

Electronic Thesis and Dissertation Repository

10-26-2011 12:00 AM

Structure and Dynamics of the Membrane Protein Bacteriorhodopsin Studied by Mass Spectrometry


Yan Pan, *The University of Western Ontario*

Supervisor: Dr. Lars Konermann, *The University of Western Ontario*

A thesis submitted in partial fulfillment of the requirements for the Doctor of Philosophy degree
in Chemistry

© Yan Pan 2011

Follow this and additional works at: <https://ir.lib.uwo.ca/etd>

 Part of the [Analytical Chemistry Commons](#), and the [Biochemistry, Biophysics, and Structural Biology Commons](#)

Recommended Citation

Pan, Yan, "Structure and Dynamics of the Membrane Protein Bacteriorhodopsin Studied by Mass Spectrometry" (2011). *Electronic Thesis and Dissertation Repository*. 294.
<https://ir.lib.uwo.ca/etd/294>

This Dissertation/Thesis is brought to you for free and open access by Scholarship@Western. It has been accepted for inclusion in Electronic Thesis and Dissertation Repository by an authorized administrator of Scholarship@Western. For more information, please contact wlsadmin@uwo.ca.

STRUCTURE AND DYNAMICS OF THE MEMBRANE PROTEIN
BACTERIORHODOPSIN STUDIED BY MASS SPECTROMETRY

(Spine title: Membrane Proteins Studied by Mass Spectrometry)

(Thesis format: Integrated-Article)

By

Yan Pan

Graduate Program in Chemistry

A thesis submitted in partial fulfillment
of the requirements for a degree of
Doctor of Philosophy

The School of Graduate and Postdoctoral Studies
The University of Western Ontario
London, Ontario, Canada

© Yan Pan 2011

CERTIFICATE OF EXAMINATION

Supervisor

Examiners

Dr. Lars Konermann

Dr. Zhifeng Ding

Supervisory Committee

Dr. François Lagugné-Labarthe

Dr. Stanley D. Dunn

Dr. Michael Siu

The thesis by

Yan Pan

entitled:

**Structure and Dynamics of the Membrane Protein
Bacteriorhodopsin Studied by Mass Spectrometry**

is accepted in partial fulfillment of the
requirements for the degree of
Doctor of Philosophy

Date

Chair of the Thesis Examination Board

Abstract

Membrane proteins continue to represent a major challenge for most analytical techniques. Using bacteriorhodopsin (BR) as model system, this work aims to develop mass spectrometry (MS)-based approaches for exploring the structure, dynamics and folding of membrane proteins.

As the first step, BR in its native lipid environment was exposed to hydroxyl radicals, which were produced by laser photolysis of hydrogen peroxide. It was found that the resulting methionine (Met) labeling pattern was consistent with the known BR structure. This finding demonstrates that laser-induced oxidative Met labeling can provide structural information on membrane proteins. In subsequent experiments, the effects of different denaturing agents (heat, acid, and SDS) on the BR conformation were investigated. It was demonstrated that each of these non-native conditions results in unique structural features that give rise to characteristic Met labeling patterns. These results highlight the ability of laser-induced oxidative labeling to detect conformational changes of membrane proteins.

Obtaining better insights into the structural properties of SDS-denatured BR is particularly important because this form of protein is widely used as starting point for folding studies. Combining oxidative labeling with site-directed mutagenesis and fluorescence measurements, this work yielded a detailed structural model of SDS-denatured BR. Subsequently, pulsed oxidative labeling coupled with rapid mixing and MS was used to characterize short-lived intermediates that become populated during BR refolding. The combination of pulsed oxidative labeling and stopped-flow spectroscopy provided key

structural insights into the kinetic mechanism by which the SDS-denatured protein inserts and folds into the lipid bilayer.

Complementary to oxidative labeling, hydrogen/deuterium exchange (HDX) MS was employed to examine the structure and dynamics of BR under various physiochemical conditions. Structural features of different detergent/lipid-bound BR samples were characterized by their HDX kinetics. Comparative HDX experiments of BR were carried out in the dark (resting state) and under illumination where the induced retinal isomerization mediates proton transport (functioning state). Isotope exchange was found to be much faster during light exposure than in the dark. This observation reveals that structural dynamics of the protein scaffold are "accelerated" by motions of the retinal, reflecting a direct coupling between protein dynamics and function.

Keywords: membrane protein, bacteriorhodopsin, mass spectrometry, oxidative labeling, hydroxyl radical, hydrogen/deuterium exchange, protein dynamics, membrane protein folding.

Co-Authorship Statement

The work in Chapters 1- 5 was published in the following articles:

Pan, Y. and Konermann, L. Membrane Protein Structural Insights from Chemical Labeling and Mass Spectrometry. *Analyst* 2010, 135: 1191-1200. Reproduced with permission. © 2010 The Royal Society of Chemistry

Pan, Y., Stocks, B. B., Brown, L., and Konermann, L. Structural Characterization of an Integral Membrane Protein in its Natural Lipid Environment by Oxidative Methionine Labeling and Mass Spectrometry. *Analytical Chemistry* 2009, 81:28–35. Reproduced with permission. © 2009 American Chemical Society

Pan, Y., Brown, L. and Konermann, L. Mapping the Structure of an Integral Membrane Protein under Semi-Denaturing Conditions by Laser-Induced Oxidative Labeling and Mass Spectrometry. *Journal of Molecular Biology* 2009, 394: 968-981. Reproduced with permission. © 2009 Elsevier

Pan, Y., Brown, L. and Konermann, L. Site-Directed Mutagenesis Combined with Oxidative Methionine Labeling for Probing Structural Transitions of a Membrane Protein. *Journal of The American Society for Mass Spectrometry* 2010, 21: 1947-1956. Reproduced with permission. © 2010 Elsevier

Pan, Y., Brown, L. and Konermann, L. Kinetic Folding Mechanism of an Integral Membrane Protein Examined by Pulsed Oxidative Labeling and Mass Spectrometry. *Journal of Molecular Biology* 2011, 410:146-458. Reproduced with permission. © 2011 Elsevier

Pan, Y., Brown, L. and Konermann, L. Hydrogen-Deuterium Exchange SEC/ESI-MS and Optical Spectroscopy as Complementary Tools for Studying the Structure and Dynamics of a Membrane Protein. *Int. J. Mass Spectrom.* [H/D Exchange Special Issue] 2011, 302:3-11. Reproduced with permission. © 2011 Elsevier

The original draft for each of these articles was prepared by the author. Subsequent revisions were made by the author, Dr. Lars Konermann and other co-authors. Dr. Leonid Brown provided the raw BR protein. All experimental work and data analyses were performed by the author under the supervision of Dr. Lars Konermann.

Acknowledgments

I would like to take the opportunity to express my sincerest gratitude to my supervisor Dr. Lars Konermann for his excellent mentoring and strong support. I also thank him for offering me many opportunities to study new skills, for providing me free spaces to exert my potential, and for giving me extremely constructive suggestions and help on my career development. I have benefited tremendously from his outstanding insights and expertise in protein mass spectrometry. He guided me into the amazing world of proteins that deserve all my efforts and struggles. I really enjoyed my Ph.D. studies in Konermann lab, which will be the most valuable experience in my life. I wish I could work here longer, learning more and contributing more.

Thanks to my thesis examiners: Dr. Zhifeng Ding, Dr. François Laguné-Labarthe, Dr. Stanley D. Dunn and Dr. Michael Siu. Thanks to all professors who taught me in UWO. Thanks to Prof. Leonid Brown in Guelph University for collaborating on this challenging project. Thanks to Prof. Mel Usselman and Graduate Coordinator Ms. Darlene McDonald for helping my admission to the Department of Chemistry. I am grateful to UWO where I lived a simple but fruitful life over the past 4 years.

Thanks to my fellow group members, Yuhong, Jinxi, Jenna, Bradley, Elias, Mahasilu, Xin, Brian, Yalda, Siavash, Anil and Dupe, for their friendship and helpful discussion. A special thank to Bradley for sharing both his experimental skills and native Canadian culture.

Thanks to NSERC for the generous financial support in the form of Canada Graduate Scholarship.

Finally, I thank my family members. My gratitude and guilt are beyond my words.

Table of Contents

CERTIFICATE OF EXAMINATION	ii
Abstract.....	iii
Co-Authorship Statement	v
Acknowledgments	vi
Table of Contents	vii
List of Tables	xii
List of Figures.....	xiii
List of Symbols and Abbreviations	xv
Chapter-1 Introduction	1
1.1 Membrane Proteins	1
<i>1.1.1 General Background</i>	<i>1</i>
<i>1.1.2 α-Helical Membrane Proteins.....</i>	<i>3</i>
<i>1.1.3 β-Barrel Membrane Proteins</i>	<i>5</i>
1.2 Membrane Protein Structure and Dynamics	6
<i>1.2.1 Non-Mass Spectrometry Techniques.....</i>	<i>6</i>
<i>1.2.2 Mass Spectrometry-Based Approaches</i>	<i>11</i>
<i>1.2.2.1 Hydrogen/Deuterium Exchange Mass Spectrometry.....</i>	<i>12</i>
<i>1.2.2.2 Covalent Labeling Versus Hydrogen/Deuterium Exchange</i>	<i>16</i>
<i>1.2.2.3 Site-Specific Covalent Labeling</i>	<i>18</i>
<i>1.2.2.4 Hydroxyl Radical Labeling</i>	<i>21</i>
1.3 Membrane Protein Folding.....	27
<i>1.3.1 Protein Folding Mechanism.....</i>	<i>27</i>
<i>1.3.2 Membrane Protein Folding Mechanism</i>	<i>29</i>
<i>1.3.3 Folding Kinetics of Membrane Proteins</i>	<i>32</i>
1.4 Electrospray Ionization Mass Spectrometry (ESI-MS)	36
<i>1.4.1 The ESI Process</i>	<i>36</i>
<i>1.4.2 Mass Analyzers.....</i>	<i>37</i>

1.4.2.1	<i>Quadrupole Mass Analyzer</i>	38
1.4.2.2	<i>Time of Flight (TOF) Mass Analyzer</i>	39
1.5	Scope of this Thesis	40
1.6	References	42
Chapter-2	Structural Characterization of Bacteriorhodopsin in Its Natural Lipid Environment by Oxidative Methionine Labeling and Mass Spectrometry	49
2.1	Introduction	49
2.2	Experimental	55
2.2.1	<i>Materials</i>	55
2.2.2	<i>Laser-Induced Oxidative Labeling</i>	56
2.2.3	<i>Intact Protein Analysis</i>	57
2.2.4	<i>Peptide Mapping and HPLC/MS analysis</i>	57
2.3	Results and Discussion	59
2.3.1	<i>Intact Protein Analysis</i>	59
2.3.2	<i>Peptide Mapping</i>	60
2.3.3	<i>Tandem Mass Spectrometry</i>	61
2.3.4	<i>Structural Interpretation</i>	66
2.4	Conclusions	66
2.5	References	69
Chapter-3	Mapping the Structure of Bacteriorhodopsin under Semi-Denaturing Conditions by Laser-Induced Oxidative Labeling and Mass Spectrometry	72
3.1	Introduction	72
3.2	Experimental	75
3.2.1	<i>Sample Preparation</i>	75
3.2.2	<i>Optical Spectroscopy and Oxidative Labeling</i>	77
3.2.3	<i>Peptide Mapping and UPLC/MS Analysis</i>	78
3.2.4	<i>Data Analysis</i>	79
3.3	Results and Discussion	81

3.3.1	<i>Optical Spectroscopy</i>	81
3.3.2	<i>Oxidative Methionine Labeling</i>	86
3.3.3	<i>Structural Interpretation - Low pH</i>	91
3.3.4	<i>Structural Interpretation - SDS Exposure</i>	92
3.3.5	<i>Structural Interpretation - BR after Heat Exposure</i>	99
3.4	Conclusions	100
3.5	References	102
Chapter-4	Kinetic Folding Mechanism of Bacteriorhodopsin Examined by Pulsed Oxidative Labeling and Mass Spectrometry	105
4.1	Introduction	105
4.2	Experimental	109
4.2.1	<i>Materials and Sample Preparation</i>	109
4.2.2	<i>Stopped-flow Spectroscopy</i>	111
4.2.3	<i>Continuous-Flow Mixing and Oxidative Labeling</i>	111
4.2.4	<i>Peptide Mapping and Quantification of Oxidative Labeling</i>	113
4.3	Results and Discussion	114
4.3.1	<i>Stopped-Flow Spectroscopy</i>	114
4.3.2	<i>Pulsed Oxidative Labeling</i>	119
4.3.3	<i>Implications for the BR Folding Mechanisms</i>	122
4.4	Conclusions	126
4.5	References	129
Chapter-5	H/D Exchange Mass Spectrometry and Optical Spectroscopy as Complementary Tools for Studying the Structure and Dynamics of Bacteriorhodopsin	132
5.1	Introduction	132
5.2	Experimental	135
5.2.1	<i>Proteins and Reagents</i>	135
5.2.2	<i>Optical Spectroscopy</i>	137

5.2.3	<i>Hydrogen/Deuterium Exchange</i>	137
5.2.4	<i>Liquid Chromatography/Mass Spectrometry</i>	138
5.3	Results and Discussion	139
5.3.1	<i>Optical Spectroscopy</i>	139
5.3.2	<i>Size Exclusion Chromatography/ESI-MS</i>	142
5.3.3	<i>Hydrogen/Deuterium Exchange SEC/ESI-MS</i>	143
5.4	Conclusions	152
5.5	References	156
Chapter-6	Hydrogen Exchange Mass Spectrometry Reveals Light-Induced Changes in the Structural Dynamics of a Biomolecular Machine	160
6.1	Introduction	160
6.2	Experimental	164
6.2.1	<i>Reagents and Sample Preparation</i>	164
6.2.2	<i>Hydrogen/Deuterium Exchange Under Light/Dark Conditions</i>	165
6.2.3	<i>Liquid Chromatography/Mass Spectrometry</i>	166
6.2.3	<i>Flash Absorption Spectroscopy</i>	167
6.3	Results and Discussion	168
6.3.1	<i>HDX Measurements on Purple Membranes</i>	168
6.3.2	<i>HDX Measurements on Monomeric BR</i>	170
6.3.3	<i>Casting the HDX Kinetics in a Thermodynamic/Kinetic Model</i>	176
6.3.4	<i>Mechanistic Origin of Differences in Light/Dark HDX Behavior</i>	177
6.4	Conclusions	180
6.5	References	182
Chapter-7	Summary and Future Work	186
7.1	Summary	186
7.2	Future Work	188

7.2.1 <i>Application of Laser-Induced Oxidative Labeling</i>	188
7.2.2 <i>Application of HDX/MS for Membrane Proteins</i>	190
7.3 References	191
Appendix-1 Permissions	192
Curriculum Vitae	198

List of Tables

Chapter-5

Table 5-1. Parameters obtained from fitting the HDX kinetics 149

Table 5-2. Amino acid sequence of BR. 150

Chapter-6

Table 6-1. Structural and thermodynamic parameters associated with the HDX 179

List of Figures

Chapter-1

Figure 1-1. Schematic of a lipid bilayer and associated membrane proteins.....	2
Figure 1-2. General workflow for covalent labeling of membrane proteins.....	20
Figure 1-3. Schematic representation of the mechanism of ion formation in ESI.....	37

Chapter-2

Figure 2-1. X-ray structure of bacteriorhodopsin.....	53
Figure 2-2. Amino acid sequence of BR.....	54
Figure 2-3. Deconvoluted ESI mass distributions of intact BR.....	62
Figure 2-4. ESI mass spectra of selected tryptic peptides.....	63
Figure 2-5. Oxidation levels of various tryptic peptides.....	64
Figure 2-6. Partial MS/MS product ion spectra.....	64
Figure 2-7. Partial MS/MS product ion spectra obtained after fragmentation.....	65

Chapter-3

Figure 3-1. Side view and top view of BR (pdb code: 1XJI).....	83
Figure 3-2. UV-Vis absorption spectra and fluorescence emission spectra.....	84
Figure 3-3. ESI mass spectra of selected BR tryptic peptides T7 and T1.....	87
Figure 3-4. Partial MS/MS spectra of the tryptic peptide T1.....	88
Figure 3-5. Laser-induced oxidative labeling of methionine residues in BR.....	89
Figure 3-6. Schematic representation of native BR in the purple membrane.....	95
Figure 3-7. F_u^{corr} values of individual Met residues in native L93M BR.....	97

Figure 3-8. Partial MS/MS product ion spectra obtained after fragmentation	98
----------------------------------------------------------------------------------	----

Chapter-4

Figure 4-1. Stopped-flow Trp fluorescence kinetics.....	115
Figure 4-2. Stopped-flow UV-Vis absorption spectra	117
Figure 4-3. Close-up view of the initial 10 s during BR refolding	118
Figure 4-4. ESI mass spectra of tryptic peptides T1	121
Figure 4-5. Schematic of refolded BR in bicelles	123

Chapter-5

Figure 5-1. UV-Vis absorption spectra and fluorescence emission spectra of BR	140
Figure 5-2. Deconvoluted mass distributions obtained by SEC/ESI-MS	144
Figure 5-3. Deconvoluted ESI mass distributions of native BR	146
Figure 5-4. HDX kinetics of BR under five different solvent conditions	148

Chapter-6

Figure 6-1. HDX kinetics of native BR in purple membranes.....	169
Figure 6-2. BR photocycle kinetics monitored by time-resolved absorption.....	171
Figure 6-3. Mass distributions of monomeric BR at selected HDX time points	172
Figure 6-4. Kinetic behavior of monomeric BR under illumination.....	174
Figure 6-5. Schematic diagram depicting the properties of monomeric BR.....	178

List of Symbols and Abbreviations

BR, bacteriorhodopsin

BO, bacterioopsin (BR without retinal)

CD, circular dichroism

CHAPS, 3-[(3-cholamidopropyl)dimethylammonio]-1-propanesulfonate

CMC, critical micelle concentration

DGK, diacylglycerol kinase

DsbB, Disulfide bond-forming protein B

DM, n-dodecyl-D-maltoside

DMPC, L- α -1,2-dimyristoylphosphatidylcholine

EPR, electron paramagnetic resonance

ESI, electrospray ionization

FRET, Förster resonance energy transfer

FTIR, Fourier transform infrared spectroscopy

HDX, hydrogen/deuterium exchange

KcsA, potassium channel

LHCII, the major plant light-harvesting complex II

L93M, mutated BR with Leucine at position 93 substituted with Methionine

V179M, mutated BR with Valine at position 179 substituted with Methionine

NMR, nuclear magnetic resonance

NATA, N-acetyl tryptophanamide

SDS, sodium dodecyl sulfate

SEC, size exclusion chromatography

MS, mass spectrometry

MALDI, matrix-assisted laser desorption ionization

MetO, methionine sulfoxide

OmpA, outer membraner protein A

$\cdot\text{OH}$, hydroxyl radical

ε , the extinction coefficient

ΔG° , standard Gibb's free energy change

K_{op} , opening equilibrium constant

M, molar, concentration (mol/L)

m/z, the mass to charge ratio

Chapter-1 Introduction

1.1 Membrane Proteins

1.1.1 General Background

Simply speaking, proteins do almost everything in living cells. All functions of living organisms, such as metabolism, energy conversion, communication, regulation, reproduction and structural support, are related to proteins. Proteins are linear biopolymers composed of 20 different amino acids, which are linked to each other by peptide bonds. Most proteins can perform their specific biological functions only after folding into unique three-dimensional structures.¹ The architecture of proteins can be divided into four hierarchical levels: (1) **Primary structure**: the amino acid sequence. DNA (or RNA in some viruses) encodes the primary protein structure. (2) **Secondary structure**: the local arrangement of the peptide backbone into α -helices, β -sheets, turns, and coiled regions. Different secondary structure elements can be present in the same protein molecule. (3) **Tertiary structure**: the overall shape of a single polypeptide chain. Tertiary structure completely defines the structure of a protein molecule. (4) **Quaternary structure**: the shape or structure that results from the interaction of more than one polypeptide chain, usually called subunits, which function as parts of a protein complex. Proteins can be divided into three main classes: globular proteins, fibrous proteins, and membrane proteins. Almost all globular proteins are water-soluble, and many are enzymes. Fibrous proteins often provide structural support. Membrane proteins often serve as receptors for cell signaling or transporters to provide channels for polar or charged molecules to pass through the cell membrane.

Each living cell is surrounded by a biological membrane that is an organized assembly of lipids and associated membrane proteins. The lipids are arranged as a bilayer. The associated membrane proteins can be classified into two groups: integral (intrinsic) and peripheral (extrinsic) membrane proteins based on the nature of the lipid bilayer-protein interactions as shown in Figure 1-1. Most biological membranes contain both types of membrane proteins. *Integral membrane proteins* are permanently attached to the membrane and have one or more segments that are embedded in the lipid bilayer. They associate tightly with the membrane through hydrophobic interactions and can be separated

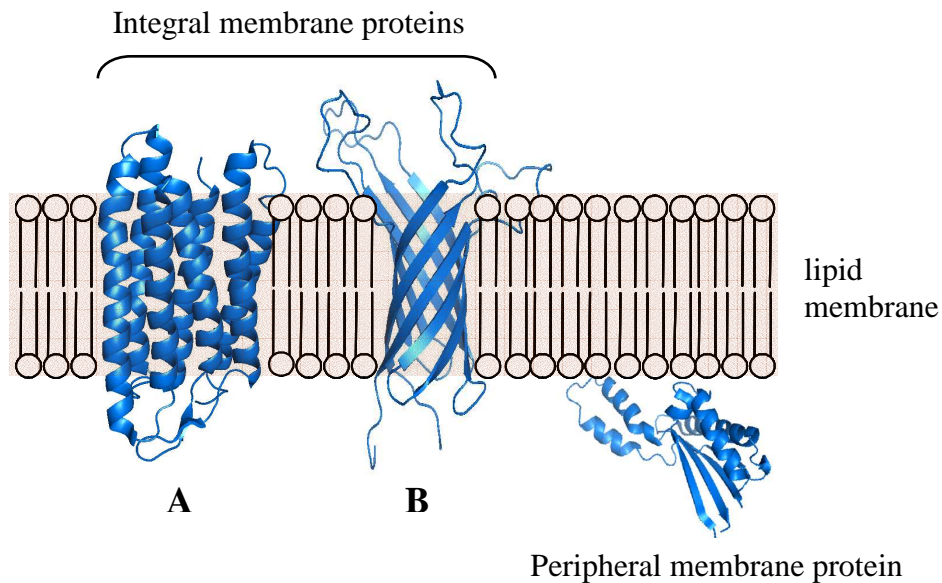


Figure 1-1. Schematic of a lipid bilayer and associated membrane proteins.

A: α -helical membrane protein; B: β -barrel membrane protein.

from the membrane only by treatment with agents that disrupt membranes. These proteins are generally free to diffuse laterally in the lipid matrix. Most *peripheral membrane proteins* are loosely attached to protruding portions of integral membrane proteins, or interact with lipid head groups.

The presence of a membrane is essential for living systems as it provides a physical barrier between the cell and its environment. Many functions of the membrane are mediated by integral membrane proteins. These proteins are key players in a variety of important cellular processes including ion and solute transport (ion channels and transporters), energy conversion (respiration, ATP synthesis), and cell signaling (G-protein coupled receptors and growth factor receptors). Based on their secondary structure, integral membrane proteins are divided into two classes: 1) α -helical and 2) β -barrel membrane proteins.

1.1.2 α -Helical Membrane Proteins

The vast majority of integral membrane proteins are α -helical. They represent an estimated 20%~25% of all open reading frames (ORFs) in fully sequenced genomes.² This type of protein possesses one or more transmembrane helices that are connected by extramembrane loops (Figure 1-1). A conspicuous characteristic in the amino acid sequence is the presence of hydrophobic stretches of approximately 20 nonpolar residues, which are just enough to span the hydrophobic core of a typical bilayer in an α -helical conformation.³ Loops that protrude into the aqueous phase on both sides are usually hydrophilic. A few polar groups can be included in the helical sequence, provided that the helix remains hydrophobic on average or that group polarity is diminished, such as in ion pairs or protonated state. Also,

the interior of transmembrane regions is often lined with hydrophilic residues, giving rise to amphipathic helices. The net hydrophobicity favors the association of these helices into membrane interior relative to the aqueous milieu. As a result, hydrophobic effects drive the formation of transmembrane helices.^{4,5}

Statistical analyses of transmembrane helices show that large hydrophobic amino acids such as leucine, isoleucine, valine and phenylalanine prefer the lipid-exposed surface to the protein interior. It is remarkable that glycine and proline are abundant in transmembrane helices although they tend to be helix breakers. About 60% of transmembrane helices contain significant bends or other distortions.⁵ These occurrences emphasize the important contribution of the hydrophobic environment to the stabilization of hydrogen bonding and helix formation. Aromatic side chains, particular tryptophan and tyrosine, are often located near the termini of helices. Additionally, even though cysteine is abundant, no disulfides have been found in transmembrane regions.⁴

Unlike soluble proteins whose structure is stabilized mostly by the hydrophobic effect, the importance of hydrophobic interactions is minimal for transmembrane helices that are dominated by non-polar residues in a bilayer milieu. Inter-helix side chain hydrogen bonds have been identified in a number of membrane proteins, but their impacts on overall stability and folding were found to be modest.^{5,6} In contrast, extensive van der Waals interactions play a major role in stabilizing the helical packing in the bilayer.^{4,5} These helices exhibit a narrow distribution of packing angles with a strong preference at $\sim 20^\circ$ that favors inter-helix side chain interdigitation. Small residues such as glycine, alanine and

serine, preferably appear at the helix-helix interface where they are often involved in specific interactions. Setting aside prosthetic groups and lipid interactions, helix packing is the dominant factor to provide specific helix-helix recognition and stabilization.^{4,5}

1.1.3 *β -Barrel Membrane Proteins*

β -Barrel membrane proteins occur in the outer membrane of Gram-negative bacteria.^{7,8}

The outer membrane protects the bacteria from hostile environments, while these proteins serve as channels to permit the entry of small solutes such as nutrients. β -Barrel proteins also occur in eukaryotes in the outer membrane of mitochondria and chloroplasts. β -Barrel membrane proteins account for 2 ~ 3 % of all ORFs.² All these species share a common architecture (Figure 1-1), composed of an antiparallel β -barrel, with loops protruding outside the membrane. Transmembrane β -barrels of known structure consist of 8 to 22 β -strands that roll up, forming a solvent accessible channel with a minimum diameter of 7 Å. The number of strands must be even to permit the β -sheet to close up on itself. The N and C termini are at the periplasmic barrel end. All strands are antiparallel and tilted by 30 ~ 60° relative to the membrane normal. The side chains at the solvent-exposed surface are often polar.⁷ In contrast, the outer surface of the barrel exposed to the membrane consists of hydrophobic side chains with two girdles of aromatic residues in the lipid head group regions. Since the transmembrane segments are β -strands, every second residue is facing the lipids and hence needs to be hydrophobic. Compared to helical membrane proteins, the sequences of β -barrel proteins tend to be relatively hydrophilic, usually containing alternating hydrophobic and hydrophilic residues.^{7,8}

1.2 Membrane Protein Structure and Dynamics

1.2.1 *Non-Mass Spectrometry Techniques*

Membrane proteins comprise ~30% of the human genome.⁹ More than half of all known drug targets are membrane proteins.¹⁰ Despite their biomedical importance, relatively little is known about the structure and function of these species, when compared to their globular counterparts. For example, among the more than 60,000 coordinate files currently available in the protein data bank (PDB) (<http://www.pdb.org/>) there are only ca. 200 unique membrane protein structures (<http://blanco.biomol.uci.edu/>).¹¹

X-ray crystallography and NMR are classical techniques for determining the structure of soluble proteins. X-ray crystallography has long been the “gold standard” to obtain protein structure at atomic resolution. Since the first three-dimensional structure of myoglobin was solved,^{12, 13} over 39000 X-ray crystal structures of proteins and other biological molecules have been determined. Around 85% of the protein structures available in the PDB were determined by X-ray crystallography. X-ray crystallography can solve the structures of very large molecules. However, the target protein must be available in large amounts (milligrams) and very high purity, in order to initiate successful crystallization. Moreover, this technique is limited to native proteins, because partially unfolded species do not crystallize. NMR spectroscopy is another indispensable technique for examining protein structure and dynamics.¹⁴ NMR investigations can yield three-dimensional structures of proteins with a high resolution, similar to what is achievable by X-ray crystallography. Roughly 15% of the protein structures in the PDB were obtained by NMR. NMR spectroscopy is often the only way to obtain high resolution information on partially or

wholly unstructured proteins. However, NMR is typically limited to relatively small proteins.¹⁵

As noted earlier, the native fold of globular proteins is characterized by a hydrophobic core, and an exterior that is dominated by polar and charged side chains. This architecture results in high water solubility and a low tendency to aggregate. In contrast, membrane proteins exhibit a large hydrophobic surface area that is in contact with alkyl chains of the lipid bilayer. Hydrophilic regions are usually limited to segments that interact with polar lipid head groups and/or that protrude out of the membrane plane, e.g., cytoplasmic or extracellular loops. A number of charged and polar residues may also be found in the interior, particularly for systems that act as pores or transporters, and that contain internal water molecules.¹⁶ Once removed from the lipid bilayer, membrane proteins tend to undergo rapid denaturation and/or aggregation caused by the exposure of hydrophobic surface elements to the aqueous solvent. The most common strategy for stabilizing isolated membrane proteins is the solubilization in detergent micelles. However, the micellar environment represents a less-than-perfect mimic of the membrane bilayer. As a result, the occurrence of structural changes and aggregation can often not be completely eliminated.¹⁷ The use of bicelles (bilayered micelles)¹⁸ or liposomes (lipid vesicles)¹⁹ can sometimes represent a useful alternative.

Membrane proteins are amenable to the same structure determination methods as globular proteins, *albeit* with a much lower success rate. The first X-ray crystal structures of myoglobin appeared in 1950s,^{12, 13} but it took almost thirty additional years until the first

membrane protein structure was published.²⁰ In many cases, a key prerequisite for successful X-ray studies on membrane proteins is the proper choice of detergent molecules that co-crystallize with the protein, while at the same time preventing precipitation.¹⁷ Bicelle-mediated crystallization has been reported as well.¹⁸ Detergent-solubilized membrane protein complexes tend to be quite large, and the resulting slow rotational diffusion causes peak broadening in solution NMR experiments which complicates the acquisition of high quality spectra.²¹ Nonetheless, structural information on a few membrane proteins has been obtained using this approach.²² Although still in its infancy, the application of solid-state NMR methods to liposome-reconstituted systems represents a promising novel strategy.²³ In addition, the use of magic-angle spinning NMR spectroscopy to systems with very long rotational correlation times has been demonstrated.²⁴

As a result of the difficulties associated with the application of X-ray and NMR techniques to membrane proteins, there is a considerable interest in low resolution methods capable of providing at least some structural information.²⁵ Probably the simplest of these strategies are Kyte-Doolittle hydrophathy analyses which yield secondary structure predictions (e.g. transmembrane helices vs. loops) on the basis of the amino acid sequence.²⁶ While the reliability of these prediction schemes is limited, they allow hypotheses regarding structure and topology to be developed which can then be tested experimentally, e.g., by protease protection assays.²⁷ Cysteine (Cys) scanning mutagenesis represents a more informative but very labor intensive approach.²⁸ This method requires the availability of a genetically engineered Cys free background construct. Individual Cys residues are then incorporated in

specific locations. Subsequently the protein is exposed to a thiol specific coupling reagent, and the extent of reaction is monitored using a fluorescence-based readout or other detection methods. Only those Cys residues that are accessible to the labeling reagent will react readily. In this way it is possible to obtain fairly accurate information on the locations of loops and transmembrane regions, as well as some insights into packing interactions. Additional topological information can be obtained by using a combination of membrane permeable and impermeable reagents.²⁸ In a Herculean effort, Kaback and coworkers²⁹ subjected over 400 positions of the 417 amino acids of the protein lac permease to this Cys substitution technique, resulting in a three-dimensional model that was later found to be largely consistent with a X-ray crystal structure.³⁰

Low resolution spectroscopic methods have also been widely used to probe the global conformation of membrane proteins. For instance, in the far-UV region (190-250nm), different forms of secondary structure result in characteristic CD patterns. Hence, CD spectroscopy is commonly used to estimate the secondary structure of membrane proteins.³¹ The fluorescence of tryptophans is sensitive to environment. Most membrane proteins contain tryptophan residues. Fluorescence spectroscopy is thus often employed for detecting global or local structural changes in response to alterations in the solvent environment. For membrane proteins that contain additional chromophores, UV-Vis spectroscopy can be used to monitor the structural changes.

A well defined protein structure usually represents a prerequisite for function, but it has been widely accepted that protein structure is not static. Proteins are in constant motion,

sampling different conformational substates around the average structure.³²⁻³⁴ The relative probabilities of these conformational substates are governed by the Boltzmann distribution. The kinetics of inter-conversion among these substates are defined by free energy barriers. These structural fluctuations are thought to be essential for protein functions such as enzyme catalysis, ligand binding, signaling, and transport. Native proteins represent a fine-tuned balance between a highly ordered and stable conformation that ensures specificity, and a state that remains dynamic enough to maintain functionality. Characterizing protein dynamics is thus important for understanding the function and stability.³²

Several experimental and computational methods are available for probing the dynamic properties of proteins. Classical crystallography can provide limited information about protein dynamics by theoretical estimates of uncertainty in atomic positions using B-factors. Recent developments such as time-resolved X-ray techniques have permitted more detailed dynamic information to be gained.³⁵ NMR spectroscopy is a powerful technique for providing insights into protein dynamics at different time scales. Relaxation measurements yield time-dependent correlation functions that can be interpreted in terms of internal dynamics.³⁶ Molecular dynamics simulations have emerged as one of the most important tools for examining protein conformational dynamics over the past decade.^{37, 38} The main advantage of such computer simulations is that they can provide unbeatable details about individual molecular motions as a function of time. To validate the simulation methodology, however, experimental data are required.

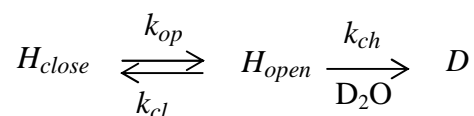
1.2.2 Mass Spectrometry-Based Approaches

With the advent of electrospray ionization (ESI)³⁹ and matrix-assisted laser desorption/ionization (MALDI),⁴⁰ mass spectrometry (MS) has become an indispensable tool, not only for studying protein sequences and post-translational modifications,⁴¹ but also for examining their conformation, folding and dynamics.⁴² Experiments on membrane proteins mostly employ liquid chromatography (LC)/ESI-MS, but the application of MALDI-MS has been demonstrated as well.⁴³ Similar to other analytical techniques, however, the application of MS to membrane proteins continues to be challenging.⁴⁴ Nonetheless, following pioneering work in the late 1990s,⁴⁵⁻⁴⁷ this area is now experiencing continuous growth⁴⁸⁻⁵¹ and even large-scale projects in membrane proteomics have become feasible.^{9, 52-54} Other interesting applications include the use of nanoESI-MS for the analysis of intact membrane protein assemblies. This approach provides information on subunit stoichiometries and lipid-protein interactions.^{55, 56} The applicability of cross-linking to membrane proteins has been demonstrated as well.⁵⁷

MS is an analytical technique that measures the mass-to-charge ratio of ions in the gas phase. For non-experts it may not be straightforward to see how these measurements can be used for probing the structure and dynamics of proteins in solution. Key to MS-based structural methods is the use of labeling strategies.⁵⁸ These approaches rely on the principle that factors such as polypeptide conformation, solvent exposure and structural dynamics modulate the labeling behavior of specific sites on the protein. Labeling causes mass changes that leads to peak shifts in the spectrum. Structural information can be obtained by analyzing the mass changes of protein fragments in a spatially-resolved manner.

1.2.2.1 Hydrogen/Deuterium Exchange Mass Spectrometry

Amide hydrogen/deuterium exchange (HDX) is one of the most popular labeling methods for studying the structure and dynamics of soluble proteins, and the technique has also been applied to a few membrane proteins.^{6, 59-63} HDX experiments rely on the fact that exposure of a protein to D₂O induces N-H → N-D conversion at backbone amide linkages. Solvent-exposed protein regions that are not involved in hydrogen bonding undergo rapid exchange, with rate constants approaching the "chemical" HDX rate constant k_{ch} of completely unprotected amides.⁶⁴ k_{ch} is primarily dependent on the nature of amino acids and neighboring residues at given pH and temperature. Because both acid and base can catalyze HDX, there is a minimum value of k_{ch} at ~ pH 2.5. Importantly, HDX at hydrogen-bonded N-H groups can be slowed down by as much as eight orders of magnitude. Exchange at these protected sites is mediated by protein structural fluctuations that involve the transient disruption of H-bonds and provide temporary solvent access.^{65, 66} These fluctuations may be interpreted as opening/closing events that are associated with rate constants k_{op} and k_{cl} , respectively. The HDX mechanism can be described as follows:



The overall exchange rate constant k_{HDX} is given by

$$k_{HDX} = \frac{k_{op} k_{ch}}{k_{cl} + k_{ch} + k_{op}} \quad (1-1)$$

The assumption of the exchangeable site being predominantly in its closed state implies that $k_{op} \ll k_{cl}$, such that equation (1-1) becomes:

$$k_{HDX} = \frac{k_{op}k_{ch}}{k_{cl} + k_{ch}} \quad (1-2)$$

This expression leads to the two distinct EX2 and EX1 regimes. In the commonly encountered EX2 limit, characterized by $k_{cl} \gg k_{ch}$, the overall exchange-rate constant k_{HDX} is given by

$$k_{HDX} = \frac{k_{op}k_{ch}}{k_{cl}} = K_{op}k_{ch} \quad (1-3)$$

where K_{op} is the equilibrium constant of the unfolding reaction of a protein. K_{op} depends on the structure and dynamics of proteins. Under these conditions the probability of HDX occurring during a single opening event is very small, such that numerous opening/closing cycles are required before isotope exchange takes place. EX2 measurements offer an avenue toward the thermodynamic characterization of proteins, because the free energy difference (ΔG^0) of the open event is given by

$$\Delta G^0 = -RT \ln K_{op} = -RT \ln \frac{k_{HDX}}{k_{ch}} \quad (1-4)$$

where the value of k_{ch} are known from the literature.⁶⁴ Spreadsheets for calculating k_{ch} at individual side chains can be downloaded from Dr. Walter Englander's web site (<http://hx2.med.upenn.edu/>).

In the EX1 limit ($k_{ch} \gg k_{cl}$) multiple amide hydrogens in an open region become simultaneously deuterated during a single unfolding event.^{66, 67} In this case, equation (1-2) becomes

$$k_{HDX} = k_{op} \quad (1-5)$$

such that the HDX behavior of the protein reflects the kinetics of the opening event. HDX of native proteins usually occurs in the EX2 regime. Semi-denaturing conditions sometimes favor the EX1 regime. EX1 behavior can also be promoted by using basic pH which increases k_{ch} .⁶⁴

HDX events affect two fundamental parameters, nuclear spin and mass. The former can be detected by NMR. The later can be identified by MS. In addition, the change in mass also leads to alterations of vibrational frequencies, which enable the use of FTIR-based HDX measurements. Traditionally, two-dimensional NMR spectroscopy has been the primary detection method of choice for HDX experiments,^{65, 68} but in recent years LC/ESI-MS has taken over as the more popular technique. Advantages of MS include its superior sensitivity, tolerance to paramagnetic ligands or co-factors, no strict limitations to molecular weight, and the possibility to readily distinguish between EX1 and EX2 modes of exchange.^{69, 70} The EX2 regime is characterized by a unimodal peak that progressively shifts to higher mass over time. In the case of EX1, a bimodal mass distribution is observed, in which the low mass peak represents the protected/folded conformer and the high mass peak represents the globally unfolded conformer. EX1 measurement provides a unique opportunity to detect and characterize the transient globally unfolded conformer.

For globular proteins, the degree of solvent exposure in the native state is *not* a primary determinant of HDX rates. In other words, even N-H...O=C groups that are located at the protein surface can be highly resilient to exchange, as long as the fraction of time spent in the dissociated (N-H O=C) form is small.⁷¹ Hence, HDX experiments on globular proteins do not necessarily provide structural information *per se*, but rather insights into protein conformational dynamics. In the case of membrane proteins the situation might be somewhat different, because solvent (D₂O) access to membrane-embedded or micelle-protected regions could well become a limiting factor for the HDX rate. At present, there does not appear to be an adequate knowledge base to resolve this interesting issue.

The standard or bottom-up HDX/MS protocol starts with exposure of a native unlabeled protein to D₂O-based buffer.⁷² Aliquots are removed from the reaction mixture at selected labeling times. These samples are then exposed to pH 2.5 where the intrinsic HDX rates are at a minimum, and the protein is digested by pepsin or other acidic proteases.⁷² LC separation followed by ESI-MS allows the mass shifts of individual protein fragments to be measured, such that a spatially-resolved picture of the deuterium incorporation is obtained for each time point. The occurrence of isotope back exchange necessitates that all of the steps following acid quenching have to be carried out in a very short amount of time, typically 10 to 20 minutes, and at a temperature close to 0 °C. Several groups have subjected isotopically labeled peptides or proteins to gas-phase fragmentation methods with the goal of enhancing spatial resolution and preventing back-exchange. This approach is called top-down HDX/MS.⁷³⁻⁷⁵

While there have been a few MS-based HDX studies on short transmembrane peptides⁷⁶ and membrane-associated proteins,⁷⁷ the application of the bottom-up HDX/MS protocol to integral membrane proteins remains challenging. Along with solubility issues, a general problem is the difficulty of generating peptic fragments in sufficiently high yield during the short time interval available, and under low temperature conditions.⁷⁸ Despite these challenges, Busenlehner et al. succeeded in generating spatially-resolved HDX profiles for two detergent solubilized membrane proteins, microsomal glutathione transferase 1⁵⁹ and cytochrome *c* oxidase.⁶⁰ Pepsinolysis of these two proteins may be favored by the presence of relatively large extra-membrane regions. Rey et al. revealed the conformational dynamics of the bovine mitochondrial ADP/ATP carrier by developing a separation method for detergent removal.^{62, 79} The application of bottom-up HDX/MS to SDS-denatured bacteriorhodopsin and γ -glutamyl carboxylase yielded spatially-resolved structural information with ~50% protein sequence.^{6, 61} In recent work, Griffin et al.⁶³ were able to study the conformational dynamics of the β_2 -adrenergic G-protein coupled receptor by the HDX/MS. Pepsin efficiency in that study was promoted by conducting the digestion step at 22 °C instead of using the customary 0 °C. It was reported that this elevated temperature did not significantly enhance back exchange, which is surprising considering the results of earlier studies.^{70, 72} A possible alternative to the bottom-up HDX/MS protocol for membrane proteins could be the use of top-down experiments employing ECD or ETD. Thus far top-down HDX MS have only been reported for water-soluble species.^{75, 80}

1.2.2.2 Covalent Labeling Versus Hydrogen/Deuterium Exchange

In addition to HDX, a large number of MS-based methods for probing protein structures

rely on the use of hydrophilic covalent probes that irreversibly modify solvent-accessible side chains. The data obtained in this way reflect the dominant protein structure(s) present in solution. This is quite different from HDX, where the overall isotope exchange behavior can be governed by weakly populated non-native conformers.⁸¹ Compared to a "labile" modification technique such as HDX, the stable nature of most covalent modifications facilitates certain aspects of the analysis. For example, in addition to digestion and LC separation it is possible to incorporate purification and concentration steps. Scrambling of covalently attached moieties during MS/MS is generally of no concern. Peptide mapping in covalent labeling experiments typically involves tryptic digestion which leads to specific peptide bond cleavage on the C-terminal side of arginine and lysine, unless these residues are followed by proline.⁸² In contrast, pepsin and other acidic proteases used for HDX approaches provide cleavage patterns that are largely unpredictable.⁷²

It is a convenient feature of the HDX approach that an isotopically labeled peptide will show almost the same elution behavior as the unlabeled peptide under given LC conditions. In contrast, covalent labeling will alter retention times on a reverse-phase (RP) column, such that differentially modified peptides of a given sequence will not co-elute. For example, the introduction of hydrophilic modifications (such as oxidation events) will shorten retention times under RPLC conditions. Despite the use of a specific protease the resulting chromatograms can be quite complicated. It may take some efforts to ensure that all possible modifications for a given peptide have been accounted for. In addition, the introduction of covalent modifications may alter peptide ionization efficiencies,⁸³ such that a quantitative determination of the labeling level is not always straightforward.

Another point to consider is the possible occurrence of structural changes following the labeling event. HDX is generally considered to be "benign" in this regard, meaning that changes in protein structure and stability as a result of deuterium incorporation are not very dramatic.^{67, 84} In contrast, the introduction of covalent modifications can result in marked structural changes. Thus, it has to be ensured that the experiments are conducted under carefully controlled conditions where the measured covalent labeling pattern reflects the protein conformation of interest, and not an artificially altered structure. Approaches that have been used to monitor the extent of these potential artifacts include optical measurements,⁸⁵ as well as first-order,⁸⁶ and second-order⁸⁷ kinetic analyses. Some covalent probes react with the protein so quickly that the labeling process goes to completion before major structural changes can occur. When used under single-exposure conditions, these techniques are therefore believed to provide an artifact-free reflection of the protein structure. An example of such approaches is the laser-induced oxidative labeling,⁸⁸ which will be discussed in the following Chapters.

1.2.2.3 Site-Specific Covalent Labeling

A host of hydrophilic reagents have been developed to covalently label proteins. Some of those compounds react only with a specific type of side chains, whereas others are more non-specific. The acetylation of Lys represents an example of a specific labeling strategy,⁸⁹ but numerous reagents targeting other residues (*e.g.*, Cys, Met, Arg, Glu, Asp, His, Trp and Tyr) have been developed as well.⁹⁰ Many of these specific labeling agents have been applied to the structural studies of membrane proteins. The general workflow of these experiments starts with labeling membrane proteins, followed by limited proteolysis of the

protein and analyzing the resulting peptides by LC/MS. Tandem mass spectrometry (MS/MS) is then used to identify the labeling sites (Figure 1-2). As an alternative to this "bottom-up" approach, the experiments may be conducted in a "top-down" fashion.^{48, 91}

The hydrophilic oxidizing agent chloramine T has been employed for mapping methionine accessibility of human erythrocyte membrane band 3 protein.⁹² For the native protein, Met oxidation was found to occur at solvent-accessible sites, but not in membrane protected regions. Enhanced oxidation was found for several Met residues after detergent exposure, indicating the occurrence of structural changes in a transmembrane segment.

Tetra-nitromethane can specifically induce nitrosylation at tyrosine residues and was used to probe the topology of vesicle-reconstituted glycine receptor.⁹³ Several modifications were identified by proteolysis of the SDS solubilized protein followed by LC-MS/MS. Interestingly, two of these sites (Tyr223 and Tyr228) were found to be located in a putative transmembrane helix, but based on the labeling data it was concluded that the corresponding segment likely forms an extramembrane loop.

A variety of hydrophobic photoreactive probes were used for monitoring conformational switching events of the nicotinic acetylcholine receptor in response to changes in transmembrane potential.⁹⁴ Oocytes expressing the protein were manipulated using a voltage-clamp setup in the presence of the labeling agent. Voltage changes and labeling on/off conditions were coordinated by a shutter that controlled exposure of the protein to a UV light source. Differences in the labeling pattern measured under different voltage

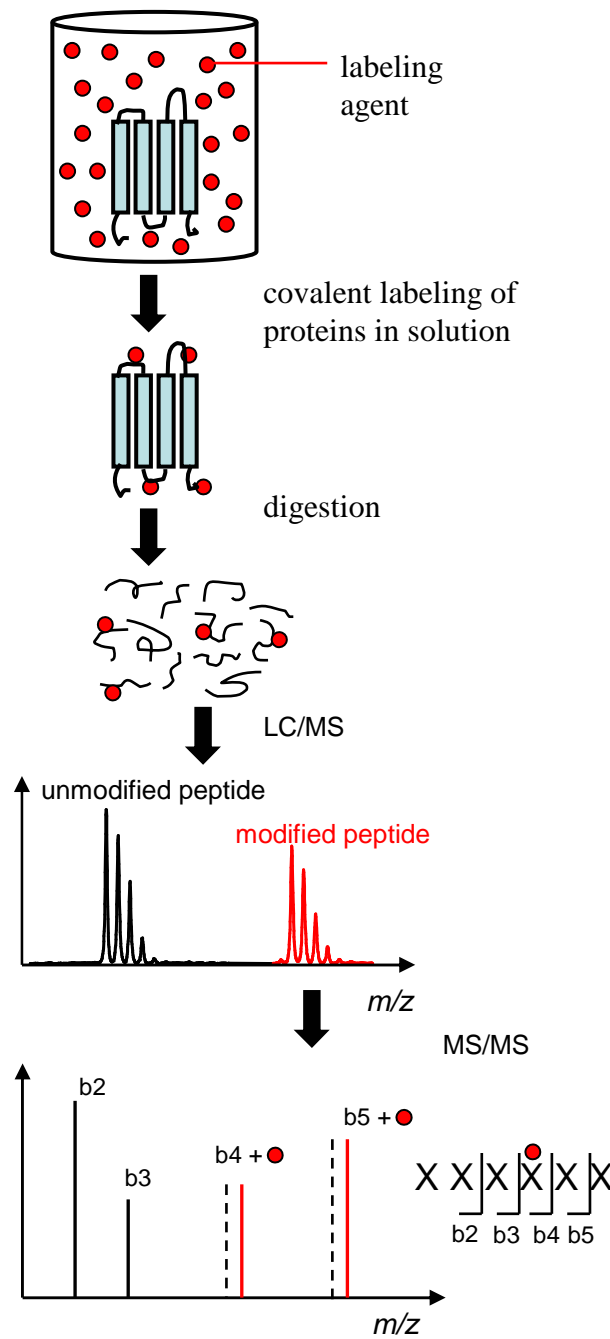


Figure 1-2. General workflow for covalent labeling of membrane proteins with subsequent MS analysis.

conditions provided insights into the voltage-induced conformational changes.

Acetylation of lysine residues was employed to monitor interactions between rhodopsin and a transducin-derived short peptide.⁸⁹ It was demonstrated that light exposure of membrane samples alters the solvent accessibility of several acetylation sites, and that binding of the light-activated protein to the peptide modifies the solvent exposure of some cytoplasmic loops. Protein-protein interactions were also explored by Wen et al.⁹⁵ who applied 1-ethyl-3-(3-dimethylaminopropyl) carbodiimide hydrochloride for labeling Asp and Glu in the membrane-associated FMO protein of a photosynthetic bacterium. In this way information was obtained about the way this protein interacts with the transmembrane reaction center complex. Those studies,^{89, 95} as well as related experiments,⁹⁶ demonstrate that covalent modification techniques not only provide information regarding membrane protein structures and conformational switching events, but also about noncovalent binding to other molecules. The term "footprinting" is often used in this context, referring to experiments where access of a labeling agent to a protein surface is blocked by the presence of a binding partner. Note, however, that some researchers employ this term in a somewhat broader context, more or less synonymous with "covalent labeling".⁹⁷

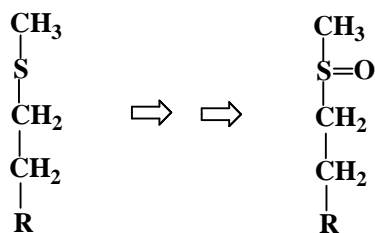
1.2.2.4 Hydroxyl Radical Labeling

Of the numerous covalent labeling agents, hydroxyl radical ($\cdot\text{OH}$) represents the most widely used non-specific covalent probe because of its small size and high reactivity.^{67, 86, 88, 98} This species can be generated in a number of ways, e.g., by using electrochemical,⁹⁹ photochemical,^{88, 100} radiolytic,⁸⁶ and corona discharge¹⁰¹ methods, as well as Fenton

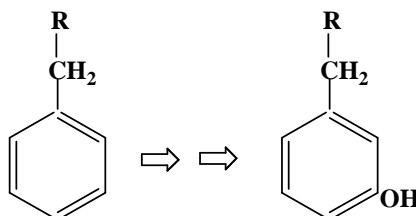
chemistry.¹⁰² $\cdot\text{OH}$ has been shown to generate oxidative modifications for at least 14 out of the 20 amino acid side chains, whereas backbone cleavage is uncommon if the conditions are chosen properly.⁸⁶ Oxidative labeling of proteins with known structures generally results in spatial oxidation patterns that are consistent with the solvent exposure of individual residues.

The overall degree to which any given target site undergoes labeling is determined by a combination of solvent accessibility and intrinsic reactivity.^{86, 103} The sulfur-containing residues Cys and Met are the most reactive, followed by the aromatic side chains Trp, Tyr, and Phe. Also His, Leu, Ile, Arg, Lys, Val, Pro, Gln, and Glu represent potential modification sites.¹⁰⁴ The remaining 4 residues Gly, Ala, Asp and Asn are not useful as probes because of their very low reactivity. Although radical reactions can proceed through complex mechanisms which is not always well understood, the most frequently observed products are amino acids with an oxygen atom incorporated shown as follows:¹⁰⁵

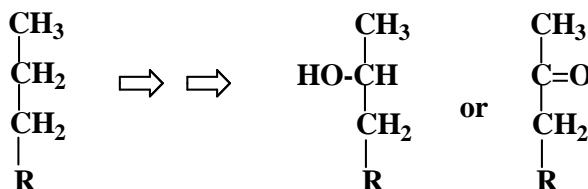
1) Oxidation of sulfur-containing residues: the reactions of $\cdot\text{OH}$ radical with Met and Cys residues take place at the sulfur atom. For Met, the formation of methionene sulfoxide results in +16 Da mass shift.



2) Oxidation of aromatic unsaturated residues: $\cdot\text{OH}$ usually attacks aromatic rings by addition reactions. Subsequently, the resulting radical species react with O_2 yielding +16 Da or higher integer multiple increase in mass.



3) Oxidation of aliphatic residues: carbon-centered radicals that form by hydrogen abstraction often react with O_2 to generate unstable peroxide radical, which eventually convert to hydroxyl or ketone groups, resulting in +16 Da or +14 Da mass shifts.



Overall, despite the highly complex reaction mechanisms, exposure of a protein to $\cdot\text{OH}$ typically culminates in the incorporation of oxygen atoms into amino acid side chains, resulting in easily recognizable +16 Da or multiple shifts in the mass spectrum.⁸⁶ Less abundant products associated with other mass shifts may be formed as well.^{67, 86}

For interpreting the combined effects of conformational and chemical factors on the reactivity of a given side chain i , it has been proposed that the second order rate constant¹⁰³

k_i for the reaction with $\cdot\text{OH}$ can be modeled as

$$k_i = \alpha_i \times k_i^{\text{int}} \quad (1-6)$$

where k_i^{int} represents the "intrinsic" rate constant that applies in case of a completely unprotected side chain. Each of the 20 residues is characterized by a specific k_i^{int} value.⁸⁶

The dimensionless parameters α_i depend on the protein conformation. Complete protection corresponds to $\alpha_i = 0$ (no labeling), whereas for a fully solvent accessible side chain $\alpha_i = 1$.

Oxidative labeling has been used for structural studies on water soluble proteins since that late 1990s.¹⁰⁶ Surprisingly, it was not until quite recently that this approach has been adopted for experiments on membrane proteins. For example, Fenton chemistry was applied for oxidative labeling of membrane protein *in vivo* using a large scale proteomics-type approach.¹⁰⁷ In this way it was possible to monitor structural transitions of the outer membrane protein OmpF in living *Escherichia coli* cells. Oxidation was found at Met and aromatic residues, but also for Asp, Leu, Val, and Ser side chains. Oxidation sites were mapped predominantly to regions of the protein that are known to be solvent accessible on the basis of X-ray structural data. An extension of this approach to *in vivo* studies on mammalian membrane proteins could provide researchers with new avenues for deciphering the mechanisms of membrane-coupled biochemical processes.

Irradiation of water with γ -rays generates $\cdot\text{OH}$ and other radiolytic species that induce protein oxidation.⁸⁵ Such a radiolysis method was applied to study the prepore to pore transition of the *Bacillus anthracis* protective antigen.¹⁰⁸ LC/MS/MS revealed that

oxidation occurred at various types of residues, including Met, Tyr, Trp, and Ile/Val. The differential labeling patterns seen in the two switching states were in partial agreement with a computational model of the pore, for which no X-ray structure is available. The data obtained provide valuable input for future refinements of the proposed pore structure.

Radiolytic oxidative labeling can also be performed by exposure of a protein solution to pulsed X-ray radiation from a synchrotron. This method was applied to monitor photo-induced structural transitions of rhodopsin, which is a member of the G-protein coupled receptor family.¹⁰⁹ Surprisingly, considerable oxidative labeling was observed not only in solvent-exposed regions, but also in transmembrane segments that would be expected to be protected based on existing X-ray data. The authors of that study attributed this behavior to the presence of functionally important ordered water molecules which are known to be present in the protein center.¹⁰⁹

As noted in previously, covalent modifications may induce structural changes that can lead to experimental artifacts.⁸⁷ ·OH labeling is no exception in that oxidative modifications may induce altered protein conformations.¹¹⁰ However, structural changes caused by ·OH labeling are often quite small.^{100, 111} One contributing factor for the lack of drastic structural changes after oxidation is the small size of the attached oxygen atoms, when compared to other labeling and/or crosslinking agents.¹¹² Moreover, oxidative modifications predominantly affect residues on the protein surface, which usually have a considerable degree of conformational freedom. Despite the relatively small magnitude of oxidation-induced conformational changes, the possible occurrence of structural damage is

an aspect that has to be carefully considered when analyzing $\cdot\text{OH}$ labeling experiments.

Hambly and Gross were the first to point out that the extent of possible artifacts due to oxidation-induced conformational changes is related to the time scale of $\cdot\text{OH}$ exposure. Conformational changes in response to covalent modifications can occur within fractions of a millisecond.¹¹³ Labeling times for the techniques discussed so far (radiolysis or Fenton chemistry induced radical labeling) are considerably longer, ranging from tens of milliseconds to several minutes.^{106, 114} Radical attacks during such a relatively extended labeling period may lead to the exposure of previously buried side chains, and $\cdot\text{OH}$ labeling of these newly exposed sites would then result in oxidation events that do not reflect the original protein structure.¹⁰³

Artifacts of this type can be avoided by using a strategy where the protein experiences a single $\cdot\text{OH}$ labeling pulse that is shorter than the fastest possible conformational changes. Such an approach was realized by using a nanosecond-pulsed KrF excimer laser (248 nm) for the photolysis of H_2O_2 . Quasi-single exposure conditions can be implemented by directing a train of laser pulses at an optical window in a protein flow tube.^{88, 100, 115} With the addition of an appropriate radical scavenger, the duration of the resulting $\cdot\text{OH}$ labeling pulses can be reduced down to the microsecond time range. This rapid laser-induced radical labeling may be preferable over other radical labeling approaches, but thus far this technique has been applied only to some soluble proteins.

1.3 Membrane Protein Folding

1.3.1 Protein Folding Mechanism

Most proteins adopt highly ordered structures under physiological conditions. The native conformation represents the biologically active state of a protein. Protein folding *in vivo* often starts when the nascent polypeptide chain emerges from the ribosome.¹¹⁶ The conformational space accessible to a polypeptide chain is astronomically large. How can proteins fold into a specific structure on a biologically relevant timescale? This puzzle, called “Levinthal’s paradox”, has attracted immense scientific interest.¹¹⁷ The area of protein folding is, however, more than just an intellectual challenge. Insight into protein folding mechanisms is critical for understanding a wide range of diseases that are linked to misfolding and aggregates, such as Alzheimer’s, Parkinson’s, mad cow disease and others.¹¹⁸ In the long term, the knowledge of protein folding will help us predict structure from sequence, and finally guide us to design new proteins or biomolecules for desired applications.¹¹⁹

Exposure of a native protein to chemical denaturants or extremes of pH and temperature can induce the transition to a largely disordered state. In 1960s Anfinsen discovered that unfolded soluble proteins can spontaneously refold to their native conformation once the denaturant is removed.¹²⁰ This discovery implies that, at least for globular proteins, the unique three-dimensional structure of a protein must be encoded by its linear amino acid sequence. The native state of a protein corresponds to the conformation with the lowest overall free energy. Spontaneous refolding *in vitro* often goes to completion within milliseconds to seconds.¹ How do proteins find the native states so quickly? Folding

through a random search can not occur, because it would take infinite time. It was thus assumed that there must be defined pathways to simplify the choices in folding. Two models prevailed in the 1980s. One is the “framework model”, which postulates that proteins fold through a stable secondary structure that forms before the tertiary structure is locked in place.¹²¹ In contrast, the “hydrophobic collapse model” suggests that a protein would rapidly collapse around its hydrophobic side chains such that folding can take place in a confined volume.¹²² The secondary structure would be directed by native-like tertiary interactions.

Conventionally, stopped-flow spectroscopy (CD, fluorescence, or UV-Vis) has been the primary tool for exploring folding kinetics.¹²³ However, structural information obtained from spectroscopic probes is typically limited to global structure features. The search for folding mechanism has driven significant advances in experimental techniques for monitoring folding events. For example, FRET (Förster resonance energy transfer) and EPR (electron paramagnetic resonance) were developed to detect site-specific contacts.¹²⁴ Φ -value analysis can characterize transition states during protein folding.¹²⁵ HDX coupled with NMR is able to provide residue-specific structural information on folding intermediates.^{65,126} Mass spectrometry in conjunction with pulsed HDX or covalent labeling was also demonstrated to be an attractive approach to explore folding kinetics and folding intermediates.^{127, 128}

These new experimental techniques uncovered much new information on folding kinetics. Important findings include that chymotrypsin inhibitor II was shown to fold in a

cooperative two-state model without detectable kinetic intermediates.¹²⁹ Φ -value analysis of the transition state showed that secondary and tertiary structure are formed in parallel as chymotrypsin inhibitor II undergoes a general collapse.¹³⁰ These studies challenged both the framework and hydrophobic collapse model. A new view involving “folding funnels” has recently emerged.^{131, 132} In this view, protein folding is seen as biased conformational diffusion on a funnel-like energy landscape. The denatured state of a protein populates a large ensemble of structures. Folding is the inevitable consequence of the requirement to lower the free energy. Folding processes are microscopically heterogeneous and may proceed by numerous pathways instead of a single pathway. In general, folding energy landscapes are rugged that are suboptimal for folding through which the polypeptide chain has to navigate to the native state. Local minima can give rise to the formation of folding intermediates. The overall folding kinetics are determined by the shape of the energy landscape. The energy landscape picture provides a conceptual framework for understanding both two-state and multi-state folding kinetics. Folding funnels can explain many experimental observations that are otherwise paradoxical, and thus this model has now been generally accepted.

1.3.2 Membrane Protein Folding Mechanism

The investigation of membrane protein folding has greatly lagged, compared to the considerable progress with soluble proteins. *In vivo*, α -helical membrane proteins are folded and inserted co-translationally into biological membranes with the assistance of translocons.² In 1980, Khorana et al. demonstrated that functional bacteriorhodopsin (BR) could be regenerated from a fully denatured state.^{133, 134} The regeneration of BR *in vitro*

provides the first evidence that Anfinsen's hypothesis holds true for integral membrane proteins: membrane proteins exist at a free energy minimum. The amino acid sequence contains all information needed to define the tertiary structure of membrane proteins. This pioneering work initiated *in vitro* folding studies of membrane proteins. However, the folding experiments of α -helical membrane proteins were found to be notoriously difficult. After considerable efforts, five additional α -helical membrane proteins (LHCII, DGK, DsbB, KcsA, 5-HT receptor) have so far been denatured and then refolded into model membranes.^{135, 136}

The “**Two-stage model**” was first proposed by Popot and Engelman to explain the folding mechanism of α -helical membrane proteins.³ It divides the folding processes into two stages: (1) insertion and (2) helix association. The first stage comprises spontaneous insertion of a polypeptide chain into a lipid bilayer and simultaneous secondary structure formation. For an integral membrane protein, the hydrophobic effect drives the spontaneous membrane insertion. However, even the most hydrophobic polypeptides can not insert into the lipid bilayer without concomitant secondary structure formation. Huge free-energy increases would incur with the loss of hydrogen bonds between the polypeptide backbone and water molecules. The energetic penalty occurring upon desolvation of the polypeptide backbone forces it to assume regular secondary structure as long as it is embedded in a hydrophobic environment.¹³⁷ In this model, individual transmembrane helices are considered to be independently stable structures. Experimental studies on different membrane proteins show that many helices are independently stable, but some are stabilized by tertiary contacts.¹³⁸ During stage 2, transmembrane helices interact with one

another to give rise to the final native tertiary structure.

Membrane protein folding is intimately linked to the interactions between the protein and the bilayer. A lipid bilayer has two chemically distinct regions. The hydrophobic core in the center is roughly 30 Å thick and dominated by hydrocarbon chains. Each interface region is ca. 15 Å thick, and consists of lipid head groups as well as layers of water molecules. Considering that partitioning an exposed peptide backbone to the hydrophobic core entails very large energetic penalties, and that the thickness of the interfaces is sufficient to accommodate a helix lying parallel to the membrane plane, Jacobs and White expanded the two-stage model into “**Four-stage model**”: partitioning, folding, insertion and association.¹³⁹ Hydrophobic peptide segments are thought to first bind to the interface, then partition into the interface and simultaneous helix formation occurs, finally the individual helices insert the lipid bilayer followed by helix association.¹⁴⁰ Recent simulation studies on a model transmembrane peptide support this model.^{141, 142}

The biogenesis of β -barrel membrane proteins is very different from that of helical proteins. *In vivo*, outer membrane proteins are secreted into the periplasm. Periplasmic chaperones bind these proteins to prevent their aggregation and ferry them to the outer membrane.⁷ Most outer membrane proteins are thought to insert and fold spontaneously into the outer membrane *in vivo*. In 1990, functional porin was refolded *in vitro* from a random coil conformation for the first time.¹⁴³ Since then, 17 β -barrel proteins have been refolded *in vitro*. Because of the modest hydrophobicity of individual β -strands, many β -barrel membrane proteins can be extracted from the membrane in a fully unfolded form when

treated with urea or guanidinium chloride. Unlike individual helices, individual β -strands are not stable in the hydrocarbon core of the bilayer. The simplest way to satisfy all the hydrogen bonding requirements in a sheet is to wrap it up into a barrel. Therefore, the folding of β -barrel proteins can not follow the two-stage model as helical membrane proteins do. In contrast, the insertion and folding should be highly coupled process. Extensive folding studies on OmpA and recent folding studies on PagP by Φ -value analysis support such a concerted insertion-folding mechanism.^{144, 145}

1.3.3 Folding Kinetics of Membrane Proteins

Experimental protein folding studies can be divided into two categories. In equilibrium experiments, the conformation of the protein is studied as a function of denaturant concentration. Measurements are taken only after a thermodynamic equilibrium has been established. In kinetic studies, conformational changes are monitored as a function of time, following rapid alteration of solvent conditions. Equilibrium studies sometimes yield structural information of partially folded species that may resemble short-lived intermediates.¹⁴⁶ Kinetic experiments remain the most direct approach for gaining insights into time-dependent structural changes.¹⁴⁷ To study the folding kinetics of a membrane protein, suitable folding conditions have to be identified, under which the unfolded protein can refold efficiently into model membranes.

Temperature, pH and chemical denaturants have been used to unfold membrane proteins. Both extreme pH (acid or base) and temperature are incapable of reversibly unfolding α -helical membrane proteins for folding studies.¹³⁶ Urea and guanidine hydrochloride

(GdnHCl) are unable to denature most α -helical membrane proteins. For example, neither 8 M urea or 6 M GdnHCl perturbed the tertiary structure of BR.¹⁴⁸ However, many β -barrel proteins such as OmpA, OmpF, OmpG and OmpT, can be unfolded by 8 M urea or 6 M GdnHCl, and then refolded.¹³⁶ An efficient and widely used denaturant for membrane proteins is SDS. SDS exposure can often lead to the denaturation of α -helical membrane proteins. It thus plays an essential role in studying α -helical membrane protein folding. BR, LHCII, DAGK and DsbB have been denatured by SDS and refolded successfully *in vitro*.¹³⁶ Although SDS has shown a strong ability to disrupt the tertiary structure of α -helical membrane proteins, SDS denatured states often retain residual structures. These species seem more like membrane-bound intermediates with pre-formed core structures. SDS is not an excellent denaturant in the view of understanding the folding from an entirely unfolded polypeptide chain to a folded native structure. However, SDS denaturation is so far the most successful approach to provide a reference state for exploring α -helical membrane protein folding. Interesting, SDS does not appear to be very effective in denaturing β -barrel membrane proteins.¹⁴³

Once denatured membrane proteins are available, the second challenge is to identify optimal refolding conditions. In sharp contrast to the folding of soluble proteins that is entirely defined within the sequence, membrane protein folding is defined by both the polypeptide sequence and the model membrane (typically micelles or lipid bilayers). Lipid/detergent composition, organization, and lipid-protein interactions can be important for shaping the folding energy landscape of membrane proteins. According to refolding conditions identified,¹³⁶ there is a bias against anionic detergents for folding. Small

sonicated vesicles and thinner bilayers provide a kinetic advantage for the folding of β -barrel proteins.¹⁴⁵ Besides specific protein-lipid interactions, the most important bilayer properties include curvature elastic energy and hydrophobic match.⁵ In addition, buffering pH, ionic strength and temperature can be important factors. For example, pH 6 is the optimal condition for BR folding. The folding efficiency decreases notably at pH 8.¹⁴⁹ In short, favorable refolding conditions involve in the right combination of lipid/detergent composition, lipid vesicle size, buffer, pH and temperature.

Kinetic folding experiments involve the availability of a trigger as well as techniques for measuring folding events in a time-resolved and spatially-resolved manner. The methods employed for membrane protein folding are similar to those for soluble proteins. Stopped-flow mixing is the predominant method to trigger a membrane protein folding on the time scale of milliseconds to minutes. Classical optical spectroscopy (CD, Fluorescence, and UV-Vis) plays the predominant role in detecting structural changes in these folding experiments.¹⁴⁹⁻¹⁵¹ Recently some new methods have been developed with improved spatial resolutions. Site-specific fluorescence was used to detect the membrane insertion events of individual helices of BR.¹⁵² EPR was applied to monitor the solvent accessibility and the position of particular residues during LHCII folding.²⁵ Φ -value analysis has been used to characterize the transition state during PagP and BR folding.^{144, 153} NMR and MS which have proven to be powerful tools for probing folding kinetics of soluble proteins,¹²⁶⁻¹²⁸ however, remain untapped for studying the folding kinetics of membrane proteins.

There are only few kinetic folding studies on membrane proteins, because it is hard to find

appropriate refolding conditions. So far, the studies of folding kinetics *in vitro* have focused on three α -helical membrane proteins, BR,^{149, 150, 154, 155} LHCII,¹⁵⁶ DGK,¹⁵⁷ and a β -barrel protein OmpA.¹⁴⁴ BR, as the first integral membrane protein to be refolded *in vitro*, has been a paradigm for membrane protein folding. BR functions as a light-driven proton pump in archaebacterium *Halobacterium salinarum*. Each BR monomer consists of bacterioopsin (BO) and a retinal. The BO polypeptide chain folds into seven transmembrane helices (A-G) which are connected by short extra-membrane loops.^{158, 159} The retinal is bound to the protein (helix G) via a protonated Schiff base. BR represents an excellent system for folding studies. It is stable, easy to be expressed and purified, folds reversibly in micelles or lipid bilayers, contains tryptophan residues and a bound retinal chromophore that can serve as optical probes.

The *in vitro* BR refolding is typically conducted by diluting SDS-denatured proteins into bicelles or lipid vesicles in the presence of retinal. The folding kinetics of BR have been extensively investigated using stopped-flow spectroscopy.^{149-151, 154} It was proposed that the folding process involves at least one partially folded apoprotein, followed by the noncovalent binding of retinal to the apoprotein, and finally covalent Schiff base formation that represents the acquisition of native structure. Some studies indicated that the folding kinetics of BR are both sequence-dependent and lipid-dependent.^{149,160,161} These pioneering studies had a major impact on the general understanding of α -helical membrane protein folding. However, structural information on folding intermediates and even the starting point SDS-denatured state is quite limited. A comprehensive characterization of these important conformers is required for deciphering the BR folding mechanism.

1.4 Electrospray Ionization Mass Spectrometry (ESI-MS)

1.4.1 *The ESI Process*

The principle of all mass spectrometric techniques is to analyze the mass-to-charge ratio (m/z) of ions in the gas phase. Ions can be produced in many ways. Electrospray ionization (ESI) is a soft ionization technique. The advent of ESI-MS in the 1980s provided a means to observe spectra of intact proteins,⁴² a discovery honored with the Chemistry Nobel Prize (to John Fenn in 2002). Matrix-assisted laser desorption/ionization (MALDI)¹⁶² is another soft ionization technique for protein studies. Yet, the direct coupling of solution phase chemistry and gas phase detection tends to make ESI-MS a more natural choice for many protein experiments.

The ESI source has undergone continued development, but the general arrangement has remained the same (Figure 1-3). The analyte is introduced to the source in solution either from a syringe pump or as the eluent flow from liquid chromatography. The analyte solution flow passes through the electrospray capillary to which a high potential is applied (typically 2.5 to 5 kV). Under the influence of this potential, the analyte solution exiting from the capillary tip forms a mist of small droplets. A carrier gas such as nitrogen is often used to help nebulize the liquid and help evaporate the solvent. As the droplets traverse the space between the needle tip and the cone, solvent evaporation occurs. Then, each droplet shrinks until it reaches the point at which the surface tension can no longer sustain the charge (the Rayleigh limit), and the droplets break up. This produces smaller droplets that can repeat the same process until the analyte transformed into a full gas phase ion. The analyte can be singly or multiply charged. Not all ions pick up the same number of charges,

therefore a number of peaks (charge state distribution) are commonly observed in the ESI mass spectrum of a protein.¹⁶³

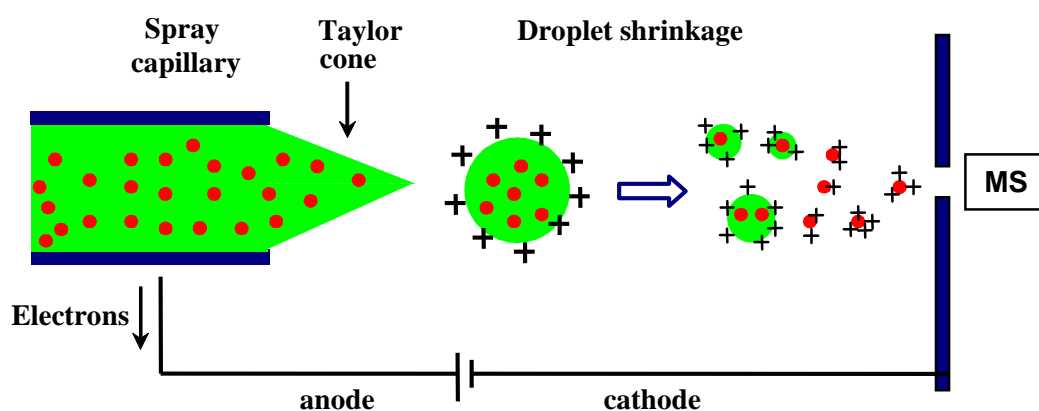


Figure 1-3. Schematic representation of the mechanism of ion formation in ESI.

1.4.2 Mass Analyzers

Mass analysis of the analyte ions is undertaken by mass analyzer. There are various types of mass analyzer, including quadrupole, time-of-flight (TOF), ion trap, and Fourier transform ion cyclotron resonance (FT-ICR) mass analyzers. Many mass spectrometers use two or more mass analyzers for tandem mass spectrometry (MS/MS), such as triple

quadrupoles and quadrupole-TOF (Q-TOF) instruments. The latter type of mass spectrometer was used in this thesis. The principle of quadrupole and TOF analyzers will be briefly discussed.

1.4.2.1 Quadrupole Mass Analyzer

A quadrupole mass analyzer is composed of four parallel rods. Each opposing rod pair is connected together electrically, and a radio frequency (RF) voltage is applied between one pair of rods and the other. A direct current voltage is then superimposed on the RF voltage. Ions produced in the source of the instrument are then focused and travel down the quadrupole between the rods. Their motion will depend on the oscillating electric fields and their mass-to-charge ratio. Only ions with a certain m/z will reach the detector for a given ratio of voltages. Other ions have unstable trajectories and will collide with the rods. This permits selection of ions with a particular m/z or allows the operator to scan for a range of m/z values by continuously varying the applied voltage.

Quadrupole mass spectrometers usually have low resolution (<4000), low mass range (<4000) and slow scan rates. But this mass analyzer excels at applications where particular ions of interest are studied because they can stay tuned on a selected ion for extended periods of time. Quadrupoles are thus generally placed in tandem to enable them to perform fragmentation studies in modern mass spectrometers. The most common type is the triple quadrupole mass spectrometer that has three consecutive quadrupoles arranged in series to incoming ions. The first quadrupole (Q1) acts as a mass filter to select ions of interest. The second quadrupole (Q2) serves as a collision cell where only RF are applied (non-mass

filtering) and selected ions from the Q1 are fragmented. The resulting fragment ions are analyzed by the third quadrupole (Q3). Replacing the Q3 with a TOF mass analyzer results in another popular hybrid Q-TOF mass spectrometer.

1.4.2.2 Time of Flight (TOF) Mass Analyzer

TOF mass analyzers use an electric field to accelerate ions. When an ion with charge z is accelerated into the flight tube by the voltage U , its potential energy is converted to kinetic energy. The resulting velocity (v) of the ion after acceleration is determined by equation 1-7. The velocity of ions flying along the field-free time-of-flight tube will not change. Therefore the time (t) required for the ion to reach the detector is obtained by equation 1-8:

$$v = \sqrt{\frac{2zU}{m}} \quad (1-7)$$

$$t = \frac{L}{v} = L\sqrt{\frac{m}{z} \frac{1}{2U}} \quad (1-8)$$

where m is the mass of the ion and L is the length of the flight tube. Ions with different m/z have different drift times and hence are separated in the flight tube. Lighter ions will reach the detector first. From this time and the known instrument parameters a mass spectrum can be obtained after converting the measured time (t) to m/z .

If ions with same m/z entering the flight tube have energy dispersion, the resolution of TOF will be decreased dramatically. One efficient method to correct the kinetic energy

dispersion in the direction of ion flight is using a reflectron. The reflectron uses a constant electrostatic field to reverse the ion beam toward the detector. The more energetic ions penetrate deeper into the reflectron, and take a slightly longer path to the detector. Less energetic ions of the same charge-to-mass ratio penetrate a shorter distance into the reflectron and, correspondingly, take a shorter path to the detector. Ions with same m/z but slightly different in kinetic energy can reach the detector at the same time after the reflection. Without a reflectron, the TOF resolution is no more than 4000. A reflectron-TOF can achieve much higher resolution ($\sim 20,000$ in some models) and high accuracy (< 5 ppm). The other advantages of TOF mass spectrometers are fast analyzing ions simultaneously and extremely high mass range (over 10,000).

1.5 Scope of this Thesis

Using bacteriorhodopsin (BR) as model system, this work aims at developing novel MS-based approaches for exploring the structure, dynamics and folding of integral membrane proteins.

Compared to other covalent labeling strategies, laser-induced hydroxyl radical ($\cdot\text{OH}$) labeling has obvious advantages: the microsecond $\cdot\text{OH}$ lifetime implies that this technique can be free of oxidation-induced structural artifacts under controlled conditions. Even more important is that the technique is potentially suitable for detecting temporal structural changes of proteins during folding/unfolding processes. However, so far, the method has not been applied to membrane proteins. In the first step, native BR in its natural lipid environment was exposed to laser-induced hydroxyl radicals with the aim to validate the

method. The resulting labeling patterns agree well with the X-ray structure of native BR (Chapter-2). In subsequent studies, the labeling approach was applied to probe the structure of semi-denatured BR samples induced by heat, acid or SDS. Mapping the structure of SDS denatured BR is particularly important because this form of protein is widely used as starting point for folding studies. Combining site-directed mutagenesis with oxidative labeling and spectroscopic studies, a detailed structure model of SDS-denatured BR was developed (Chapter-3). Taking advantage of the very rapid radical bursts induced by laser photolysis, the pulsed radical labeling in conjunction with rapid mixing and MS was used for characterizing short-lived BR folding intermediates. For the first time, the MS-based oxidative labeling approach provided key structural insights into the folding mechanism of a membrane protein (Chapter-4).

Complementary to covalent labeling, hydrogen/deuterium exchange (HDX) with MS is another powerful tool for protein studies. HDX experiments were carried out for characterizing the structural features of various BR samples (Chapter-5). To explore and correlate membrane protein dynamics and function, comparative HDX experiments of BR were carried out in the dark (resting state) and under illumination where the light-induced retinal isomerization mediates the vectorial proton transport (functioning state). Our results suggest that structural fluctuations/dynamics of the protein scaffold are "accelerated" by motions of the retinal, reflecting a direct coupling between protein dynamics and function (Chapter-6).

1.6 References

- (1) Pain, R. H. *Mechanisms of Protein Folding*, 2nd ed.; Oxford University Press: New York, 2000.
- (2) Elofsson, A.; Heijne, G. V. *Annu. Rev. Biochem.* **2007**, *76*, 125-140.
- (3) Popot, J.-L.; Engelman, D. M. *Biochemistry* **1990**, *29*, 4031-4037.
- (4) Popot, J.; Engelman, D. *Annual Review of Biochemistry* **2000**, *69*, 881-922.
- (5) Bowie, J. U. *Nature* **2005**, *438*, 581-589.
- (6) Joh, N. H.; Min, A.; Faham, S.; Whitelegge, J. P.; Yang, D.; Woods, V. L.; Bowie, J. U. *Nature* **2008**, *453*, 1266-1270.
- (7) Tamm, L. K.; Hong, H.; Liang, B. *Biochim. Biophys. Acta* **2004**, *1666*, 250-263.
- (8) Haltia, T.; Freire, E. *Biochim. Biophys. Acta* **1995**, *1241*, 295-322.
- (9) Wu, C. C.; Yates III, J. R. *Nat. Biotechnol.* **2003**, *21*, 262-267.
- (10) George, S. R.; O'Dowd, B. F.; Lee, S. P. *Nat. Rev. Drug Discov.* **2002**, *1*, 808-820.
- (11) White, S. H. *Nature* **2009**, *459*, 344-346.
- (12) Kendrew, J. C.; Bodo, G.; Dintzis, H. M.; Parrish, R. G.; Wyckoff, H. W.; Phillips, D. C. *Nature* **1958**, *181*, 662-666.
- (13) Fersht, A. R. *Nat. Struct. Biol.* **2002**, *9*, 245-246.
- (14) Fischer, M. W. F.; Majumdar, A.; Zuiderweg, E. R. P. *Prog. Nucl. Mag. Res. Spectr.* **1998**, *33*, 207 - 272.
- (15) Brutscher, B.; Brüwchweiler, R.; Ernst, R. R. *Biochemistry* **1997**, *36*, 13043-13053.
- (16) Garczarek, F.; Gerwert, K. *Nature* **2006**, *439*, 109-112.
- (17) Ostermeier, C.; Michel, H. *Curr. Op. Struct. Biol.* **1997**, *7*, 697-701.
- (18) Faham, S.; Boulting, G. L.; Massey, E. A.; Yohannan, S.; Yang, D.; Bowie, J. U. *Protein Sci.* **2005**, *14*, 836-840.
- (19) Dencher, N. A. *Biochemistry* **1986**, *25*, 1195-1200.
- (20) Deisenhofer, J.; Epp, O.; Miki, K. H., R.; Michel, H. *Nature* **1985**, *318*, 618-624.
- (21) Yeagle, P. L.; Albert, A. In *Modern Magnetic Resonance*; Webb, G. A., Ed.; Springer Netherlands: Dordrecht, The Netherlands, 2006, pp 335-343.
- (22) Arora, A.; Abilgaard, F.; Bushweller, J. H.; Tamm, L. K. *Nat. Struct. Biol.* **2001**, *8*, 334-338.
- (23) Park, S. H.; Prytulla, S.; De Angelis, A. A.; Brown, J. M.; Kiefer, H.; Opella, S. J. *J. Am. Chem. Soc.* **2006**, *128*, 7402-7403.
- (24) Mainz, A.; Jehle, S.; van Rossum, B. J.; Oschkinat, H.; Reif, B. *J. Am. Chem. Soc.* **2009**, *131*, 15968-15969.
- (25) Dockter, C.; Volkov, A.; Bauer, C.; Polyhach, Y.; Joly-Lopez, Z.; Jeschke, G.; Paulsen, H. *Proc. Natl. Acad. Sci. U.S.A.* **2009**, *106*, 18485-18490.

- (26) Kyte, J.; Doolittle, R. *J. Mol. Biol.* **1982**, *157*, 105-132.
- (27) Lorenz, H.; Hailey, D. W.; Wunder, C.; Lippincott-Schwartz, J. *Nat. Protocols* **2006**, *1*, 276-279.
- (28) Bogdanov, M.; Zhang, W.; Xie, J.; Dowhan, W. *Methods* **2005**, *36*, 148-171.
- (29) Frillingos, S.; Sahin-Tótha, M.; Wua, J.; Kaback, H. R. *FASEB J.* **1998**, *12*, 1281-1299.
- (30) Abramson, J.; Smirnova, I.; Kasho, V.; Verner, G.; Kaback, H. R.; Iwata, S. *Science* **2003**, *301*, 610-615.
- (31) Manley, D. M.; McComb, M. E.; Perreault, H.; Donald, L. J.; Duckworth, H. W.; O'Neil, J. D. *Biochem.* **2000**, *39*, 12303-12311.
- (32) Henzler-Wildman, K. A.; Lei, M.; Thai, V.; Kerns, S. J.; Karplus, M.; Kern, D. *Nature* **2007**, *450*, 913-918.
- (33) Frauenfelder, H.; Sligar, S. G.; Wolynes, P. G. *Science* **1991**, *254*, 1598-1603.
- (34) Henzler-Wildman, K.; Kern, D. *Nature* **2007**, *450*, 964-972.
- (35) Schotte, F.; Lim, M.; Jackson, T. A.; Smirnov, A. V.; Soman, J.; Olson, J. S.; Phillips, G. N.; Wulff, M.; Anfinsen, P. A. *Science* **2003**, *300*, 1944-1947.
- (36) Mittermaier, A.; Kay, L. E. *Science* **2006**, *312*, 224-228.
- (37) Agarwal, P. A. *Microbial Cell Factories* **2006**, *5*, 1-12.
- (38) Wang, Y.; Schulten, K.; Tajkhorshid, E. *Structure* **2005**, *13*, 1107-1118.
- (39) Fenn, J. B. *Angew. Chem. Int. Ed.* **2003**, *42*, 3871-3894.
- (40) Karas, M.; Hillenkamp, F. *Anal. Chem.* **1988**, *60*, 2299-2301.
- (41) Aebersold, R.; Mann, M. *Nature* **2003**, *422*, 198-207.
- (42) Kaltashov, I. A.; Eyles, S. J. *Mass Spectrometry in Biophysics*; John Wiley and Sons, Inc.: Hoboken, NJ, 2005.
- (43) Trimpin, S.; Deinzer, M. L. *Anal. Chem.* **2007**, *79*, 71-78.
- (44) Trimpin, S.; Brizzard, B. *BioTechniques* **2009**, *46*, 409-419.
- (45) Ball, L. E.; Oatis, J. E.; Dharmasiri, K.; Busman, M.; Wang, J.; Cowden, L. B.; Galijatovic, A.; Chen, N.; Crouch, R. K.; Knapp, D. R. *Protein Sci.* **1998**, *7*, 758-764.
- (46) Whitelegge, J. P.; Gundersen, C. B.; Faull, K. F. *Protein Sci.* **1998**, *7*, 1423-1430.
- (47) Hufnagel, P.; Schweiger, U.; Eckerskorn, C.; Oesterhelt, D. *Anal. Biochem.* **1996**, *243*, 46-54.
- (48) Zabrouskov, V.; Whitelegge, J. P. *J. Proteome Res.* **2007**, *6*, 2205-2210.
- (49) Morgner, N.; Kleinschroth, T.; Barth, H.-D.; Ludwig, B.; Brutschy, B. *J. Am. Soc. Mass Spectrom.* **2007**, *18*, 1429-1438.
- (50) Weinglass, A. B. In *Protein Mass Spectrometry*; Whitelegge, J. P., Ed.; Elsevier: Amsterdam, 2009; Vol. 52, pp 197-212.
- (51) Whitelegge, J. P. In *Protein Mass Spectrometry*; Whitelegge, J. P., Ed.; Elsevier:

- Amsterdam, 2009; Vol. 52, pp 179-196.
- (52) Galetskiy, D.; Susnea, I.; Reiser, V.; Adamska, I.; Przybylski, M. *J. Am. Soc. Mass Spectrom.* **2008**, *19*, 1004-1013.
- (53) Weiner, J. H.; Li, L. *Biochim. Biophys. Acta* **2008**, *1778*, 1698-1713.
- (54) Carroll, J.; Altman, M. C.; Fearnley, I. M.; Walker, J. E. *Proc. Natl. Acad. Sci. U.S.A.* **2007**, *104*, 14330-14335.
- (55) Barrera, N. P.; Di Bartolo, N.; Booth, P. J.; Robinson, C. V. *Science* **2008**, *321*, 243-246.
- (56) Barrera, N. P.; Isaacson, S. C.; Zhou, M.; Bavro, V. N.; Welch, A.; Schaedler, T. A.; Seeger, M. A.; Miguel, R. N.; Korkhov, V. M.; Veen, H. W.; Venter, H.; Walmsley, A. R.; Tate, C. G.; Robinson, C. V. *Nature Methods* **2009**, *6*, 585-587.
- (57) Zhang, H.; Tang, X.; Munske, G. R.; Tolic, N.; Anderson, G. A.; Bruce, J. E. *Mol. Cell. Proteomics* **2009**, *8*, 409-420.
- (58) Fitzgerald, M. C.; West, G. M. *J. Am. Soc. Mass Spectrom.* **2009**, *20*, 1193-1206.
- (59) Busenlehner, L. S.; Codreanu, S. G.; Holm, P. J.; Bhakat, P.; Hebert, H.; Morgenstern, R.; Armstrong, R. N. *Biochemistry* **2004**, *43*, 11145-11152.
- (60) Busenlehner, L. S.; Salomonsson, L.; Brzezinski, P.; Armstrong, R. N. *Proc. Natl. Acad. Sci. U.S.A.* **2006**, *103*, 15398-15403.
- (61) Hebling, C. M.; Morgan, C. R.; Stafford, D. W.; Jorgenson, J. W.; Rand, K. D.; Engen, J. R. *Anal. Chem.* **2010**, *82*, 5415-5419.
- (62) Rey, M.; Mrzek, H.; Pompach, P.; Novk, P.; Pelosi, L.; Brandolin, G.; Forest, E.; Havlek, V.; Man, P. *Anal. Chem.* **2010**, *82*, 5107-5116.
- (63) Zhang, X.; Chien, E. Y. T.; Chalmers, M. J.; Pascal, B. D.; Gatchalian, J.; Stevens, R. C.; Griffin, P. R. *Anal. Chem.* **2010**, *82*, 1100-1108.
- (64) Bai, Y.; Milne, J. S.; Mayne, L.; Englander, S. W. *Proteins: Struct. Funct. Genet.* **1993**, *17*, 75-86.
- (65) Krishna, M. M. G.; Hoang, L.; Lin, Y.; Englander, S. W. *Methods* **2004**, *34*, 51-64.
- (66) Eyles, S. J.; Kaltashov, I. A. *Methods* **2004**, *34*, 88-99.
- (67) Konermann, L.; Tong, X.; Pan, Y. *J. Mass Spectrom.* **2008**, *43*, 1021-1036.
- (68) Hughson, F. M.; Wright, P. E.; Baldwin, R. L. *Science* **1990**, *249*, 1544-1548.
- (69) Engen, J. R. *Anal. Chem.* **2009**, *81*, 7870-7875.
- (70) Englander, S. W. *J. Am. Soc. Mass Spectrom.* **2006**, *17*, 1481-1489.
- (71) Chetty, P. S.; Mayne, L.; Lund-Katz, S.; Stranz, D. D.; Englander, S. W.; Phillips, M. C. *Proc. Natl. Acad. Sci. U.S.A.* **2009**, *106*, 19005-19010.
- (72) Smith, D. L.; Deng, Y.; Zhang, Z. *J. Mass Spectrom.* **1997**, *32*, 135-146.
- (73) Deng, Y.; Pan, H.; Smith, D. L. *J. Am. Chem. Soc.* **1999**, *121*, 1966-1967.
- (74) Jørgensen, T. J. D.; Gårdsvoll, H.; Ploug, M.; Roepstorff, P. *J. Am. Chem. Soc.* **2005**, *127*, 2785-2793.

- (75) Pan, J.; Han, J.; Borchers, C. H.; Konermann, L. *J. Am. Chem. Soc.* **2009**, *131*, 12801–12808.
- (76) Stelzer, W.; Poschner, B. C.; Stalz, H.; Heck, A. J.; Langosch, D. *Biophys. J.* **2008**, *95*, 1326-1335.
- (77) Man, P.; Montagner, C.; Vernier, G.; Dublet, B.; Chenal, A.; Forest, E.; Forge, V. *J. Mol. Biol.* **2007**, *368*, 464-472.
- (78) Rietschel, B.; Bornemann, S.; Arrey, T. N.; Baeumlisberger, D.; Karas, M.; Meyer, B. *Proteomics* **2009**, *9*, 5553-5557.
- (79) Rey, M.; Man, P.; Cléménçon, B.; Trézéguet, V.; Brandolin, G.; Forest, E.; Pelosi, L. *J. Bio. Chem.* **2010**, *285*, 34981-34990.
- (80) Abzalimov, R. R.; Kaltashov, I. A. *Anal. Chem.* **2010**, *82*, 942-950.
- (81) Maity, H.; Maity, M.; Krishna, M. M. G.; Mayne, L.; Englander, S. W. *Proc. Natl. Acad. Sci. U.S.A.* **2005**, *102*, 4741-4746.
- (82) Manea, M.; Mez, G.; Hudecz, F.; Przybylski, M. *Journal of Peptide Science* **2007**, *13*, 227-236.
- (83) Cech, N. B.; Krone, J. R.; Enke, C. G. *Anal. Chem.* **2001**, *73*, 208-213.
- (84) Konermann, L.; Simmons, D. A. *Mass Spectrom. Rev.* **2003**, *22*, 1-26.
- (85) Tong, X.; Wren, J. C.; Konermann, L. *Anal. Chem.* **2007**, *79*, 6376-6382.
- (86) Xu, G.; Chance, M. R. *Chem. Rev.* **2007**, *107*, 3514-3543.
- (87) Mendoza, V. L.; Vachet, R. W. *Anal. Chem.* **2008**, *80*, 2895-2904.
- (88) Hambly, D. M.; Gross, M. L. *J. Am. Soc. Mass Spectrom.* **2005**, *16*, 2057-2063.
- (89) Wang, X.; Kim, S.-H.; Ablonczy, Z.; Crouch, R. K.; Knapp, D. R. *Biochemistry* **2004**, *43*, 11153-11162.
- (90) Mendoza, V. L.; Vachet, R. W. *Mass Spectrom. Rev.* **2009**, *28*, 785-815.
- (91) Novak, P.; Kruppa, G. H.; Young, M. M.; Schoeniger, J. *J. Mass Spectrom.* **2004**, *39*, 322-328.
- (92) Li, C.; Takazaki, S.; Jin, X.; Kang, D.; Abe, H.; Hamasaki, N. *Biochemistry* **2006**, *45*, 12117-12124.
- (93) Leite, J. F.; Cascio, M. *Biochemistry* **2002**, *41*, 6140-6148.
- (94) Leite, J. F.; Blanton, M. P.; Shahgholi, M.; Dougherty, D. A.; Lester, H. A. *Proc. Natl. Acad. Sci. U.S.A.* **2003**, *100*, 13054-13059.
- (95) Wen, J.; Zhang, H.; Gross, M. L.; Blankenship, R. E. *Proc. Natl. Acad. Sci. U.S.A.* **2009**, *106*, 6134-6139.
- (96) Weinglass, A. B.; Whitelegge, J. P.; Hu, Y.; Verner, G. E.; Faull, K. F.; Kaback, H. R. *EMBO J.* **2003**, *22*, 1467-1477.
- (97) Gau, B. C.; Sharp, J. S.; Rempel, D. L.; Gross, M. L. *Anal. Chem.* **2009**, *81*, 6563–6571.
- (98) Sharp, J. S.; Sullivan, D. M.; Cavanagh, J.; Tomer, K. B. *Biochemistry* **2006**, *45*, 6260-6266.

- (99) McClintock, C.; Kertesz, V.; Hettich, R. L. *Anal. Chem.* **2008**, *80*, 3304-3317.
- (100) Aye, T. T.; Low, T. Y.; Sze, S. K. *Anal. Chem.* **2005**, *77*, 5814-5822.
- (101) Maleknia, S. D.; Downard, K. *Mass Spectrom. Rev.* **2001**, *20*, 388-401.
- (102) Lim, J.; Vachet, R. W. *Anal. Chem.* **2003**, *75*, 1164-1172.
- (103) Tong, X.; Wren, J. C.; Konermann, L. *Anal. Chem.* **2008**, *80*, 2222-2231.
- (104) Xu, G.; Chance, M. R. *Anal. Chem.* **2005**, *77*, 4549-4555.
- (105) Takamoto, K.; Chance, M. R. *Annu. Rev. Biophys. Biomol. Struct.* **2006**, *35*, 251-276.
- (106) Maleknia, S. D.; Brenowitz, M.; Chance, M. R. *Anal. Chem.* **1999**, *71*, 3965-3973.
- (107) Zhu, Y.; Guo, T.; Park, J.-H.; Li, X.; Meng, W.; Datta, A.; Bern, M.; Lim, S. K.; Sze, S. K. *Mol. Cell. Proteomics* **2009**, *8*, 1999-2010.
- (108) Smedley, J. G.; Sharp, J. S.; Kuhn, J. F.; Tomer, K. B. *Biochemistry* **2008**, *47*, 10694-10704.
- (109) Angel, T. E.; Gupta, S.; Jastrzebska, B.; Palczewski, K.; Chance, M. R. *Proc. Natl. Acad. Sci. U.S.A.* **2009**, *106*, 14367-14372.
- (110) Sharp, J. S.; Tomer, K. B. *Biophys. J.* **2007**, *92*, 1682-1692.
- (111) Wong, J. W. H.; Maleknia, S. D.; Downard, K. M. *Anal. Chem.* **2003**, *75*, 1557-1563.
- (112) Sinz, A. *J. Mass Spectrom.* **2003**, *38*, 1225-1237.
- (113) Gruebele, M. *Annu. Rev. Phys. Chem.* **1999**, *50*, 485-516.
- (114) Sharp, J. S.; Becker, J. M.; Hettich, R. L. *Anal. Chem.* **2004**, *76*, 672-683.
- (115) Konermann, L.; Stocks, B. B.; Czarny, T. *Anal. Chem.* **2010**, *82*, 6667-6674.
- (116) Ferbitz, L.; Maier, T.; Patzelt, H.; Bukau, B.; Deuerling, E.; Ban, N. *Nature* **2004**, *431*, 590-596.
- (117) Zwanzig, R.; Szabo, A.; Bagchi, B. *Proc. Natl. Acad. Sci. U.S.A.* **1992**, *89*, 20-22.
- (118) Dobson, C. M. *Nature* **2003**, *426*, 884-890.
- (119) Schnepf, R.; Hörth, P.; Bill, E.; Wieghardt, K.; Hildebrandt, P.; Haehnel, W. *J. Am. Chem. Soc.* **2001**, *123*, 2186-2195.
- (120) Anfinsen, C. B. *Science* **1973**, *181*, 223-230.
- (121) Kim, P. S.; Baldwin, R. L. *Ann. Rev. Biochem.* **1982**, *51*, 459-489.
- (122) Daggett, V.; Fersht, A. R. *Trends Biochem. Sci.* **2003**, *28*, 18-25.
- (123) Roder, H.; Maki, K.; Cheng, H. *Chem. Rev.* **2006**, *106*, 1836-1861.
- (124) Shastry, M. C. R.; Roder, H. *Nat. Struct. Biol.* **1998**, *5*, 385-392.
- (125) Fersht, A. R. *Proc. Natl. Acad. Sci. U.S.A.* **2000**, *97*, 1525-1529.
- (126) Roder, H.; Elöve, G. A.; Englander, S. W. *Nature* **1988**, *335*, 700-704.
- (127) Jha, S. K.; Udgaonkar, J. B. *J. Biol. Chem.* **2007**, *282*, 37479-37491.
- (128) Stocks, B. B.; Konermann, L. *J. Mol. Biol.* **2010**, *398*, 362-373.

- (129) Jackson, S. E.; Fersht, A. *Biochem.* **1991**, *30*, 10428-10435.
- (130) Otzen, D. E.; Itzhaki, L. S.; elMasry, N. F.; Jackson, S. E.; Fersht, A. R. *Proc. Natl. Acad. Sci. U.S.A.* **1994**, *91*, 10422-10425.
- (131) Dill, K. A.; Chan, H. S. *Nat. Struct. Biol.* **1997**, *4*, 10-19.
- (132) Fersht, A. R. *Nat. Rev. Mol. Cell Biol.* **2008**, *9*, 650-654.
- (133) Huang, K.; Bayley, H.; Khorana, H. G. *Proc. Natl. Acad. Sci. U.S.A.* **1980**, *77*, 323-327.
- (134) Huang, K.; Bayley, H.; Liao, M.; London, E.; Khorana, H. G. *J. Biol. Chem.* **1981**, *256*, 3802-3809.
- (135) Booth, P. J.; Clarke, J. *Proc. Natl. Acad. Sci. U.S.A.* **2010**, *107*, 3947-3948.
- (136) Stanley, A. M.; Fleming, K. G. *Arch. Biochem. Biophys.* **2008**, *469*, 46-66.
- (137) White, S. H.; Wimley, W. C. *Annu. Rev. Biophys. Biomol. Struct.* **1999**, *28*, 319-365.
- (138) Lazarova, T.; Brewin, K. A.; Stoeber, K.; Robinson, C. R. *Biochemistry* **2004**, *43*, 12945-12954.
- (139) White, S. H.; Ladokhin, A. S.; Jayasinghe, S.; Hristova, K. *J. Biol. Chem.* **2001**, *276*, 32395-32398.
- (140) Killian, J. A.; Heijne, G. V. *Trends Biochem. Sci.* **2000**, *25*, 429-434.
- (141) Milik, M.; Skolnick, J. *Biophys. J.* **1995**, *69*, 1382-1386.
- (142) Ulmschneider, M. B.; Doux, J. P. F.; Killian, J. A.; Smith, J. C.; Ulmschneider, J. P. *J. Am. Chem. Soc.* **2010**, *132*, 3452-3460.
- (143) Eisele, J. L.; Rosenbusch, J. P. *J. Biol. Chem.* **1990**, *265*, 10217-10220.
- (144) Huysmans, G. H. M.; Baldwin, S. A.; Brockwell, D. J.; Radford, S. E. *Proc. Natl. Acad. Sci. U.S.A.* **2010**, *107*, 4099-4104.
- (145) Kleinschmidt, J. H.; Tamm, L. K. *J. Mol. Biol.* **2002**, *324*, 319-330.
- (146) Eliezer, D.; Yao, J.; Dyson, H. J.; Wright, P. E. *Nat. Struct. Biol.* **1998**, *5*, 148-155.
- (147) Gianni, S.; Ivarsson, Y.; Jemth, P.; Brunori, M.; Travaglini-Allocatelli, C. *Biophys. Chem.* **2007**, *128*, 105-113.
- (148) Chen, G. Q.; Gouaux, E. *Biochem.* **1999**, *38*, 15380-15387.
- (149) Riley, M. L.; Wallace, B. A.; Flitsch, S. L.; Booth, P. J. *Biochemistry* **1997**, *36*, 192-196.
- (150) Booth, P. J.; Fitch, S. L.; Stern, L. J.; Greenhalgh, D. A.; Kim, P. S.; Khorana, H. G. *Nat. Struct. Biol.* **1995**, *2*, 139-143.
- (151) Booth, P. J.; Farooq, A. *Eur. J. Biochem* **1997**, *246*, 674-680.
- (152) Compton, E. L. R.; Farmer, N. A.; Lorch, M.; Mason, J. M.; Moreton, K. M.; Booth, P. J. *J. Mol. Biol.* **2006**, *357*, 325-338.
- (153) Curnow, P.; Booth, P. J. *Proc. Natl. Acad. Sci. U.S.A.* **2009**, *106*, 773-778.
- (154) Booth, P. J. *Folding & Design* **1997**, *2*, R85-R92.

- (155) Allen, S. J.; Curran, A. R.; Templer, R. H.; Meijberg, W.; Booth, P. J. *J. Mol. Biol.* **2004**, *342*, 1279-1291.
- (156) Horn, R.; Paulsen, H. *J. Mol. Biol.* **2002**, *318*, 547-556.
- (157) Nagy, J. K.; Lonzer, W. L.; Sanders, C. R. *Biochem.* **2001**, *40*, 8971-8980.
- (158) Subramaniam, S.; Hirai, T.; Henderson, R. *Phil. Trans. R. Soc. Lond. A* **2002**, *360*, 859-874.
- (159) Luecke, H.; Schobert, B.; Richter, H.; Cartailler, J.; Lanyi, J. K. *J. Mol. Biol.* **1999**, *291*, 899-911.
- (160) Kim, J.; Booth, P. J.; Allen, S. J.; Khorana, H. G. *J. Mol. Biol.* **2001**, *308*, 409-422.
- (161) Allen, S. J.; Curran, A. R.; Templer, R. H.; Meijberg, W.; Booth, P. J. *J. Mol. Biol.* **2004**, *342*, 1293-1304.
- (162) Tanaka, K. *Angew. Chem. Int. Ed.* **2003**, *42*, 3861-3870.
- (163) Kebarle, P.; Verkerk, U. H. *Mass Spectrom. Rev.* **2009**, *28*, 898-917.

Chapter-2 Structural Characterization of Bacteriorhodopsin in Its Natural Lipid Environment by Oxidative Methionine Labeling and Mass Spectrometry

2.1 Introduction

Mass spectrometry (MS) has become an indispensable tool for studying protein structure, dynamics, interactions, and function.^{1, 2} Due to its high sensitivity and high-throughput capabilities, MS provides structural biologists with an arsenal of methods that are complementary to traditional techniques such as NMR spectroscopy and X-ray crystallography. Many MS-based approaches employ labeling steps in bulk solution, making use of the fact that target site reactivities are modulated by the protein conformation. Tightly folded regions can provide significant protection, whereas amino acids located in partially unfolded or highly dynamic areas are modified more readily. Spatially-resolved information can be obtained through the analysis of protein fragments after labeling. This can be achieved using traditional "bottom-up" approaches, where proteolytic peptides are analyzed by LC-MS/MS, or by "top-down" strategies that involve the dissociation of intact proteins in the gas phase.^{3, 4} HDX is one of the most popular labeling methods.⁵⁻⁸ In addition, there is a host of covalent modification approaches, many of which target specific reactive side chains such as Lys or Cys.⁹⁻¹¹

Hydroxyl radicals ($\cdot\text{OH}$) represent a probe that is being widely used for the oxidative labeling of proteins.¹²⁻¹⁹ In contrast to many other covalent labeling agents, $\cdot\text{OH}$ normally exhibits a low specificity that allows it to react with a wide range of target sites. A number

of different methods are available for hydroxyl radical production, all of which have their unique advantages and limitations (see refs.^{12, 13, 15}). Despite the highly complex reaction mechanisms, exposure of a protein to $\cdot\text{OH}$ usually culminates in the incorporation of oxygen atoms into amino acid side chains, resulting in easily recognizable +16 Da shifts in the mass spectrum.¹² The overall degree to which any given target site undergoes labeling is determined by a combination of solvent accessibility and intrinsic reactivity.^{12, 20} The presence of sulfur atoms in Met and Cys makes these two residues most reactive, followed by the aromatic side chains of Trp, Tyr, and Phe. Also His, Leu, Ile, Arg, Lys, Val, Pro, Gln, and Glu represent possible modification sites.^{21, 22} $\cdot\text{OH}$ labeling of proteins with known structures generally results in spatial oxidation patterns that are highly consistent with the solvent exposure of individual residues. Met side chains, however, represent a special case because formation of the corresponding sulfoxide (MetO)²³ can take place even for residues that are deeply buried.²⁴⁻²⁷ The basis of this unusual behavior has not been uncovered yet. Proposals have been made that the effect might be due to processes involving solvated electrons²⁸ or intramolecular radical transfer,²⁹ rather than direct contact with $\cdot\text{OH}$. Based on the results of those previous reports,^{24-26, 28, 29} the validity of using Met oxidation levels as a structural probe remains unclear. Interestingly, protein stability measurements based on MetO levels have been shown to be feasible,¹⁷ highlighting that much remains to be learned about the behavior of Met under oxidative labeling conditions.

Every living cell is surrounded by a lipid bilayer that contains integral membrane proteins. The overall character of these proteins is amphipathic, i.e., they possess a large hydrophobic surface area that interacts with the membrane alkyl chains, whereas loops

extending into the aqueous phase on both sides are mostly hydrophilic. Membrane proteins are involved in essential processes such as energy conversion, transport, signal transduction, and cell-cell interactions. Up to 30% of all proteins encoded by the human genome are estimated to be membrane proteins³⁰, and many of them represent potential drug targets.³¹ Unfortunately, the fact that membrane proteins are water insoluble makes them notoriously difficult to work with. Their hydrophobic exterior tends to result in aggregation and precipitation; it also interferes with the growth of crystals that are amenable to X-ray structure determination. Because *in situ* studies are often not feasible, experimentalists commonly resort to surfactant-solubilized species. However, removal of the lipid bilayer often interferes with the structural integrity of the protein, and does not offer long-term protection against aggregation.³² As a result of these difficulties, membrane proteins are vastly underrepresented in databases, representing only 1% of all known protein structures.³⁰

Similar to other analytical techniques, the application of MS to membrane proteins continues to be much less common than studies on their water soluble counterparts.³³ Nonetheless, following pioneering work in the late 1990s,³⁴⁻³⁶ this area is experiencing continuous growth, and even large-scale proteomics projects are gradually becoming practicable.^{37, 38} Experiments on membrane proteins mostly employ LC/ESI-MS, but the application of MALDI-MS has been demonstrated as well.³⁹ Notable progress is also being made in MS-based *structural* studies on membrane proteins, e.g., by using protease protection assays for the determination of topological features.⁴⁰ The successful application of HDX/MS to surfactant-solubilized species has been demonstrated,^{41, 42} and it was even

shown that HDX patterns of short transmembrane peptides can be analyzed by direct infusion of liposome solutions.⁴³ In addition, various covalent labeling techniques have been used, e.g., for structural mapping,⁴⁴ monitoring protein-ligand interactions,^{45, 46} and for detecting conformational changes.⁴⁷

For reasons unknown, ·OH labeling has been largely overlooked as an approach for structural studies on membrane proteins. This is surprising, considering the popularity of this technique for investigations on water-soluble species. One potential issue is the fact that many membrane proteins are methionine rich,^{48, 49} keeping in mind that the reactivity of this amino acid has been found to be problematic in previous oxidative labeling experiments (see above).

Using bacteriorhodopsin (BR) as a model system, this study reports the first application of laser-induced ·OH labeling¹⁹ for the structural characterization of a membrane protein in its natural lipid bilayer environment. BR is the main component of the *Halobacterium salinarum* purple membrane, and it probably represents the best characterized membrane protein.⁵⁰⁻⁵³ The purple color is due to the presence of a retinal chromophore which is bound to Lys216 via a protonated Schiff base. Trans/cis isomerization of this chromophore allows the protein to act as a light-driven proton pump.⁵⁴ The BR polypeptide chain comprises 248 amino acids that fold into seven transmembrane helices which are connected by short extra-membrane loops. The helices are oriented roughly perpendicular to the membrane plane (Figure 2-1).^{55, 56}

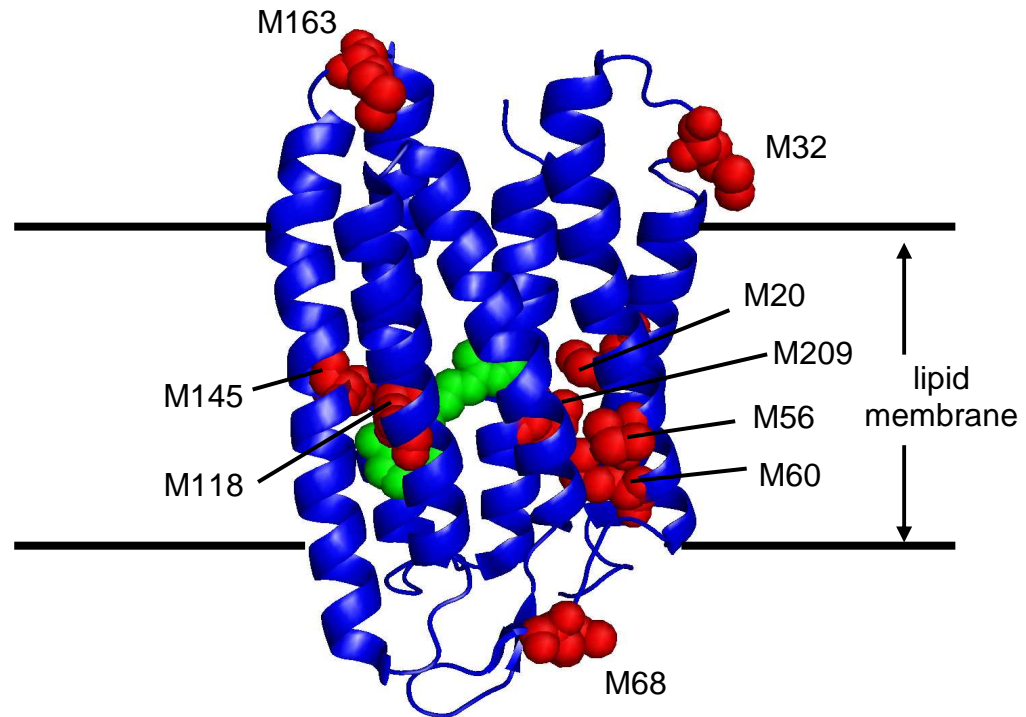


Figure 2-1. X-ray structure of bacteriorhodopsin (pdb code: 1XJI) with its seven transmembrane helices. The nine methionines are shown in red, and the retinal chromophore is depicted in green. Also shown is the approximate location of the lipid bilayer relative to the protein.

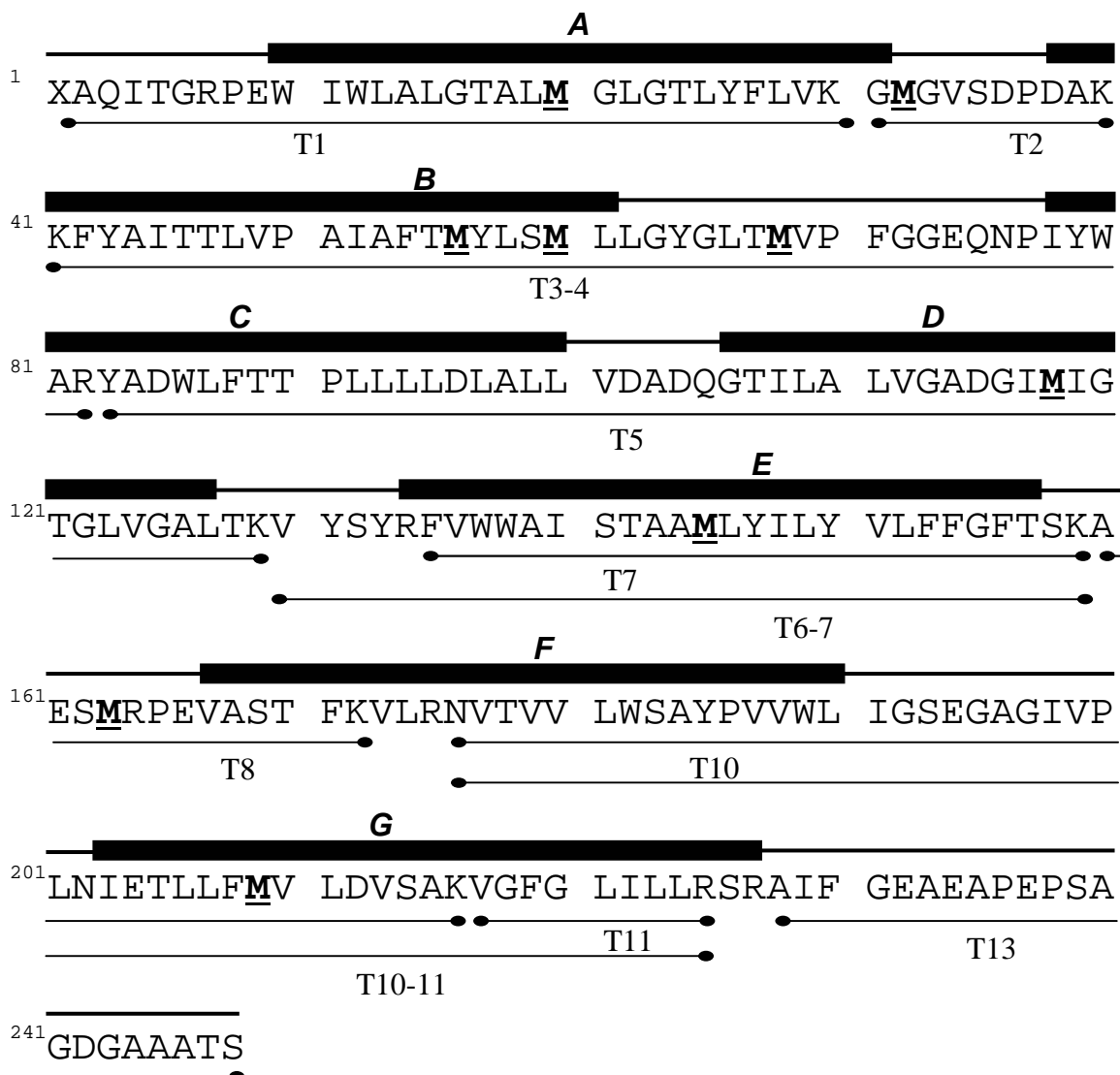


Figure 2-2. Amino acid sequence of BR (pdb code 1XJI). Transmembrane helices (A-G) are represented as black boxes. Tryptic peptides (T1, T2, ...) used in this study are indicated as double-headed lines. T3-4, T6-7 and T10-11 represent peptides resulting from missed cleavages. Methionines are highlighted. The N-terminal "X" represents pyroglutamate.³⁶

BR contains nine methionines, six of which are located in transmembrane helices, and three in connecting loops (Figures 2-1, 2-2). In the purple membrane BR molecules are packed in clusters of three, forming a two-dimensional hexagonal lattice.^{57, 58} The protein accounts for 75% (by weight) of the membrane, the remainder consists of a variety of neutral and acidic diether lipids.^{59, 60} These lipids fill the space between BR trimers, and they also occupy the center of the trimeric rings.

Peptide mapping and tandem MS experiments in this study reveal an unexpected oxidative labeling behavior for BR, with methionine oxidation as the only observable covalent modification. It is demonstrated that the extent of MetO formation is highly correlated with the protein structure, allowing the differentiation between buried and solvent exposed regions. Based on these findings we propose that Met oxidation studies could become a valuable tool for monitoring the structure, folding, and dynamics of membrane proteins.

2.2 Experimental

2.2.1 Materials

Purple membranes were isolated from *Halobacterium salinarum*, strain L33, transformed with a plasmid encoding the protein (bop) and resistance to novobiocin.⁶¹ Cell growth, harvesting, disruption, and purple membrane purification by sucrose gradient centrifugation were performed according to standard procedures.⁶² The final aqueous stock solutions obtained by this method had a protein concentration of ca. 170 μ M, contained 40% sucrose, and were stored at -80 °C prior to analysis. Protein concentrations were

determined by UV-Vis spectroscopy using a Cary 100 spectrophotometer (Varian, Mississauga, ON, Canada) based on a molar absorption coefficient of $\epsilon_{280} = 65,000 \text{ M}^{-1} \text{ cm}^{-1}$ for purple membrane/SDS solutions.⁵⁰ Sequencing-grade modified trypsin was purchased from Promega (Madison, WI). RapiGest SF was obtained from Waters Corporation (Milford, MA). SDS, ammonium bicarbonate, and formic acid were from Sigma (St. Louis, MO). All chemicals were used without further purification.

2.2.2 Laser-Induced Oxidative Labeling

Covalent labeling of the protein was performed following a procedure similar to that previously described by Hambly and Gross.^{19, 63} A KrF excimer laser (GAM EX 100/125, Orlando, FL) producing 18 ns pulses at 248 nm, 16 Hz and 62.5 mJ per pulse was used to generate hydroxyl radicals through photolysis of H_2O_2 within a 100 μm i.d. flow capillary made of fused silica (TSP100170 Polymicro Technologies, Phoenix, AZ). The laser beam was focused onto this capillary by a 500 mm lens, with a capillary-lens distance of 26 cm. A UV transparent window was created by removing the polyimide coating from the capillary using a butane torch. The width of the laser spot at the capillary was determined to be *ca.* 2 mm, corresponding to a volume of about 16 nL being irradiated during each laser pulse. 200 μL of purple membrane suspension (protein concentration 10 μM with 15 μM glutamine, 3% sucrose), and different concentrations of H_2O_2 (up to 0.2%, corresponding to *ca.* 60 mM, at pH 6.8) were loaded into a glass syringe and flushed through the flow capillary at 40 $\mu\text{L min}^{-1}$ using a syringe pump (Harvard Apparatus, Boston, MA). Glutamine and other organic species in the solution (membrane lipids and the protein itself)

act as radical scavengers and limit the duration of the labeling pulse to *ca.* 1 μ s.⁶³ Under these conditions every protein molecule is exposed only to a single labeling pulse. This characteristic, along with the extremely short pulse duration eliminates possible oxidation-induced structural artifacts^{19, 63} which are of potential concern for covalent labeling strategies involving longer exposure times.¹¹ Control experiments (not shown) carried out on purple membranes in the absence of sucrose resulted in data virtually identical to those discussed below. The capillary outflow was collected in a microcentrifuge tube that contained 10 μ L 1 μ M catalase at pH 6.8 for removal of residual H₂O₂, thereby avoiding secondary oxidation reactions.²⁶ Previous work has demonstrated that the mere presence of H₂O₂ in the concentration range used here does not affect the structure and stability of proteins, as long as no oxidation reactions take place.¹⁷

2.2.3 Intact Protein Analysis.

A phase extraction method was used to recover oxidatively labeled BR from the purple membrane suspension.⁶⁴ Following oxidative labeling, 100 μ L of purple membrane suspension was mixed on a vortex for 10 s with 400 μ L chloroform /methanol/water (22:56:22 v/v/v). The mixture was centrifuged at 13000 g for 5 minutes which resulted in a layer of precipitated protein at the interface. After carefully removing the upper aqueous and the lower chloroform phase, the precipitate was dissolved in 100 μ L formic acid.

2.2.4 Peptide Mapping and HPLC/MS analysis

200 μ L aliquots of the oxidatively labeled sample at pH 6.8 were lyophilized. Subsequently,

the dry powder was dissolved in 65 μL of 50 mM aqueous ammonium bicarbonate buffer (pH 8) containing 0.1% (w/v) RapiGest SF. Protein solubilization by this acid-labile surfactant enhances the susceptibility to enzymatic cleavage without inhibiting endopeptidase activity, and without interfering with LC-MS analyses.^{48, 65} The resulting sample solution was boiled at 100 $^{\circ}\text{C}$ for 3 min and then cooled to room temperature, followed by digestion with sequencing-grade trypsin overnight at 37 $^{\circ}\text{C}$ using a 1:20 (w/w) enzyme: protein ratio. The digests were flash-frozen in liquid nitrogen and stored at -80 $^{\circ}\text{C}$.

All experiments were performed on a Q-TOF Ultima API mass spectrometer (Waters, Milford, MA) equipped with a Z-spray electrospray ionization (ESI) source. Spectra were acquired in positive ion mode at a sprayer voltage of 3 kV and a desolvation temperature of 200 $^{\circ}\text{C}$. For intact protein analysis, the formic acid solution was infused directly into the ion source at a flow rate of 10 $\mu\text{L min}^{-1}$. Experimental spectra were converted to mass distributions using the MaxEnt 1 routine provided by the instrument manufacturer. For peptide analysis, the mass spectrometer was coupled to a Waters 1525 μHPLC system employing a C18 2.1 mm \times 100 mm (Symmetry 300) column (Waters). For each injection 25 μL of digested sample were loaded onto the LC column without prior RapiGest removal. Solvent A was 0.1% aqueous formic acid, and solvent B consisted of 50:50 (v/v) acetonitrile/isopropanol with 0.065% formic acid. Elution was carried out at a flow rate of 50 $\mu\text{L min}^{-1}$. A linear gradient was run from 0 to 45% B in 45 min, then from 45% to 58% B in 5 min, from 58% to 80% B in 45 min, finally from 80% to 100% B in 5 min. Most peptides eluted in a range between 15 and 80 min. Confirmation of peptide identities and localization of oxidation sites was performed by tandem MS in data-dependent acquisition

mode, employing collision-induced dissociation in an Ar-filled hexapole cell.

Oxidation levels are reported by plotting the fraction of unmodified peptide, F_u , vs. the hydrogen peroxide percentage. F_u is defined as A_u/A_{tot} , where A_u is the integrated area under the isotope distribution of the unmodified species, and A_{tot} is the total area of the unmodified peptide plus that of the oxidatively modified form(s). This procedure is widely used in the $\cdot\text{OH}$ labeling literature.^{12, 16, 20, 25, 66-68} It has been argued that F_u values measured in this way should only be interpreted in a semi-quantitative way, because unmodified and labeled peptides may exhibit different ionization efficiencies.^{67, 69} However, the first-order kinetics commonly observed during peptide and protein $\cdot\text{OH}$ labeling suggest that these differences are not very pronounced.¹² Also, it will be seen that most tryptic peptides studied here are large, such that slight modifications (MetO formation, in particular) will not affect their ionization efficiencies too much. No evidence for differences in ionization efficiency were found upon carbodiimide labeling of peptides, which represents a much more severe modification than MetO formation.^{45, 70}

2.3 Results and Discussion

2.3.1 Intact Protein Analysis

Aqueous purple membrane suspensions containing native BR were oxidatively labeled, employing the photochemical cleavage of H_2O_2 by a nanosecond laser pulse as $\cdot\text{OH}$ source. ESI-MS analysis of the unlabeled protein reveals a mass of (26783 ± 1) Da, in close agreement with the value expected from the amino acid sequence (26783.6 Da).³⁶ Control experiments carried out in the absence of H_2O_2 and laser exposure reveal a small +16 Da

satellite peak, indicating a low level of background oxidation (Figure 2-3A). This finding is not surprising, given that BR contains nine Met residues which are prone to spontaneous oxidation during protein isolation and/or storage.⁷¹ BR does not contain any cysteines. Other small peaks in the mass distribution of Figure 3A are attributed to trace contaminants such as metal cations. Oxidative labeling of the protein by laser exposure in 0.05% H₂O₂ results in major peaks shifted by +16, +32, and +48 Da (Figure 2-3C). Higher oxidation states are likely present, but obscured by noise in the data. Experiments carried out in the presence of H₂O₂, but without laser irradiation (Figure 2-3B), resulted in a mass distribution very similar to that in Figure 2-3A. This control experiment confirms that covalent labeling in our experiments is indeed caused by photochemically produced radicals, and that the extent of undesired secondary oxidation processes is insignificant.²⁶

2.3.2 Peptide Mapping

Several different methods have been reported for the mapping of BR.^{38, 39, 48, 72} Here, the covalently labeled protein was solubilized using an acid-labile surfactant⁶⁵ prior to digestion and LC/ESI-MS analysis, as described in the Experimental section. The data analysis in this work was based on the 11 most intense tryptic peptides, yielding a protein sequence coverage of 97% (Figure 2-2). The spectral quality for these fragments (Figure 2-4) is considerably higher than for the intact protein (Figure 2-3). Oxidative labeling of intact purple membrane suspensions was carried out on solutions containing 0% (control), 0.02%, 0.1%. The resulting tryptic peptides reveal drastically different oxidation characteristics. For example, T8 represents the protein segment that is most readily labeled. In 0.02% H₂O₂ both the unmodified form and a +16 Da species are observed at comparable

signal intensities (Figure 2-4B). After labeling in 0.1% H₂O₂ (Figure 2-4C) the signal of the unmodified peptide is close to 0.2. A totally different behavior is seen for T7, where the unmodified form remains dominant under all conditions (Figure 2-4E-G).

The labeling data can be visualized by plotting the fraction of unmodified peptide, F_u , vs. the hydrogen peroxide percentage (Figure 2-5). The ten peptides can be grouped into three categories based on their oxidation behavior. (i) No labeling is detectable for T11 and T13, corresponding to $F_u \approx 1$. (ii) T1, T5, T6-7, T7, and T10 exhibit moderate labeling, with F_u values that remain in the range of 0.8 even for the highest peroxide concentration used. (iii) T2, T8, and T3-4 represent protein regions that are most susceptible to oxidation with F_u values as low as 0.2.

2.3.3 Tandem Mass Spectrometry

MS/MS experiments confirm that all observed covalent modifications are due to sulfoxide (MetO) formation. Labeling at non-methionyl residues was not detectable, although very small amounts of other products cannot be ruled out. As an example, Figure 2-6 compares MS/MS data of unlabeled and singly oxidized T8. Fragmentation yields unmodified y⁹ ions in both cases. In contrast, the signals for y¹⁰ (and y¹¹) are shifted by 16 Da, thus confirming that the oxygen atom is located on Met163 (Figure 2-6). Analogous data (not shown) were obtained for the other single-Met peptides. Of particular interest is T3-4 with its three Met residues. Fragmentation of the singly labeled peptide (Figure 2-7) reveals that oxidation is restricted to Met68, as seen from the +16 Da shifts for y¹⁵ - y¹⁷ (Figure 2-7B-D, F-H), along with unmodified y¹⁴ fragments in both cases (Figure 2-7A, E).

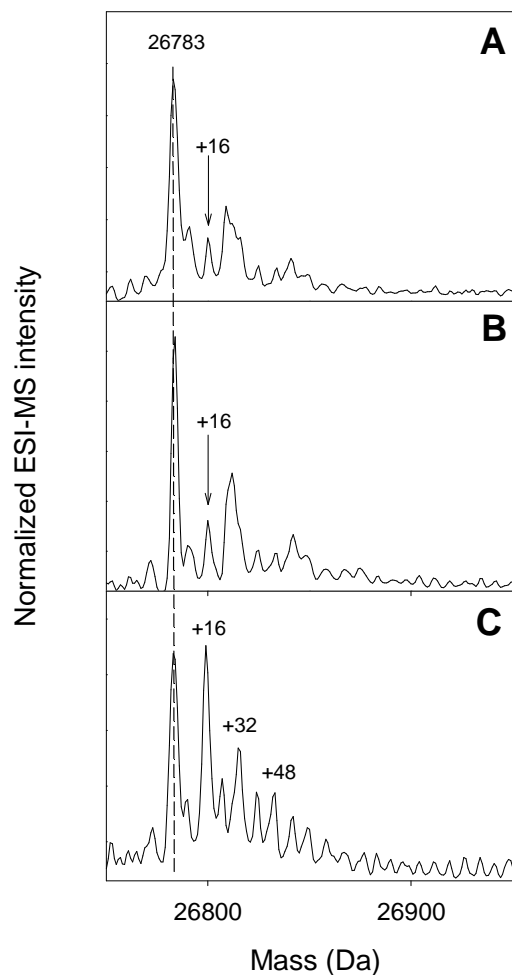


Figure 2-3. Deconvoluted ESI mass distributions of intact BR under different oxidative labeling conditions. (A) no laser irradiation, no H_2O_2 (control); (B) no laser irradiation, 0.1% H_2O_2 (control); (C) after laser irradiation, 0.05% H_2O_2 . Note that the retinal chromophore is lost during sample preparation, but was present during labeling. Peaks designated as +16, +32, and +48 represent the incorporation of one, two, and three oxygen atoms, respectively

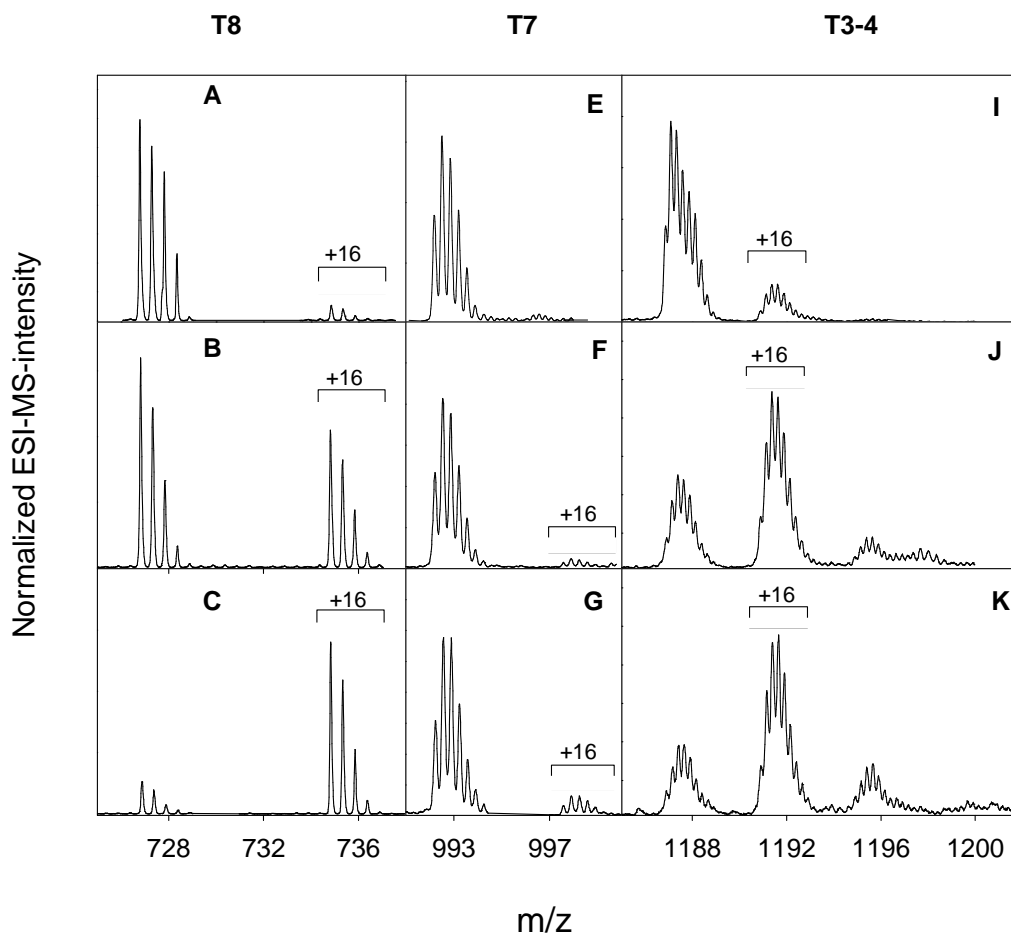


Figure 2-4. ESI mass spectra of selected tryptic peptides obtained under different oxidative labeling conditions: T8 (A-C, doubly charged), T7 (E-G, triply charged), and T3-4 (I-K, quadruply charged). First row of panels (A, E, I), unlabeled controls; second row (B, F, J), 0.02% H₂O₂; third row (C, G, K), 0.1% H₂O₂.

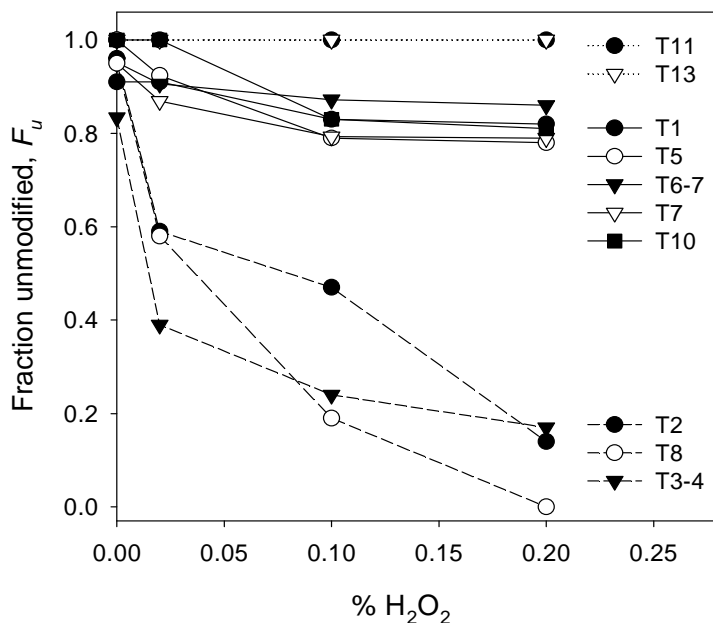


Figure 2-5. Oxidation levels of various tryptic peptides, expressed as fraction unmodified (F_u) and plotted as a function of H_2O_2 percentage.

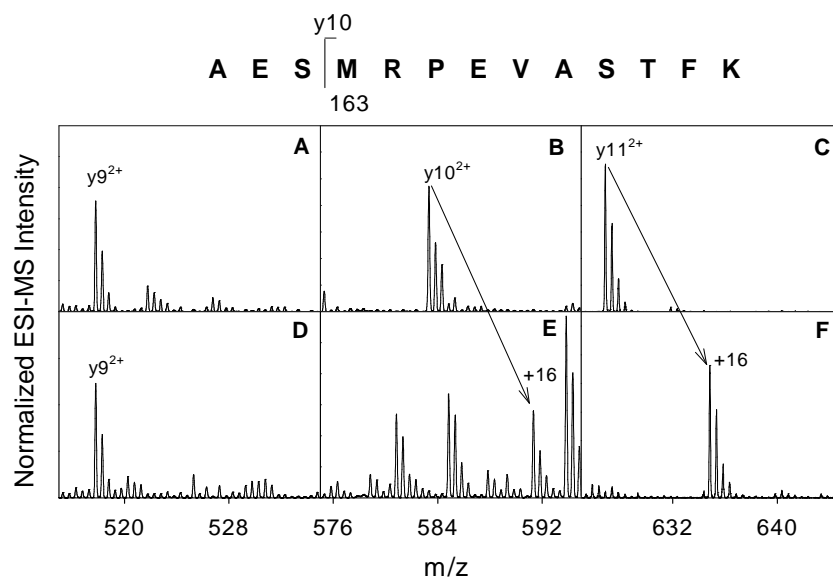


Figure 2-6. Partial MS/MS product ion spectra obtained after fragmentation of $[T8 + 2H]^{2+}$ (unlabeled peptide, panels A-C), and of the singly oxidized species $[T8^{OX} + 2H]^{2+}$ (panels D-F). Shown at the top of the Figure is the sequence of T8.

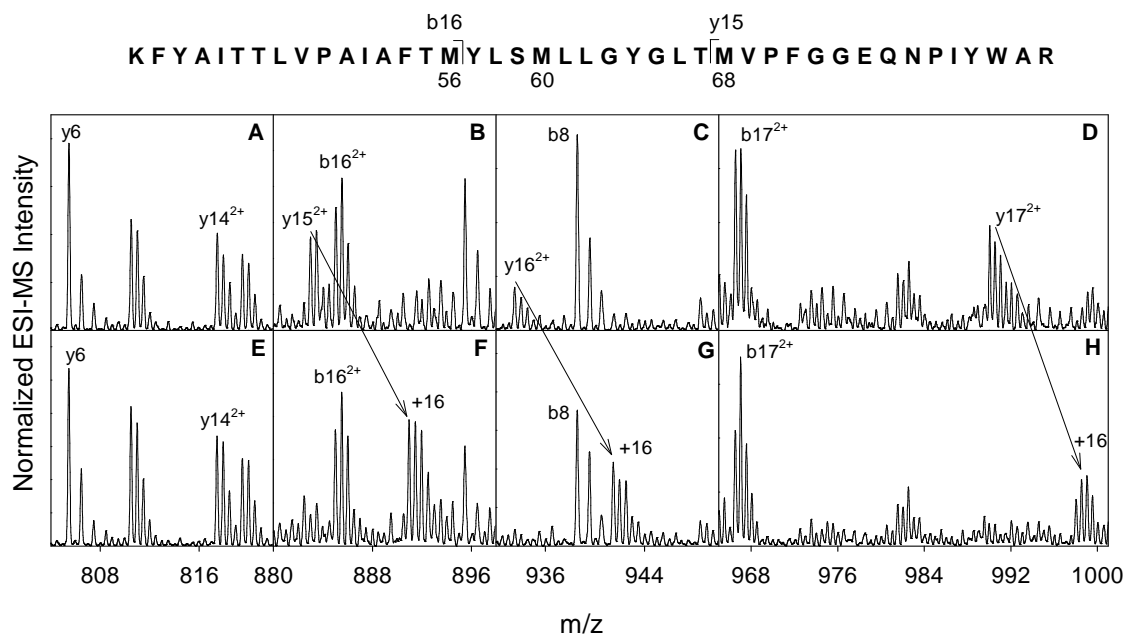


Figure 2-7. Partial MS/MS product ion spectra obtained after fragmentation of $[T3-4 + 4H]^{4+}$ (unlabeled peptide, panels A-D), and of the singly oxidized species $[T3-4^{OX} + 4H]^{4+}$ (panels E-H). For further explanations, see the caption of Figure 2-6.

No modifications were found for the other two methionines (see e.g. the b16 signals in Figure 2-7, B and F), confirming that Met56 and Met60 remain unlabeled. The observation of exclusive Met oxidation reveals a remarkable chemical selectivity. This finding contrasts earlier studies on various water-soluble proteins by laser-induced oxidation^{19, 27, 63} (and other ·OH labeling strategies), which always found a host of additional oxidation sites, besides methionine.

2.3.4 Structural Interpretation

The peptide data of Figure 2-5, along with the MS/MS analyses discussed in the preceding section reveal that the Met residues 20, 56, 60, 118, 145, and 209 are labeled to a much lesser extent than Met32, Met68, and Met163. This dramatic difference is most pronounced in 0.2% H_2O_2 where the two groups exhibit F_u values around 0.8 and below 0.2, respectively. Comparison with the crystal structure of BR (Figure 2-1) reveals that the former group of methionines is part of the tightly packed protein core that is embedded in the lipid membrane. In contrast, the easily oxidized residues Met32, Met68, and Met163 are located in surface loops that are exposed to the aqueous environment. Thus, spatially resolved MS measurements of Met oxidation provide structural information that is fully consistent with the known BR structure.^{55, 73}

2.4 Conclusions

Many previous oxidative labeling studies have taken advantage of the fact that hydroxyl radicals can react with a wide variety of amino acid side chains, leading to modifications at multiple different sites. The extent of oxidative labeling is generally found to be well correlated with the solvent exposure of the corresponding residues. However, inclusion of Met oxidation levels in these data sets has been problematic due to extensive MetO formation even at deeply buried methionyl side chains.²⁴⁻²⁹ As a result, Met oxidation could not thus far be used as a reliable probe of protein structure. We note, however, that the unusual reactivity of methionyl side chains only leads to difficulties with data interpretation when considering Met oxidation within the context of labeling levels seen for other residues. The results of this work demonstrate that unambiguous structural information can

be obtained by comparing the oxidation levels of various methionines among each other. In this way it is possible to differentiate residues located in solvent exposed loops from those that are shielded within the protein core.

The oxidative labeling data presented in this study are unusual in that MetO formation is the *only* detectable type of covalent modification occurring in the entire protein. This behavior is quite different from that observed for water-soluble proteins in previous studies, where oxidative labeling of at least 14 out of the 20 naturally occurring amino acids is normally observed.¹² Without doubt, one contributing factor for the remarkable chemical selectivity seen here is the presence of nine methionines in BR, which is a much higher number than for previously studied proteins. Competition of these extremely rapidly reacting sites (having rate constants close to the diffusion limit)⁷⁴ with less reactive side chains will automatically result in significant protection against oxidation for other residues. An additional factor could be the presence of bilayer lipids. Just like virtually all other bio-organic compounds, these species are expected to act as radical scavengers.^{68, 74} Extensive radical absorption by scavengers will tend to protect the protein from covalent labeling, except for Met residues which represent the most reactive "oxidation hot spots".

It might be argued that the specific oxidation of Met is not as structurally informative as the largely non-selective labeling observed in previous $\cdot\text{OH}$ footprinting studies on water-soluble proteins. However, non-selective labeling tends to result in overwhelmingly complex spectra, unpredictable MS/MS fragmentation patterns, and considerable difficulties in quantifying oxidation data in a spatially-resolved manner. Selective labeling

of only one type of residue, on the other hand, greatly facilitates the data analysis and interpretation. This has been demonstrated in the current work, where six Met residues in the protein core could be readily distinguished from three that are located in solvent exposed loops. The fact that many membrane proteins are methionine rich^{48, 49} makes the application of Met labeling all the more useful for this type of system. Membrane protein function, folding, and dynamics continue to be most challenging research topics,⁵¹ and the application of Met oxidative labeling could become a valuable experimental tool in these areas. Protein engineering methods⁷⁵ can be used for inserting further methionines in various positions of interest. Based on the medium size and mildly hydrophobic character of Met (Kyte-Doolittle score 1.9)⁷⁶ many of these substitutions would be expected to leave the structure and dynamics of membrane proteins unaltered, thereby providing valuable additional probes for ·OH labeling.

Overall, the proof-of-principle experiments in this work demonstrate that oxidative labeling with MS detection allows structural information to be gained for membrane proteins in their natural lipid bilayer environment. The use of artificial surfactant micelle systems that can interfere with the native protein structure is not required for this approach. The technique will be most valuable for the many membrane proteins that so far have not been amenable to X-ray crystallography or electron diffraction.

2.5 References

- (1) Kaltashov, I. A.; Eyles, S. J. *Mass Spectrometry in Biophysics*; John Wiley and Sons, Inc.: Hoboken, NJ, 2005.
- (2) Heck, A. J. R.; Van den Heuvel, R. H. H. *Mass Spectrom. Rev.* **2004**, *23*, 368-389.
- (3) Zubarev, R. A.; Zubarev, A. R.; Savitski, M. M. *J. Am. Soc. Mass Spectrom.* **2008**, *19*, 753-761.
- (4) Pan, J.; Han, J.; Borchers, C. H.; Konermann, L. *J. Am. Chem. Soc.* **2008**, *130*, 11574-11575.
- (5) Englander, S. W. *J. Am. Soc. Mass Spectrom.* **2006**, *17*, 1481-1489.
- (6) Smith, D. L.; Deng, Y.; Zhang, Z. *J. Mass Spectrom.* **1997**, *32*, 135-146.
- (7) Wales, T. E.; Engen, J. R. *Mass Spectrom. Rev.* **2006**, *25*, 158-170.
- (8) Chalmers, M. J.; Busby, S. A.; Pascal, B. D.; He, Y.; Hendrickson, C. L.; Marshall, A. G.; Griffin, P. R. *Anal. Chem.* **2006**, *78*, 1005-1014.
- (9) Jha, S. K.; Udgaonkar, J. B. *J. Biol. Chem.* **2007**, *282*, 37479-37491.
- (10) Chen, H.; Schuster, M. C.; Sfyroera, G.; Geisbrecht, B. V.; Lambris, J. D. *J. Am. Soc. Mass Spectrom.* **2008**, *19*, 55-65.
- (11) Mendoza, V. L.; Vachet, R. W. *Anal. Chem.* **2008**, *80*, 2895-2904.
- (12) Xu, G.; Chance, M. R. *Chem. Rev.* **2007**, *107*, 3514-3543.
- (13) Konermann, L.; Tong, X.; Pan, Y. *J. Mass Spectrom.* **2008**, *43*, 1021-1036.
- (14) Maleknia, S. D.; Wong, J. W. H.; Downard, K. M. *Photochem. Photobiol. Sci.* **2004**, *3*, 741-748.
- (15) McClintock, C.; Kertesz, V.; Hettich, R. L. *Anal. Chem.* **2008**, *80*, 3304-3317.
- (16) Sharp, J. S.; Sullivan, D. M.; Cavanagh, J.; Tomer, K. B. *Biochemistry* **2006**, *45*, 6260-6266.
- (17) West, G. M.; Tang, L.; Fitzgerald, M. C. *Anal. Chem.* **2008**, *80*, 4175-4185.
- (18) Bridgewater, J. D.; Lim, J.; Vachet, R. W. *Anal. Chem.* **2006**, *78*, 2432-2438.
- (19) Hambly, D. M.; Gross, M. L. *J. Am. Soc. Mass Spectrom.* **2005**, *16*, 2057-2063.
- (20) Tong, X.; Wren, J. C.; Konermann, L. *Anal. Chem.* **2008**, *80*, 2222-2231.
- (21) Takamoto, K.; Chance, M. R. *Annu. Rev. Biophys. Biomol. Struct.* **2006**, *35*, 251-276.
- (22) Xu, G.; Chance, M. R. *Anal. Chem.* **2005**, *77*, 4549-4555.
- (23) Xu, G.; Chance, M. R. *Anal. Chem.* **2005**, *77*, 2437-2449.
- (24) Sharp, J. S.; Becker, J. M.; Hettich, R. L. *Anal. Biochem.* **2003**, *313*, 216-225.
- (25) Sharp, J. S.; Becker, J. M.; Hettich, R. L. *Anal. Chem.* **2004**, *76*, 672-683.
- (26) Xu, G.; Kiselar, J.; He, Q.; Chance, M. R. *Anal. Chem.* **2005**, *77*, 3029-3037.
- (27) Aye, T. T.; Low, T. Y.; Sze, S. K. *Anal. Chem.* **2005**, *77*, 5814-5822.

- (28) Maleknia, S. D.; Kiselar, J. G.; Downard, K. M. *Rapid Commun. Mass Spectrom.* **2002**, *16*, 53-61.
- (29) Kiselar, J. G.; Maleknia, S. D.; Sullivan, M.; Downard, K. M.; Chance, M. R. *Int. J. Radiat. Biol.* **2002**, *78*, 101-114.
- (30) Wu, C. C.; Yates III, J. R. *Nat. Biotechnol.* **2003**, *21*, 262-267.
- (31) George, S. R.; O'Dowd, B. F.; Lee, S. P. *Nat. Rev. Drug Discov.* **2002**, *1*, 808-820.
- (32) Ostermeier, C.; Michel, H. *Curr. Op. Struct. Biol.* **1997**, *7*, 697-701.
- (33) Barrera, N. P.; Di Bartolo, N.; Booth, P. J.; Robinson, C. V. *Science* **2008**, *321*, 243-246.
- (34) Ball, L. E.; Oatis, J. E.; Dharmasiri, K.; Busman, M.; Wang, J.; Cowden, L. B.; Galijatiovic, A.; Chen, N.; Crouch, R. K.; Knapp, D. R. *Protein Sci.* **1998**, *7*, 758-764.
- (35) Whitelegge, J. P.; Gundersen, C. B.; Faull, K. F. *Protein Sci.* **1998**, *7*, 1423-1430.
- (36) Hufnagel, P.; Schweiger, U.; Eckerskorn, C.; Oesterhelt, D. *Anal. Biochem.* **1996**, *243*, 46-54.
- (37) Weiner, J. H.; Li, L. *Biochim. Biophys. Acta* **2008**, *1778*, 1698-1713.
- (38) Blonder, J.; Conrads, T. P.; Yu, L.; Terunuma, A.; Janini, G. M.; Issaq, H. J.; Vogel, J. C.; Veenstra, T. D. *Proteomics* **2004**, *4*, 31-45.
- (39) Trimpin, S.; Deinzer, M. L. *Anal. Chem.* **2007**, *79*, 71-78.
- (40) Wu, C. C.; MacCoss, M. J.; Howell, K. E.; Yates III, J. R. *Nat. Biotechnol.* **2003**, *21*, 532-538.
- (41) Joh, N. H.; Min, A.; Faham, S.; Whitelegge, J. P.; Yang, D.; Woods, V. L.; Bowie, J. U. *Nature* **2008**, *453*, 1266-1270.
- (42) Busenlehner, L. S.; Salomonsson, L.; Brzezinski, P.; Armstrong, R. N. *Proc. Natl. Acad. Sci. U.S.A.* **2006**, *103*, 15398-15403.
- (43) Demmers, J. A. A.; Haverkamp, J.; Heck, A. J. R.; Koeppe, R. E.; Killian, A. *Proc. Natl. Acad. Sci. U.S.A.* **2000**, *97*, 3189-3194.
- (44) Leite, J. F.; Cascio, M. *Biochemistry* **2002**, *41*, 6140-6148.
- (45) Weinglass, A. B.; Whitelegge, J. P.; Hu, Y.; Verner, G. E.; Faull, K. F.; Kaback, H. R. *EMBO J.* **2003**, *22*, 1467-1477.
- (46) Wang, X.; Kim, S.-H.; Ablonczy, Z.; Crouch, R. K.; Knapp, D. R. *Biochemistry* **2004**, *43*, 11153-11162.
- (47) Leite, J. F.; Blanton, M. P.; Shahgholi, M.; Dougherty, D. A.; Lester, H. A. *Proc. Natl. Acad. Sci. U.S.A.* **2003**, *100*, 13054-13059.
- (48) Yu, Y.; Gilar, M.; Gebler, J. C. *Rapid Commun. Mass Spectrom.* **2004**, *18*, 711-715.
- (49) Ablonczy, Z.; Kono, M.; Crouch, R. K.; Knapp, D. R. *Anal. Chem.* **2001**, *73*, 4774-4779.
- (50) Huang, K.; Bayley, H.; Liao, M.; London, E.; Khorana, H. G. *J. Biol. Chem.* **1981**, *256*, 3802-3809.

- (51) Curnow, P.; Booth, P. J. *Proc. Natl. Acad. Sci. U.S.A.* **2007**, *104*, 18970-18975.
- (52) Oesterhelt, D.; Brauchle, C.; Hampp, N. *Q. Rev. Biophys.* **1991**, *24*, 425-478.
- (53) Birge, R. R.; Gillespie, N. B.; Izaguirre, E. W.; Kusnetzow, A.; Lawrence, A. F.; Singh, D.; Song, W.; Schmidt, E.; Stuart, J. A.; Seetharaman, S.; Wise, K. J. *J. Phys. Chem. B* **1999**, *103*, 10746-10766.
- (54) Subramaniam, S.; Henderson, R. *Nature* **2000**, *406*, 653-657.
- (55) Faham, S.; Boulting, G. L.; Massey, E. A.; Yohannan, S.; Yang, D.; Bowie, J. U. *Protein Sci.* **2005**, *14*, 836-840.
- (56) Henderson, R.; Unwin, P. N. *Nature* **1975**, *257*, 28-32.
- (57) Wan, C.; Qian, J.; Johnson, C. K. *Biophys. J.* **1993**, *65*, 927-938.
- (58) Blaurock, A. E.; Stoeckenius, W. *Nat. New Biol.* **1971**, *233*, 152-155.
- (59) Szundi, I.; Stoeckenius, W. *Proc. Natl. Acad. Sci. U.S.A.* **1987**, *84*, 3681-3684.
- (60) Taneva, S. G.; Koynova, R.; Tenchov, B. *FEBS Lett.* **1994**, *345*, 154-158.
- (61) Ni, B.; Chang, M.; Duschl, A.; Lanyi, J.; Needleman, R. *Gene* **1990**, *90*, 169-172.
- (62) Oesterhelt, D.; Stoeckenius, W. *Methods Enzymol.* **1974**, *31*, 667-678.
- (63) Hambly, D. M.; Gross, M. L. *Int. J. Mass Spectrom.* **2007**, *259*, 124-129.
- (64) Wessel, D.; Flugge, U. I. *Anal. Biochem.* **1984**, *138*, 141-143.
- (65) Yu, Y.; Gilar, M.; Lee, P. J.; Bouvier, S. P.; Gebler, J. C. *Anal. Chem.* **2003**, *75*, 6023-6028.
- (66) Wong, J. W. H.; Maleknia, S. D.; Downard, K. M. *Anal. Chem.* **2003**, *75*, 1557-1563.
- (67) Xu, G.; Takamoto, K.; Chance, M. R. *Anal. Chem.* **2003**, *75*, 6995-7007.
- (68) Tong, X.; Wren, J. C.; Konermann, L. *Anal. Chem.* **2007**, *79*, 6376-6382.
- (69) Cech, N. B.; Enke, C. G. *Mass Spectrom. Rev.* **2001**, *20*, 362-387.
- (70) Weinglass, A. B.; Soskine, M.; Vazquez, J.; Whitelegge, J. P.; Faull, K. F.; Kaback, H. R.; Schuldiner, S. *J. Biol. Chem.* **2005**, *280*, 7487-7492.
- (71) Vogt, W. *Free Radical Biol. Med.* **1995**, *18*, 93 - 105.
- (72) Hixson, K. K.; Todriguez, N.; Camp II, D. G.; Strittmatter, E. F.; Lipton, M. S.; Smith, R. D. *Electrophoresis* **2002**, *23*, 3224-3232.
- (73) Seigneuret, M.; Kainosho, M. *FEBS* **1993**, *327*, 7-12.
- (74) Buxton, G. V.; Greenstock, C. L.; Helman, W. P.; Ross, A. B. *J. Phys. Chem. Ref. Data* **1988**, *17*, 513-886.
- (75) Vazquez-Ibar, J.; Guan, L.; Weinglass, A. B.; Verner, G.; Gordillo, R.; Kaback, H. R. *J. Biol. Chem.* **2004**, *279*, 49214-49221.
- (76) Kyte, J.; Doolittle, R. *J. Mol. Biol.* **1982**, *157*, 105-132.

Chapter-3 Mapping the Structure of Bacteriorhodopsin under Semi-Denaturing Conditions by Laser-Induced Oxidative Labeling and Mass Spectrometry

3.1 Introduction

Experimental studies on the structure and folding of membrane proteins represent considerable challenges. X-ray crystallography, NMR spectroscopy and other techniques have provided a wealth of information on water-soluble species, whereas the general understanding of membrane proteins continues to lag behind. This situation represents a critical bottleneck because of the central role that membrane proteins play in cellular transport, energy conversion, signaling, and as drug targets.¹ Fortunately, the past few years have witnessed encouraging progress in the biophysical characterization of membrane proteins.²⁻⁷ For example, novel insights into the molecular interactions that stabilize membrane protein structures have recently emerged.^{8,9}

Most structural studies on both water-soluble and membrane proteins focus on the native conformation. Yet, partially disordered conformers can play biologically important roles as well, for example as folding intermediates,¹⁰⁻¹² during amyloidogenesis,¹³ for ligand-binding,^{14,15} and for membrane translocation.¹⁶ The native state of every protein is in equilibrium with various semi-unfolded species.¹⁷ In a physiological environment the concentrations of these excited states are usually very low (as dictated by the Boltzmann distribution). However, their formation can be promoted in a mildly denaturing solvent environment.^{10,17} Non-native proteins usually do not crystallize, but NMR spin relaxation

measurements¹⁸ and hydrogen/deuterium exchange (HDX) approaches¹⁹ have been successfully applied in a number of cases. Once again, however, the overwhelming majority of these studies have been conducted on water-soluble proteins.

Electrospray ionization mass spectrometry (ESI-MS) is becoming an increasingly important tool for the characterization of membrane proteins, e.g., for determining molecular weights,²⁰ for probing covalent modifications,²¹ and for large-scale proteomics projects.²² Intact multiprotein/surfactant complexes have been successfully analyzed by ESI-MS, a development that might pave the way towards measurements on the subunit composition of membrane protein assemblies.²³ Membrane protein conformations and dynamics have been explored in HDX experiments with ESI-MS detection.^{8, 24, 25} Another particularly promising approach is the use of ESI-MS-based covalent labeling techniques for structural studies. Numerous labeling reagents with different specificities are available that induce covalent modifications on amino acid side chains.²⁶ The utility of these compounds is based on the principle that solvent-exposed sites exhibit a higher reactivity than those in inaccessible locations. The exact positions of covalently labeled sites can be determined by peptide mapping and MS/MS. Solvent exposure data generated in this way provide insights into protein tertiary structures.²⁷⁻³¹

Hydroxyl radical ($\cdot\text{OH}$) represents a particularly interesting covalent labeling probe. This species can be generated by electrochemical, photochemical, radiolytic or redox-based methods, and it can react with at least 14 out of the 20 amino acid side chains.^{32, 33} Most of the oxidative modifications generated in this way are easily recognizable as +16 Da

modifications in the resulting mass distributions, but less abundant products associated with other mass shifts may also be formed.³³⁻³⁶ Oxidative labeling has been used for the structural mapping of numerous water-soluble biomolecular systems,^{33, 35, 37-39} as well as a few membrane proteins.^{40, 41}

In Chapter-2, we applied ·OH labeling to native purple membranes. It was found that oxidative modifications on BR exclusively occurred at Met residues under the conditions used. BR contains a total of nine methionines (Figure 3-1a), whereas cysteines are absent. MetO formation is known to be a preferred oxidative process,³³ but the complete lack of oxidation at other residues in BR is nonetheless somewhat surprising. Most importantly, however, it was demonstrated that Met labeling provides structural information. Extensive MetO formation occurred at M32, M68, and M163 which are solvent exposed in loop regions. The labeling levels at the remaining six Met residues were several fold lower, consistent with their locations in solvent-inaccessible regions of the purple membrane. Many membrane proteins are rich in methionine, and hence the mapping of Met oxidation represents a promising approach for obtaining structural information on these species *in situ*, i.e., in their natural lipid environment. This simple method could become a useful complement to the current practice of generating numerous cysteine mutants for tagging experiments aimed at exploring membrane protein structures and topologies.^{42, 43}

The aim of the present work is to characterize the structure of a membrane protein under semi-denaturing conditions, using bacteriorhodopsin (BR) as a model system. This work employs a combination of optical spectroscopy and oxidative labeling for characterizing

the structure of BR under partially denaturing conditions. Data obtained for the native protein are compared to measurements carried out in the presence of acid, SDS, and after exposing the protein to heat. Previous studies have shown that all three conditions modify the properties of BR to a certain extent. The exact nature of these changes, however, remains a matter of debate. Much of the ongoing controversy regarding the structure of BR in the presence of denaturants stems from complications with the interpretation of CD spectra for proteins within membrane sheets.^{44, 45} Additionally, in the case of SDS-containing solutions detergent binding to peptide carbonyl groups affects differences in the absorption of left and right circular polarized light.⁴⁶ The oxidative labeling technique used here represents an alternative structural approach. We demonstrate that each of the tested conditions results in structural features that give rise to characteristic Met oxidation patterns and spectroscopic signatures. Oxidative labeling experiments on BR variants that contain additional Met residues make it possible to probe the solvent accessibility of the protein with an even better coverage. This work demonstrates how the combination of oxidative labeling with protein engineering and optic measurements can provide insights into structural aspects of membrane proteins.

3.2 Experimental

3.2.1 *Sample Preparation*

Purple membranes from *H. salinarum* were harvested and purified by sucrose gradient centrifugation as described in Chapter-2. Cell lines expressing the L93M and V179M variants were a generous gift from Janos K. Lanyi (University of California at Irvine).

Purification of these mutant proteins was performed in the same way as for wt BR. The expected masses of intact wt BR, L93M BR, and V179M BR based on the amino acid sequences (including retinal) were calculated as 27050 Da,⁴⁷ 27068 Da, and 27082 Da, respectively. Intact mass measurement of all three BR samples confirmed these theoretical mass values to within ± 1 Da. The amino acid substitutions of the two mutated proteins were further verified by tryptic peptide mapping and ESI-MS/MS (data not shown). All protein samples were stored at -80 °C prior to analysis. Sequencing-grade modified trypsin was purchased from Promega (Madison, WI). The acid-labile surfactant RapiGest SF was obtained from Waters (Milford, MA). SDS, ammonium bicarbonate, sodium phosphate, potassium phosphate, formic acid and NATA were from Sigma (St. Louis, MO). All chemicals were used as received.

Structural studies on BR were carried out by exposing purple membranes to four different solvent conditions. For experiments on the native protein, native purple membranes or mutants were suspended in 10 mM sodium phosphate buffer at pH 7. Acidic samples were generated by addition of HCl to pH 2.5. Lower pH values induced excessive aggregation and hence were not used in this work. SDS samples were exposed to 0.2% (w/v) (7 mM) sodium dodecyl sulphate in 10 mM sodium phosphate buffer (pH 7). The critical micelle concentration of SDS under these conditions is 5 mM.⁴⁸ SDS samples containing higher detergent concentrations (up to 2%) yielded experimental results very similar to those discussed above for 0.2% (data not shown). Heat-exposed BR was obtained by incubating samples containing 10 mM sodium phosphate buffer (pH 7) in a water bath at 100 °C for 8 minutes, followed by cooling to room temperature (22 ± 1 °C). After these procedures all

samples were sonicated in a water bath (Fisher Scientific, FS60, Ottawa, Ontario, Canada) for 15 minutes, followed by equilibration at room temperature for six hours.

3.2.2 Optical Spectroscopy and Oxidative Labeling

UV-Vis absorption data were recorded on a Varian Cary 100 spectrophotometer (Varian, Mississauga, Ontario, Canada). Fluorescence emission spectra were acquired on a Fluorolog-3 instrument (Horiba Jobin Yvon, Edison, NJ) with an excitation wavelength of 280 nm. All optical measurements were performed at a protein concentration of 15 μM at room temperature. Protein-free solutions were used as blanks.

Covalent labeling of BR was performed as described in Chapter-2. Briefly, solutions with a total protein concentration of 12 μM were pumped through a 100 μm i.d. flow capillary made of fused silica (TSP100170 Polymicro Technologies, Phoenix, AZ) at 40 $\mu\text{L min}^{-1}$. The sample solution also contained 0.05% (15 mM) H_2O_2 , 3% sucrose, and 15 mM glutamine as radical scavenger.³⁹ A KrF excimer laser (GAM EX 100/125, Orlando, FL) producing 18 ns pulses at 248 nm and 16 Hz was used to generate hydroxyl radicals by peroxide photolysis. Each laser pulse induces labeling of a 16 nL portion of sample. The resulting single-exposure flow segments are separated by 24 nL portions of non-labeled solution, estimated on the basis of a plug flow approximation.⁴⁹ These conditions were chosen in order to eliminate oxidation-induced structural artifacts, as discussed in detail elsewhere.³⁹ Capillary outflow aliquots of 100 μL were collected in microcentrifuge tubes containing 10 μL of 1 μM catalase (pH 7) for removal of residual H_2O_2 . To ensure catalase activity the collection tube also contained 10 μL of 200 mM phosphate buffer (pH 7) for

acidic samples, and 300 μL water in the case of SDS experiments. Control experiments carried out with and without H_2O_2 revealed the occurrence of secondary oxidation reactions at a low level,⁵⁰ corresponding to an average difference in oxidation background of less than 2%.

3.2.3 Peptide Mapping and UPLC/MS Analysis

100 μL aliquots of unlabeled control samples or labeled BR samples were lyophilized. Subsequently, the dry powder was dissolved in 40 μL of 50 mM ammonium bicarbonate buffer (pH 8) containing 0.1% (w/v) RapiGest. Dissolution was achieved by extensive vortex mixing followed by 15 minutes of sonication in a water bath. For native, heated, and acidic BR the resulting solutions were digested directly with trypsin for 24 h at 37 °C using a 1:20 (w/w) enzyme: protein ratio. SDS interferes with digestion and had to be removed by K^+ precipitation. For this purpose 8 μL 1.0 M potassium phosphate buffer (pH 8) was added to the SDS sample solutions. The resulting precipitate was removed by centrifugation at 13,000 g for 5 minutes. The supernatant was digested as described above. All digests were flash-frozen in liquid nitrogen and stored at -80 °C.

Protein digests were analyzed on a Q-TOF Ultima API mass spectrometer (Waters) equipped with a Z-spray ESI source. Spectra were acquired in positive ion mode at a sprayer voltage of 3 kV and a desolvation temperature of 250 °C. The mass spectrometer was coupled to an Acquity UPLC system (Waters) employing a 1.7 μm C18 BEH 130 column (2.1 mm \times 100 mm). For each injection 5 μL of digested sample were loaded onto the UPLC column without prior lipid or RapiGest removal. Solvent A was 0.1% aqueous

formic acid, and solvent B consisted of 50:50 (v/v) acetonitrile/isopropanol with 0.065% formic acid. Chromatographic separations were carried out at 40°C with a flow rate of 100 $\mu\text{L min}^{-1}$. A linear gradient was run from 3 to 5% B in 4 minutes, then from 15% to 40% B in 7 minutes, from 40% to 70% B in 2 minutes, from 70% to 85% B in 10 minutes, and finally from 85% to 100% B in 6 minutes. Most peptides eluted in a range between 7 and 24 min. Peptide identities were confirmed by MS/MS in data-dependent acquisition mode, employing collision-induced dissociation (CID) in an Ar-filled hexapole cell. Oxidation labeling sites were determined in offline MS/MS experiments, by collecting the UPLC eluent in a 96-well plate. These samples were then injected into the mass spectrometer using a TriVersa NanoMate (Advion, Ithaca, NY) chip-based ion source.

3.2.4 Data Analysis

The degree of methionine oxidation for each peptide is reported as the "fraction unmodified", F_u , which is calculated from the ESI-MS data as

$$F_u = \frac{A_u}{A_u + A_{ox}} \quad (3-1)$$

where A_u and A_{ox} are the integrated peak areas of the unmodified species and its oxidation product(s), respectively. Eq. 3-1 is based on the commonly made assumption that differences in the ionization efficiency between unmodified peptides and the oxidation products are negligible.^{33, 51} Some peptides and their oxidation products gave rise to the formation of sodium adducts, which were also included for calculating A_u and A_{ox} . No particular considerations are required for tryptic peptides that contain a single methionine, but T3-4 with its three Met residues (M56, M60, and M68) requires special treatment. The

F_u of M68 can be calculated from the T3-4 labeling data using a modified version of Eq. 3-1

$$F_u(M68) = \frac{A_u}{A_u + A_{ox}(+16) + A_{ox}(+32) + A_{ox}(+48)} \quad (3-2)$$

and the combined oxidation levels of M56 and M60 are reflected in the expression

$$F_u(M56/M60) = \frac{A_u + A_{ox}(+16)}{A_u + A_{ox}(+16) + A_{ox}(+32) + A_{ox}(+48)} \quad (3-3)$$

where +16, +32, and +48 refer to signals arising from singly, doubly, and triply oxidized T3-4. The validity of Eqs. 3-2 and 3-3 is based on the MS/MS results of Figure 3-5.

Not all of the observed protein oxidation is attributable to laser-induced labeling. Significant oxidation can occur prior to H₂O₂/laser exposure during pre-treatment of the samples (especially for heated BR, see Results and Discussion). As noted above, a low basal level of oxidation (< 2%) is also caused by the presence of H₂O₂ in the solution. To take into account these background effects we have to distinguish three different parameters: (i) F_u^{app} is the apparent F_u obtained by applying Eq. 3-1 directly to data obtained after labeling. (ii) F_u^{bgr} represents the F_u of BR that has undergone oxidation as a result of various background processes. The corresponding samples were treated in exactly the same way as those in the oxidative labeling experiments, except that the H₂O₂-containing solutions were not exposed to laser irradiation. (iii) F_u^{corr} reflects the actual extent of laser-induced labeling, corrected for background oxidation. Let R_u be the relative peak area of an unmodified peptide in the mass spectrum, and R_{ox} the relative area

of the corresponding oxidation product(s) with $R_u + R_{ox} = 1$. Using the superscript notation defined above, it can be stated that

$$F_u^{corr} = \frac{R_u^{app}}{R_u^{app} + R_{ox}^{app} - R_{ox}^{bgr}} \quad (3-4)$$

After considering that $(1 - R_{ox}^{bgr}) = R_u^{bgr} = F_u^{bgr}$, and $R_u^{app} = F_u^{app}$ we obtain the relationship

$$F_u^{corr} = \frac{F_u^{app}}{F_u^{bgr}} \quad (3-5)$$

which provides a simple tool for quantifying the actual amount of laser-induced oxidative labeling in the presence of background oxidation. All F_u values calculated in this work represent an average of at least three independent measurements. Error bars reflect the maximum deviation from each average value.

3.3 Results and Discussion

3.3.1 Optical Spectroscopy

BR in its native purple membrane environment displays an absorption band with a maximum at 568 nm, attributable to the retinal chromophore (Figure 3-2A).^{52, 53} Although the protein contains eight tryptophans (Figure 3-1B), it is only weakly UV fluorescent in its native state (Fig. 3-2B). The Trp fluorescence properties of BR may be modulated by several factors.⁵⁴ However, the low emission intensity observed here for the native protein is largely due to the fact that most Trp residues (in particular W86, W138, W182, and W189, Figure 3-1B) are in close spatial proximity to the retinal chromophore, such that their emission is quenched by FRET.⁵⁵

Exposure of BR to pH 2.5 results in a shift of the retinal absorption maximum to around 602 nm (Figure 3-2A). Protonation of D85 has been shown to be chiefly responsible for this spectroscopic change.⁵⁶ An elevated background in the absorption spectrum is attributed to light scattering, suggesting partial aggregation.⁵⁷ The level of Trp fluorescence quenching remains virtually unchanged under acidic conditions (Figure 3-2B). Consistent with recent X-ray data,⁵⁶ these observations indicate that the retinal remains attached to the protein at low pH, and that its orientation relative to the Trp residues is similar as in the native state.

BR in SDS exhibits a prominent absorption peak at 392 nm, whereas the 568 nm signal has disappeared (Figure 3-2A). The 392 nm band is commonly attributed to free retinal.^{53, 58, 59} Indeed, control experiments carried out on the isolated chromophore in protein-free SDS solution resulted in an absorption band very similar to that in Figure 3-2A, with a maximum at 394 nm (data not shown). This finding confirms that residual interactions between the retinal and the protein (and/or the membrane lipids) are absent or extremely weak. A fourfold increase in the Trp fluorescence intensity (Figure 3-2B) is consistent with a disruption of the Trp to retinal FRET, a result that also points to removal of the chromophore from its binding pocket.⁵⁵

Previous calorimetry studies have shown that BR exhibits a reversible premelting transition at ~78 °C, which is followed by a main transition at ~96 °C that is irreversible.^{53, 60} Irreversibly denatured protein was produced in this study by heating to 100 °C, followed by cooling to room temperature. The retinal absorption spectrum measured after this heat treatment is weak, with faint bands around 570 and 390 nm (Figure 3-2A). We attribute this

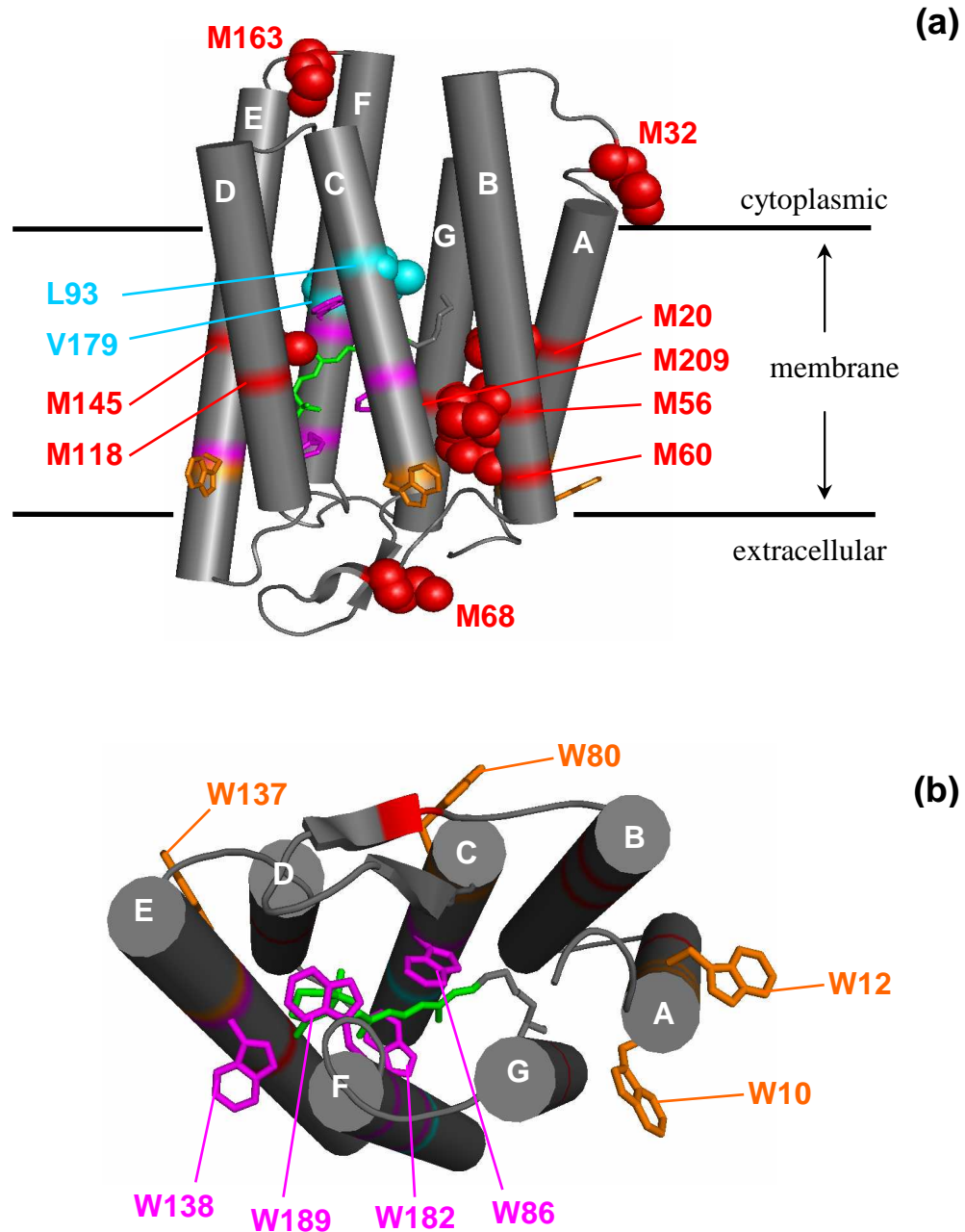


Figure 3-1. Side view (a) of BR (pdb code: 1XJI) and top view (b) from the extracellular. Transmembrane helices (A-G) are shown in gray cylinders; methionines are in red spheres. Also shown are leucine 93 and valine 179 (blue spheres) which were converted to methionines for some experiments. Tryptophan side chains that are in close proximity to the retinal (shown in green) are highlighted in purple sticks. Other tryptophans are shown in orange.

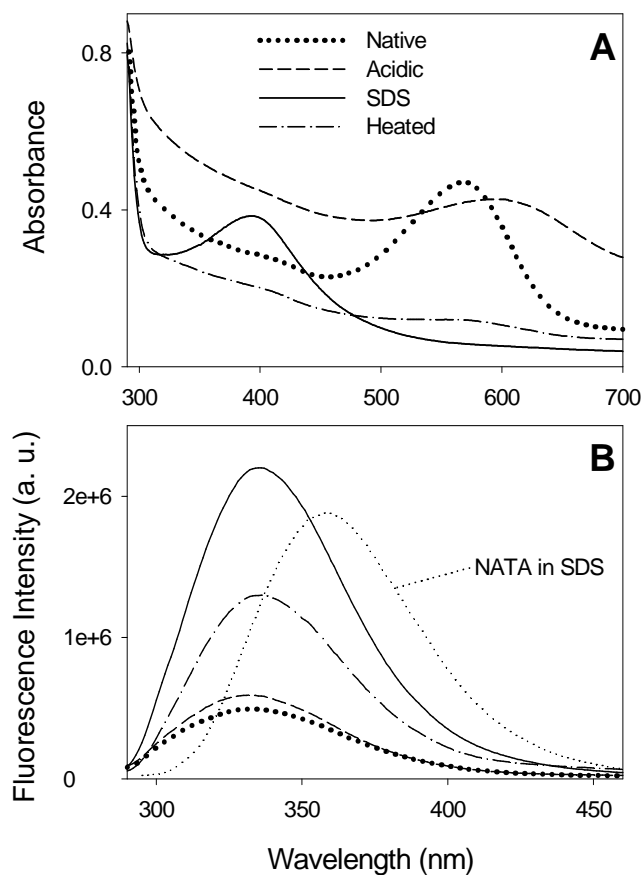


Figure 3-2. (A) UV-Vis absorption spectra and (B) fluorescence emission spectra of BR under different conditions. Dotted lines, pH 7 (native protein); dashed line, pH 2.5; solid line, pH 7 in 0.2% SDS; dash-dotted line, pH 7 after heating to 100 °C. Also shown in panel B are fluorescence data for 20 μ M NATA in 0.2% SDS, normalized to account for the different concentration and the number of chromophores per molecule.

behavior to partial dissociation of the retinal from the protein, followed by aggregation of the chromophore in the solvent. Evidence for partial retinal release from its binding pocket also comes from the fluorescence data in Figure 3-2B, which show an almost threefold increase in emission intensity as the result of a reduced Trp-retinal energy transfer efficiency. In addition, thermal decomposition of retinal could occur under these conditions as well.

In summary, the data in Figure 3-2A report the retinal binding state under the various experimental conditions. The retinal remains attached to the protein at acidic pH. Heat treatment of the protein induces partial retinal release, whereas a complete disruption of the retinal-protein interactions occurs in SDS. These findings are in agreement with the results of previous work.^{45, 53, 56, 58, 61} Fluorescence data of Figure 3-2B also provide some information on the degree of protein unfolding in response to the three denaturing agents. In particular, the fluorescence emission maximum reflects the degree of Trp solvent exposure. Native and acidic BR in Figure 3-2B both have their emission maxima at 333 nm. A slight shift to 336 nm is observed for the heated and SDS samples. Transferring a Trp residue from a nonpolar environment to the aqueous phase generally results in a red shifted emission.^{62, 63} However, the 3 nm change observed here for SDS and heat denaturation has to be considered very minor. For comparison, Figure 3-2B also contains data for NATA in SDS, which mimics the properties of an exposed Trp side chain in a detergent-containing solvent environment. The NATA emission maximum is dramatically red shifted to 360 nm. Taken together, these data imply that all the Trp residues in BR remain almost completely shielded from the aqueous environment under all conditions used. This conclusion will be

complemented with the results of oxidative labeling (see below).

3.3.2 Oxidative Methionine Labeling

Laser-induced oxidative labeling, tryptic peptide mapping, and MS/MS were employed for studying the solvent accessibility of individual regions in native BR, as well as for acidified, SDS containing, and heated samples. The resulting tryptic peptides of these different BR samples are the same as shown in Figure 2-2, yielding a sequence coverage of 97%. As an example, Figure 3-3 illustrates the behavior for fragment T7. The extent of oxidative labeling for this peptide is minimal for all solvent conditions used. In contrast, T1 shows a low oxidation level only for native and acidic BR, whereas labeling of the SDS and heated samples results in pronounced +16 Da signals (Figure 3-3, E-H).

MS/MS data of tryptic peptides were employed for identifying the location of oxidation sites. Consistent with our earlier results on native BR in Chapter-2, it was found that the oxidation of Met residues to sulfoxide (MetO) is the only identifiable covalent modification, regardless of the solvent conditions used. Exploring the basis of this remarkable Met selectivity is beyond the scope of the current work. Selected MS/MS data are depicted in Figure 3-4, where results for peptide T1 from unlabeled BR (panels A-C) are shown together with those for oxidized T1 after laser-induced labeling (panels D-F). It is seen that y_n -ions with $n > 10$ are shifted by 16 Da, identifying M20 as the oxidative labeling site. MS/MS data for oxidized T3-4 obtained under different conditions (data not shown) confirm that the single oxidation of T3-4 reflects MetO formation at M68 for all BR samples studies here, as shown in Figure 2-4.

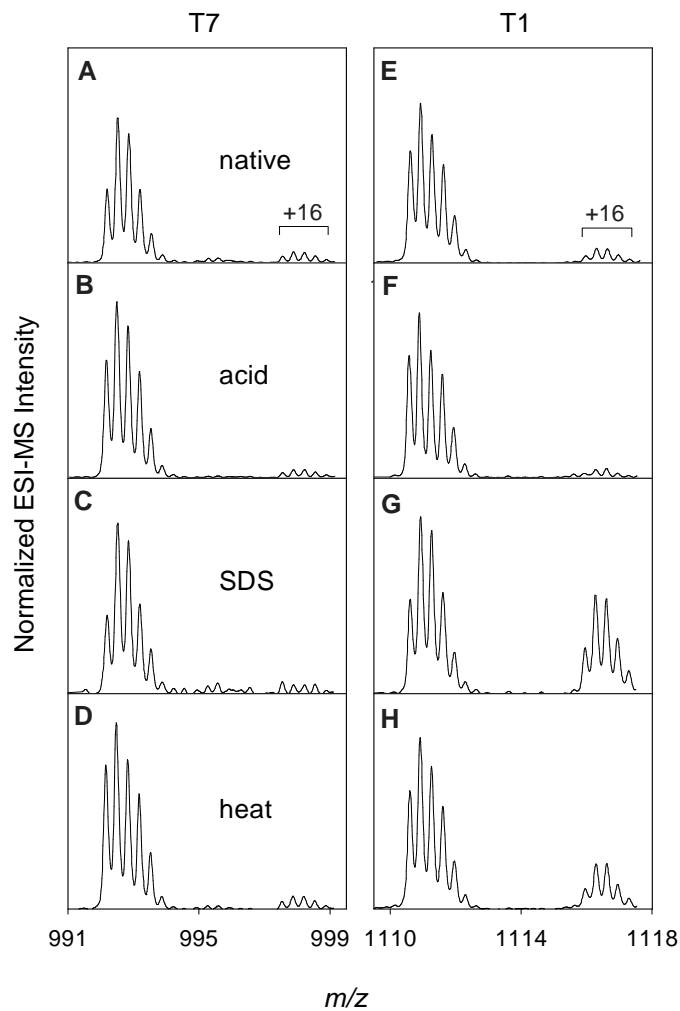


Figure 3-3. ESI mass spectra of selected BR tryptic peptides T7 (A-D) and T1 (E-H) after oxidative labeling under different conditions: First row of panels (A, E), native BR; second row (B, F), pH 2.5; third row (C, G), in 0.2% SDS; fourth row (D, H), after heat exposure. Both peptides shown in this figure are triply charged.

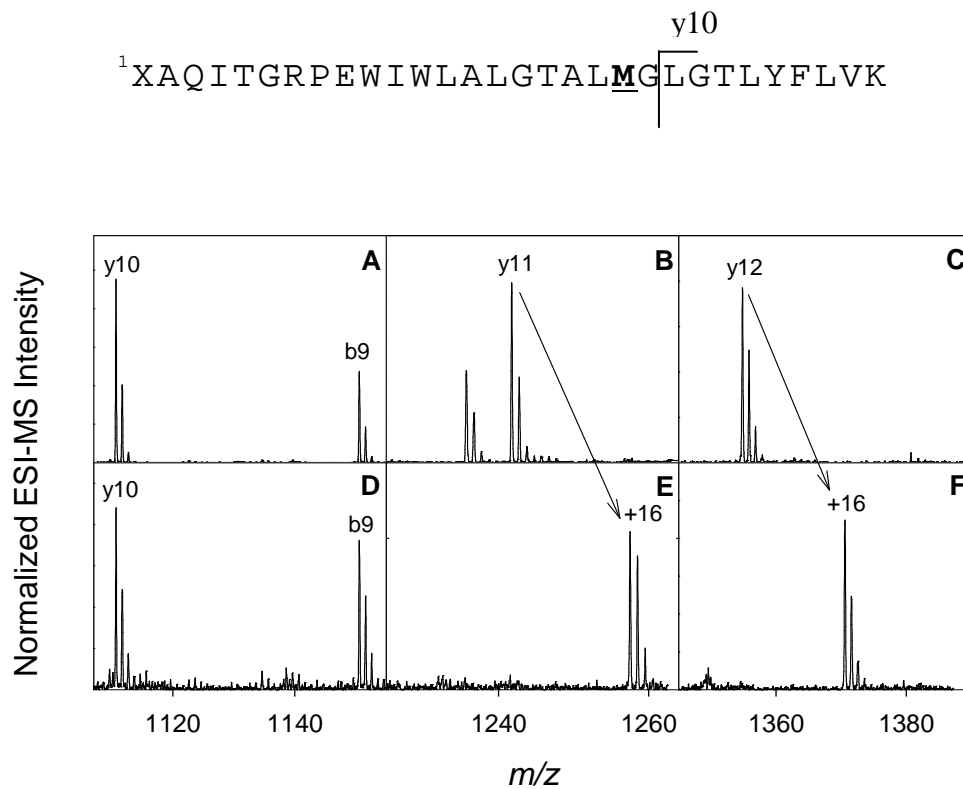


Figure 3-4. Partial MS/MS spectra of the tryptic peptide T1 from unlabeled BR (m/z 1110.60, A-C), and for the peptide (T1 + 16) after laser-induced oxidative labeling of BR in SDS (m/z 1115.93, D-F). The precursor ion is triply charged.

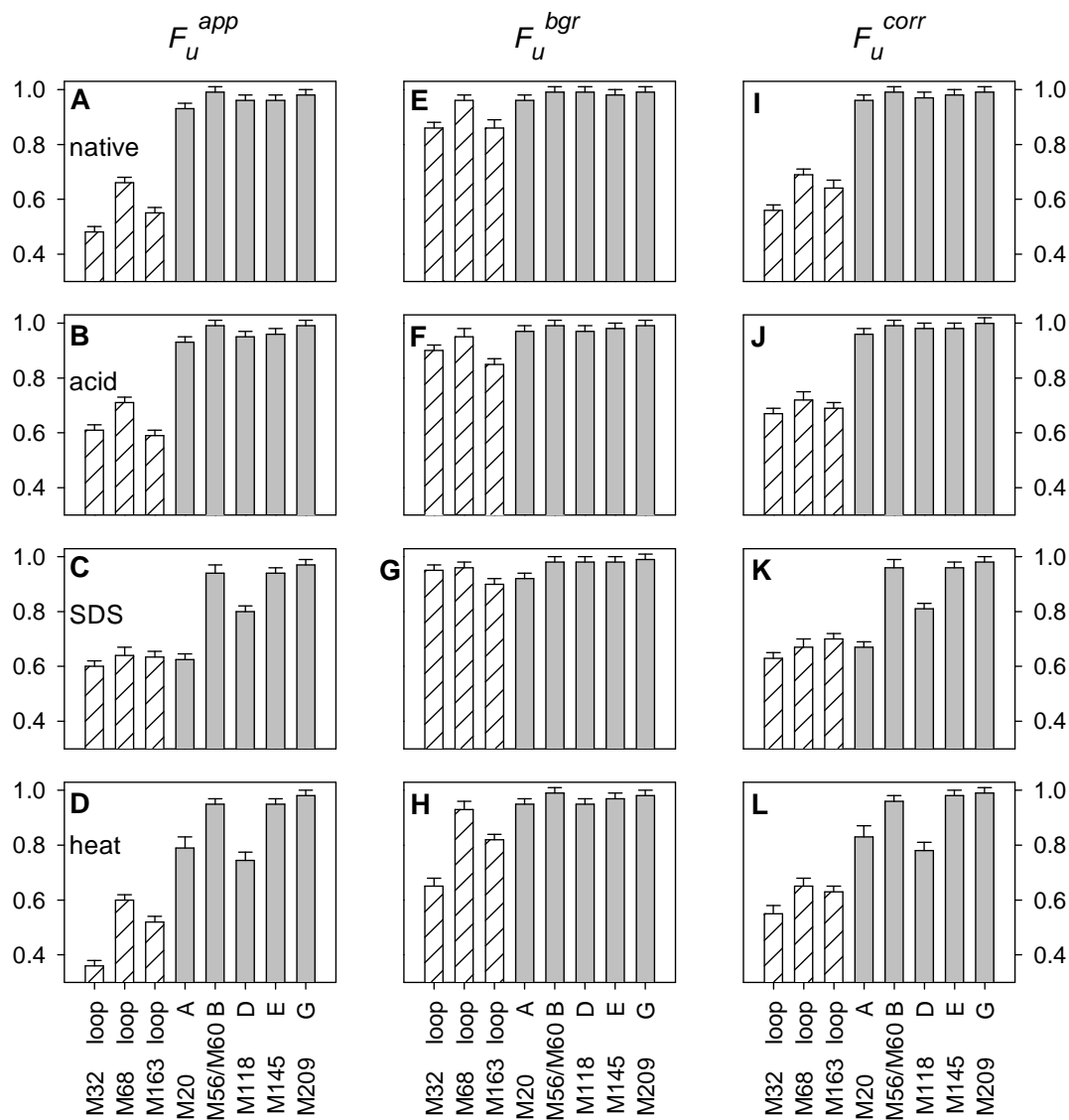


Figure 3-5. Laser-induced oxidative labeling of methionine residues in BR. Shown is the fraction unmodified, F_u , obtained in three different ways: (A-D), uncorrected values F_u^{app} ; (E-H), background oxidation levels F_u^{bgr} ; (I-L), values obtained after background correction (F_u^{corr}). The first row of panels refers to native purple membrane samples; row 2 is for acidified BR, row 3 is for SDS samples, and row 4 is for heated BR. Hatched bars represent data for M32, M68, and M163. Also shown along the bottom are the locations of individual Met residues in helices A, B, D, E, or G.

For discussing the oxidative labeling behavior of individual methionines it is convenient to consider "fraction unmodified" (F_u) values, calculated as outlined in the Experimental section. Met side chains that are completely shielded are characterized by $F_u \approx 1$, whereas exposure to the solvent leads to $F_u < 1$. Application of Equation 3-1 directly to the uncorrected oxidative labeling data yields the F_u^{app} progressions depicted in Figure 3-5A-D. For assessing the level of background oxidation, experiments were carried out on all four types of samples in the presence of H_2O_2 but without laser irradiation (Figure 3-5, E-H). The F_u^{bgr} patterns obtained in this way reveal that background oxidation is quite predominant for M32 and M163. Both of these residues are positioned in solvent exposed loops on the cytoplasmic side of native BR (Figure 3-1). Background oxidation of M32 and M163 is most pronounced after heating (Figure 3-5H), consistent with earlier studies on other proteins that have demonstrated spontaneous MetO formation at elevated temperature.^{57, 64} As a side aspect, we note that these covalent modifications may contribute to the irreversible nature of BR thermal denaturation.⁶⁴ Equation 3-5 allows the calculation of background corrected F_u^{corr} values from the F_u^{app} and F_u^{bgr} measurements. The F_u^{corr} progressions obtained in this way exclusively reflect oxidation events that are caused by laser-induced labeling (Figure 3-5, I-L).

Inspection of the corrected oxidation data (Figure 3-5, I-L) reveals that M32, M68, and M163 exhibit F_u^{corr} values in the range of 0.6 to 0.7 for all solvent conditions studied. Because only ca. 40% of the solution is being laser irradiated (see Experimental section), $F_u^{corr} \approx 0.6$ corresponds to the maximum possible degree of labeling, reflecting complete solvent exposure of the affected side chains. The observation of nearly complete oxidative

labeling for M32, M68, and M163 is consistent with the positioning of these residues in solvent-exposed loops of native BR (Figure 3-1). The data (Figure 3-5, J-L) demonstrate that this solvent exposure is retained under partially denaturing conditions. This finding is particularly noteworthy in the case of SDS (Figure 3-5K), as one might suspect that steric shielding by detergent binding to solvent exposed methionines^{59, 65, 66} could lead to partial protection from oxidation. Our results imply that any such detergent-mediated shielding at protruding loops is insignificant.

The results for native BR (Figure 3-5I) show a striking difference in the labeling behavior of the three solvent accessible methionines (M32, M68, and M163), and the six Met residues that are buried within the purple membrane. The latter are characterized by F_u^{corr} values close to unity, which attests to their lack of solvent exposure. This behavior is consistent with our earlier oxidative labeling data in Chapter-2, as well as with the results of NMR spectroscopy.⁶⁷ The dramatic labeling differences of solvent accessible and inaccessible methionines in Figure 3-5I reaffirms the validity of using MetO formation as a structural probe in our experiments. This is a non-trivial conclusion, considering that the high reactivity of methionine can lead to oxidation even for non-exposed residues under some conditions.^{51, 68-72} The data of Figure 3-5I demonstrate that such aberrant behavior does not occur for the experimental settings used here.

3.3.3 *Structural Interpretation - Low pH*

Of the three denaturants studied here, the effects of low pH on the BR structure are best understood. Recently it has even been possible to crystallize the protein under acidic

conditions, revealing that the overall structure of the lipid/protein membranes only undergoes relatively subtle conformational changes.⁵⁶ Thus, unlike for many soluble proteins acid does not induce large-scale unfolding of BR. Consistent with those X-ray data, the oxidative labeling pattern of acidified BR (Figure 3-5J) is almost indistinguishable from that measured for the native protein (Figure 3-5I), demonstrating that M20 (helix A), M56/M60 (helix B), M118 (helix D), M145 (helix E), and M209 (helix G) remain completely shielded from the solvent at low pH. Also, the optical data of Figure 3-2 confirm that all Trp residues maintain their hydrophobic environment, and that the retinal remains in its binding pocket under acidic conditions.

3.3.4 Structural Interpretation - SDS Exposure

SDS disrupts the purple membrane and results in BR monomers.^{58, 61} As noted earlier (Figure 3-2), SDS exposure also leads to hydrolytic loss of the retinal chromophore. Obtaining better insights into the protein structure under these conditions is of particular importance because of the widespread use of SDS-solubilized state as the starting point for refolding studies.⁵⁻⁸ On the basis of CD measurements it has been suggested that the helical content of the protein in SDS is reduced from the native state value of 74% down to 42%.⁴⁵ However, this interpretation has been questioned because of the unique challenges associated with BR structural studies by CD.⁴⁴⁻⁴⁶ FRET measurements have shown that SDS exposure leads only to a very small (2 Å) increase in the interhelix distance between B and F.⁴⁶ NMR spectroscopy reveals that BR fragments retain a native-like helicity in SDS,⁷³ but the conformational propensities of these segments may be different in the context of the full-length protein. Hence, there is no consensus regarding the degree of

secondary structure loss and unfolding induced by SDS.⁴⁶

Oxidative labeling of BR in SDS reveals that M20 (helix A) becomes almost completely solvent accessible with $F_u^{corr} = 0.67$ (Figure 3-5K). Significant deprotection is also seen for M118 (helix D, $F_u^{corr} = 0.80$). In contrast, M56/M60, M145, and M209 retain F_u^{corr} values close to unity, which means that these residues remain shielded from the solvent. A lack of water exposure is also evident for the eight Trp residues as seen from the fluorescence data in Figure 3-2B. These observations imply that a large protein core is preserved upon BR solubilization in SDS, where a substantial number of residues remain inaccessible to water. This behavior is different from structural models of other SDS-denatured proteins, where the detergent is believed to disrupt the majority of all tertiary interactions, as well as unravel most secondary structure elements.^{59, 65, 66}

In native BR all of M20, M56, M60, M118, M145, and M209 are arranged in close spatial proximity to the retinal (Figure 3-1). It is remarkable that SDS selectively enhances the solvent accessibility of M20 and M118, while the four other methionines remain fully protected. To account for this labeling pattern we will consider two possible scenarios. (i) It could be envisioned that retinal loss creates a water-filled channel in the protein center, while leaving the apo-protein structure largely intact. Oxidative labeling of M20 and M118 could then occur after $\cdot\text{OH}$ diffusion into this cavity. However, it is difficult to reconcile this proposal with the observation of selective labeling for just two residues. For example, M118 and M145 are directly adjacent to each other in the native retinal binding pocket (Figure 3-1), but only the former gets oxidized in SDS. Also, the fact that the Trp residues

maintain a nonpolar environment (Figure 3-2B) argues against an SDS-denatured state that bears an internal water-filled cavity. (ii) An alternative model for BR in SDS represents a more likely scenario, where hydrolytic retinal loss leads to collapse of the binding pocket such that water remains largely excluded from the protein core. We propose that the solvent exposure of M20 and M118 can be accounted for by partial breakdown of helices A and D, concomitant with exposure of the unraveled regions to the bulk (Figure 3-6). The possible involvement of such "extrusion phenomena" for partially denatured membrane proteins has been noted earlier.⁷⁴ Evidence for partial unfolding of helix D in SDS also comes from earlier fluorescence tagging experiments.⁷⁵ The outside faces of the remaining helical elements will be surrounded by detergent molecules in a micellar fashion, such that a hydrophobic environment is maintained. Complete extrusion of helix A is unlikely, because this would imply solvent exposure for W10 and W12. In the fluorescence spectrum of Figure 3-2B such a scenario would result in a pronounced red-shifted shoulder. The lack of such a spectral feature implies that the N-terminal residues of helix A remain protected.

Unfortunately, the absence of Met residues in helices C and F does not allow direct structural information on these helices to be obtained by oxidative labeling. For gaining a better understanding of the structure of SDS-denature BR, two BR variants (L93M and V179M) were examined, which provide potential oxidation sites in helix C or F (Figure 3-1a), respectively. In this way, each helix is covered by at least one potential oxidative labeling site. Trypsinolysis of L93M BR and V179M BR resulted in similar peptides to wild type BR. The newly introduced methionines in L93M and V179M variants are located in peptides T5 and T10-11 (Figure 2-2), respectively. Similar to wt BR, after exposing

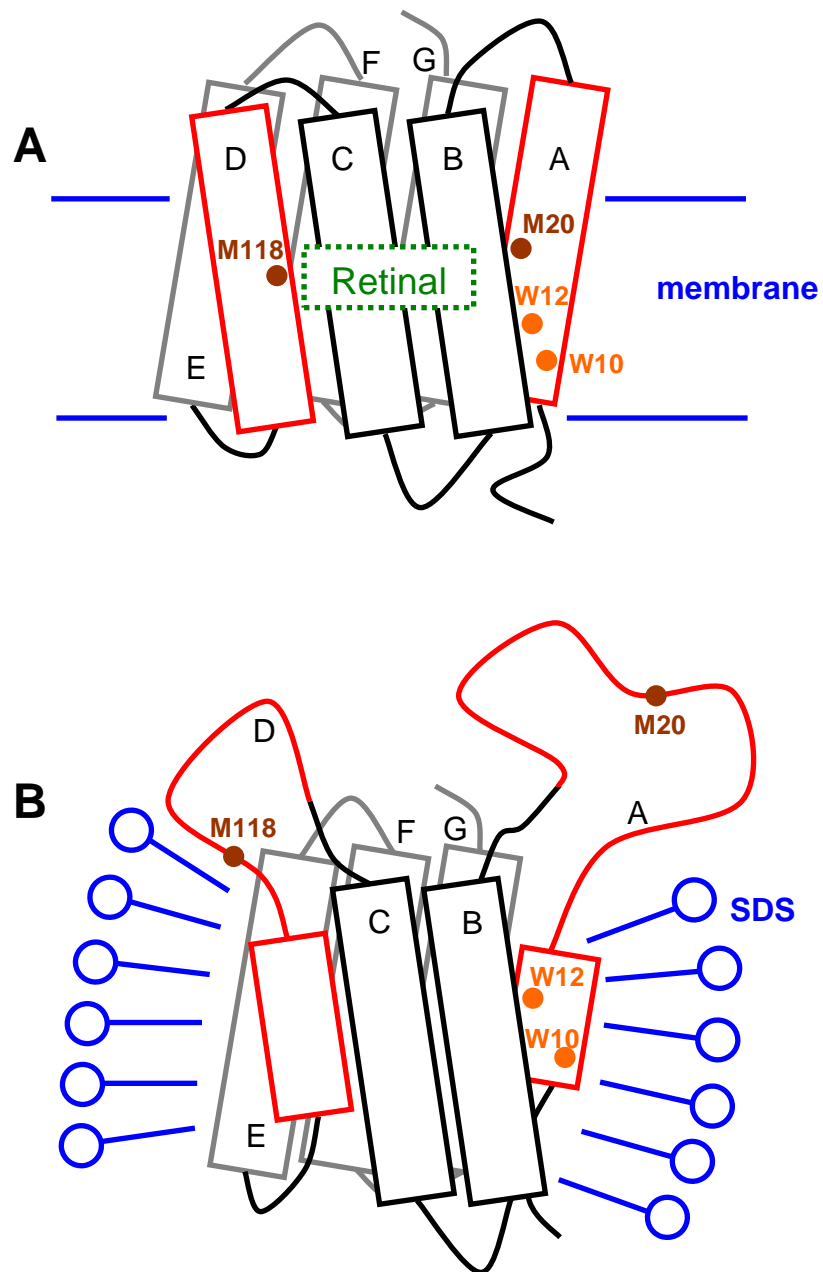


Figure 3-6. Schematic representation of (A) native BR in the purple membrane, and (B) the proposed SDS-solubilized state where M20 (helix A) and M118 (helix D) becomes solvent accessible, and W10 and W12 remain non-exposed. Possible detergent binding to the unfolded segments in (B) is not shown.

these BR variants to $\cdot\text{OH}$ labeling, MetO formation (corresponding to a +16 Da mass shift) was the only detectable type of covalent modification. Laser-induced oxidative labeling was conducted for both native BR variants and SDS-denatured variants.

A comprehensive overview of the protein labeling behavior under native conditions and SDS state is obtained by considering the F_u^{corr} values of individual Met residues (Figure 3-7). As expected, only the three loop-exposed methionines (M32, M68, and M163) were extensively oxidized in native state. SDS denaturation did not affect the extensive oxidation of the loop methionines. In contrast, the denatured protein showed obvious oxidation on peptide T5 and T1 for both variants. MS/MS data of the oxidized T5 from SDS-denatured L93M BR (Figure 3-8), as well as SDS-denatured V179M BR (not shown), confirm that M118 is the only oxidative labeling site in these two variants, whereas the newly introduced M93 remains protected. In addition, Figure 3-7d reveals that SDS denaturation affects neither the protection of M209, nor that of the substituted M179.

The labeling behavior of the two engineered residues M93 and M179 indicates that helices C and F remain essentially solvent-inaccessible in the SDS state. Based on these findings that M56/M60 (helix B), M93 (helix C), M145 (helix E), M179 (helix F) and M209 (G) keep unlabeled, it is suggested that helices B, C, E, F, and G continue to be largely protected in SDS micelles, as shown in the structural model (Figure 3-6B).

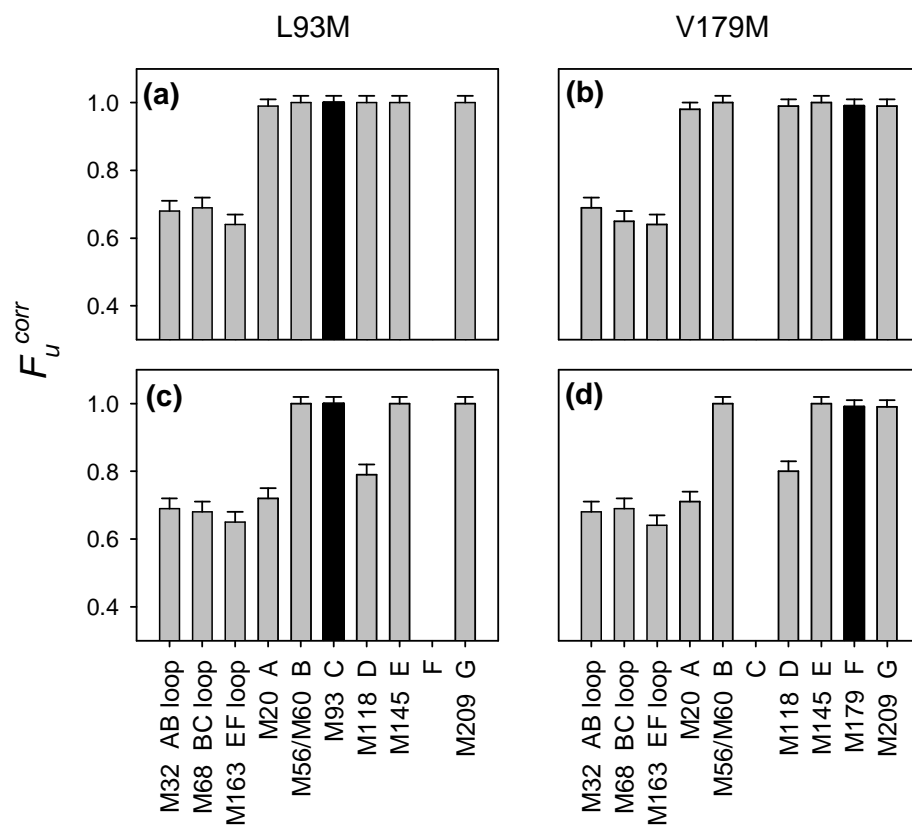


Figure 3-7. F_u^{corr} values of individual Met residues in native L93M BR (a), native V179M BR (b), and of the two protein variants after SDS denaturation (c) and (d). Highlighted in black are results for the L93M and V179M amino acid substitutions. Data for naturally occurring Mets are in gray

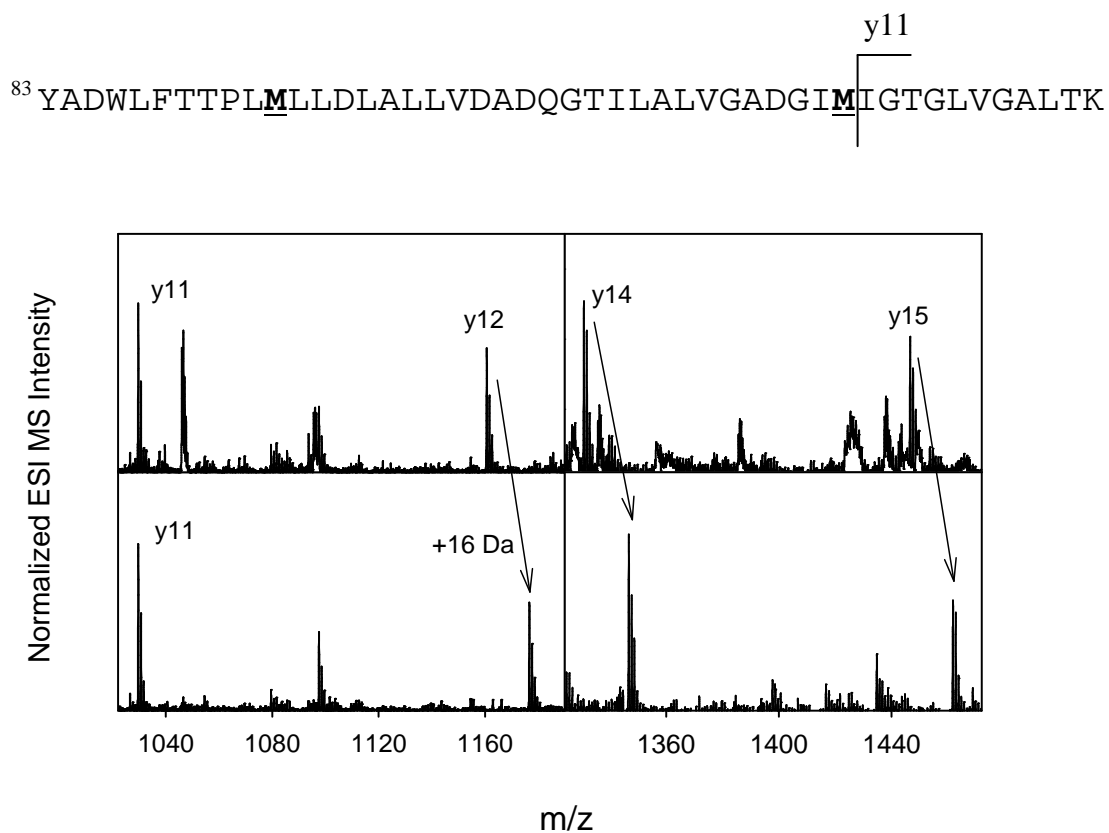


Figure 3-8. Partial MS/MS product ion spectra obtained after fragmentation of unlabeled T5 of L93M BR (the first row), and of the oxidized T5 + 16 Da species (the second row). Shown at the top of the Figure is the sequence of T5. Arrows indicate +16 Da mass shifts due to oxidative labeling of M118.

It is noted that the observed lack of solvent exposure for M56/M60, M93, M145, M179 and M209 in SDS state does not provide direct proof for the intactness of the corresponding helices B, C, E, F and G. In principle, protection from solvent access at these residues could not be ruled out if the micelle-embedded protein segments in Figure 3-6B were to adopt a more disordered, yet compact conformation. In view of the strong evidence for considerable helical structure in the SDS-state of BR,^{45, 46, 73} however, the situation depicted in Figure 3-6B represents a far more likely scenario.

To test if the structure of BR in SDS is affected by the presence of the retinal in the solution, oxidative labeling was also carried out on the retinal-free protein (bacterioopsin, BO) in SDS. The resulting BO labeling pattern (not shown) was found to be indistinguishable from that of SDS-solubilized BR in Figure 3-5K. In agreement with the optical data of Figure 3-2, this result supports the view that residual protein/retinal interactions are very weak or absent.

3.3.5 Structural Interpretation - BR after Heat Exposure

Earlier studies on the irreversible thermal denaturation of BR found that cooling of purple membranes to room temperature after heating to 100 °C leads to limited breakdown of the trimeric packing.⁵³ In addition, partial loss of retinal takes place (Figure 3-2). Alterations of the protein's helical structure upon thermal denaturation have been suggested based on infrared spectroscopy and HDX measurements.^{76, 77} Dynamic light scattering indicates partial disruption of the purple membrane patches.⁷⁷

Labeling of heated BR leads to significant oxidation of M20 (helix A) and M118 (helix D) with $F_u^{corr} \approx 0.8$, whereas M56, M60, M145, and M209 remain fully protected (Figure 3-5L). This pattern is reminiscent of that observed in SDS (Figure 3-5K). We thus propose that the structural model of Figure 3-6B with partial unfolding of helices A and D similarly applies to heated BR as well. The measured F_u^{corr} values imply, however, that the breakdown of helix A is less pronounced in the latter case. Instead of being surrounded by a detergent micelle, the heat-denatured protein is expected to be embedded within a partially intact purple membrane.⁷⁷

3.4 Conclusions

Characterizing the conformation of semi-denatured membrane proteins remains a challenging task. The current work demonstrates the application of oxidative methionine labeling and mass spectrometry for experiments of this kind, complemented by optical spectroscopy and site-directed mutagenesis. The distinction between solvent accessible and protected Met residues provides medium-resolution insights into protein structural changes. The present work confirms the structural resilience of purple-membrane embedded BR against acidic pH. In contrast, both SDS exposure and thermal denaturation induce marked conformational changes. Selective solvent exposure of M20 and M118 under these two conditions reflects partial unfolding of helices A and D.

The introduction of two additional Met residues (M93 and M179) makes it possible to probe the solvent accessibility of this protein with a better coverage. Out of the eleven

methionines, eight are located in transmembrane regions, such that every BR helix is covered by at least one potential labeling site. SDS solubilization makes M20 and M118 significantly more solvent accessible. But M56/M60, M93, M145, M179 and M209 remain solvent inaccessible. Based on those labeling data and the results of spectroscopy experiments, we proposed a structural model of SDS-denatured BR: SDS induces hydrolytic retinal loss and release of the chromophore into the solvent, which is accompanied by collapse of the retinal binding pocket and partial unfolding/extrusion of helices A and D. In contrast, helices B, C, E, F, and G remain largely intact and form a solvent-inaccessible residue core surrounded by SDS micelles, although the cytoplasmic side is most likely to be disordered (indicated by HDX studies in Chapter-4).

This work uses MetO formation as an easily identifiable covalent modification for monitoring the solvent accessibility of individual BR segments. This strategy is particularly suitable for membrane proteins, because many of these species are methionine rich.^{78, 79} Here we exploit the fact that X \rightarrow M substitutions in membrane proteins tend to be structurally benign due to the medium size and mildly hydrophobic character of methionine.⁸⁰ In this way it is possible to engineer additional labeling sites into the protein, thereby enhancing the level of structural detail. In principle, it would be possible to conduct studies on protein constructs that contain multiple substituted methionines. This work followed a more cautious strategy that minimizes the possibility of mutation-induced structural artifacts by studying one substitution at a time. The combination of protein engineering and oxidative labeling employed here should also be suitable for monitoring the structure and conformational transitions of other membrane proteins.

3.5 References

- (1) George, S. R.; O'Dowd, B. F.; Lee, S. P. *Nat. Rev. Drug Discov.* **2002**, *1*, 808-820.
- (2) Bowie, J. U. *Nature* **2005**, *438*, 581-589.
- (3) Booth, P. J.; Curnow, P. *Curr. Op. Struct. Biol.* **2009**, *19*, 8-13.
- (4) White, S. H. *Nature* **2009**, *459*, 344-346.
- (5) Curnow, P.; Booth, P. J. *Proc. Natl. Acad. Sci. U.S.A.* **2007**, *104*, 18970-18975.
- (6) Faham, S.; Yang, D.; Bare, E.; Yohannan, S.; Whitelegge, J. P.; Bowie, J. U. *J. Mol. Biol.* **2004**, *335*, 297-305.
- (7) Curnow, P.; Booth, P. J. *Proc. Natl. Acad. Sci. U.S.A.* **2009**, *106*, 773-778.
- (8) Joh, N. H.; Min, A.; Faham, S.; Whitelegge, J. P.; Yang, D.; Woods, V. L.; Bowie, J. U. *Nature* **2008**, *453*, 1266-1270.
- (9) Joh, N. H.; Oberai, A.; Yang, D.; Whitelegge, J. P.; Bowie, J. U. *J. Am. Chem. Soc.* **2009**, *131*, 10846-10847.
- (10) Hughson, F. M.; Wright, P. E.; Baldwin, R. L. *Science* **1990**, *249*, 1544-1548.
- (11) Skach, W. R. *Nat. Struct. Mol. Biol.* **2009**, *16*, 606-612.
- (12) Booth, P. J.; Fitsch, S. L.; Stern, L. J.; Greenhalgh, D. A.; Kim, P. S.; Khorana, H. G. *Nat. Struct. Biol.* **1995**, *2*, 139-143.
- (13) Dobson, C. M. *Nature* **2003**, *426*, 884-890.
- (14) Wright, P. E.; Dyson, H. J. *J. Mol. Biol.* **1999**, *293*, 321-331.
- (15) Gunasekaran, K.; Tsai, C.-J.; Kumar, S.; Zhan, D.; Nussinov, R. *Trends Biochem. Sci.* **2003**, *28*, 81-85.
- (16) Dyson, H. J.; Wright, P. E. *Nat. Struct. Biol.* **1998**, *5*, 499-503.
- (17) Bai, Y.; Sosnick, T. R.; Mayne, L.; Englander, S. W. *Science* **1995**, *269*, 192-197.
- (18) Mittermaier, A.; Kay, L. E. *Science* **2006**, *312*, 224-228.
- (19) Krishna, M. M. G.; Hoang, L.; Lin, Y.; Englander, S. W. *Methods* **2004**, *34*, 51-64.
- (20) Whitelegge, J. P.; Gundersen, C. B.; Faull, K. F. *Protein Sci.* **1998**, *7*, 1423-1430.
- (21) Manzanares, D.; Rodriguez-Capote, K.; Liu, S.; Haines, T.; Ramos, Y.; Zhao, L.; Doherty-Kirby, A.; Lajoie, G.; Possmayer, F. *Biochemistry* **2007**, *46*, 5604-5615.
- (22) Weiner, J. H.; Li, L. *Biochim. Biophys. Acta* **2008**, *1778*, 1698-1713.
- (23) Barrera, N. P.; Di Bartolo, N.; Booth, P. J.; Robinson, C. V. *Science* **2008**, *321*, 243-246.
- (24) Busenlehner, L. S.; Salomonsson, L.; Brzezinski, P.; Armstrong, R. N. *Proc. Natl. Acad. Sci. U.S.A.* **2006**, *103*, 15398-15403.
- (25) Stelzer, W.; Poschner, B. C.; Stalz, H.; Heck, A. J.; Langosch, D. *Biophys. J.* **2008**, *95*, 1326-1335.
- (26) Mendoza, V. L.; Vachet, R. W. *Mass Spectrom. Rev.* **2009**, *28*, 785-815.

- (27) Yu, E. T.; Hawkins, A.; Eaton, J.; Fabris, D. *Proc. Natl. Acad. Sci. U.S.A.* **2008**, *105*, 12248-12253.
- (28) Leite, J. F.; Cascio, M. *Biochemistry* **2002**, *41*, 6140-6148.
- (29) Wang, X.; Kim, S.-H.; Ablonczy, Z.; Crouch, R. K.; Knapp, D. R. *Biochemistry* **2004**, *43*, 11153-11162.
- (30) Weinglass, A. B.; Whitelegge, J. P.; Hu, Y.; Verner, G. E.; Faull, K. F.; Kaback, H. R. *EMBO J.* **2003**, *22*, 1467-1477.
- (31) Leite, J. F.; Blanton, M. P.; Shahgholi, M.; Dougherty, D. A.; Lester, H. A. *Proc. Natl. Acad. Sci. U.S.A.* **2003**, *100*, 13054-13059.
- (32) Cheal, S. M.; Ng, M.; Barrios, B.; Miao, Z.; Kalani, A. K.; Meares, C. F. *Biochemistry* **2009**, *48*, 4577-4586.
- (33) Xu, G.; Chance, M. R. *Chem. Rev.* **2007**, *107*, 3514-3543.
- (34) Konermann, L.; Tong, X.; Pan, Y. *J. Mass Spectrom.* **2008**, *43*, 1021-1036.
- (35) McClintock, C.; Kertesz, V.; Hettich, R. L. *Anal. Chem.* **2008**, *80*, 3304-3317.
- (36) West, G. M.; Tang, L.; Fitzgerald, M. C. *Anal. Chem.* **2008**, *80*, 4175-4185.
- (37) Wong, J. W. H.; Maleknia, S. D.; Downard, K. M. *J. Am. Soc. Mass Spectrom.* **2005**, *16*, 225-233.
- (38) Bridgewater, J. D.; Lim, J.; Vachet, R. W. *J. Am. Soc. Mass Spectrom.* **2006**, *17*, 1552-1559.
- (39) Hambly, D. M.; Gross, M. L. *J. Am. Soc. Mass Spectrom.* **2005**, *16*, 2057-2063.
- (40) Smedley, J. G.; Sharp, J. S.; Kuhn, J. F.; Tomer, K. B. *Biochemistry* **2008**, *47*, 10694-10704.
- (41) Li, C.; Takazaki, S.; Jin, X.; Kang, D.; Abe, Y.; Hamasak, N. *Biochemistry* **2006**, *45*, 12117-12124.
- (42) Bogdanov, M.; Zhang, W.; Xie, J.; Dowhan, W. *Methods* **2005**, *36*, 148-171.
- (43) Frillingos, S.; Sahin-Tótha, M.; Wua, J.; Kaback, H. R. *FASEB J.* **1998**, *12*, 1281-1299.
- (44) Wallace, B. A.; Teeters, C. L. *Biochemistry* **1987**, *26*, 65-70.
- (45) Riley, M. L.; Wallace, B. A.; Flitsch, S. L.; Booth, P. J. *Biochemistry* **1997**, *36*, 192-196.
- (46) Renthal, R. *Biochemistry* **2006**, *45*, 14559-14566.
- (47) Whitelegge, J. P.; Halgand, F.; Souda, P.; Zabrouskov, V. *Exp. Rev. Proteomics* **2006**, *3*, 585-596.
- (48) Jacquier, J. C.; Desbene, P. L. *J. Chrom. A* **1996**, *743*, 307-314.
- (49) Konermann, L. *J. Phys. Chem. A* **1999**, *103*, 7210-7216.
- (50) Xu, G.; Chance, M. R. *Anal. Chem.* **2005**, *77*, 4549-4555.
- (51) Sharp, J. S.; Becker, J. M.; Hettich, R. L. *Anal. Chem.* **2004**, *76*, 672-683.
- (52) Szundi, I.; Stoeckenius, W. *Proc. Natl. Acad. Sci. U.S.A.* **1987**, *84*, 3681-3684.

- (53) Wang, J.; Heyes, C. D.; El-Sayed, M. A. *J. Phys. Chem.* **2002**, *106*, 723-729.
- (54) Plotkin, J. B.; Sherman, W. V. *Biochem.* **1984**, *23*, 5353-5360.
- (55) Kalisky, O.; Feitelson, J.; Ottolenghi, M. *Biochemistry* **1981**, *20*, 203-209.
- (56) Okumura, H.; Murakami, M.; Kouyama, T. *J. Mol. Biol.* **2005**, *351*, 481-495.
- (57) Benjwal, S.; Verma, S.; Röhm, K.-H.; Gursky, O. *Protein Sci.* **2006**, *15*, 635-639.
- (58) Torres, J.; Sepulcre, F.; Padros, E. *Biochemistry* **1995**, *34*, 16320-16326.
- (59) Michaux, C.; Pomroy, N. C.; Prive, G. G. *J. Mol. Biol.* **2008**, *375*, 1477-1488.
- (60) Jackson, M. B.; Sturtevant, J. M. *Biochemistry* **1978**, *17*, 911-915.
- (61) London, E.; Khorana, H. G. *J. Biol. Chem.* **1982**, *257*, 7003-7011.
- (62) van Holde, K.; Johnson, W.; Shing Ho, P. *Principles of Physical Biochemistry*, second ed.; Pearson Prentice Hall: Upper Saddle River, NJ, 2006.
- (63) Nölting, B.; Golbik, R.; Fersht, A. R. *Proc. Natl. Acad. Sci. U.S.A.* **1995**, *92*, 10668-10672.
- (64) Liu, J.; Konermann, L. *J. Am. Soc. Mass Spectrom.* **2009**, *20*, 819-828.
- (65) Jones, M. N. *Chem. Soc. Rev.* **1992**, *21*, 127-136.
- (66) Turro, N. J.; Lei, X. *Langmuir* **1995**, *11*, 2525-2533.
- (67) Seigneuret, M.; Kainosho, M. *FEBS* **1993**, *327*, 7-12.
- (68) Sharp, J. S.; Becker, J. M.; Hettich, R. L. *Anal. Biochem.* **2003**, *313*, 216-225.
- (69) Xu, G.; Kiselar, J.; He, Q.; Chance, M. R. *Anal. Chem.* **2005**, *77*, 3029-3037.
- (70) Aye, T. T.; Low, T. Y.; Sze, S. K. *Anal. Chem.* **2005**, *77*, 5814-5822.
- (71) Maleknia, S. D.; Kiselar, J. G.; Downard, K. M. *Rapid Commun. Mass Spectrom.* **2002**, *16*, 53-61.
- (72) Kiselar, J. G.; Maleknia, S. D.; Sullivan, M.; Downard, K. M.; Chance, M. R. *Int. J. Radiat. Biol.* **2002**, *78*, 101-114.
- (73) Pervushin, K.; Orekhov, V. Y.; Popov, A. I.; Musina, L. Y.; Arseniev, A. S. *Eur. J. Biochem* **1994**, *219*, 571-583.
- (74) Hamasaki, N.; Abe, Y.; Tanner, M. J. A. *Biochemistry* **2002**, *41*, 3852-3854.
- (75) Compton, E. L. R.; Farmer, N. A.; Lorch, M.; Mason, J. M.; Moreton, K. M.; Booth, P. J. *J. Mol. Biol.* **2006**, *357*, 325-338.
- (76) Muller, J.; Muster, C.; Salditt, T. *Biophys. J.* **2000**, *78*, 3208-3217.
- (77) Taneva, S. G.; Caaveiro, J. M.; Muga, A.; Goni, F. M. *FEBS Lett.* **1995**, *367*, 297-300.
- (78) Yu, Y.; Gilar, M.; Gebler, J. C. *Rapid Commun. Mass Spectrom.* **2004**, *18*, 711-715.
- (79) Ablonczy, Z.; Kono, M.; Crouch, R. K.; Knapp, D. R. *Anal. Chem.* **2001**, *73*, 4774-4779.
- (80) Kyte, J.; Doolittle, R. *J. Mol. Biol.* **1982**, *157*, 105-132.

Chapter-4 Kinetic Folding Mechanism of Bacteriorhodopsin Examined by Pulsed Oxidative Labeling and Mass Spectrometry

4.1 Introduction

Membrane proteins play a key role in numerous biochemical processes. They constitute one third of the human proteome, and many of them represent important drug targets. Membrane protein misfolding caused by genetic defects can lead to various diseases.¹ Studying the folding mechanisms of membrane proteins is essential for understanding how altered structures lead to aberrant function. Despite their biological significance, the general understanding of membrane protein folding mechanisms is quite rudimentary, compared to the staggering amount of information that has been amassed for soluble species.²⁻⁴ This imbalance is caused largely by the extreme hydrophobicity of membrane proteins, and their tendency to aggregate once removed from the natural bilayer environment.⁵

These difficulties notwithstanding, encouraging recent progress in the general understanding of membrane protein structure and folding has been made.⁶⁻⁸ *In vitro* folding experiments commence by generating a solubilized denatured state, e.g., in SDS or urea.⁹ Membrane proteins under these non-native conditions often retain significant secondary and tertiary structure.^{8, 10} These (semi)denatured species are then refolded by exposure to micelles, bicelles,¹¹ or lipid vesicles¹² which serve as surrogate for the natural membrane. The number of membrane proteins that have been successfully refolded increases steadily.⁹

¹³⁻¹⁷ Methods originally developed for soluble proteins, such as thermodynamic measurements and ϕ -value analyses,¹⁸ are now also being applied to membrane proteins.¹⁹⁻²² Despite these advances, however, a consensus folding mechanism has not emerged yet. For α -helix bundles a two-stage model has been proposed, according to which insertion of independently stable helices into the bilayer is followed by helix association.²³ However, it has now become clear that additional steps are usually required for the formation of native membrane protein structures.^{5, 24-26}

Deciphering the temporal sequence of events during folding requires time-resolved structural investigations. Similar to studies on soluble proteins,^{27, 28} the detection and characterization of short-lived intermediates is a key requirement for piecing together kinetic folding pathways. An arsenal of techniques has been developed for characterizing transiently populated conformers,²⁹ but the applicability of these tools to membrane proteins is limited. Stopped-flow spectroscopy remains the most common technique in this area. Unfortunately, the data obtained in this way provide only global information, and details of the structural changes remain hidden. Engineered fluorescence tags³⁰ or spin labels³¹⁻³³ can offer additional insights. Nonetheless, there remains a need to establish robust techniques capable of monitoring the kinetics of membrane protein structural changes in a spatially resolved fashion.

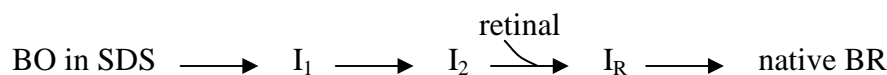
Covalent labeling of amino acid side chains in combination with mass spectrometry (MS) provides an interesting approach for examining protein conformations and interactions.

Exposure to a hydrophilic labeling agent induces modifications at solvent-accessible sites, whereas buried residues are protected. MS-based peptide mapping can then be used to determine the locations and the extent of labeling, thereby providing structural information.^{34, 35} Hydroxyl radical ($\cdot\text{OH}$) is a widely used covalent probe that can induce oxidative modifications (typically +16 Da)³⁶⁻³⁸ at accessible side chains. This oxidative labeling strategy has been applied for monitoring conformational changes and ligand binding of several membrane proteins under equilibrium conditions.³⁹⁻⁴² Hydroxyl radical may be formed in different ways,³⁶ e.g., by using an excimer laser for the photolysis of H_2O_2 . This approach makes it possible to generate very brief ($\sim 1 \mu\text{s}$) "bursts" of $\cdot\text{OH}$.³⁷ The ensuing labeling pulses are suitable for characterizing short-lived folding intermediates in rapid-mixing or temperature-jump experiments.⁴³ The feasibility of this approach has been demonstrated for several water-soluble proteins.⁴⁴⁻⁴⁷ Here we report the first application of pulsed $\cdot\text{OH}$ labeling for millisecond time-resolved folding studies on the membrane protein Bacteriorhodopsin (BR).

BR represents the main component of the *Halobacterium salinarum* purple membrane. A considerable number of studies have focused on the BR photocycle and its associated proton transfer events.⁴⁸⁻⁵⁰ Even more important in the context of the current work is the role of BR as a model system for *in vitro* folding experiments.^{8, 13, 51-53} BR refolding typically starts from the SDS-denatured state. SDS solubilizes the protein in monomeric form, concomitant with hydrolysis of the Schiff base linkage and retinal loss.^{54, 55} The retinal-free protein is referred to as Bacterioopsin (BO). Mixing of SDS-denatured BO with bicelles or vesicles in the presence of free retinal regenerates native BR monomers.¹³ The

kinetic mechanism of this process has been explored by stopped-flow fluorescence,⁵⁶ CD,⁵⁷ UV-Vis spectroscopy,^{51, 58} and by mutational analyses.⁵⁹ Those studies culminated in a proposed kinetic folding mechanism that may be summarized as⁵¹

<Scheme 1>



where I_1 and I_2 denote retinal-free intermediates. Interactions with retinal start to take place once I_2 is formed, whereas the earlier conformational changes proceed independently of the chromophore.^{51, 56-59} I_R represents a noncovalent protein-retinal complex.^{13, 54, 60} Formation of the Schiff base linkage ultimately yields native BR.^{51, 56}

Developing a reaction scheme for the BR refolding process has been a big step forward.^{51, 56-59} Nonetheless, many aspects remain incompletely understood. Most importantly, it has not been possible yet to conduct an in-depth structural characterization of the various intermediates. Even the structural feature of the SDS-denatured state is not clear. Also, the time scale of I_1 formation (milliseconds vs. seconds) remains a matter of debate.^{59, 61, 62} While <Scheme 1> includes only a single noncovalently bound I_R species,⁵¹ the involvement of two sequential I_R forms has been proposed on the basis of biphasic retinal binding data.^{13, 54, 62} More recently, it has been suggested that two spectroscopically distinct I_R intermediates become populated in parallel, rather than sequentially.⁵⁶

In the previous work (Chapter-3), combining covalent labeling with site-directed

mutagenesis and spectroscopic measurements, we proposed a detailed structural model of SDS-denatured state (Figure 3-6B). SDS exposure induces helices A and D largely unfolded and most likely extruded from the residual core. Met residues in these helices (M20 and M118) become solvent-accessible in SDS state, whereas they are protected in native BR. Nonetheless, the SDS-denatured protein retains significant structure, with a central region that remains inaccessible to water, and with partially intact helices B, C, E, F, and G. It is consistent with CD measurements that suggest a helical content of 42% for BO in SDS, down from the native value of 74%.⁵⁷ After figuring out the structural feature of the starting point of BR refolding, the aim of the current study is to gain additional insights into the structural changes that accompany the BR folding. By exposing the protein to ·OH labeling pulses at selected time points during the folding reaction it is possible to track which of its 9 Met residues undergo time-dependent changes in solvent accessibility. Comparative measurements with and without retinal reveal which of the structural changes are associated with cofactor binding. By complementing covalent labeling with stopped-flow measurements it becomes possible to establish links between time-dependent changes in Met accessibility, Trp fluorescence, and retinal UV-Vis absorption.

4.2 Experimental

4.2.1 Materials and Sample Preparation

Purple membranes from *Halobacterium salinarum* were harvested and purified by sucrose gradient centrifugation as described in Chapter-2. Sequencing-grade modified trypsin was purchased from Promega (Madison, WI). RapiGest SF was obtained from Waters (Milford,

MA). SDS, ammonium bicarbonate, sodium phosphate, potassium phosphate, formic acid, NATA and all-*trans*-retinal were from Sigma (St. Louis, MO). DMPC was obtained from Avanti (Alabaster, AL) and CHAPS was from Calbiochem (San Diego, CA). All chemicals were used as received, and all measurements were conducted at room temperature.

Delipidated BO in SDS was prepared following established procedures with minor modifications.^{62, 63} Briefly, 20 μL of purple membrane stock suspension were added to 400 μL chloroform/methanol/triethylamine (100:80:1 v/v/v), followed by sonication and vortex mixing for 30 minutes to facilitate Schiff base hydrolysis and retinal dissociation. Addition of buffer (50 mM sodium phosphate at pH 6, unless noted otherwise) in a 1:1 volume ratio followed by 10 seconds of vortex mixing resulted in phase separation. Delipidated BO was recovered as a precipitate at the interface after centrifugation at 13,000 g for 5 minutes. Phase separation and protein recovery were repeated twice. The delipidated BO precipitate was dissolved in buffer containing 5% w/v SDS using vortex mixing and sonication for 30 minutes. The resulting solution was then diluted to 0.2% SDS with buffer, followed by 30 minutes of vortexing and sonication. After subsequent centrifugation to remove any insoluble material, the SDS-solubilized BO was dialyzed twice against 3 L buffer containing 0.2% SDS to remove residual organic solvent. UV absorption measurements confirmed the absence of retinal after this procedure. The BO concentration in the resulting samples was on the order of 20 μM , determined based on a molar absorption coefficient of $\epsilon_{280} = 65,000 \text{ M}^{-1} \text{ cm}^{-1}$.¹³ Refolding buffer was prepared by sonicating 2% DMPC and 2% CHAPS (w/v) in phosphate buffer (pH 6) for 30 minutes as described previously.⁶²

4.2.2 Stopped-flow Spectroscopy

Stopped-flow measurements were conducted on a Biologic SFM 300 (Molecular Kinetics, Indianapolis, IN) system employing 2-syringe mixing in a 1:1 volume ratio. Syringe 1 contained refolding buffer, and syringe 2 contained 6 μM SDS-denatured BO as well as 30 mM glutamine. The latter was added to maintain consistency with the oxidative labeling conditions (see below). For experiments yielding refolded BR, 1.3 mole equivalents all-*trans*-retinal in ethanol were added to syringe 2 prior to mixing with refolding buffer. The final reaction mixture contained 3 μM protein, 1% DMPC, 1% CHAPS, 0.1% SDS, 15 mM glutamine, and less than 0.2% (v/v) ethanol. For NATA control experiments, the protein in syringe 2 was replaced by 50 μM NATA. Stopped-flow absorption spectra were collected using a photodiode array detector, with a diode wavelength separation of 3 nm. Water was used as baseline reference. Spectra were collected every 60 ms for the first 6 s, every 0.5 s from 6 s to 56 s, every 1 s from 56 s to 600 s. The integration time was 20 ms in all cases, and the observation cell had a 1 cm path length. Stopped-flow fluorescence measurements were performed using a Biologic MOS-250 module, using a 1 ms integration time per data point for the first 10 ms of the reaction. Longer integration times were used for later data points. Tryptophan excitation was at 280 nm with 5 nm bandwidth, and fluorescence was recorded at 340 nm with 20 nm bandwidth.

4.2.3 Continuous-Flow Mixing and Oxidative Labeling

Folding experiments with pulsed oxidative labeling were performed using a custom built two-syringe continuous-flow device described previously.⁴⁴ The contents of syringes 1 and 2 were the same as for the stopped-flow measurements above, except that the protein

concentration in syringe 2 was 20 μM , while maintaining a retinal:protein molar ratio of 1.3. Also, 0.24% (v/v) H_2O_2 was added to syringe 1. Both syringes were advanced at 60 $\mu\text{L min}^{-1}$ simultaneously by using a syringe pump (Harvard Apparatus, Boston, MA). Folding was initiated at a custom-built mixer⁴⁴ that was connected to a reaction capillary with an i.d. of 100 μm . The average reaction time is proportional to the distance traveled by the solution downstream of the mixer. A pulsed KrF excimer laser (GAM EX 100/125, Orlando, FL) operated at 48 Hz and 62 mJ pulse⁻¹ was used to generate $\cdot\text{OH}$ by photolysis of H_2O_2 . Approximately 35% of the total protein in the reaction capillary was irradiated, estimated on the basis of a laminar flow approximation.⁶⁴ Glutamine in the reaction mixture acts as radical scavenger that reduces the duration of the covalent labeling pulse to $\sim 1 \mu\text{s}$.³⁷ The condition was chosen to eliminate oxidation-induced structural artifacts.⁶⁵ Pulsed labeling was performed at selected folding time points (20 ms to 10 s) by irradiating the protein at specific positions along the reaction capillary. The mixer performance was verified optically.²⁸ Mixing efficiency were also confirmed by labeling fully refolded BR at different capillary positions. Experiments for a reaction time of "zero", corresponding to SDS-denatured protein prior to initiation of folding, were conducted by omitting DMPC/CHAPS and retinal from the mixing experiment. Measurements corresponding to a reaction time of one day were conducted using manual mixing; for this purpose refolded BR and BO samples were equilibrated for one day in the dark. Two-syringe mixing was employed for the latter samples similar to the procedure outlined above, ensuring that the composition of the final mixture was identical to all other time points.

4.2.4 Peptide Mapping and Quantification of Oxidative Labeling

120 μL aliquots of capillary outflow were collected in microcentrifuge tubes containing 10 μL of 2 μM catalase and 10 μL of 200 mM methionine amide at pH 7 for deactivation of residual H_2O_2 .⁶⁶ For $t = 0$ samples, the collection vials contained 25 μL of 2 μM catalase, 10 μL of 200 mM methionine amide and 350 μL water, to ensure catalase activity even in the presence of elevated amounts of SDS. Labeled samples and unlabeled controls were lyophilized. Subsequently, the dry powder was dissolved in 50 μL of 50 mM ammonium bicarbonate buffer (pH 8) containing 0.2% (w/v) of the acid-labile surfactant RapiGest. The resulting solutions were digested with trypsin for 24 h at 40 °C using a 1:10 (w/w) enzyme: protein ratio. Only for $t = 0$ samples, 10 μL 1.0 M potassium phosphate buffer (pH 8) was added and the resulting SDS precipitate was removed by centrifugation. The supernatant was digested as for the other samples. Peptide analyses and oxidation level measurements by electrospray MS were performed as described previously in Chapter-3, using a Q-TOF Ultima API mass spectrometer (Waters, Milford, MA) and an Acquity UPLC system (Waters) with a C18 column. The identity of tryptic peptides, as well as those of MetO oxidation sites, was confirmed by MS/MS.

The oxidation behavior of Met residues in their corresponding tryptic peptides is reported as "fraction unmodified" (F_u). This value was calculated as $F_u = A_u / (A_{ox} + A_u)$, where A_u and A_{ox} are the integrated peak areas of the unmodified and the oxidized peptide, respectively. Protonated as well as sodiated ions were considered for this procedure. A background correction was performed for all data points. In Chapter 3, we used the notation F_u^{corr} to emphasize the fact that a background correction had been performed. The

superscript *corr* is omitted in this study to improve readability of the text.

4.3 Results and Discussion

4.3.1 Stopped-Flow Spectroscopy

BR was refolded by mixing of SDS-denatured BO, free retinal, and DMPC/CHAPS bicelles. The Trp fluorescence kinetics associated with regeneration of native BR exhibit a rapid rise with an apparent rate constant k_{app} of 250 s^{-1} . This is followed by a bi-exponential decay with k_{app} values of 0.16 s^{-1} and 0.027 s^{-1} (Figure 4-1a). The decrease in emission intensity can be attributed to retinal binding, which causes FRET quenching.^{51, 67} Refolding in the absence of retinal yields "native" BO (Figure 4-2b).⁵¹ Similar to the data of Figure 4-1a an initial rapid rise (175 s^{-1}) is seen under these conditions. The emission intensity in Figure 4-2b continues to grow in a bi-exponential fashion (0.28 s^{-1} , 0.1 s^{-1}), reflecting an increasingly nonpolar environment for one or more of the eight Trp residues.⁵¹

Based on observations very similar to those depicted in Figure 4-1, the presence of two apoprotein intermediates I_1 and I_2 on the BR folding pathway has previously been suggested (Scheme 1).⁵¹ It is well established that I_2 is generated on a time scale of a few seconds.^{51, 59} In contrast, the kinetics of the initial step are more controversial. Early work suggested that I_1 forms within ca. 1 s.^{61, 62} In later studies it was implied that this first intermediate might be formed on a much faster (millisecond) time scale,⁵⁹ which is more in line with the behavior of many water-soluble proteins.^{68, 69} Notably, the rapid initial rise ($k_{app} \approx 200 \text{ s}^{-1}$) observed for both BR and BO can *not* be taken as direct evidence of a rapid conformational

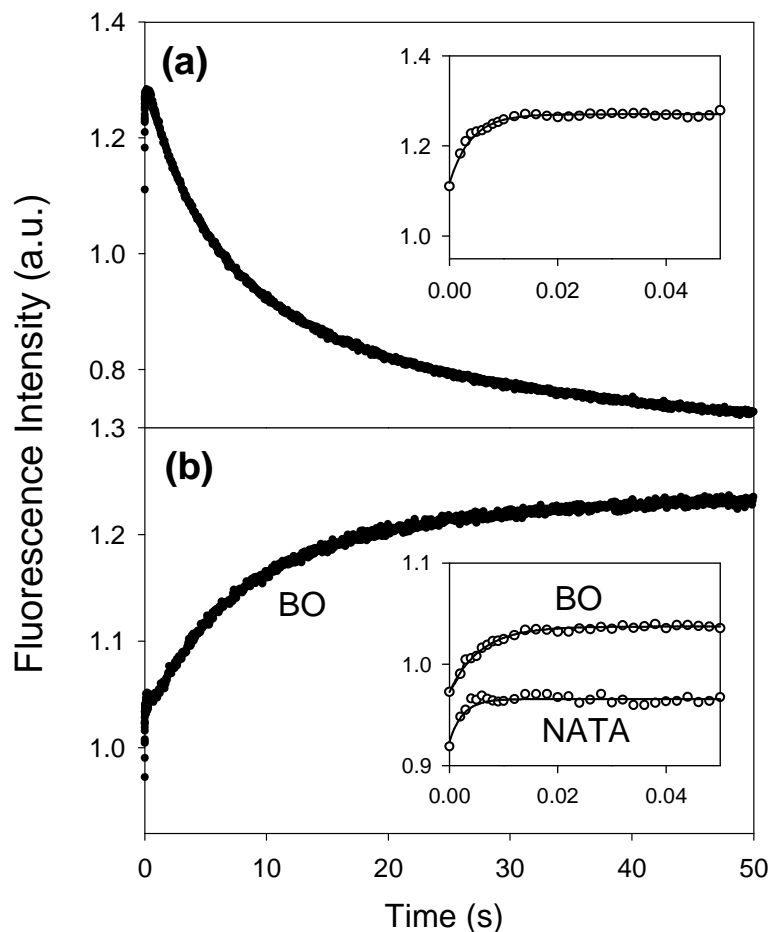


Figure 4-1. Stopped-flow Trp fluorescence kinetics acquired during protein folding in DMPC/CHAPS bicelles, with $\lambda_{ex} = 280$ nm, $\lambda_{em} = 340$ nm. (a) Folding of BR in the presence of retinal; (b) folding of BO in the absence of retinal. Insets show data for the initial 50 ms. Also included in (b) are data for mixing of NATA in SDS with refolding buffer. Exponential fitting of the protein folding kinetics yields apparent rate constants of (a) 250 s^{-1} , 0.16 s^{-1} , 0.027 s^{-1} ; (b) 175 s^{-1} ; 0.28 s^{-1} , 0.1 s^{-1} . For the NATA experiment an apparent rate constant of 350 s^{-1} is obtained.

change, because a similar feature is seen upon mixing bicelles with the Trp derivative NATA (Figure 4-1b, inset).⁵¹ Nonetheless, the fluorescence data of Figure 4-1 do not exclude the possibility of millisecond conformational changes during BR and BO refolding. We will return to this point when discussing ·OH labeling data (see below).

Additional insights into protein-retinal interactions can be obtained by tracking the UV-Vis absorption spectrum of the chromophore throughout the folding reaction (Figure 4-2a). Free retinal in DMPC/CHAPS exhibits an absorption maximum around 385 nm. After 10 s the retinal peak has shifted to ~399 nm, reflecting formation of the noncovalent protein-retinal complex I_R . The appearance of a strongly red-shifted band with λ_{max} around 560 nm commences on a much slower time scale (tens of seconds to minutes), indicative of Schiff base formation between retinal and K216.⁷⁰

UV-Vis kinetic traces for three selected wavelengths are depicted in Figure 4-2b. The disappearance of free retinal is represented by a decreasing absorption at 382 nm. The rise and subsequent fall at 439 nm reflects the formation and decay of at least one noncovalent I_R intermediate, whereas the slow rise at 559 nm is associated with native BR formation. The kinetics of these absorbance changes are well described by bi-exponential fits with k_{app} values on the order of 0.1 s^{-1} and 0.006 s^{-1} (see caption of Figure 4-2 for details). A close-up view of the spectroscopic traces confirms that the initial ~0.5 s of BR folding occur without retinal participation (Figure 4-3). Following this initial lag phase, I_R formation is evident from the absorption increase at 439 nm between 0.5 s and 10 s (Figure 4-3b). Simultaneously, noncovalent protein-retinal interactions lead to quenching of the Trp

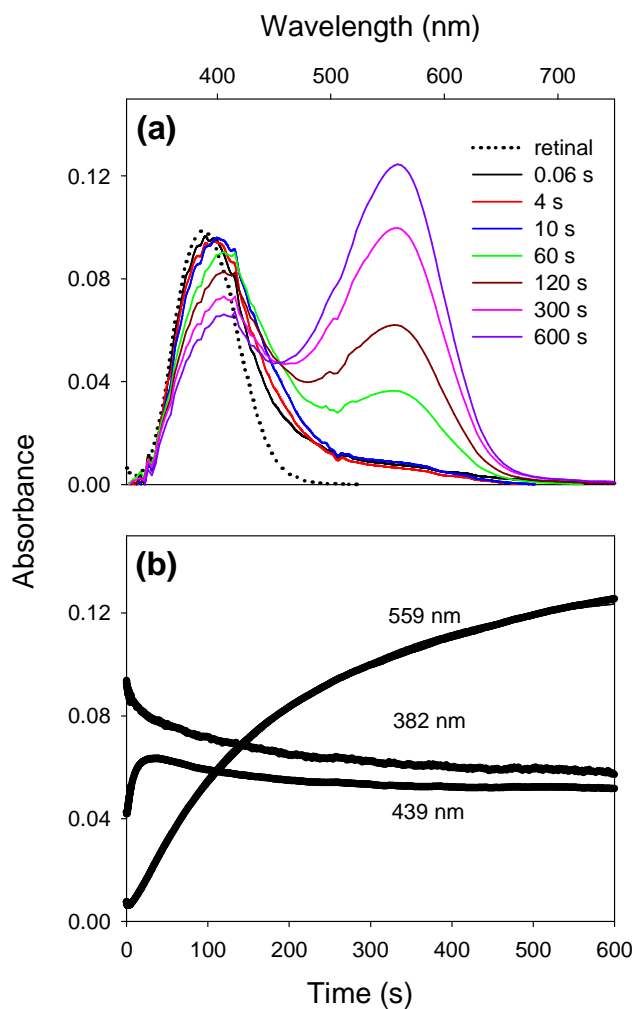


Figure 4-2. (a) Stopped-flow UV-Vis absorption spectra, collected during protein refolding in the presence of retinal. Also included is the spectrum of free retinal in the same solvent as the protein after mixing. (b) Kinetic absorption changes at three selected wavelengths. Exponential fitting yields the following apparent rate constants: 382 nm, 0.09 s^{-1} and 0.006 s^{-1} ; 439 nm, 0.11 s^{-1} and 0.008 s^{-1} ; 559 nm, 0.1 s^{-1} and 0.005 s^{-1} .

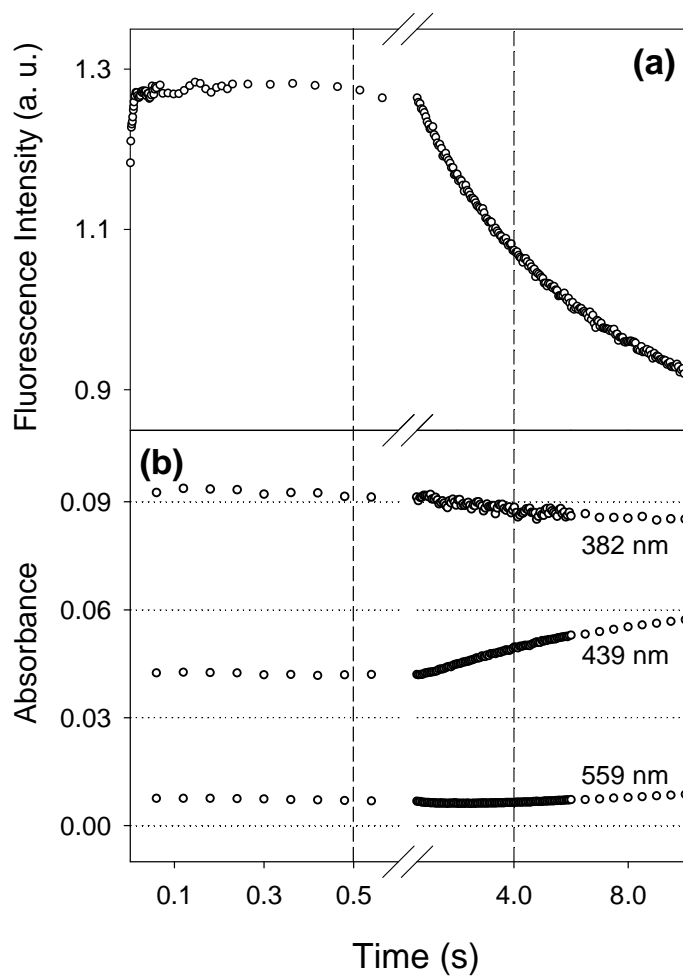


Figure 4-3. Close-up view of the initial 10 s during BR refolding, monitored by (a) stopped-flow Trp fluorescence and (b) UV-Vis absorption spectroscopy. Vertical dashed lines highlight reaction times of 0.5 s and 4 s. Note that the time axis is not linear.

emission (Figure 4-3a), implying that the retinal moves relatively close to its native position in the binding pocket.

The spectroscopic data depicted here, as well as the interpretations offered here are consistent with previous reports.^{51, 56-59} The primary purpose of including these optical measurements is to allow a side-by-side comparison with the ·OH labeling data discussed in the following section.

4.3.2 Pulsed Oxidative Labeling

Earlier work (Chapter-2 and Chapter-3) has demonstrated that MetO formation at solvent accessible methionine side chains represents the dominant oxidation pathway for BR under ·OH labeling conditions. The nine methionines can be divided into three groups according to their oxidation behavior: (i) M32, M68, and M163 are located in solvent accessible loops. These residues undergo oxidative labeling both in native and in SDS-denatured BR; (ii) M56/60 (helix B), M145 (E), and M209 (G) are always protected, consistent with residual structure in the SDS state; (iii) M20 (A) and M118 (D) are solvent accessible in SDS, but not in native BR. The locations of all nine methionines are highlighted in Figure 3-1. Wild-type BR does not possess Met residues in helices C and F, but site-directed mutagenesis was employed to probe the behavior of these regions in Chapter-3. It was found that methionines introduced into helices C and F behaved just as those of group *ii*, i.e., they are always protected. These engineered protein variants therefore do not offer any additional perspective for the kinetic studies conducted here, and wild-type protein was chosen for the current work.

Oxidative labeling was performed by exposing BR to a $\sim 1 \mu\text{s}$ $\cdot\text{OH}$ pulse at various time points during refolding, using a custom built continuous-flow mixing device.^{44, 45} The short duration of the labeling event ensures that oxidation-induced structural artifacts are negligible.^{37, 65} The labeling behavior of individual Met residues in BR can be tracked by monitoring proteolytic peptides that are generated by trypsin digestion after $\cdot\text{OH}$ exposure. This procedure yields a total of thirteen tryptic peptides, referred to as T1 to T13 as shown in Figure 2-2. Examples of unprocessed MS data are depicted in Figure 4-4. Peptide T1 reports on the labeling behavior of M20. A high level of oxidation occurs in the SDS state ($t = 0$ ms, Figure 4-4a), evident from the a strong T1+16 signal which reflects MetO formation at M20. The intensity of T1+16 drops to background levels within 20 ms (Figure 4-4b). A very different behavior is seen for T5 (M118), where pronounced MetO formation persists for much longer reaction times (Figure 4-4, f-h). The intensity of the corresponding T5+16 signal decreases to background levels only after several seconds (Figure 4-4i). The MS signals of several peptides show sodium adduction (such as T5+Na, Figure 4-4, f-j). These adducts are a common occurrence in electrospray MS, and their inclusion for quantitative data analyses is straightforward.

It is customary to report the extent of oxidative labeling as "fraction unmodified", F_u . Protected Met residues do not undergo oxidation, and hence these sites are characterized by $F_u \approx 1$. In contrast, solvent accessible methionines show significantly lower F_u values. For the conditions used here *ca.* 35% of the protein molecules in the reaction mixture undergo $\cdot\text{OH}$ exposure.⁶⁴ This implies that F_u values around 0.65 are expected for Met residues that

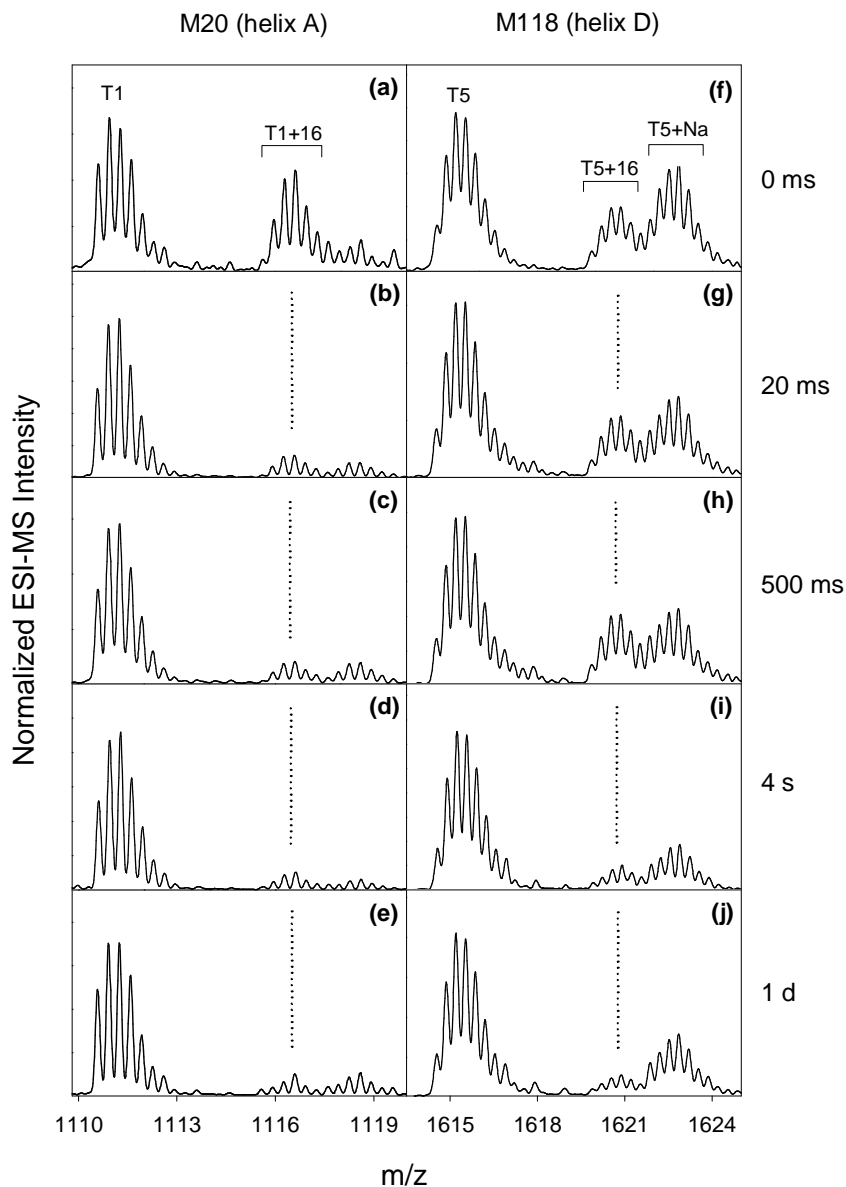


Figure 4-4. ESI mass spectra of tryptic peptides T1 (M20, helix A, panels a-e) and T5 (M118, helix D, panels f-j) obtained after pulsed $\cdot\text{OH}$ labeling at different time points during BR folding. Labeling time points are denoted along the right hand side. Dotted vertical lines were included to highlight the temporal changes of the T1+16 and T5+16 oxidation products. All peptide ions are triply charged.

are completely solvent accessible. Temporal F_u profiles were generated for all nine Met residues. It turns out that the nine Met residues can be grouped into 3 categories: *i.*) M56/60 (B), M145 (E), and M209 (G) (shown in blue in Figure 4-5I) are completely protected throughout the entire reaction. *ii.*) the loop residues M32, M68, and M163 (shown in red in Figure 4-5I) remain exposed during the folding. F_u plots M145 and M163 are exemplified (Figure 4-5II, a). These data provide an important control, confirming that the \cdot OH labeling conditions before and after mixing are not affected by differential radical scavenging. *iii.*) M20 and M118 (shown in orange in Figure 4-5I) undergo changes of solvent accessibility during the folding reaction. M20 of helix A is fully exposed only at $t = 0$, and complete protection is achieved within 20 ms (Figure 4-5II, b). Helix D exhibits a different behavior as evidenced by the behavior of M118, which only becomes protected after 4 s (Figure 4-5II, c). The degree of solvent exposure at $t = 0$ is slightly lower for M118 ($F_u = 0.73$) than for M20 ($F_u = 0.62$). This finding is consistent with earlier results obtained under equilibrium conditions (Chapter-3).

Oxidative labeling experiments analogous to those just described were also conducted in the absence of retinal. For the most part, the resulting BO folding data are very similar to those for BR. The only notable difference is the behavior of M118 in helix D (Figure 4-5II, f), which retains extensive solvent exposure throughout the entire reaction.

4.3.3 Implications for the BR Folding Mechanisms

The \cdot OH labeling data of this work provide evidence of a rapid conformational change during BR folding that goes to completion within 20 ms (Figure 4-5II, b). This rapid

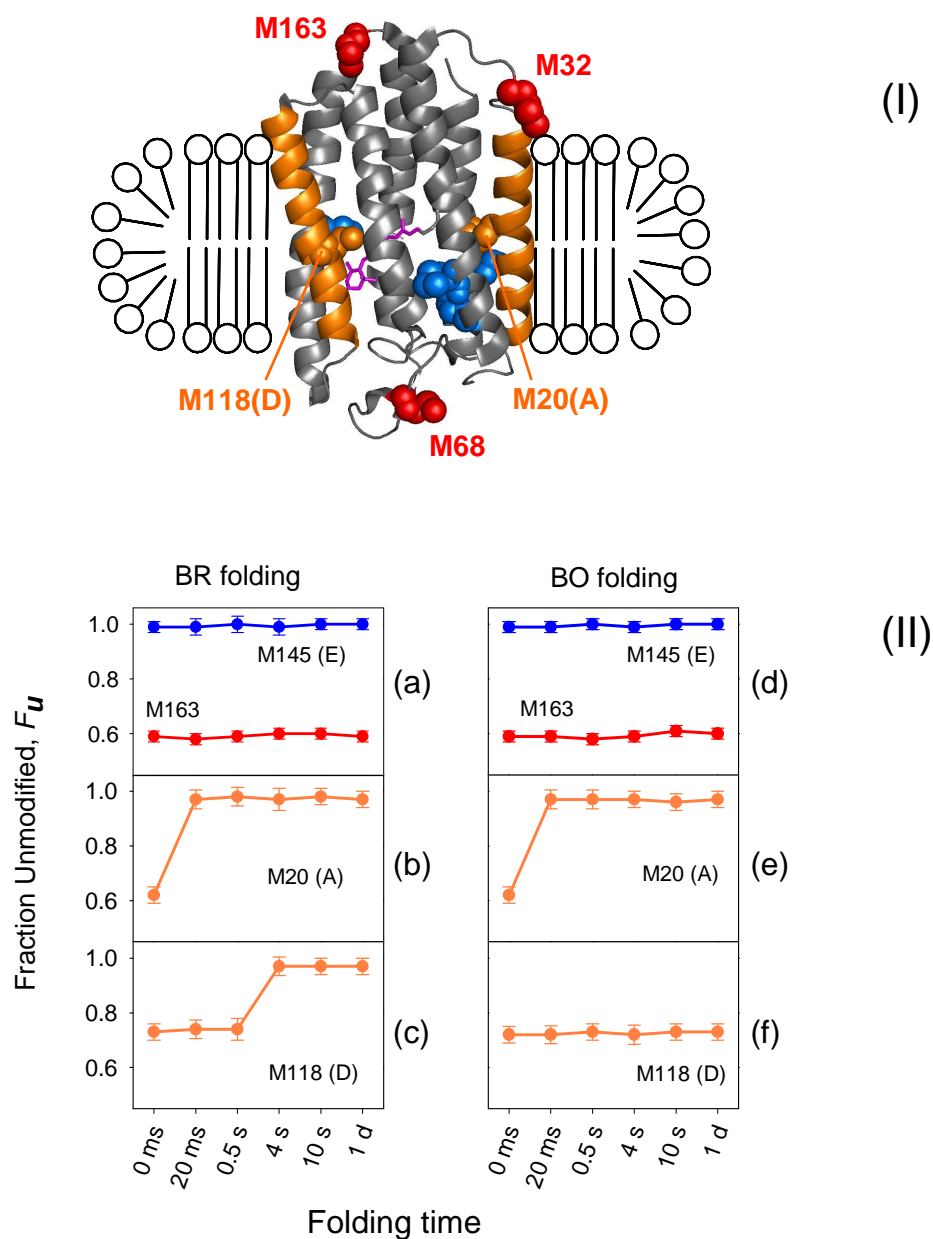


Figure 4-5. (I) Schematic of refolded BR in bicelles. Methionines located in loops are depicted in red; M56, M60, M145 and M209 are in blue; M20, M118 and their locations (helices A and D) are shown in orange. Retinal is in purple sticks. (II) Pulsed $\cdot\text{OH}$ labeling behavior of selected Met residues for BR folding or BO folding (without retinal). The extent of oxidation is expressed as "fraction unmodified" (F_u). Each data point represents the average of three independent experiments. Error bars indicate standard deviations.

structural transition leads to complete protection of the initially solvent-exposed M20. The most likely explanation of this event is folding of helix A from its largely disordered SDS conformation. This step is consistent with formation of an early intermediate I_1 in Scheme 1.⁵⁹ Observation of virtually the same M20 labeling kinetics with and without retinal (Figure 4-5II, e) confirms that this initial step is not affected by interactions with the cofactor. The transition from I_1 to I_2 is not associated with changes in Met solvent accessibility. However, the occurrence of this step is evident from a slow fluorescence increase for BO (Figure 4-1b), reflecting alterations in the Trp surroundings towards a more nonpolar environment.⁵¹

In the presence of retinal, formation of I_2 is immediately followed by noncovalent binding of the cofactor to yield I_R , concomitant with emission quenching as well as an absorption rise at 439 nm. It is evident from Figure 4-3 that this process extends over at least 10 s. Interaction of retinal with the protein also triggers the transition of M118 from a solvent accessible to a protected orientation, an event that goes to completion within only 4 s (Figure 4-5II, c). The transition is attributable to folding of helix D. In the absence of retinal (BO folding) this transition does not take place. While this step is dependent on the presence of retinal, it does not require formation of the Schiff base which occurs on a much slower time scale. Notably, ·OH labeling reveals *complete* protection for M118 after 4 s, whereas spectroscopic changes are *still ongoing* at $t = 4$ s (Figure 3-4). In other words, not all the events associated with formation of I_R occur with the same kinetics, implying that an additional kinetic intermediate must be involved.¹⁸ Thus, our data reveal the existence of an "early" and a "late" form of I_R . These two forms will be referred to as I_R^* ($t \approx 4$ s) and I_R^{**}

($t \approx 10$ s), respectively. Similar proposals were put forward earlier on the basis of UV-Vis measurements.^{13, 54, 62}

It is interesting to speculate on the structural features of I_R^* . In native BR the retinal ionone ring interacts with. It has been suggested that this interaction represents a key stabilizing feature of helix D,^{70, 71} along with contacts between D and C, E.⁷² M118 is no longer solvent accessible in I_R^* , suggesting that interactions between this residue and the ionone ring have been established. At the same time, the retinal orientation within the binding pocket remains very much non-native (evident from incomplete Trp quenching, Figure 4-3, $t = 4$ s). A scenario that might account for these observations is that in I_R^* the ionone ring is in close proximity to M118, while the hydrophilic aldehyde group remains in contact with solvent water. Such a situation is in line with the expectation that retinal insertion into the binding pocket should start with the most hydrophobic part (the ionone ring), whereas the least hydrophobic part (the aldehyde group) will be buried last. Such an arrangement should be possible if the retinal were placed close to (and roughly parallel to) helix D, with its aldehyde group protruding into the aqueous environment. The retinal entry point into the binding pocket remains a matter of debate.^{73, 74} Considering the linear dimensions of retinal and its positioning in native BR (Figure 3-1), our proposed I_R^* structure is compatible with entry from the extracellular side. Clearly, further evidence is needed to confirm the suggestions made in the paragraph regarding the retinal orientation in the I_R^* intermediate.

The transition from I_R^* to I_R^{**} is associated with a further drop in fluorescence intensity during the 4 s \rightarrow 10 s time interval (Figure 4-3a). This implies that the retinal moves

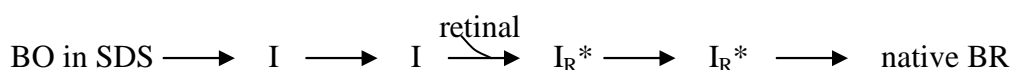
towards its native position during this phase. W86, W138, W182, and W189 are in close spatial contact with the retinal in native BR as shown in Figure 3-1B, and hence quenching of these four residues will be chiefly responsible for the declining emission level during the step from I_R^* to I_R^{**} . Ultimately, formation of the Schiff-base linkage on a time scale of several minutes leads to native BR. As noted earlier, this final step is associated with an absorption increase at 559 nm (Figure 4-2).

4.4 Conclusions

This work used pulsed $\cdot\text{OH}$ labeling with MS detection, in combination with stopped-flow spectroscopy for probing structural changes during BR folding. The characterization of short-lived conformers by oxidative labeling has previously been demonstrated for soluble proteins,⁴⁴⁻⁴⁷ whereas the extension of this approach to membrane proteins in this study is new. The optical data presented here are in agreement with previous investigations,^{51, 57-59} while time-resolved information on the solvent accessibility of individual Met residues provides additional perspectives.

<Scheme 1> remains a useful framework for describing the overall structural changes associated with BR folding and retinal binding. Similar to earlier work,^{13, 54, 62} however, our data present evidence of an "early" and a "late" form of I_R . A modified minimal reaction scheme for the folding of BR can therefore be expressed as follows:

<Scheme 2>



The transition from SDS-denatured BO to an initial intermediate I_1 goes to completion within 20 ms. This process involves formation of helix A, while helix D remains disordered. It is likely that formation of I_1 occurs simultaneously with BO insertion into the bicelle, as envisioned by some membrane protein folding models.^{5, 23-25} Formation of I_2 occurs more slowly, on the order of several seconds. This transition involves consolidation of the protein structure, leading to an increasingly hydrophobic environment for several Trp residues. Noncovalent binding of retinal takes place once I_2 is formed, inducing the folding of helix D. The intermediate generated in this way is indicated as I_R^* in Scheme 2. The ~4 s time scale of helix D formation observed here is consistent with a 0.33 s^{-1} phase that has previously been observed for this step in fluorescence tagging experiments.³⁰ I_R^* may represent a state where the retinal has entered its binding pocket "head first" from the extracellular side, such that the ionone ring interacts with M118 while the aldehyde tail remains in contact with the aqueous environment. As the retinal then settles further into the pocket (evident from ongoing UV-Vis spectral changes and enhanced Trp quenching), the final intermediate I_R^{**} is generated. I_R^{**} formation goes to completion within ~10 s. Establishment of the covalent linkage between the retinal aldehyde group and Lys216 occurs on a time scale of minutes, resulting in native BR.

A sequential folding pathway as in <Scheme 2> is consistent with earlier investigations,^{51, 57-59} and it is also supported by recent time-resolved spin labeling experiments.³³ Nonetheless, the occurrence of parallel events as suggested in some studies^{59, 75} cannot be ruled out. The retinal binding mechanism observed here may be different from the processes occurring during BR reconstitution from apomembrane.⁷² While our *in vitro* data

provide some evidence for retinal entry from the extracellular side, such a scenario is unlikely to occur *in vivo* considering that retinal is produced intracellularly.

It is emphasized that <Scheme 2> should still be considered a *minimal* model. Structural changes in addition to those discussed here are likely required to bring about the overall transition from SDS-denatured BO to native BR. Also, slow (tens of minutes) changes may occur after BR formation as the chromophore equilibrates into the dark-adapted state.^{59, 75,}

⁷⁶ One point that remains somewhat unclear is whether the earliest intermediate detected in our experiments is entirely equivalent to the "I₁" species proposed by Booth and coworkers.^{51, 59}

Overall, this study demonstrates how pulsed covalent labeling can provide mechanistic insights into kinetic folding transitions of membrane proteins. The information obtained in this way is complementary to data obtained by classical stopped-flow spectroscopy. It is hoped that this multi-pronged strategy will also be applicable to other membrane protein systems, thereby narrowing the existing knowledge gap in this area.

4.5 References

- (1) Sander, C. R.; Myer, J. K. *Annu. Rev. Biophys. Biomol. Struct.* **2004**, *33*, 25-51.
- (2) Hartl, F. U.; Hayer-Hartl, M. *Nat. Struct. Mol. Biol.* **2009**, *16*, 574-581.
- (3) Fersht, A. R. *Nat. Rev. Mol. Cell Biol.* **2008**, *9*, 650-654.
- (4) Service, R. F. *Science* **2008**, *321*, 784-786.
- (5) MacKenzie, K. R. *Chem. Rev.* **2006**, *106*, 1931-1977.
- (6) Bowie, J. U. *Nature* **2005**, *438*, 581-589.
- (7) Lee, J. K.; Stroud, R. M. *Curr. Opin. Struct. Biol.* **2010**, *20*, 464-470.
- (8) Joh, N. H.; Min, A.; Faham, S.; Whitelegge, J. P.; Yang, D.; Woods, V. L.; Bowie, J. U. *Nature* **2008**, *453*, 1266-1270.
- (9) Lorch, M.; Booth, P. J. *J. Mol. Biol.* **2004**, *344*, 1109-1121.
- (10) Schleich, J. P.; Kim, M.; Joh, N. H.; Bowie, J. U.; Park, C. *J. Mol. Biol.* **2010**, *406*, 545-551.
- (11) Sanders, C. R.; Prosser, R. S. *Structure* **1998**, *6*, 1227-1234.
- (12) Dencher, N. A. *Biochemistry* **1986**, *25*, 1195-1200.
- (13) Huang, K.; Bayley, H.; Liao, M.; London, E.; Khorana, H. G. *J. Biol. Chem.* **1981**, *256*, 3802-3809.
- (14) Surrey, T.; Jahnig, F. *Proc. Natl. Acad. Sci. U.S.A.* **1992**, *89*, 7457-7461.
- (15) Otzen, D. E. *J. Mol. Biol.* **2003**, *330*, 641-649.
- (16) Lau, F. W.; Bowie, J. U. *Biochem.* **1997**, *36*, 5884-5892.
- (17) Horn, R.; Paulsen, H. *J. Mol. Biol.* **2002**, *318*, 547-556.
- (18) Fersht, A. R. *Structure and Mechanism in Protein Science*; W. H. Freeman & Co.: New York, 1999.
- (19) Hong, H.; Tamm, L. K. *Proc. Natl. Acad. Sci. U.S.A.* **2004**, *101*, 4065-4070.
- (20) Curnow, P.; Booth, P. J. *Proc. Natl. Acad. Sci. U.S.A.* **2007**, *104*, 18970-18975.
- (21) Huysmans, G. H. M.; Baldwin, S. A.; Brockwell, D. J.; Radford, S. E. *Proc. Natl. Acad. Sci. U.S.A.* **2010**, *107*, 4099-4104.
- (22) Otzen, D. E. *Protein Eng. Des. Sel.* **2011**, *24*, 139-149.
- (23) Popot, J.-L.; Engelman, D. M. *Biochemistry* **1990**, *29*, 4031-4037.
- (24) Engelman, D. M.; Chen, Y.; Chin, C. N.; Curran, A. R.; Dixon, A. M.; Dupuy, A. D.; Lee, A. S.; Lehnert, U.; Matthews, E. E.; Reshetnyak, Y. K.; Senes, A.; Popot, J. L. *FEBS Lett.* **2003**, *555*, 122-125.
- (25) White, S. H.; Wimley, W. C. *Annu. Rev. Biophys. Biomol. Struct.* **1999**, *28*, 319-365.
- (26) Klein-Seetharaman, J. *Trends Pharmacol. Sci.* **2005**, *26*, 183-189.
- (27) Gianni, S.; Ivarsson, Y.; Jemth, P.; Brunori, M.; Travaglini-Allocatelli, C. *Biophys.*

- Chem.* **2007**, *128*, 105-113.
- (28) Uzawa, T.; Nishimura, C.; Akiyama, S.; Ishimori, K.; Takahashi, S.; Dyson, H. J.; Wright, P. E. *Proc. Natl. Acad. Sci. U.S.A.* **2008**, *105*, 13859-13864.
- (29) Bartlett, A. I.; Radford, S. E. *Nat. Struct. Mol. Biol.* **2009**, *16*, 582-588.
- (30) Compton, E. L. R.; Farmer, N. A.; Lorch, M.; Mason, J. M.; Moreton, K. M.; Booth, P. J. *J. Mol. Biol.* **2006**, *357*, 325-338.
- (31) Dockter, C.; Volkov, A.; Bauer, C.; Polyhach, Y.; Joly-Lopez, Z.; Jeschke, G.; Paulsen, H. *Proc. Natl. Acad. Sci. U.S.A.* **2009**, *106*, 18485-18490.
- (32) Volkov, A.; Dockter, C.; Polyhach, Y.; Paulsen, H.; Jeschke, G. *J. Phys. Chem. Lett.* **2010**, *1*, 663-667.
- (33) Krishnamani, V.; Lanyi, J. K. *Biophys. J.* **2011**, *100*, 1559-1567.
- (34) Mendoza, V. L.; Vachet, R. W. *Mass Spectrom. Rev.* **2009**, *28*, 785-815.
- (35) Weinglass, A. B. In *Protein Mass Spectrometry*; Whitelegge, J. P., Ed.; Elsevier: Amsterdam, 2009; Vol. 52, pp 197-212.
- (36) Xu, G.; Chance, M. R. *Chem. Rev.* **2007**, *107*, 3514-3543.
- (37) Hambly, D. M.; Gross, M. L. *J. Am. Soc. Mass Spectrom.* **2005**, *16*, 2057-2063.
- (38) Sharp, J. S.; Becker, J. M.; Hettich, R. L. *Anal. Chem.* **2004**, *76*, 672-683.
- (39) Orban, T.; Gupta, S.; Palczewski, K.; Chance, M. R. *Biochemistry* **2010**, *49*, 827-834.
- (40) Li, C.; Takazaki, S.; Jin, X.; Kang, D.; Abe, H.; Hamasaki, N. *Biochemistry* **2006**, *45*, 12117-12124.
- (41) Zhu, Y.; Guo, T.; Park, J.-H.; Li, X.; Meng, W.; Datta, A.; Bern, M.; Lim, S. K.; Sze, S. K. *Mol. Cell. Proteomics* **2009**, *8*, 1999-2010.
- (42) Smedley, J. G.; Sharp, J. S.; Kuhn, J. F.; Tomer, K. B. *Biochemistry* **2008**, *47*, 10694-10704.
- (43) Gruebele, M. *Nature* **2010**, *468*, 640-641.
- (44) Stocks, B. B.; Konermann, L. *Anal. Chem.* **2009**, *81*, 20-27.
- (45) Stocks, B. B.; Konermann, L. *J. Mol. Biol.* **2010**, *398*, 362-373.
- (46) Chen, J.; Rempel, D. L.; Gross, M. L. *J. Am. Chem. Soc.* **2010**, *132*, 15502-15504.
- (47) Kiselar, J. G.; Chance, M. R. *J. Mass Spectrom.* **2010**, *45*, 1373-1382.
- (48) Lanyi, J. K. *Annu. Rev. Physiol.* **2004**, *66*, 665-688.
- (49) Subramaniam, S.; Hirai, T.; Henderson, R. *Phil. Trans. R. Soc. Lond. A* **2002**, *360*, 859-874.
- (50) Haupts, U.; Tittor, J.; Oesterhelt, D. *Annu. Rev. Biophys. Biomol. Struct.* **1999**, *28*, 367-399.
- (51) Booth, P. J.; Fitsch, S. L.; Stern, L. J.; Greenhalgh, D. A.; Kim, P. S.; Khorana, H. G. *Nat. Struct. Biol.* **1995**, *2*, 139-143.
- (52) Booth, P. J.; Curnow, P. *Curr. Op. Struct. Biol.* **2009**, *19*, 8-13.

- (53) Kessler, M.; Gottschalk, K. E.; Janovjak, H.; Muller, D. J.; Gaub, H. E. *J. Mol. Biol.* **2006**, *357*, 644-654.
- (54) London, E.; Khorana, H. G. *J. Biol. Chem.* **1982**, *257*, 7003-7011.
- (55) Torres, J.; Sepulcre, F.; Padros, E. *Biochemistry* **1995**, *34*, 16320-16326.
- (56) Allen, S. J.; Curran, A. R.; Templer, R. H.; Meijberg, W.; Booth, P. J. *J. Mol. Biol.* **2004**, *342*, 1279-1291.
- (57) Riley, M. L.; Wallace, B. A.; Flitsch, S. L.; Booth, P. J. *Biochemistry* **1997**, *36*, 192-196.
- (58) Booth, P. J.; Farooq, A. *Eur. J. Biochem* **1997**, *246*, 674-680.
- (59) Lu, H.; Marti, T.; Booth, P. J. *J. Mol. Biol.* **2001**, *308*, 437-446.
- (60) Schreckenbach, T.; Walckhoff, B.; Oesterhelt, D. *Biochemistry* **1978**, *17*, 5353-5359.
- (61) Booth, P. J. *Folding & Design* **1997**, *2*, R85-R92.
- (62) Booth, P. J.; Farooq, A.; Flitsch, S. L. *Biochemistry* **1996**, *35*, 5902-5909.
- (63) Huang, K.; Bayley, H.; Khorana, H. G. *Proc. Natl. Acad. Sci. U.S.A.* **1980**, *77*, 323-327.
- (64) Konermann, L.; Stocks, B. B.; Czarny, T. *Anal. Chem.* **2010**, *82*, 6667-6674.
- (65) Gau, B. C.; Sharp, J. S.; Rempel, D. L.; Gross, M. L. *Anal. Chem.* **2009**, *81*, 6563-6571.
- (66) Xu, G.; Kiselar, J.; He, Q.; Chance, M. R. *Anal. Chem.* **2005**, *77*, 3029-3037.
- (67) Kalisky, O.; Feitelson, J.; Ottolenghi, M. *Biochemistry* **1981**, *20*, 203-209.
- (68) Yang, W. Y.; Gruebele, M. *Nature* **2003**, *423*, 193-197.
- (69) Roder, H.; Shastry, M. C. R. *Curr. Opin. Struct. Biol.* **1999**, *9*, 620-626.
- (70) Pan, Y.; Brown, L.; Konermann, L. *J. Mol. Biol.* **2009**, *394*, 968-981.
- (71) Grigorieff, N.; Ceska, T. A.; Downing, K. H.; Baldwin, J. M.; Henderson, R. *J. Mol. Biol.* **1996**, *259*, 393-421.
- (72) Rüdiger, M.; Tittor, M.; Gerwert, K.; Oesterhelt, D. *Biochemistry* **1997**, *36*, 4867-4874.
- (73) Isralewitz, B.; Izrailev, S.; Schulten, K. *Biophys. J.* **1997**, *73*, 2972-2979.
- (74) Schadel, S. A.; Heck, M.; Maretzki, D.; Filipek, S.; Teller, D. C.; Palczewski, K.; Hofmann, K. P. *J. Biol. Chem.* **2003**, *278*, 24896-24903.
- (75) Lu, H.; Booth, P. J. *J. Mol. Biol.* **2000**, *299*, 233-243.
- (76) Patzelt, H.; Simon, B.; terLaak, A.; Kessler, B.; Kühne, R.; Schmieder, P.; Oesterhelt, D.; Oschkinat, H. *Proc. Natl. Acad. Sci. U.S.A.* **2002**, *99*, 9765-9770.

Chapter-5 H/D Exchange Mass Spectrometry and Optical Spectroscopy as Complementary Tools for Studying the Structure and Dynamics of Bacteriorhodopsin

5.1 Introduction

Membrane proteins are involved in many essential processes, including oxidative phosphorylation, photosynthesis, signaling, and transport. Moreover, membrane proteins represent important drug targets.¹ Despite their tremendous importance, the general understanding of membrane protein structure and function is miniscule when compared to the amount of information that is available for their water-soluble counterparts. More than 99.6 % of all known protein structures are for water-soluble species,² although roughly one third of the sequences encoded by the human genome are believed to be membrane proteins.³ This imbalance is due to the fact that most membrane proteins are exceedingly difficult to work with. Once removed from their natural bilayer environment, they tend to undergo rapid denaturation and aggregation because of their extreme hydrophobicity. Some degree of stabilization can be achieved by embedding isolated membrane proteins in detergent micelles, bicelles (bilayered micelles), or lipid vesicles.⁴ However, precipitation often still takes place in these surrogate environments. The application of traditional high resolution structure determination methods such as X-ray crystallography⁵ and NMR spectroscopy⁶ to membrane proteins has been demonstrated, but the success rate of these strategies is low. Alternative techniques that are capable of providing low to medium level structural information are therefore of considerable interest.⁷

Following its inception in the early 1990s,^{8, 9} hydrogen/deuterium exchange (HDX) in conjunction with electrospray ionization mass spectrometry (ESI-MS) has evolved into one of the most commonly used tools for probing the structure, dynamics, and folding of water-soluble proteins.¹⁰⁻¹³ Prior to that, NMR-based HDX studies had already become a well established technique.¹⁴⁻¹⁶ HDX experiments rely on the fact that exposure of a protein to D₂O induces N-H → N-D conversion at backbone amide linkages. Disordered protein regions that are not involved in hydrogen bonding undergo rapid exchange, with rate constants approaching those of isolated dipeptides.¹⁷ In contrast, HDX at hydrogen-bonded N-H groups is slowed down by as much as eight orders of magnitude. Exchange at these protected sites is mediated by protein structural fluctuations that involve the transient disruption of H-bonds and provide temporary solvent access.^{13, 16} HDX/MS is typically conducted under exchange-in conditions, where an unlabeled protein is exposed to D₂O.^{9, 18} Aliquots are taken at selected labeling times, followed by acid quenching at pH 2.5. The protein is then digested by pepsin or other acidic proteases at 0 °C,¹⁹ and the mass shifts of individual fragments are determined by LC/MS. In this way the HDX pattern can be uncovered in a spatially-resolved manner as a function of time.¹⁰⁻¹³

Various HDX strategies have also been applied to membrane proteins. Instead of using MS detection, however, past studies in this area have largely relied on vibrational (FTIR) spectroscopy.²⁰⁻²² Upon N-H → N-D conversion the amide II band shifts from 1550 cm⁻¹ to 1450 cm⁻¹, such that global HDX information can be obtained by deconvolution of infrared spectra.^{23, 24} The use of ESI-MS for membrane protein HDX studies remains rare, and only a handful of studies have reported the successful application of the standard proteolytic

digestion approach.²⁵⁻²⁸ Experiments of this kind are hampered not only by solubility issues, but also by the difficulty of generating proteolytic fragments from membrane proteins in sufficiently high yield within a short time at low temperature and pH.²⁹

In an attempt to enhance the general applicability of HDX/ESI-MS to membrane proteins, this work explores the isotope exchange behavior of bacteriorhodopsin (BR) from *Halobacterium salinarum*. Electron microscopy³⁰ and X-ray crystallography⁵ have revealed that the 248 residue polypeptide chain of this protein folds into seven transmembrane helices that are connected by six solvent-exposed loops, similar to the G protein-coupled receptors of higher organisms.³¹⁻³³ The seven BR helices surround a central retinal chromophore that is bound to Lys216 via a protonated Schiff-base, giving the protein its characteristic purple color. In its native environment BR is packed in clusters of three that form a two-dimensional hexagonal lattice referred to as purple membrane.³⁰ Trans/cis isomerization of the retinal allows the protein to act as a light-driven proton pump.

While the structure of native BR is well known, there continue to be uncertainties regarding the properties of this protein in environments other than the purple membrane. In particular, the structure of the SDS-denatured state continues to be a matter of debate,³⁴ although this form frequently serves as starting point for BR folding experiments.³⁵ Using a combination of optical spectroscopy and HDX/MS, this work explores the properties of five different types of samples: BR in its native purple membrane, as well as solubilized in two different detergents (SDS and DM), refolded BR in bicelles, and after cleavage of the Schiff-base linkage. Owing to the experimental difficulties outlined above, we focus on the HDX

behavior of the intact protein, but it is hoped that the experiments described here provide the groundwork for future spatially-resolved studies.^{27, 28}

5.2 Experimental

5.2.1 Proteins and Reagents

Purple membranes from *H. salinarum* were harvested and purified as described in Chapter-2, resulting in aqueous stock suspensions with a BR concentration of ~170 μ M. Samples were stored at -80 °C prior to analysis. Deuterium oxide was obtained from Cambridge Isotope Laboratories (Andover, MA). SDS, DM, sodium phosphate, formic acid, hydroxylamine, and all-*trans*-retinal were from Sigma (St. Louis, MO). DMPC was procured from Avanti (Alabaster, AL) and CHAPS from Calbiochem (San Diego, CA).

To ensure consistency with previous work³⁶ all protein solutions were adjusted to pH 6 using 50 mM sodium phosphate buffer (referred to simply as "buffer", unless noted otherwise). Five types of different protein samples were examined. (i) For studies on native BR, purple membrane stock suspensions were prepared in buffer at a protein concentration of 100 μ M. (ii) DM-solubilized protein was obtained by exposing native BR stock suspensions to 0.1 % DM in buffer. These solutions were vortex-mixed for 30 seconds, followed by sonication in a water bath (Fisher Scientific, FS60, Ottawa, Ontario, Canada) for 15 minutes, and equilibration at room temperature for six hours. (iii) Bleached membranes^{21, 37, 38} were prepared by exposing 10 μ M native BR suspensions in buffer to 0.5 M hydroxylamine at pH 7.7. Subsequently the samples were irradiated for 30 h by 546

nm light from a Xe/Hg lamp, using the fiber optics-coupled output of a Biologic SFM 4S/Q (Molecular Kinetics, Indianapolis, IN) spectrometer. The resulting suspension was dialyzed twice against 3 L buffer (5 mM, pH 6) to remove hydroxylamine. The final bleached sample was lyophilized and resuspended in water to a protein concentration of 100 μ M in buffer.

(iv) SDS-denatured protein was produced by exposing native BR stock suspension to 1.25% (w/v) SDS, followed by vortex mixing, sonication and equilibration as for the DM samples. The CMC of SDS under the conditions here is around 0.1 % (\approx 3 mM).³⁹ A higher concentration was used here to ensure the detergent concentration remained well above the CMC even after dilution during HDX. (v) Refolded BR was prepared from SDS-denatured bacterioopsin (BO) following established procedures.⁴⁰ Briefly, native BR purple membranes were exposed to chloroform/methanol/triethylamine (100:100:1 v/v/v). Addition of 0.1 M buffer in a 1:1 volume ratio followed by 10 seconds of vortex mixing resulted in phase separation. Delipidated BO was recovered as a precipitate at the interface. Phase separation and recovery of the protein interphase were repeated twice. The final pellet of delipidated BO was dissolved in an aqueous solution of 5% w/v SDS. The SDS-solubilized BO was diluted to 0.2% SDS and dialyzed against 10 mM buffer containing 0.2% SDS to remove residual organic solvent. To initiate refolding, the resulting delipidated BO solution in 0.2 % SDS / 10 mM buffer was vortex mixed with an equal volume of buffer containing 2% DMPC / 2% CHAPS bicelles at pH 6. All-*trans*-retinal (1:1 retinal:protein molar ratio) was added simultaneously from ethanol stock. The final refolding buffer contained 1 % DMPC/1 % CHAPS/0.1 % SDS, and 0.1 % ethanol. The solution was equilibrated for one day at room temperature in the dark.

5.2.2 Optical Spectroscopy

UV-Vis absorption measurements were carried out on a Cary 100 spectrophotometer (Varian, Mississauga, Ontario, Canada). Trp fluorescence emission spectra were acquired on a Fluorolog-3 instrument (Horiba Jobin Yvon, Edison, NJ) with an excitation wavelength of 280 nm. All optical measurements were performed at a protein concentration of 7 μ M at room temperature, using protein-free solutions as blanks.

5.2.3 Hydrogen/Deuterium Exchange

Isotope exchange was initiated by mixing 100 μ M protein solutions, prepared as described above, and D₂O-based buffer (with a pH meter reading of 6) at room temperature in a 1:4 volume ratio. After initiation of labeling, 35 μ L aliquots were removed at various time points ranging from one to 120 minutes. These aliquots were quenched by mixing with 6 μ L of 500 mM buffer (pH 2) for a final pH of 2.5, followed by flash freezing in liquid nitrogen. Zero time point controls (m_0) for the correction of artifactual in-exchange were performed by exposing protein solutions to a mixture of labeling and quenching buffer. Maximally deuterated samples (m_{100}) for the correction of back-exchange were prepared by incubating 20 μ M BR in 0.4% SDS containing 80% D₂O at pH_{read} 11.8 and 40 °C for 30 h. Relative HDX levels were determined as ⁹

$$\text{deuteration level} = (m - m_0) / (m_{100} - m_0) \quad (5-1)$$

In this expression m is the mass of the protein, and m_0 and m_{100} are the values of the corresponding control measurements. The procedure used for determining m_{100} induces retinal loss, and hence the measured mass had to be corrected by adding 284.4 Da (mass of

free retinal) and subtracting 18 Da (loss of water after Schiff base formation) for those sample that contained the chromophore. The kinetic data were fitted to the biexponential expression:

$$\text{deuteration level} = A_1(1-\exp[-k_1t]) + A_2(1-\exp[-k_2t]) \quad (5-2)$$

where A_1 and A_2 are the hydrogen fractions that undergo labeling with apparent k_{ex} rate constants of k_1 and k_2 , respectively.

5.2.4 Liquid Chromatography/Mass Spectrometry

LC/MS measurements were conducted by using a Waters Acquity UPLC (Milford, MA) with a Waters SEC column (BioSuite, 4 μm UHR SEC, 4.6 mm \times 300 mm), employing isocratic chloroform/methanol/water/formic acid (400/400/90/25/ v/v/v/v) flow at 0.25 mL min^{-1} under quenching conditions (pH 2.5, 0 $^\circ\text{C}$). The column and extensively coiled solvent delivery lines were embedded in an ice bath. For each injection 20 μL of sample were loaded onto the column. The protein eluted after about 10 minutes. The SEC column was coupled to the Z-spray ESI source of a Q-TOF Ultima API mass spectrometer (Waters). Spectra were acquired in positive ion mode at a sprayer voltage of 3 kV and desolvation temperature of 250 $^\circ\text{C}$. Experimental data were converted to mass distributions using the MaxEnt 1 routine provided by the instrument manufacturer for determination of m , m_0 , and m_{100} in Eq. 5-1. Using maximally deuterated control samples, amide back exchange was determined to be around 10 %.

5.3 Results and Discussion

5.3.1 Optical Spectroscopy

Prior to exploring structural aspects of BR by HDX/MS, it is instructive to study the five different types of samples highlighted in this work by traditional spectroscopic tools. The retinal absorption spectrum is sensitive to the protein conformation. Native light-adapted BR in its purple membrane environment has its absorption maximum at 568 nm, indicative of the covalently linked chromophore in a structurally intact environment.⁴¹ For the SDS-solubilized protein a maximum at 392 nm is observed (Figure 5-1A). This dramatic blue shift is caused by hydrolytic cleavage of the Schiff-base linkage. SDS denaturation also affects the emission properties of the eight Trp residues.⁴² Native BR exhibits a relatively low fluorescence intensity, mainly because of FRET-based retinal quenching (Figure 5-1B).⁴³ SDS induces a five-fold increase in Trp fluorescence intensity (Figure 5-1B). These spectroscopic changes reflect the transition to a partially unfolded structure, concomitant with Schiff-base hydrolysis and release of the detergent-solubilized retinal into the solvent.⁴⁴ The lack of a major red shift in the emission reveals that SDS-denaturation does not cause significant water-exposure of Trp residues. The optical spectra obtained here for native BR and the SDS-denatured form are consistent with earlier observations in Chapter-3. The reason for including these data in Figure 5-1 is to facilitate a comparison with results obtained under the other experimental conditions.

The structural changes that occur upon solubilization of the protein are highly dependent on the detergent used. DM-solubilized BR exhibits an absorption maximum at the same

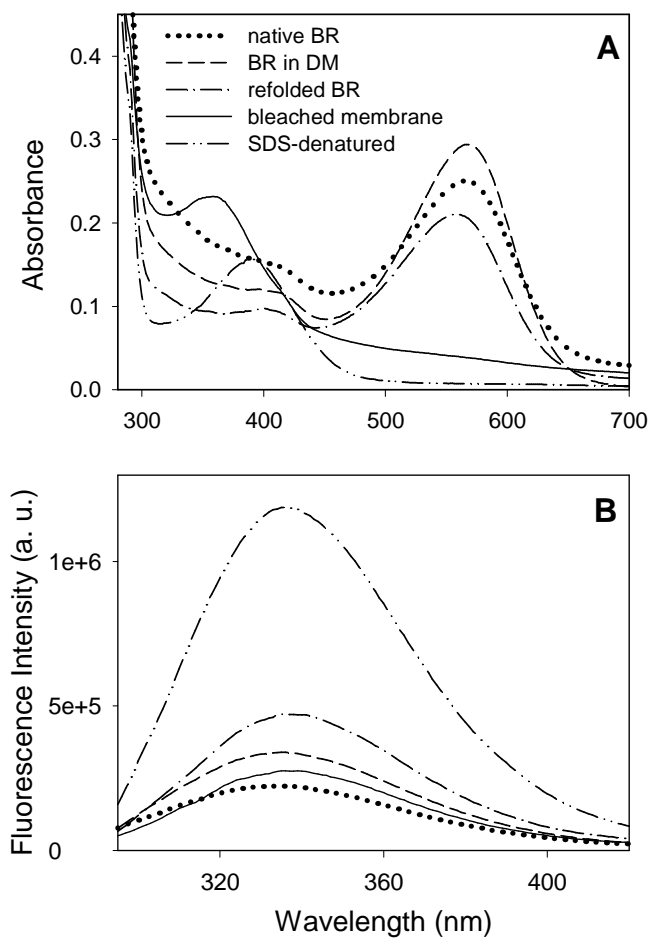


Figure 5-1. (A) UV-Vis absorption spectra and (B) fluorescence emission spectra of BR. The five line styles represent different experimental conditions as noted in panel A.

wavelength as the native protein (Figure 5-1A), and the fluorescence intensity increases only moderately, by a factor of less than two (Figure 5-1B). This behavior is consistent with previous NMR work⁴⁵ and indicates that the DM-solubilized protein retains a structure similar to the native state, despite the breakdown of membrane-bound BR trimers into monomeric units.⁴⁶ Our data reiterate the generally accepted view of DM as a "mild" detergent that tends to preserve membrane protein structure and (to some extent) function,⁴⁷⁻⁴⁹ whereas SDS typically induces extensive structural perturbations.⁴⁴

Purple membrane bleaching by hydroxylamine entails cleavage of the retinal-protein linkage and retinaloxime formation,³⁷ a step that is accompanied by a major change in λ_{max} to 358 nm (Figure 5-1A). AFM studies have shown that this process leaves the trimeric BR structure inside the membrane largely intact, but induces loss of crystallinity.³⁸ Interestingly, the fluorescence emission properties of the bleached protein in Figure 5-1B are almost indistinguishable from those of native BR, implying that FRET-based Trp quenching by the chromophore still takes place. It can be concluded that the detached retinaloxime remains trapped inside the chromophore binding pocket, thereby putting a qualifier on earlier suggestions of chromophore "removal"²¹ under the conditions used here. Extraction of the retinaloxime from the membrane can be achieved by bovine serum albumin.⁵⁰

Exposure of SDS-denatured BO to bicelles and free retinal triggers refolding to a monomeric state.^{51, 52} The 557 nm absorption maximum of the refolded samples is close to that of native BR, indicating that the Schiff-base linkage between retinal and K216 has been

regenerated for the majority of the protein molecules (Figure 5-1A). Compared to the SDS-denatured state, the Trp fluorescence intensity of refolded BR is greatly reduced. However, the emission remains *ca.* two-fold higher than for the native protein (Figure 5-1B). The origin of this behavior is further investigated below.

5.3.2 Size Exclusion Chromatography/ESI-MS

With few exceptions,^{53, 54} MS analyses of membrane proteins require the analyte to be separated from surfactants and salts. One approach is to precipitate the protein, followed by dissolution in organic solvent/acid mixtures. Alternatively, SEC or reverse-phase chromatography can be used.⁵⁵ MS studies on intact proteins are an important tool for the detection of covalently linked co-factors and post-translational modifications.⁵⁶⁻⁵⁸ Unfortunately, the harsh solvent environment typically employed for membrane protein analyses can induce the loss of some covalently coupled moieties. For example, the MS detection of intact BR with its chromophore attached is problematic owing to the labile nature of the Schiff-base linkage. Hence, although retention of the chromophore has been demonstrated in a few instances,^{59, 60} most previous MS studies on BR involved complete or partial BO formation in the course of the analysis.⁶¹⁻⁶⁵

During the work leading up to the HDX measurements discussed below, we initially carried out SEC/ESI-MS analyses on BR at room temperature. Those conditions resulted in partial degradation of the protein-retinal complex consistent with ref. (data not shown). It was then noticed that the stability of the complex is dramatically enhanced by lowering the elution temperature to 0 °C. Analysis of native BR under these conditions results in a major signal

for the intact complex, whereas retinal-free BO is almost undetectable (Figure 5-2A). Virtually the same spectrum was obtained for BR after solubilization in DM (data not shown). In contrast, SDS-denatured protein, as well as bleached membrane samples were found to be largely devoid of the covalently linked chromophore (illustrated for an SDS sample in Figure 5-2B). These SEC/ESI-MS findings are in agreement with the optical results of Figure 5-1, which indicated that the retinal-Lys216 bond remains intact in native and DM-solubilized BR, whereas both membrane bleaching and SDS-denaturation induce cleavage of the Schiff-base linkage.

From the data of Figure 5-2A, B it can be concluded that the low temperature SEC/ESI-MS procedure used here provides an accurate reflection of the retinal binding state in bulk solution. This technique can therefore be used to determine the regeneration yield of samples that had undergone SDS denaturation and subsequent refolding. Typical SEC/ESI-MS data for refolded BR are depicted in Figure 5-2C, revealing the presence of a dominant peak for the retinal-bound protein and a less intense signal for BO. On the basis of the 8:1 peak intensity ratio the regeneration yield is $8/9 = 89\%$, which is in close agreement with the A_{568} ratio of the two samples in Figure 5-1A, as well as with previously reported values.⁴⁰ The presence of 11% BO after refolding contributes to the elevated fluorescence intensity in Figure 5-1B (dash-dotted line).

5.3.3 Hydrogen/Deuterium Exchange SEC/ESI-MS

HDX/ESI-MS protocols typically employ reverse-phase chromatography.⁶⁶ For the membrane protein experiments of this work we pursued the SEC-based strategy outlined

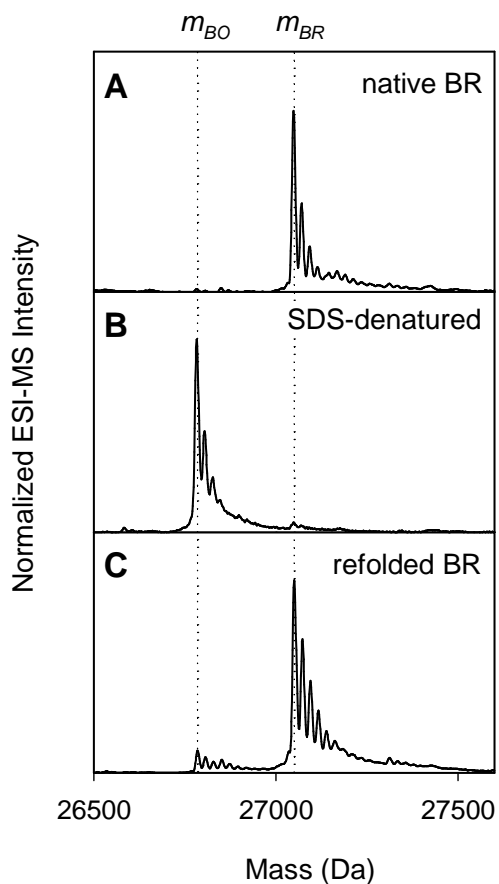


Figure 5-2. Deconvoluted mass distributions obtained by SEC/ESI-MS of unlabeled protein samples at 0 °C. (A) native BR, (B) SDS-denatured state, (C) refolded BR. Satellite peaks are due to sodium adducts. Dashed vertical lines indicate the masses expected for BO ($m_{BO} = 26784$ Da)⁵⁶ and BR ($m_{BR} = 27050$ Da).⁶⁵

above, as it allows the covalently linked chromophore to be preserved during analysis, such that co-existing BO and BR species in solution can be monitored separately. High quality intact protein HDX data were obtained for all five experimental conditions. Native BR undergoes only a relatively small mass change during the 120 min time window examined here (Figure 5-3, A-D). In contrast, much more extensive HDX is observed for the SDS-denatured state (Figure 5-3, E-H). All the samples studied in this work underwent gradual mass shifts without peak splitting, indicative of HDX in the EX2 regime.¹⁸ Satellite peaks in Figure 5-3 are due to sodium adducts, not to EX1 dynamics.¹⁸

Amide deuteration levels were determined according to Eq. 5-1 (Figure 5-4). The HDX kinetics were analyzed on the basis of a biphasic expression (Eq. 5-2), resulting in fits that are shown as solid lines in Figure 5-4 (parameters are summarized in Table 5-1). The apparent rate constants determined by this approach are on the order of $k_1 \approx 1 \text{ min}^{-1}$ and $k_2 \approx 0.1 \text{ min}^{-1}$. The kinetic amplitudes associated with these two phases represent the percentage of amide hydrogens that are weakly (A_1) and moderately protected (A_2). $A_{non-ex} = 100 - A_1 - A_2$ represents the percentage of amide hydrogens that is non-exchangeable on the time scale of our experiments.

In the case of native BR, $A_1 = 12 \%$ of the amide hydrogens are weakly protected, $A_2 = 11.7 \%$ are moderately protected, and $A_{non-ex} = 76.3 \%$ do not undergo exchange (Table 5-1). It is interesting to compare these data with the H-bonding pattern in the 1.55 Å X-ray structure of the protein. Stable H-bonds were identified by analyzing pdb file 1C3W⁵ using Swiss PDB Viewer default values,⁶⁷ i.e., a donor-acceptor distance between 2.195 and 3.3 Å, and

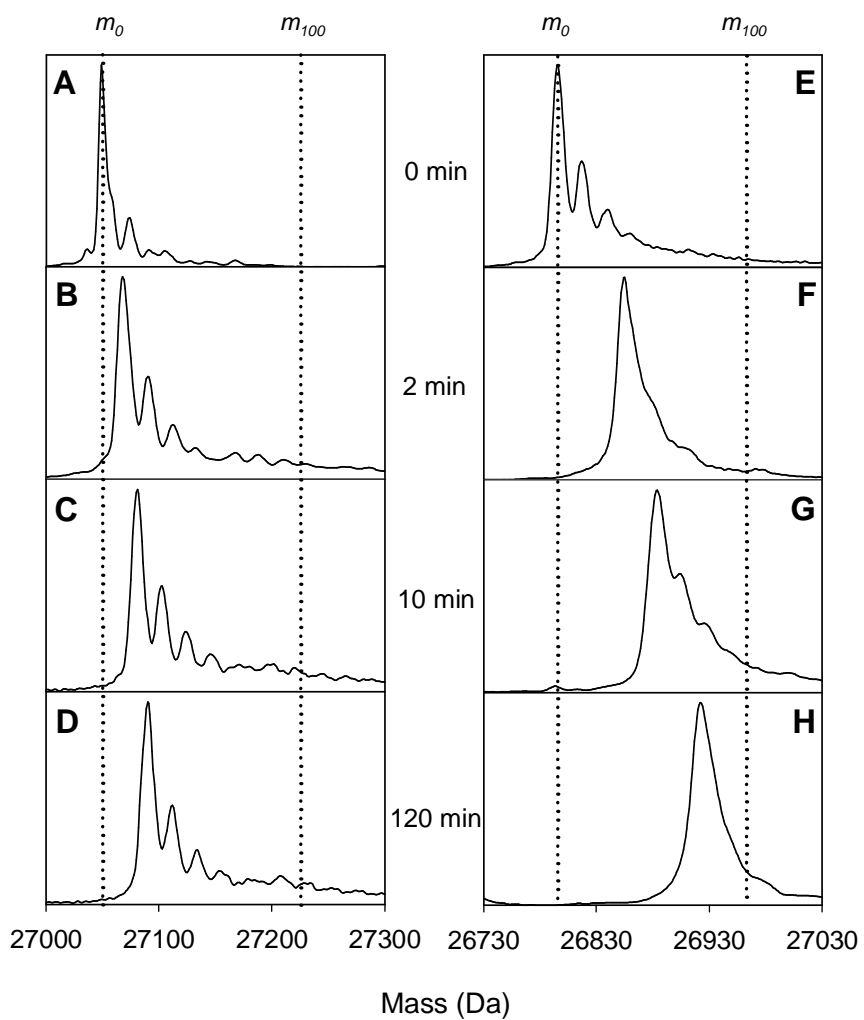


Figure 5-3. Deconvoluted ESI mass distributions of native BR (A-D) and SDS-denatured protein (E-H), obtained after HDX for exchange times of $t = 0$ min, 2 min, 10 min, and 120 min. Dotted lines represent mass values for the m_0 and m_{100} controls. The mass range for the SDS samples (panels on the right hand side) is shifted to account for the loss of retinal.

a minimum angle of 90° . According to this analysis, almost all of the amide N-H groups in the transmembrane helices are H-bonded, with the exception of a small number of residues close to the helix termini. Most of the non-bonded N-H groups are located in the extramembrane loops (Table 5-2). BR has a total of 248 residues, corresponding to 247 backbone amide bonds. Taking into account the presence of 11 prolines, the number of backbone N-H groups is 236. Table 2 shows 181 stable H-bonds, which means that an amide fraction of $181/236 = 76.7\%$ is expected to be strongly protected. This value is in very close agreement with the measured value of $A_{non-ex} = 76.3\%$. A high resilience against HDX in the seven transmembrane helices has previously been inferred from tritium exchange^{68, 69} and infrared spectroscopic HDX studies,^{20, 22} which found the total amide protection to be in the range of 71 - 80%. Our HDX kinetics show that the remaining N-H groups in native BR can be grouped in two categories. $A_2 = 11.7\%$ are likely involved in weak hydrogen bonds that do not appear in the X-ray structure when applying the criteria listed above. The remaining $A_1 = 12\%$ experience an even lower degree of protection, although their apparent rate constant ($k_1 = 1.5 \text{ min}^{-1}$) is below the value of $k_{ch} \approx 60 \text{ min}^{-1}$ that would be expected for completely exposed amides in a random coil environment.¹⁷

Solubilization of BR in SDS results in dramatically more extensive HDX. Almost half of all amide hydrogens become rapidly exchangeable ($A_1 = 46.7\%$), whereas $A_2 = 28.5\%$ undergo isotope exchange with an apparent rate constant of $k_2 = 0.028 \text{ min}^{-1}$. Only one quarter ($A_{non-ex} = 24.8\%$) of all amide hydrogens are non-exchangeable in SDS. These HDX kinetics suggest partial helix unraveling in the SDS state but with retention of a protein core that remains inaccessible to solvent water. It is consistent with our oxidative labeling

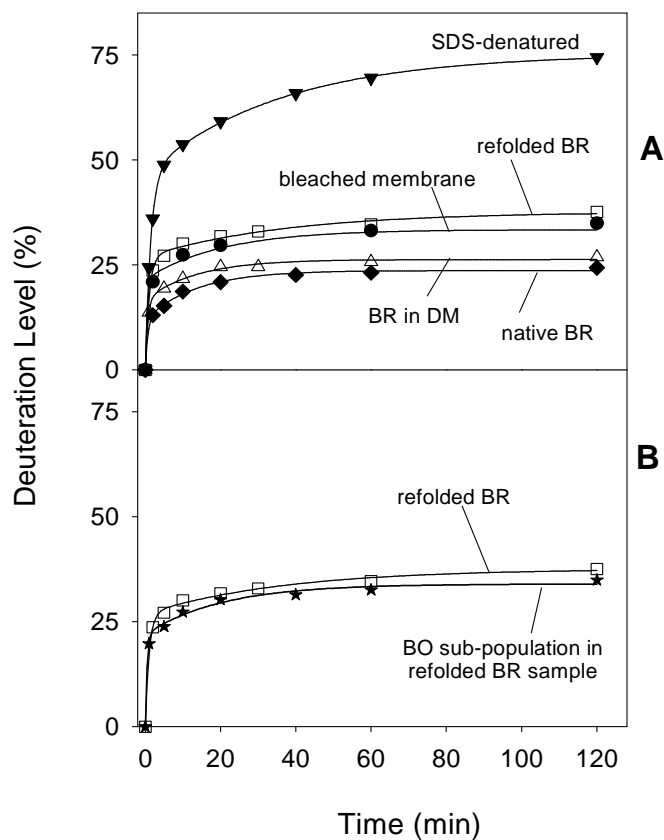


Figure 5-4. (A) HDX kinetics of BR under five different solvent conditions, normalized according to Eq. (5-1). Each data point represents an average of two or three independent measurements. The experimental error was found to be less than 2%. Solid lines are biexponential fits, using the expression of eq. (5-2). Fitting parameters are summarized in Table 5-1. (B) Refolded BR data (open squares) are identical to those in panel A. Star-shaped symbols represent the HDX behavior of the 11% BO sub-population in the refolded BR sample (see Figure 5-2C).

Table 5-1. Parameters obtained from fitting the HDX kinetics of Figure 5-4A according to the bi-exponential expression of Eq. 5-2. The percentage of "non-exchangeable" hydrogens (last column) has been calculated as $A_{non-ex} = 100 - A_1 - A_2$.

	A_1 (%)	k_1 (min ⁻¹)	A_2 (%)	k_2 (min ⁻¹)	A_{non-ex} (%)
Native BR	12.0	1.5	11.7	0.074	76.3
BR in DM	16.6	1.5	9.7	0.074	73.7
Refolded BR	26.9	0.97	10.7	0.027	62.4
bleached membrane	21.5	2.1	11.9	0.050	66.6
SDS-denatured	46.7	0.69	28.5	0.028	24.8

Table 5-2. Amino acid sequence of BR.⁷⁰ Residues that act as amide N-H hydrogen bond donor (to an amide carbonyl, or to a side chain acceptor) are underlined and bold. Hydrogen bonds were determined from the X-ray structure of native BR⁵ using the procedure outlined in the text. Non-hydrogen bonded residues include eleven prolines, as well as three short disordered segments (italicized, not seen in the X-ray structure⁵). X represents pyroglutamate.

Segment	Sequence	H-bonds
N-term.	¹ <i>X</i> <u>AQITGRP</u> ⁸	1
Helix A	⁹ <u>EWIWLALGTALMGLGTLYFLVKG</u> ³¹	21
A-B loop	³² <u>MGVS</u> ³⁵	3
Helix B	³⁶ <u>DPDAKKFYAITTLVPAIAFTMYLSML LG</u> ⁶³	24
B-C loop	⁶⁴ <u>YGLTMYPFGGEQNPIYW</u> ⁸⁰	9
Helix C	⁸¹ <u>ARYADWLFTTPLLLLDLALLV</u> ¹⁰¹	19
C-D loop	¹⁰² <u>DA</u> ¹⁰³	2
Helix D	¹⁰⁴ <u>DQGTILALVGADGIMIGTGLVGAL</u> ¹²⁷	21
D-E loop	¹²⁸ <u>TKVYS</u> ¹³²	1
Helix E	¹³³ <u>YRFVWWAISTAAMLYILYVLFEG</u> ¹⁵⁵	23
E-F loop	¹⁵⁶ <i>FTSKAESM</i> ¹⁶³	0
Helix F	¹⁶⁴ <u>RPEVASTFKVLRNVTVVLWSAYPVVWLIG</u> ¹⁹²	25
F-G loop	¹⁹³ <u>SEGAGIV</u> ¹⁹⁹	6
Helix G	²⁰⁰ <u>PLNIETLLFMVLDVSAKVGFLILLR</u> ²²⁵	23
C-term.	²²⁶ <u>SRAIFGEAEAPEPSAGDGAAATS</u> ²⁴⁸	3

studies in Chapter-3, as well as other earlier work.^{34, 36} Our data indicate that this residual core encompasses a total of $0.248 \times 236 \approx 59$ protected backbone amides.

In contrast to the behavior observed after SDS exposure, solubilization of BR in DM results in HDX kinetics that is almost indistinguishable from those of the native state (Figure 5-4, Table 5-1). Hence, the transition from the native trimeric structure in the purple membrane to a monomeric DM-solubilized state⁴⁶ induces virtually no changes to the BR structure and dynamics, as previously suggested on the basis of NMR data.⁴⁵ Bleached membranes exhibit a roughly two-fold increase in the amplitude of rapidly exchanging hydrogens (A_1) relative to native BR, whereas the value of A_2 remains more or less unchanged. Comparison with the HDX behavior of the SDS-denatured state shows that the structural perturbations induced by cleavage of the Schiff-base are relatively moderate. The percentage of non-exchangeable amide hydrogens in the bleached membranes is 66.6 %. Our findings are consistent with previous ¹³C-NMR,^{37, 71} AFM,³⁸ FRET,⁷² and infrared studies,²¹ all of which indicate that the protein structure in the bleached membrane remains similar to that of native BR, despite the loss of membrane crystallinity and the occurrence of greater disorder in some local regions. Thus, major aspects of the native BR structure are not dependent on the presence of an intact covalent linkage between protein and chromophore.

As noted in the Introduction, one intriguing feature of BR is the possibility to refold the protein in a bicelle environment after SDS denaturation.^{35, 73} In contrast to the crystalline trimeric assembly within the purple membrane, refolded BR is monomeric.^{51, 52} It remains somewhat unclear in how far individual refolded protein chains differ from the native trimer

in terms of their structure and dynamics. Optical assays of the type discussed above (Figure 5-1) are not necessarily suitable for exploring this interesting question, because the spectra represent ensemble averages. In particular, it is difficult to decide whether the presence of 11 % BO in the refolded samples (Figure 5-2C) can account for the elevated fluorescence intensity seen in Figure 5-1B, and whether the 89 % BR population is affected by structural perturbations. The SEC/ESI-MS protocol employed here allows the HDX behavior of BO and BR in the refolded samples to be monitored separately. We find that the HDX kinetics of these two co-existing sub-population are very similar to each other (Figure 5-4B), resembling the behavior seen for bleached membranes (Figure 5-4A). Thus, it can be concluded that *in vitro* refolding of the protein leads to a native-like conformation, but that structural perturbations persist for both the retinal-bound (89 %) and the retinal-free (11 %) forms. NMR data suggest that some of this disorder is attributable to loop elements that do not fully recover during BR folding *in vitro*.^{71, 74} Our findings suggest that the chromophore plays a relatively minor role as far as the formation of secondary structure is concerned.⁷⁵ This assertion is in agreement with the oxidative labeling experiments, which revealed that the retinal-free protein can fold into a conformation resembling the native state, where only one of the seven helices (D) remains partially disordered in Chapter-4

5.4 Conclusions

This work employed a combination of optical spectroscopy and ESI-MS-based methods for exploring the structure and dynamics of BR under various experimental conditions. UV-Vis absorption measurements report on the intactness of the Schiff-base linkage between protein and retinal, whereas the fluorescence intensity is sensitive to changes in

retinal-tryptophan distance. Low temperature SEC/ESI-MS was found to be an even more direct tool for probing the intactness of the sensitive Schiff-base linkage. This procedure will likely be applicable to other retinal-containing membrane proteins as well. SDS-denaturation and purple membrane bleaching induce loss of the chromophore, whereas solubilization in DM leaves the linkage intact. Bicelle-mediated refolding predominantly results in the formation of BR, whereas a smaller fraction of the protein remains in the BO state. HDX measurements by SEC/ESI-MS were shown to represent a straightforward alternative to traditional infrared spectroscopy experiments²⁰⁻²² for monitoring global changes in BR structure and dynamics. To the best of our knowledge, this study conducts the first side-by-side comparison of the HDX characteristics for this important model system under different biochemical conditions. Backbone amide hydrogens within the seven transmembrane helices of native BR are highly protected. The number of non-exchangeable hydrogens decreases in the order: native BR \approx DM-solubilized BR > bleached membranes \approx refolded BO \approx refolded BR \gg SDS-denatured state. However, even the SDS-denatured protein retains a sizeable number of protected backbone amides.

On the basis of CD measurements it has previously been suggested that SDS denaturation reduces the helical content of the protein from the native state value of 74 % down to 42 %³⁶. That interpretation has been challenged by noting that CD studies on BR are associated with unique experimental difficulties.³⁴ It is interesting to compare those previous CD data to the findings of the current work. When judging the secondary structure content of the SDS state on the basis of amide protection, our data suggest that $A_{non-ex} = 24.8$

% of all amide hydrogens are involved in stable helical elements (Table 5-2). In addition, the $A_2 = 28.5$ % moderately protected hydrogens in SDS are likely located in regions that retain some helix propensity as well. A residual helicity of 42 % in SDS as suggested in ref.³⁶ is therefore not in disagreement with our findings. It is noted, however, that caution should be exercised when estimating the secondary structure content of a membrane protein solely on the basis of HDX data, because amide protection might involve significant contributions from surrounding surfactant molecules.

It is remarkable that $\cdot\text{OH}$ labeling reveals significantly enhanced solvent accessibility for only two of the helices after SDS exposure in Chapter-3, whereas changes in amide HDX protection are much more dramatic in this work. This behavior illustrates the complementarity between the two methods. Covalent labeling strategies probe the solvent accessibility of reactive sites, whereas HDX monitors structural dynamics and the intactness of the H-bonding network.⁷⁶ From an analytical point of view, the stable nature of protein covalent labels greatly facilitates the proteolytic mapping procedure. HDX experiments are considerably more challenging in this regard, because back-exchange requires the digestion and LC separation steps to be completed in as little as about fifteen minutes.¹⁰ The situation is particularly challenging for membrane proteins where digestion efficiencies under quenching conditions tend to be low,²⁷ and where detergents often interfere with the analysis. It is therefore not surprising that membrane protein covalent labeling has become a fairly routine approach, whereas only a handful of HDX studies in this area have appeared over the past few years.²⁵⁻²⁸

Although this work provides interesting information on the global structure and dynamics of BR, the lack of a robust protocol for spatially-resolved membrane protein studies represents a severe impediment for studies in this area. In a recent study, Joh et al. applied the standard HDX/MS approach to SDS-denatured BR,²⁷ and identified less than 50% of the protein sequence. Spatially-resolved data for native BR could not be obtained. Unfortunately, we were not successful in extending the approach of that work further, neither by using pepsinolysis in bulk solution, nor by employing a pepsin column. We attribute these difficulties to the well known tendency of BR to precipitate under the acidic conditions required for HDX quenching.⁷⁷ Rietschel et al.²⁹ recently reported the successful pepsinolysis of BR, but only under conditions that are incompatible with the HDX workflow, i.e., up to 16 hours of digestion at room temperature. Nonetheless, results obtained for a number of other systems^{25, 26, 28} suggest that spatially-resolved HDX/MS studies on membrane proteins will soon cease to be considered a fringe area.

5.5 References

- (1) George, S. R.; O'Dowd, B. F.; Lee, S. P. *Nat. Rev. Drug Discov.* **2002**, *1*, 808-820.
- (2) White, S. H. *Nature* **2009**, *459*, 344-346.
- (3) Wu, C. C.; Yates III, J. R. *Nat. Biotechnol.* **2003**, *21*, 262-267.
- (4) Sanders, C. R.; Prosser, R. S. *Structure* **1998**, *6*, 1227-1234.
- (5) Luecke, H.; Schobert, B.; Richter, H.; Cartailier, J.; Lanyi, J. K. *J. Mol. Biol.* **1999**, *291*, 899-911.
- (6) Arora, A.; Abilgaard, F.; Bushweller, J. H.; Tamm, L. K. *Nat. Struct. Biol.* **2001**, *8*, 334-338.
- (7) Weinglass, A. B. In *Protein Mass Spectrometry*; Whitelegge, J. P., Ed.; Elsevier: Amsterdam, 2009; Vol. 52, pp 197-212.
- (8) Katta, V.; Chait, B. T. *Rapid Commun. Mass Spectrom.* **1991**, *5*, 214-217.
- (9) Smith, D. L.; Deng, Y.; Zhang, Z. *J. Mass Spectrom.* **1997**, *32*, 135-146.
- (10) Engen, J. R. *Anal. Chem.* **2009**, *81*, 7870-7875.
- (11) Englander, S. W. *J. Am. Soc. Mass Spectrom.* **2006**, *17*, 1481-1489.
- (12) Maier, C. S.; Deinzer, M. L. *Methods Enzymol.* **2005**, *402*, 312-360.
- (13) Eyles, S. J.; Kaltashov, I. A. *Methods* **2004**, *34*, 88-99.
- (14) Hughson, F. M.; Wright, P. E.; Baldwin, R. L. *Science* **1990**, *249*, 1544-1548.
- (15) Kim, K. S.; Fuchs, J. A.; Woodward, C. K. *Biochemistry* **1993**, *32*, 9600-9608.
- (16) Krishna, M. M. G.; Hoang, L.; Lin, Y.; Englander, S. W. *Methods* **2004**, *34*, 51-64.
- (17) Bai, Y.; Milne, J. S.; Mayne, L.; Englander, S. W. *Proteins: Struct. Funct. Genet.* **1993**, *17*, 75-86.
- (18) Konermann, L.; Tong, X.; Pan, Y. *J. Mass Spectrom.* **2008**, *43*, 1021-1036.
- (19) Rey, M.; Man, P.; Brandolin, G.; Forest, E.; Pelosi, L. *Rapid Commun. Mass Spectrom.* **2009**, *23*, 3431-3438.
- (20) Earnest, T. N.; Herzfeld, J.; Rothschild, K. J. *Biophys. J.* **1990**, *58*, 1539-1546.
- (21) Cladera, J.; Torres, J.; Padros, E. *Biophys. J.* **1996**, *70*, 2882-2887.
- (22) Downer, N. W.; Bruchman, T. J.; Hazzard, J. H. *J. Biol. Chem.* **1986**, *261*, 3640-3647.
- (23) Barth, A. *Biochim. Biophys. Acta* **2007**, *1767*, 1073-1101.
- (24) Laczko-Dobos, H.; Szalontai, B. *Biochemistry* **2009**, *48*, 10120-10128.
- (25) Busenlehner, L. S.; Codreanu, S. G.; Holm, P. J.; Bhakat, P.; Hebert, H.; Morgenstern, R.; Armstrong, R. N. *Biochemistry* **2004**, *43*, 11145-11152.
- (26) Busenlehner, L. S.; Salomonsson, L.; Brzezinski, P.; Armstrong, R. N. *Proc. Natl. Acad. Sci. U.S.A.* **2006**, *103*, 15398-15403.
- (27) Joh, N. H.; Min, A.; Faham, S.; Whitelegge, J. P.; Yang, D.; Woods, V. L.; Bowie,

- J. U. *Nature* **2008**, *453*, 1266-1270.
- (28) Zhang, X.; Chien, E. Y. T.; Chalmers, M. J.; Pascal, B. D.; Gatchalian, J.; Stevens, R. C.; Griffin, P. R. *Anal. Chem.* **2010**, *82*, 1100-1108.
- (29) Rietschel, B.; Bornemann, S.; Arrey, T. N.; Baeumlisberger, D.; Karas, M.; Meyer, B. *Proteomics* **2009**, *9*, 5553-5557.
- (30) Henderson, R.; Unwin, P. N. *Nature* **1975**, *257*, 28-32.
- (31) Palczewski, K.; Kumasaka, T.; Hori, T.; Behnke, C. A.; Motoshima, H.; Fox, B. A.; Trong, I. L.; Teller, D. C.; Okada, T.; Stenkamp, R. E.; Yamamoto, M.; Miyano, M. *Science* **2000**, *289*, 739-745.
- (32) Cherezov, V.; Rosenbaum, D. M.; Hanson, M. A.; Rasmussen, S. G. F.; Thian, F. S.; Kobilka, T. S.; Choi, H.; Kuhn, P.; Weis, W. I.; Kobilka, B. K.; Stevens, R. C. *Science* **2007**, *318*, 1258-1265.
- (33) Jaakola, V.-P.; Griffith, M. T.; Hanson, M. A.; Cherezov, V.; Chien, E. Y. T.; Lane, J. R.; Ijzerman, A. P.; Stevens, R. C. *Science* **2008**, *322*, 1211-1217.
- (34) Renthal, R. *Biochemistry* **2006**, *45*, 14559-14566.
- (35) Curnow, P.; Booth, P. J. *Proc. Natl. Acad. Sci. U.S.A.* **2009**, *106*, 773-778.
- (36) Riley, M. L.; Wallace, B. A.; Flitsch, S. L.; Booth, P. J. *Biochemistry* **1997**, *36*, 192-196.
- (37) Yamaguchi, S.; Tuzi, S.; Tanio, M.; Naito, A.; Lanyi, J. K.; Needleman, R.; Saito, H. *J. Biochem.* **2000**, *127*, 861-869.
- (38) Möller, C.; Büldt, G.; Dencher, N. A.; Engel, A.; Müller, D. J. *J. Mol. Biol.* **2000**, *301*, 869-879.
- (39) Jacquier, J. C.; Desbene, P. L. *J. Chrom. A* **1996**, *743*, 307-314.
- (40) Booth, P. J.; Farooq, A.; Flitsch, S. L. *Biochemistry* **1996**, *35*, 5902-5909.
- (41) Wang, J.; Heyes, C. D.; El-Sayed, M. A. *J. Phys. Chem.* **2002**, *106*, 723-729.
- (42) Chen, Y.; Barkley, M. D. *Biochemistry* **1998**, *37*, 9976-9982.
- (43) Kalisky, O.; Feitelson, J.; Ottolenghi, M. *Biochemistry* **1981**, *20*, 203-209.
- (44) Michaux, C.; Pomroy, N. C.; Prive, G. G. *J. Mol. Biol.* **2008**, *375*, 1477-1488.
- (45) Patzelt, H.; Ulrich, S. D.; Egbringhoff, H.; Dux, P.; Ashurst, J.; Simon, B.; Oschkinat, H.; Oesterhelt, D. *J. Biomol. NMR* **1997**, *10*, 95-106.
- (46) Seigneuret, M.; Neumann, J.-M.; Rigaut, J.-L. *J. Biol. Chem.* **1991**, *266*, 10066-10069.
- (47) Garavito, R. M.; Ferguson-Miller, S. *J. Biol. Chem.* **2001**, *276*, 32403-32406.
- (48) le Maire, M.; Champeil, P.; Moller, J. V. *Biochim. Biophys. Acta* **2000**, *1508*, 86-111.
- (49) Qin, L.; Hiser, C.; Mulichak, A.; Garavito, R. M.; Ferguson-Miller, S. *Proc. Nat. Acad. Sci. U.S.A.* **2006**, *103*, 16117-16122.
- (50) Büldt, G.; Konno, K.; Nakanishi, K.; Plöhn, H.-J.; Rao, B. N.; Dencher, N. A. *Photochem. Photobiol.* **1991**, *54*, 873-879.

- (51) Brouillette, C. G.; McMichens, R. B.; Stern, L. J.; Khorana, H. G. *Proteins: Struct. Funct. Gen.* **1989**, *5*, 38-46.
- (52) Faham, S.; Bowie, J. U. *J. Mol. Biol.* **2002**, *316*, 1-6.
- (53) Barrera, N. P.; Di Bartolo, N.; Booth, P. J.; Robinson, C. V. *Science* **2008**, *321*, 243-246.
- (54) Stelzer, W.; Poschner, B. C.; Stalz, H.; Heck, A. J.; Langosch, D. *Biophys. J.* **2008**, *95*, 1326-1335.
- (55) Whitelegge, J. P. In *Protein Mass Spectrometry*; Whitelegge, J. P., Ed.; Elsevier: Amsterdam, 2009; Vol. 52, pp 179-196.
- (56) Hufnagel, P.; Schweiger, U.; Eckerskorn, C.; Oesterhelt, D. *Anal. Biochem.* **1996**, *243*, 46-54.
- (57) Whitelegge, J. P.; Le Coutre, J.; Lee, J. C.; Engel, C. K.; Prive, G. G.; Faull, K. F.; Kaback, H. R. *Proc. Natl. Acad. Sci. U.S.A.* **1999**, *96*, 10695-10698.
- (58) Siuti, N.; Kelleher, N. L. *Nat. Methods* **2007**, *4*, 817-821.
- (59) Whitelegge, J. P.; Gundersen, C. B.; Faull, K. F. *Protein Sci.* **1998**, *7*, 1423-1430.
- (60) Schey, K. L.; Papac, D. I.; Knapp, D. R.; Crouch, R. K. *Biophys. J.* **1992**, *63*, 1240-1243.
- (61) Schaller, J.; Pellascio, B. C.; Schlunegger, U. P. *Rapid Commun. Mass Spectrom.* **1997**, *11*, 418-426.
- (62) Whitelegge, J. *Trends in Analytical Chemistry* **2005**, *24*, 576-582.
- (63) Barnidge, D. R.; Dratz, E.; Jesaitis, A. J.; Sunner, J. *Anal. Biochem.* **1999**, *269*, 1-9.
- (64) Schindler, P. A.; Vandorsselaer, A.; Falick, A. M. *Anal. Biochem.* **1993**, *213*, 256-263.
- (65) Whitelegge, J. P.; Halgand, F.; Souda, P.; Zabrouskov, V. *Exp. Rev. Proteomics* **2006**, *3*, 585-596.
- (66) Wales, T. E.; Engen, J. R. *Mass Spectrom. Rev.* **2006**, *25*, 158-170.
- (67) Guex, N.; Peitsch, M. C. *Electrophoresis* **1997**, *18*, 2714-2723.
- (68) Konishi, T.; Packer, L. *FEBS Lett.* **1977**, *80*, 455-458.
- (69) Englander, J. J.; Englander, S. W. *Nature* **1977**, *265*, 658-659.
- (70) Faham, S.; Boulting, G. L.; Massey, E. A.; Yohannan, S.; Yang, D.; Bowie, J. U. *Protein Sci.* **2005**, *14*, 836-840.
- (71) Kawamura, I.; Tanabe, J.; Ohmine, M.; Yamaguchi, S.; Tuzi, S.; Naito, A. *Photochem. Photobiol.* **2009**, *85*, 624-630.
- (72) Nannepaga, S. J.; Gawalapu, R.; Velasquez, D.; Renthal, R. *Biochemistry* **2004**, *43*, 550-559.
- (73) Huang, K.; Bayley, H.; Liao, M.; London, E.; Khorana, H. G. *J. Biol. Chem.* **1981**, *256*, 3802-3809.
- (74) Tanio, M.; Tuzi, S.; Yamaguchi, S.; Konishi, H.; Naito, A.; Needleman, R.; Lanyi, J. K.; Saitô, H. *Biochim. Biophys. Acta* **1998**, *1375*, 84-92.

- (75) Booth, P. J.; Fitsch, S. L.; Stern, L. J.; Greenhalgh, D. A.; Kim, P. S.; Khorana, H. G. *Nat. Struct. Biol.* **1995**, *2*, 139-143.
- (76) Chetty, P. S.; Mayne, L.; Lund-Katz, S.; Stranz, D. D.; Englander, S. W.; Phillips, M. C. *Proc. Natl. Acad. Sci. U.S.A.* **2009**, *106*, 19005-19010.
- (77) Mowery, P. C.; Lozier, R., H.; Chae, Q.; Tseng, G. C.; Taylor, M.; Stoeckenius, W. *Biochemistry* **1979**, *18*, 4100-4107.

Chapter-6 Hydrogen Exchange Mass Spectrometry Reveals Light-Induced Changes in the Structural Dynamics of a Biomolecular Machine

6.1 Introduction

Native proteins adopt unique structures that are linked to specific biological functions. However, these structures are not static. Numerous investigations have highlighted a close association between protein function and dynamics,¹⁻⁷ although the exact nature of this relationship remains a matter of debate.⁸⁻¹¹ Also, the term "conformational dynamics" can carry different connotations.¹² We propose the following classification:

(i) A *switching motion (SM)* represents an externally triggered conformational change. SMs are singular events that may be caused by ligand binding, covalent modifications, or an alteration in solvent environment. As a result of one of these factors, the conformational equilibrium of the protein shifts from one region of the energy landscape to another.¹³

(ii) Many proteins act as molecular machines that undergo externally driven *cyclic motions (CMs)*. In contrast to thermal fluctuations (see below), CMs require a non-thermal energy source that drives structural changes along a well-defined cyclic trajectory. For example, a number of transporters in the cell membrane exploit energy stored in an ion concentration gradient to translocate substrate molecules across lipid bilayers. This pumping action involves protein motions that expose a substrate binding site alternatively to the cytoplasmic and the extracellular surface.¹⁴⁻¹⁶ In a related fashion, the CMs of stator-rotor assemblies are energized by a proton-motive force or by nucleotide-

triphosphate hydrolysis.^{17, 18} The salient feature that distinguishes SMs from CMs is the inherently repetitive nature of the latter.

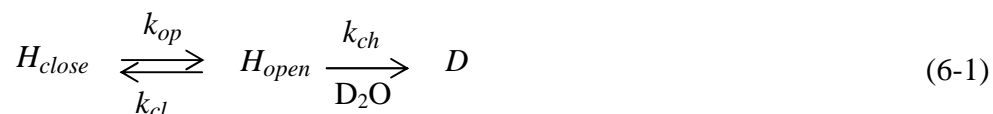
(iii) All proteins undergo incessant *thermal fluctuations (TFs)* that are coupled to random motions of the surrounding solvent.¹⁹ TFs are stochastic events that span a multitude of time and length scales, from picosecond movements of individual side chains to infrequent unfolding/refolding transitions of the entire protein.^{12, 20} At equilibrium, all states on the energy landscape are populated according to their Boltzmann weights.²¹ TFs lead to an ongoing interconversion between these states, with rates that are governed by free energy barriers.^{12, 20, 22} SMs and CMs will generally be superimposed by TFs.

In many cases the character of TFs is profoundly different before and after a SM has occurred. This relationship allows changes in protein switching state to be monitored by techniques that probe TFs.^{23, 24} In contrast, much less is known about the relationship between TFs and CMs.^{25, 26} One possibility is that TFs are more pronounced when a protein undergoes CMs. On the other hand, CMs often manifest themselves as rigid-body movements,^{27, 28} and it seems conceivable that these motions might have only minor effects on TFs. The current work explores this issue by monitoring the dynamics of a molecular machine under "engine-on" and "engine-off" conditions.

TFs can be probed by a variety of techniques. These include computer simulations,²⁹ crystallographic temperature factors,¹² single molecule fluorescence assays,³⁰ quasielastic neutron scattering,²⁶ Mössbauer spectroscopy,²⁰ and NMR spin relaxation measurements.³¹ In addition, amide hydrogen/deuterium exchange (HDX) methods are being widely used.

The readout of HDX experiments may be performed by NMR,³² infrared spectroscopy,⁶ and mass spectrometry.³³⁻³⁶ The latter approach is particularly attractive due to its conceptual simplicity, high sensitivity, the possibility to distinguish co-existing protein conformers, and the capability to study proteins that are beyond the NMR size range.

In typical continuous-labeling HDX experiments the protein is placed in a D₂O-containing environment, and deuterium incorporation is monitored as a function of time.³² Backbone amide hydrogens can reside either in a closed or in an open state.³⁷ Closed sites are protected from exchange, either by N-H···O=C hydrogen bonding or by solvent exclusion (or a combination of both). Open sites are not involved in hydrogen bonding and they are accessible to the solvent.³⁸ HDX at these unprotected sites proceeds with a chemical rate constant k_{ch} .³⁹ Most amide groups in natively folded proteins predominantly reside in a closed state. Slow HDX at these sites nonetheless takes place due to short-lived excursions to open conformations. As a result of these TFs, each amide group undergoes exchange with a characteristic rate constant k_{HDX} . Opening and closing rate constants are designated as k_{op} and k_{cl} , respectively, and the overall HDX mechanism can be described as^{32, 40}



The EX1 regime ($k_{ch} \gg k_{cl}$) is characterized by $k_{HDX} = k_{op}$. Under EX2 conditions ($k_{cl} \gg k_{ch}$) isotope exchange occurs with $k_{HDX} = K_{op} \times k_{ch}$ where $K_{op} = (k_{op} / k_{cl})$. The free energy difference associated with opening of an amide group in the EX2 regime is

$$\Delta G^{EX2} = -RT \ln K_{op} \quad (6-2)$$

Most HDX investigations in the literature have focused on the effects of SMs.^{23, 34, 41-47} Comparing "before" and "after" scenarios (such as free vs. ligand-bound), those studies exploit the fact that the stability of a protein depends on its switching state, leading to differences in the TFs that modulate the EX2 kinetics according to equation 6-2.⁴⁸ In contrast to the numerous HDX studies devoted to SMs, there appear to be no prior attempts to explore whether the HDX behavior of molecular machines is sensitive to the occurrence of CMs.

Bacteriorhodopsin (BR) is a molecular machine that acts as light-driven proton pump. In its natural purple membrane environment BR is packed as trimers that form a two-dimensional lattice. However, monomers represent the functional unit of the protein.^{49, 50} Each monomer consists of seven transmembrane helices that are connected by short loops. In addition, the protein contains a central retinal chromophore that is bound to K216 via a Schiff base. H⁺ translocation is mediated by a photocycle that starts with the light-adapted all-*trans*/15-*anti* ground state and proceeds through a number of sequential intermediates.⁵¹⁻⁵⁴ Photoisomerization of the retinal to the 13-*cis*/15-*anti* configuration represents the primary event. The resulting strained chromophore configuration drives all subsequent steps of the cycle.⁵⁴ Vectorial H⁺ translocation involves proton transfer from the Schiff base to D85, and subsequent Schiff base reprotonation by D96. Reisomerization ultimately regenerates the BR ground state. The photocycle is coupled to various protein conformational changes^{55, 56} that involve partial rotation, tilting, and bending motions of helices.⁵⁷⁻⁶⁰ In the dark, the retinal equilibrates between the all-*trans*/15-*anti* and 13-*cis*/15-*syn* forms.⁶¹ Protein structural differences between the light-adapted ground state and dark-adapted BR are

small when compared to the substantial motions that occur during the photocycle.⁶²

BR represents a suitable test system for exploring a possible relationship between CMs and TFs. Under continuous illumination the protein performs an ongoing cycle of structural transitions,^{57, 58} whereas many of these motions are absent in the dark.⁶² We probe the extent of TFs in comparative HDX measurements with and without illumination. Under properly controlled conditions our investigations reveal dramatically different isotope exchange kinetics that reflect a light-induced destabilization of the protein. It appears that this destabilization is caused by retinal-mediated mechanical agitation, which acts in a manner comparable to an internal heat source. Our findings highlight the utility of HDX techniques for studying the behavior of molecular machines.

6.2 Experimental

6.2.1 Reagents and Sample Preparation

Purple membranes from *Halobacterium salinarum* were harvested and purified by sucrose gradient centrifugation as described in Chapter-2. SDS, sodium phosphate and formic acid were from Sigma (St. Louis, MO). L- α -1,2-dimyristoylphosphatidylcholine (DMPC) was obtained from Avanti (Alabaster, AL) and 3-[(3-cholamidopropyl) dimethylammonio]-1-propanesulfonate (CHAPS) was from Calbiochem (San Diego, CA). All chemicals were used as received.

Most experiments were conducted on monomeric BR^{50, 63} that was generated by refolding of SDS-denatured bacterioopsin (BO, the retinal-free form of the protein). SDS-denatured

BO was prepared by delipidation as described in Chapter-4, and the absence of retinal was confirmed by UV-Vis spectroscopy. Monomeric BR^{50, 63} was prepared by mixing SDS-denatured BO with all-*trans* retinal from an ethanol stock solution in equimolar retinal:protein ratio. Subsequently, 10 mM phosphate refolding buffer (pH 6) containing 2% DMPC/CHAPS bicelles was added to the mixture. The regeneration yield of this procedure is on the order of 90%,⁶⁴ as confirmed on the basis of BR:BO peak intensity ratios in the mass spectra shown in Chapter-5. Monomeric BO was generated following the same procedure, but without addition of retinal. All samples were equilibrated overnight at room temperature in the dark. The resulting solutions contained 10 μ M protein, 1% DMPC, 1% CHAPS, 0.1% SDS, and less than 0.2 % (v/v) ethanol. The protein was concentrated tenfold by lyophilization and subsequent resuspension in phosphate buffer. In addition to studies on monomeric BR, we also conducted HDX measurements on intact purple membranes. For these measurements purple membrane stock suspension was diluted with phosphate buffer to a protein concentration of 100 μ M. The final buffer concentration was 100 mM. All other steps were performed as described below for the monomeric samples.

6.2.2 Hydrogen/Deuterium Exchange Under Light/Dark Conditions

All HDX experiments of this work were conducted in continuous-labeling mode. In order to promote extensive isotope exchange, HDX was conducted in mildly basic solution (pH meter reading 8.5). Chemical exchange rate constants k_{ch} under these conditions are in the range of 1000 s^{-1} , roughly three orders of magnitude higher than in neutral solution.^{39, 65} This difference in pH is the reason for the greater exchange levels observed in the current work, as compared to previous experiments that were conducted at a pH meter reading of

6 in Chapter-5. BR consists of 248 residues, 11 of which are prolines, such that the number of backbone N-H groups is 236. Isotope labeling was initiated by mixing the protein solutions with D₂O-based buffer (100 mM sodium phosphate) in a 1:4 volume ratio. The resulting solution was transferred into two identical microcentrifuge tubes (Eppendorf, Hamburg, Germany) that had their lids fitted with transparent windows made from glass cover slips and fastened with epoxy glue. Each tube contained 350 μ L protein solution. One tube was wrapped in aluminum foil and kept in the dark. The other one was continuously illuminated at 530 nm using a Thorlabs light-emitting diode (model M530L1, Newton, NJ) that was operated using a 275 mW power supply. The light source was fitted with a collimator, and the protein samples were irradiated from above through the transparent lid with a distance of 3 cm between the collimator output and the surface of the solution. Both tubes were thermostated at 26 °C in a circulating water bath; a digital resistance thermometer was used to confirm that light and dark samples were at the same temperature. 35 μ L aliquots were removed at various time points ranging from 4 minutes to 48 hours. These aliquots were quenched by mixing with 3 μ L of 2 M hydrochloric acid for a final pH of 2.4, followed by flash freezing in liquid nitrogen.

6.2.3 Liquid Chromatography/Mass Spectrometry

LC/MS measurements were conducted using the same protocol as described in Chapter-5. The low-temperature SEC/MS analysis can preserve retinal binding to BR, such that the HDX properties of BR and BO sub-populations in bulk solution could be tracked independently. Experimental spectra were converted to mass distributions using deconvolution software provided by the instrument manufacturer. Relative HDX levels of

the intact protein were determined from the deconvoluted mass distributions using the relationship³⁶

$$\text{deuteration percentage} = \frac{m - m_0}{m_{100} - m_0} \times 100\% \quad (6-3)$$

In this expression m is the measured mass (peak maximum) of the protein, and m_0 and m_{100} are the values of zero time point controls and maximally deuterated samples. Zero time point control data were obtained by exposing the protein first to the 0°C quenching solution and then to the labeling buffer. Maximally deuterated protein samples were obtained by exposing refolded BO to labeling buffer for 24 h using the same conditions as for the light/dark samples. The uncorrected labeling level of these samples was 97% (229 out of 236 amide hydrogens), indicating the occurrence of 3% back exchange during analysis. Normalized HDX kinetics (equation 6-3) was analyzed by single- or double-exponential fitting using Sigmaplot. All data shown are based on triplicate independent experiments. Error bars correspond to standard deviations. Both proteolytic digestion³⁴ and top-down strategies^{66, 67} were pursued in an effort to obtain spatially-resolved HDX information. Unfortunately, the sequence coverage of those experiments was not adequate, such that the considerations of this work must be restricted to HDX data at the intact protein level.

6.2.3 Flash Absorption Spectroscopy

Photocycle kinetics were measured by time-resolved difference spectroscopy, using a custom-built flash photolysis apparatus.⁶⁸ 0.5 mL of BR solution (prepared as above for HDX experiments) with an optical density of ~0.6 were placed in a cuvette which allowed the 532 nm second harmonic of a Nd:YAG Minilite II laser to excite the sample at a 90°

angle to the probe light beam from a Oriel QTH source. The photocycle was triggered with a 7 ns laser flash at room temperature. The resulting absorbance changes were recorded using a photomultiplier, amplifier, and Gage Compuscope AD converter. Up to 600 single-shot traces were averaged to produce an adequate signal-to-noise ratio.

6.3 Results and Discussion

6.3.1 HDX Measurements on Purple Membranes

For comparing BR structural dynamics under illumination and in the dark by HDX mass spectrometry, investigations were initially conducted on intact purple membranes. Somewhat disappointingly, the isotope exchange behavior observed under light/dark conditions for these samples is virtually indistinguishable (Figure 6-1). Consistent with earlier reports,^{69, 70} purple membranes exhibit a high degree of protection. Even after an extended labeling period of 24 h the BR deuteration level is only 43%. Although spatially-resolved HDX studies on BR are difficult,⁷¹ labeling under the conditions of Figure 6-1 is known to occur predominantly in peripheral regions, i.e., loops and helix termini.^{55, 69, 72} Possible effects of light-induced CMs are expected to be most prevalent for transmembrane segments in the vicinity of the retinal.^{55, 57, 58} Previous work⁶⁹ already implied that opening/closing events (equation 6-1) at these internal segments are exceedingly rare and/or short-lived, such that the lack of light-induced differences in Figure 6-1 is not completely surprising. Minor light-induced differences in exchange kinetics were reported in an older tritium exchange study.⁷³ However, those earlier purple membrane radiolabeling data⁷³ exhibited considerable scatter, and no error bars were reported. Under the conditions of our work we cannot confirm the effects reported in ref.⁷³ We do not

dispute that purple membranes undergo a certain "softening" upon illumination, as suggested by neutron scattering²⁶ and hydroxylaminolysis investigations.^{63, 74} Nonetheless, light-induced changes in structure and dynamics do not manifest themselves in altered HDX kinetics under the conditions of Figure 6-1.

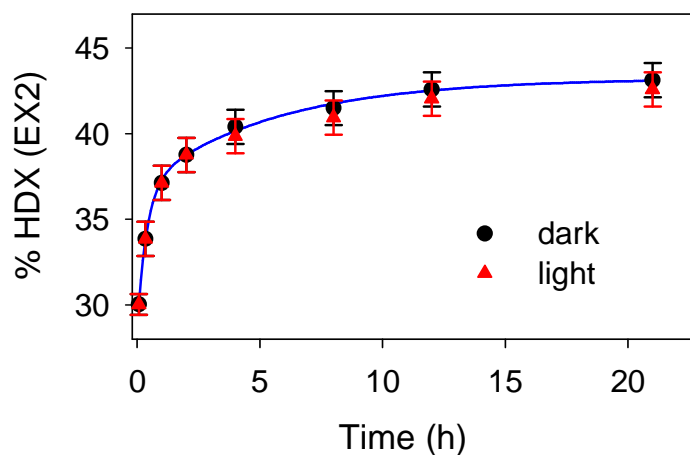


Figure 6-1. HDX kinetics of native BR in purple membranes monitored by ESI-MS. Red triangles and black circles represent data recorded under green light illumination (530 nm) and in the dark, respectively. The blue lines represent a bi-exponential fit, $D\%(t) = y_0 + a_1(1 - \exp[-k_1t]) + a_2(1 - \exp[-k_2t])$, with $y_0 = 28.7$, $a_1 = 8.1$, $k_1 = 2.56 \text{ h}^{-1}$, $a_2 = 6.4$, $k_2 = 0.18 \text{ h}^{-1}$. Isotope exchange under the conditions of this experiment proceeds in the EX2 regime; no EX1-related peak splitting was observed in the BR mass distributions (not shown).

6.3.2 HDX Measurements on Monomeric BR

Packing effects inside the purple membrane can restrict the extent of protein motions.^{75, 76} For the remainder of this study we therefore shift our attention from purple membranes to monomeric BR.^{50, 63} The monomeric form is known to undergo more extensive HDX as described in Chapter-5, reflecting greater overall dynamics with enhanced solvent access to formerly protected amide sites.⁵⁰ Flash photolysis was used to verify that monomeric BR undergoes a photocycle (Figure 6-2, black solid lines).^{28, 77-79} The protein remains active even after extensive continuous illumination (Figure 6-2, green and blue lines), mimicking the conditions used for subsequent HDX experiments. For comparison, Figure 6-2 also shows data for intact purple membranes (black broken line) which reveal photocycle kinetics that are somewhat faster than for the monomeric protein. The data of Figure 6-2 are consistent with earlier work on solubilized BR,^{80, 81} where it was shown that reprotonation of the Schiff base is slower in the absence of the purple membrane lattice. These altered kinetics extend the lifetime of the M state, and thus lead to a greater accumulation of this photocycle intermediate (as seen from the slower decay of the 420 nm signals in Figure 6-2). Overall, the data of Figure 6-2 confirm that monomeric BR is a functional molecular machine that continuously undergoes CMs upon illumination, albeit at a lower rate than purple membrane samples.

Monomeric BR exhibits HDX kinetics that are profoundly different in the dark (Figure 6-3, a-d) and under illumination (Figure 6-3, e-h). In both cases the protein exhibits a combination of EX2 and EX1 exchange. The former manifests itself as a gradual shift of the BR main peak to higher mass (highlighted in green, Figure 6-3). Superimposed on this

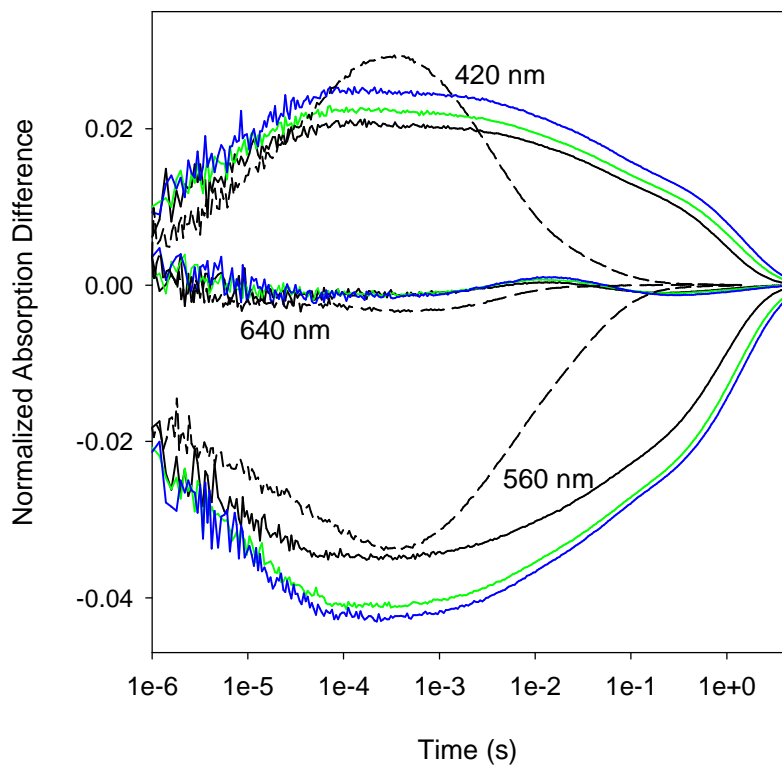


Figure 6-2. BR photocycle kinetics monitored by time-resolved absorption difference spectroscopy following a 532 nm excitation pulse at pH 8.5. The transients were recorded at 560 nm (BR ground state), 420 nm (M intermediate), and 640 nm (O intermediate). Data are shown for monomeric BR without prior continuous illumination (black solid line), after 4 h of continuous illumination (green), and after 24 hour of continuous illumination (blue). Also included are the kinetics of native purple membranes (black broken line). The data shown for each sample were normalized to the absorbance of the 568 nm retinal peak.

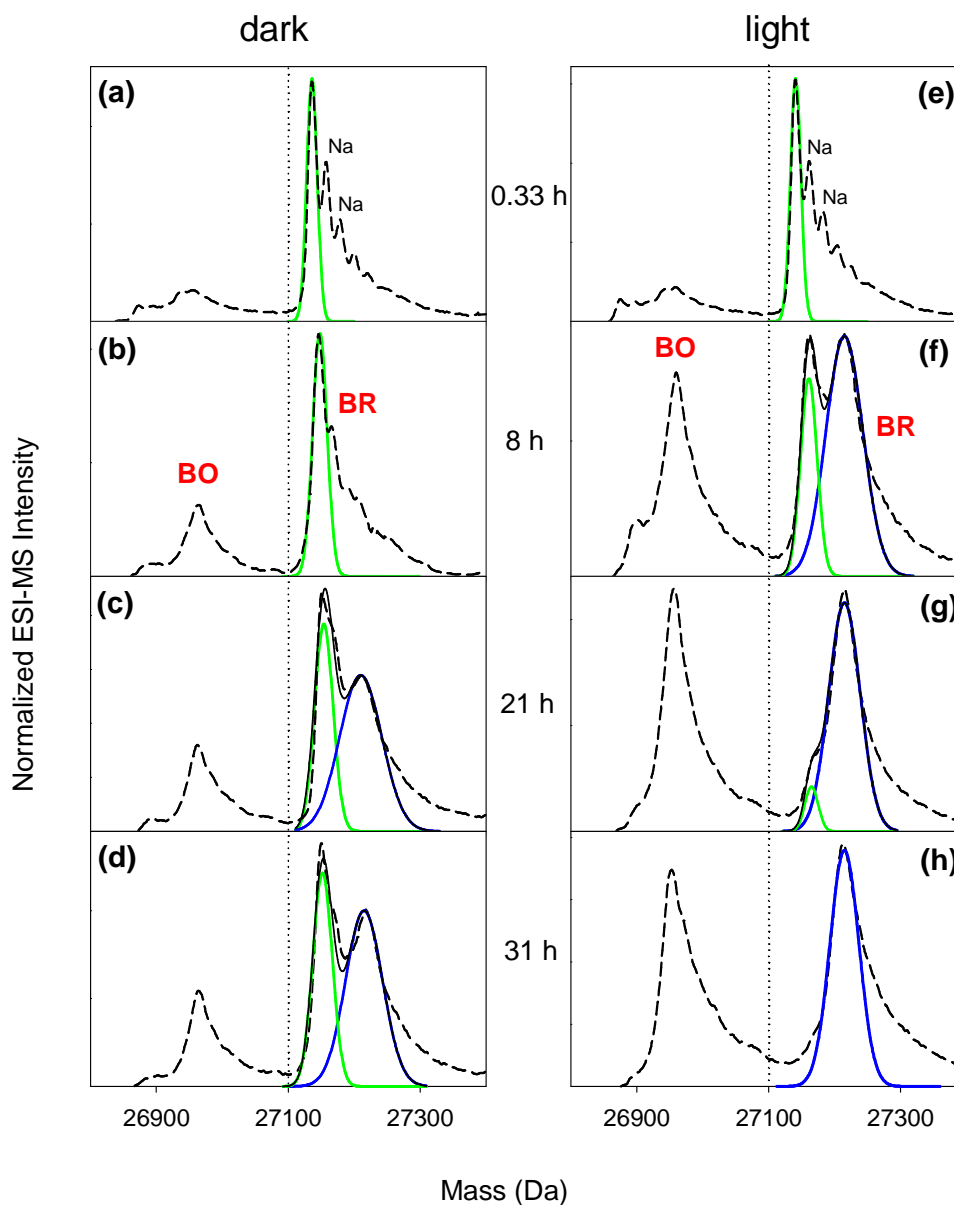


Figure 6-3. Mass distributions of monomeric BR at selected HDX time points. Panels (a)-(d) represent the behavior of samples kept in the dark. Data in panels (e)-(f) were recorded after continuous illumination of the protein. Black broken lines represent experimental spectra. Dotted horizontal lines at 27100 Da separate contributions attributable to BO and BR, as highlighted in panels (b) and (f). Gaussian curve fitting was employed to determine the locations of peak areas and maxima of BR. Green: EX2 component, blue: EX1 component, black solid line: sum of EX1 and EX2 components.

EX2 process is the appearance of a highly deuterated EX1 component that increases in magnitude over time (Figure 6-3, blue). Combined EX1/EX2 processes have previously been observed for other proteins.^{40, 82, 83} Figure 6-3 also reveals the occurrence of BR → BO conversion, leading to ca. 50% retinal loss after 31 h of illumination (Figure 6-3h). This hydrolysis reaction can also be traced by UV-Vis spectroscopy (data not shown).⁸⁴ Retinal loss is less extensive in the dark (Figure 6-3d). The occurrence of retinal loss under illumination has previously been reported for intact purple membranes, where the hydrolysis rate was shown to increase with pH. Hence, the observation of this process under the conditions of the current work (monomeric BR at pH 8.5) is not unexpected. In Figure 6-2 this degradation is not apparent because the photocycle signals were normalized to the absorption maximum of the active protein. We emphasize that the MS approach used here allows the HDX kinetics of co-existing BR and BO to be monitored separately. As a result, the BR behavior can be probed without interference from BO signals (Figure 3). In other words, the BR data discussed below exclusively reflect the properties of the intact protein, prior to retinal loss.

Least-square analyses of the measured kinetics reiterate the considerable differences in HDX behavior for the light/dark samples. Illumination enhances the EX2 rate constant by a factor of two (Figure 6-4a, see caption for fitting parameters). A similar acceleration factor is seen for the EX1 process (Figure 6-4b). BO formation under illumination proceeds with an apparent rate constant of 0.12 h^{-1} . In the dark this Schiff base hydrolysis is much slower, and the reaction rate cannot be readily determined (Figure 6-4c). The maximum of the EX1 component (blue peak envelopes in Figure 6-3) corresponds to an HDX level of

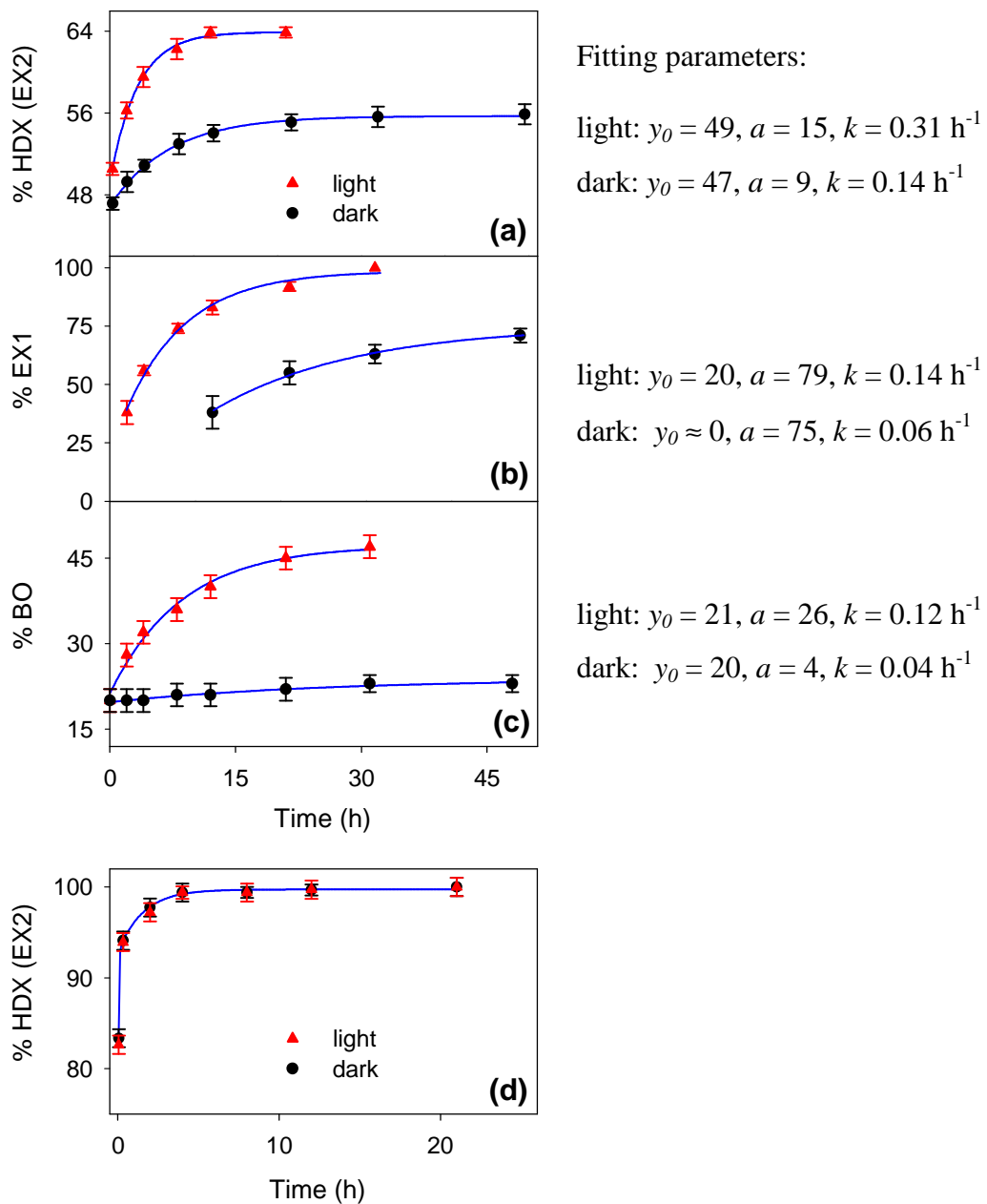


Figure 6-4. Kinetic behavior of monomeric BR under illumination (red) or in dark (black). (a) EX2 HDX kinetics, determined from the maxima of the "green" component in Figure 6-3. (b) EX1 HDX kinetics, reflecting the rise of the "blue" component relative to the "green" one in Figure 6-3. (c) Percentage of BO in the protein samples as a function of time. Blue lines are exponential fits with $y(t) = y_0 + a(1 - \exp[-kt])$, fitting parameters are shown in the figure. Panel (d) shows the results of control experiments, displaying a light/dark comparison of the EX2 HDX kinetics for pure refolded BO samples.

89% for all conditions studied. BO peak maxima in Figure 6-3 reveal somewhat higher HDX levels, between 95% and 100%.

As noted in the Methods section, care was taken to ensure that comparative light/dark experiments were conducted in an artifact-free fashion. As an additional control, HDX studies were carried out on pure BO samples, i.e., monomeric protein that had been refolded in the absence of retinal. Figure 6-4d confirms that the HDX kinetics of these chromophore-free samples are indistinguishable under illumination and in the dark. This result reinforces the conclusion that the HDX differences seen for monomeric BR (Figures 6-3, 4) are the result of light-induced protein structural dynamics.

Some readers might be tempted to ascribe the kinetic phenomena (Figure 6-3, e-h) *directly* to CMs that occur during the photocycle, possibly interpreting the EX1 "blue" peak as an accumulating photocycle intermediate. Unfortunately, such an interpretation is incorrect. The link between illumination and HDX behavior is more subtle, as can be seen from several arguments. First, the EX1 amide opening rate of $4 \times 10^{-5} \text{ s}^{-1}$ (Figure 6-4b) is many orders of magnitude slower than the $\sim 1 \text{ s}^{-1}$ photocycle turnover rate (Figure 6-2). Thus, the EX1 peak cannot represent a photocycle intermediate. Also, X-ray crystallographic studies did not reveal any photocycle intermediates with a large number of open amide hydrogens⁵⁴ that would be required HDX via equation 6-1. Most importantly, the general nature of the phenomena seen in Figure 6-3 (i.e., a combination of EX2 and EX1 with slow retinal loss) is the same in the dark and under illumination. Light exposure enhances the rates of these processes, while their overall character remains unchanged. It must be concluded that the

protein motions that mediate HDX largely correspond to *intrinsic* TFs, rather than photocycle-associated CMs. The extent of these TFs is dramatically enhanced in the presence of light-induced CMs. Thus, TFs that mediate HDX are closely coupled to photon-driven CMs, but the two types of dynamics remain distinct from each other.

6.3.3 Casting the HDX Kinetics in a Thermodynamic/Kinetic Model

The data presented here allow the development of a minimalist model that can account for the HDX behavior of monomeric BR under light/dark conditions. Our considerations are based on equation 6-1, according to which HDX is mediated by TFs that result in amide hydrogen opening/closing transitions.³² For reasons of simplicity, we assume that these fluctuations encompass distinct groups of amide hydrogens in a cooperative fashion. The interpretation of protein structural dynamics in terms of such cooperative units (foldons) is well established.^{85, 86}

For any protein, the occurrence of parallel EX1 and EX2 kinetics implies the involvement of at least four different conformational species.^{40, 83, 87} EX2 exchange reflects rapid fluctuations between the natively folded state F , and a native-like (but partially unfolded) excited species F^* . EX1 exchange can be attributed to the occurrence infrequent transitions between F and a significantly unfolded conformer U . Slow interconversion between F and U requires crossing of a major free energy barrier that is associated with a transition state TS .^{40, 83, 87} For clarity, we emphasize again that none of the four conformers F , F^* , TS , or U corresponds to a BR photocycle intermediate. Instead, the entire photocycle proceeds largely within the confines of the native conformational ensemble F . Thermally activated

excursions to F^* or U are not directly linked to vectorial proton transport.

Figure 6-5 displays the number of open hydrogens for F , F^* , TS , and U , together with the corresponding free energy values. Light and dark scenarios are distinguished by subscripts. The free energy of U is arbitrarily normalized to zero. The number of open hydrogens in U is 89%, in accordance with the EX1 signals of Figure 6-3 (blue Gaussian curves). Based on its HDX level, U is extensively unfolded while retaining some residual protection. We make the simplifying assumption that the same transition state is encountered under illumination and in the dark. The positioning of all the species in the two-dimensional diagram of Figure 6-5 is consistent with the measured HDX parameters (Table 6-1). Only the location of TS is somewhat arbitrary, since its properties cannot be ascertained with certainty from the data of this work.

6.3.4 Mechanistic Origin of Differences in Light/Dark HDX Behavior

The findings of this work reveal that illumination of monomeric BR causes sub-global as well as global destabilization of the protein. EX2 processes report on the former, whereas EX1 events are related to the latter. At the sub-global level, TFs involve a considerably larger number of EX2 sites under illumination (15%) than in the dark (9%, Table 6-1). This implies that transitions between F and F^* entail more extensive structural changes when the protein is exposed to light.²⁶ In other words, F^*_{light} represents a more unfolded conformation than F^*_{dark} (Figure 6-5). The occurrence of light-induced destabilization becomes most obvious when relating the ΔG^{EX2} values to the number of hydrogens involved. Accordingly, the average free energy required for the opening of a single EX2 site

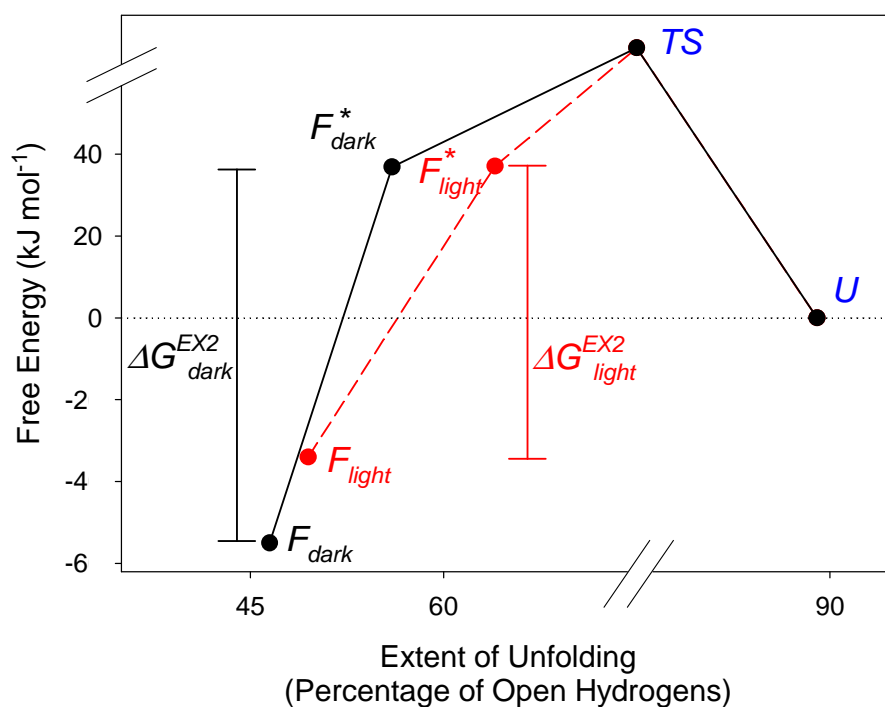


Figure 6-5. Schematic diagram, depicting the properties of monomeric BR conformers under illumination (red) and in the dark (black). Species highlighted in blue are common to both scenarios. The x -axis displays the percentage of amide hydrogens that adopt an open (unprotected) state. The y -axis represents free energy. The positioning of all species is consistent with the data displayed in Table 1. EX2 processes are mediated by fluctuations between F and F^* , whereas EX1 exchange arises due to interconversion between F and U . Note that the scaling of the free energy axis in this diagram is not linear, to emphasize differences between F_{dark} and F_{light} . Additional information is provided in the text.

Table 6-1. Structural and thermodynamic parameters associated with the HDX kinetics of monomeric BR.

	% open N-H sites in F ^a	ΔG^{EX2} (kJ/mol) ^b	% additional open N-H sites in F ^{*c}	Free energy difference Between U and F (kJ/mol)
Light	49	40.5	15	3.4 ^d
Dark	47	42.4	9	5.5 ^e

Notes:

^a EX2 burst phase amplitude (fitting parameter y_0) in Figure 6-4a.

^b Determined from equation 6- 2, with $k_{ch} \approx 1000 \text{ s}^{-1}$.^{39, 65}

^c EX2 amplitude (fitting parameter a) in Figure 6-4a.

^d Determined from the EX1 burst phase amplitude, which implies a [U]/[F] equilibrium ratio of 0.25 under illumination.

^e The ratio of the EX1 rates reflects an activation energy difference according to²² $rate_1/rate_2 = \exp(\Delta\Delta G^\ddagger/RT)$, where $|\Delta\Delta G^\ddagger| = 2.1 \text{ kJ mol}^{-1}$. In combination with (d), this implies an overall free energy difference of $(3.4 + 2.1) \text{ kJ mol}^{-1} = 5.5 \text{ kJ mol}^{-1}$.

is 4.8 kJ mol^{-1} in the dark, but only 2.7 kJ mol^{-1} during illumination. The EX1 behavior of monomeric BR suggests that illumination reduces the thermodynamic stability (i.e., the free energy difference between F and U) from 5.5 to 3.4 kJ mol^{-1} (Figure 6-5, Table 6-1). This destabilization causes U to be more highly populated in the light ($\sim 20\%$) than in the dark ($< 10\%$). In our view Schiff base hydrolysis likely occurs from U . The Schiff base is sensitive to attack by water and other nucleophiles.^{63, 88} U represents a highly unfolded conformer that will not significantly protect the Schiff base from solvent access. A light-induced equilibrium shift from F to U will therefore lead to accelerated retinal loss, consistent with the behavior seen in Figure 6-4c.

6.4 Conclusions

HDX is mediated by opening/closing events of exchangeable hydrogens that occur as the result of TFs. In this work we examined the behavior of a molecular machine, with the goal of determining whether the extent of these TFs depends on the occurrence of CMs. BR is a molecular machine that is fuelled by light. It is a simple matter to perform comparative measurements for this system under CM-on and CM-off conditions. Irrespective of the illumination state, monomeric BR undergoes two types of TFs. Small-scale EX2 fluctuations between the natively folded F and a native-like excited species F^* only affect a handful of N-H sites. In addition, F also undergoes rare EX1 transitions to a much more unfolded state U .

Amide hydrogen opening/closing events that are probed by HDX do *not* directly correspond to structural transitions between individual photocycle intermediates.^{54,57-59}

Yet, our experiments reveal dramatically enhanced HDX kinetics when the monomeric protein undergoes CMs in the presence of light. We attribute this phenomenon to a destabilizing effect of the light-driven *trans/cis* retinal switching cycle on the overall protein structure. The retinal is intimately coupled to the surrounding polypeptide elements.⁸⁹ Mechanical agitation of the chromophore is transferred to the protein scaffold, before the energy dissipates into the bulk solvent. The conversion of photon energy to mechanical motions is therefore comparable to the presence of a heat source in the protein interior. In other words, the enhanced TFs seen in our HDX experiments can be ascribed to local heating that occurs as the result of the protein's CMs. The heat involved in this phenomenon likely represents only a small fraction of the initially absorbed energy (226 kJ mol⁻¹ for a 530 nm photon). Our interpretation of retinal movements as a source of thermal energy is consistent with earlier proposals.⁸⁴ We reiterate that the light/dark comparisons of this work were conducted at the same *bulk* temperature. On its way from the retinal "hot spot" to the thermostated solvent, however, the thermal energy must pass through the protein where it enhances TFs (opening/closing events) that promote HDX. Investigations on various different systems have suggested that thermally activated conformational dynamics can "lubricate" certain aspects of protein function.^{11,26,53} In this sense, it is to be expected that the light-enhanced TFs seen here for monomeric BR facilitate certain structural events that are associated with proton translocation. In any case, the current study reveals that HDX-based TF measurements offer a window into the inner workings of molecular machines. In future work, it will be interesting to see if our findings can be corroborated for other proteins that have their function coupled to an external energy source.

6.5 References

- (1) Liang, Z.-X.; Lee, T.; Resing, K. A.; Ahn, N. G.; Klinman, J. P. *Proc. Natl. Acad. Sci. U.S.A.* **2004**, *101*, 9556-9561.
- (2) Codreanu, S. G.; Ladner, J. E.; Xiao, G.; Stourman, N. V.; Hachey, D. L.; Gilliland, G. L.; Armstrong, R. N. *Biochemistry* **2002**, *41*, 15161-15172.
- (3) Wolf-Watz, M.; Thai, V.; Henzler-Wildman, K.; Hadjipavlou, G.; Eisenmesser, E. Z.; Kern, D. *Nat. Struct. Mol. Biol.* **2004**, *11*, 945-949.
- (4) Hollien, J.; Marqusee, S. *Proc. Natl. Acad. Sci. U.S.A.* **1999**, *96*, 13674-13678.
- (5) Pagán, M.; Solá, R. J.; Griebenow, K. *Biotech. Bioeng.* **2008**, *103*, 77-83.
- (6) Zavodszky, P.; Kardos, J.; Svingor, A.; Petsko, A. G. *Proc. Nat. Acad. Sci.* **1998**, *95*, 7406-7411.
- (7) Bhabha, G.; Lee, J.; Ekiert, D. C.; Gam, J.; Wilson, I. A.; Dyson, H. J.; Benkovic, S. J.; Wright, P. E. *Science* **2011**, *332*, 234-238.
- (8) Schwartz, S. D.; Schramm, V. L. *Nat. Chem. Biol.* **2009**, *5*, 551-558.
- (9) Pisljakov, A. V.; Cao, J.; Kamerlin, S. C. L.; Warshel, A. *Proc. Natl. Acad. Sci. U.S.A.* **2009**, *106*, 17359-17364.
- (10) Kamerlin, S. C. L.; Warshel, A. *Proc. Natl. Acad. Sci. U.S.A.* **2010**, *107*, E72.
- (11) Karplus, M. *Proc. Natl. Acad. Sci. U.S.A.* **2010**, *107*, E71.
- (12) Henzler-Wildman, K.; Kern, D. *Nature* **2007**, *450*, 964-972.
- (13) Boehr, D. D.; Nussinov, R.; Wright, P. E. *Nat. Chem. Biol.* **2009**, *5*, 789-796.
- (14) Diallinas, G. *Science* **2008**, *322*, 1644-1645.
- (15) Singh, S. K.; Piscitelli, C. L.; Yamashita, A.; Gouaux, E. *Science* **2008**, *322*, 1655-1661.
- (16) Weyand, S.; Shimamura, T.; Yajima, S.; Suzuki, S.; Mirza, O.; Krusong, K.; Carpenter, E. P.; Rutherford, N. G.; Hadden, J. M.; O'Reilly, J.; Ma, P.; Saidijam, M.; Patching, S. G.; Hope, R. J.; Norbertczak, H. T.; Roach, P. C.; Iwata, S.; Henderson, P. J.; Cameron, A. D. *Science* **2008**, *322*, 709-713.
- (17) Diez, M.; Zimmermann, B.; Börsch, M.; König, M.; Schweinberger, E.; Steigmiller, S.; Reuter, R.; Felekyan, S.; Kudryavtsev, V.; Seidel, C. A.; Gräber, P. *Nat. Struct. Mol. Biol.* **2004**, *11*, 135-141.
- (18) Gennerich, A.; Vale, R. D. *Curr. Op. Cell Biol.* **2009**, *21*, 59-67.
- (19) Frauenfelder, H.; Chen, G.; Berendzen, J.; Fenimore, P. W.; Jansson, H.; McMahan, B. H.; Strope, I. R.; Swenson, J.; Young, R. D. *Proc. Natl. Acad. Sci. U.S.A.* **2009**, *106*, 5129-5134.
- (20) Ansari, A.; Berendzen, J.; Bowne, S. F.; Frauenfelder, H.; Iben, I. T.; Sauke, T. B.; Shyamsunder, E.; Young, R. D. *Proc. Natl. Acad. Sci. U.S.A.* **1985**, *82*, 5000-5004.
- (21) Bai, Y.; Sosnick, T. R.; Mayne, L.; Englander, S. W. *Science* **1995**, *269*, 192-197.

- (22) Bieri, O.; Kiefhaber, T. In *Mechanisms of Protein Folding*; Pain, R. H., Ed.; University Press: Oxford, 2000.
- (23) Liu, Y.; Belcheva, A.; Konermann, L.; Golemi-Kotra, D. *J. Mol. Biol.* **2009**, *391*, 149-163.
- (24) Sugase, K.; Dyson, H. J.; Wright, P. E. *Nature* **2007**, *447*, 1021-1027.
- (25) Pieper, J.; Renger, G. *Biochemistry* **2009**, *48*, 6111-6115.
- (26) Pieper, J.; Buchsteiner, A.; Dencher, N. A.; Lechner, R. E.; Hauß, T. *Phys. Rev. Lett.* **2008**, *100*, (228103)228101-228104.
- (27) Langosch, D.; Arkin, I. T. *Protein Sci.* **2009**, *18*, 1343-1358.
- (28) Simón-Vázquez, R.; Lazarova, T.; Perálvarez-Marín, A.; Bourdelande, J. L.; Padrós, E. *Angew. Chem. int. Ed.* **2009**, *48*, 8523-8525.
- (29) Shaw, D. E.; Maragakis, P.; Lindorff-Larsen, K.; Piana, S.; Dror, R. O.; Eastwood, M. P.; Bank, J. A.; Jumper, J. M.; Salmon, J. K.; Shan, Y.; Wriggers, W. *Science* **2010**, *330*, 341-346.
- (30) Rhoades, E.; Cohen, M.; Schuler, B.; Haran, G. *J. Am. Chem. Soc.* **2004**, *126*, 14686-14687.
- (31) Mittermaier, A.; Kay, L. E. *Science* **2006**, *312*, 224-228.
- (32) Krishna, M. M. G.; Hoang, L.; Lin, Y.; Englander, S. W. *Methods* **2004**, *34*, 51-64.
- (33) Kaltashov, I. A.; Eyles, S. J. *Mass Spectrometry in Biophysics*; John Wiley and Sons, Inc.: Hoboken, NJ, 2005.
- (34) Houde, D.; Berkowitz, S. A.; Engen, J. R. *J. Pharm. Sci.* **2011**, *100*, 2071-2086.
- (35) Miranker, A.; Robinson, C. V.; Radford, S. E.; Aplin, R.; Dobson, C. M. *Science* **1993**, *262*, 896-900.
- (36) Smith, D. L.; Deng, Y.; Zhang, Z. *J. Mass Spectrom.* **1997**, *32*, 135-146.
- (37) Hvidt, A.; Nielsen, S. O. *Adv. Protein Chem.* **1966**, *21*, 287-386.
- (38) Chetty, P. S.; Mayne, L.; Lund-Katz, S.; Stranz, D. D.; Englander, S. W.; Phillips, M. C. *Proc. Natl. Acad. Sci. U.S.A.* **2009**, *106*, 19005-19010.
- (39) Bai, Y.; Milne, J. S.; Mayne, L.; Englander, S. W. *Proteins: Struct. Funct. Genet.* **1993**, *17*, 75-86.
- (40) Konermann, L.; Tong, X.; Pan, Y. *J. Mass Spectrom.* **2008**, *43*, 1021-1036.
- (41) Johnson, R. S.; Walsh, K. A. *Protein Sci.* **1994**, *3*, 2411-2418.
- (42) Englander, J. J.; Del Mar, C.; Li, W.; Englander, S. W.; Kim, J. S.; Stranz, D. D.; Hamuro, Y.; Woods, V. L. *Proc. Natl. Acad. Sci. U.S.A.* **2003**, *100*, 7057 - 7062.
- (43) Xiao, H.; Kaltashov, I. A.; Eyles, S. J. *J. Am. Soc. Mass Spectrom.* **2003**, *14*, 506-515.
- (44) Busenlehner, L. S.; Salomonsson, L.; Brzezinski, P.; Armstrong, R. N. *Proc. Natl. Acad. Sci. U.S.A.* **2006**, *103*, 15398-15403.
- (45) Sperry, J. B.; Smith, C. L.; Caparon, M. G.; Ellenberger, T.; Gross, M. L. *Biochemistry* **2011**, *50*, 4038-4045.

- (46) Chalmers, M. J.; Busby, S. A.; Pascal, B. D.; He, Y.; Hendrickson, C. L.; Marshall, A. G.; Griffin, P. R. *Anal. Chem.* **2006**, *78*, 1005-1014.
- (47) Marcoux, J.; Manb, P.; Castellan, M.; Vives, C.; Forest, E.; Fieschi, F. *FEBS Lett.* **2009**, *583*, 835-840.
- (48) Powell, K. D.; Ghaemmaghami, S.; Wang, M. Z.; Ma, L.; Oas, T. G.; Fitzgerald, M. C. *J. Am. Chem. Soc.* **2002**, *124*, 10256-10257.
- (49) Dencher, N. A.; Sass, H. J.; Büldt, G. *Biochim. Biophys. Acta* **2000**, *1460*, 192-203.
- (50) Brouillette, C. G.; Mcnichens, R. B.; Stern, L. J.; Khorana, H. G. *Proteins: Struct. Funct. Gen.* **1989**, *5*, 38-46.
- (51) Subramaniam, S.; Hirai, T.; Henderson, R. *Phil. Trans. R. Soc. Lond. A* **2002**, *360*, 859-874.
- (52) Haupts, U.; Tittor, J.; Oesterhelt, D. *Annu. Rev. Biophys. Biomol. Struct.* **1999**, *28*, 367-399.
- (53) Heberle, J.; Fitter, J.; Sass, H. J.; Büldt, G. *Biophys. Chem.* **2000**, *85*, 229-248.
- (54) Lanyi, J. K. *Annu. Rev. Physiol.* **2004**, *66*, 665-688.
- (55) Kluge, T.; Olejnik, J.; Smilowitz, L.; Rothschild, K. J. *Biochemistry* **1998**, *37*, 10279-10285.
- (56) Shibata, M.; Yamashita, H.; Uchihashi, T.; Kandori, K.; Ando, T. *Nat. Nanotech.* **2010**, *5*, 208-212.
- (57) Luecke, H.; Schobert, B.; Richter, H. T.; Cartailler, J. P.; Lanyi, J. K. *Science* **1999**, *286*, 255-261.
- (58) Sass, H. J.; Büldt, G.; Gessenich, R.; Hehn, D.; Neff, D.; Schlesinger, R.; Berendzen, J.; Ormos, P. *Nature* **2000**, *406*, 649-653.
- (59) Hirai, T.; Subramaniam, S. *PLoS One* **2009**, *4*, e5769.
- (60) Andersson, M.; Malmerberg, E.; Westenhoff, S.; Katona, G.; Cammarata, M.; Wöhri, M. B.; Johansson, L. C.; Ewald, F.; Eklund, M.; Wulff, M.; Davidsson, J.; Neutze, R. *Structure* **2009**, *17*, 1265-1275.
- (61) Patzelt, H.; Simon, B.; terLaak, A.; Kessler, B.; Kühne, R.; Schmieder, P.; Oesterhelt, D.; Oschkinat, H. *Proc. Natl. Acad. Sci. U.S.A.* **2002**, *99*, 9765-9770.
- (62) Nishikawa, T.; Murakami, M.; Kouyama, T. *J. Mol. Biol.* **2005**, *352*, 319-328.
- (63) Subramaniam, S.; Marti, T.; Rösselet, S. J.; Rothschild, K. J.; Khorana, H. G. *Proc. Natl. Acad. Sci. U.S.A.* **1991**, *88*, 2581-2587.
- (64) Booth, P. J.; Farooq, A.; Flitsch, S. L. *Biochemistry* **1996**, *35*, 5902-5909.
- (65) Roder, H.; Elöve, G. A.; Englander, S. W. *Nature* **1988**, *335*, 700-704.
- (66) Sterling, H. J.; Williams, E. R. *Anal. Chem.* **2010**, *82*, 9050-9057.
- (67) Pan, J.; Han, J.; Borchers, C. H.; Konermann, L. *J. Am. Chem. Soc.* **2009**, *131*, 12801-12808.
- (68) Waschuk, S. A.; Bezerra, A. G.; Shi, L.; Brown, L. S. *Proc. Natl. Acad. Sci. U.S.A.* **2005**, *102*, 6879-6883.

- (69) Englander, J. J.; Englander, S. W. *Nature* **1977**, *265*, 658-659.
- (70) Downer, N. W.; Bruchman, T. J.; Hazzard, J. H. *J. Biol. Chem.* **1986**, *261*, 3640-3647.
- (71) Joh, N. H.; Min, A.; Faham, S.; Whitelegge, J. P.; Yang, D.; Woods, V. L.; Bowie, J. U. *Nature* **2008**, *453*, 1266-1270.
- (72) Earnest, T. N.; Herzfeld, J.; Rothschild, K. J. *Biophys. J.* **1990**, *58*, 1539-1546.
- (73) Konishi, T.; Packer, L. *FEBS Lett.* **1977**, *80*, 455-458.
- (74) Oesterhelt, D.; Schuhmann, L.; Gruber, H. *FEBS Lett.* **1974**, *44*, 257-261.
- (75) Hirai, T.; Subramaniam, S.; Lanyi, J. K. *Curr. Opin. Struct. Biol.* **2009**, *19*, 433-439.
- (76) Varo, G.; Lanyi, J. K. *Biochemistry* **1991**, *30*, 7165-7171.
- (77) Balashov, S. P.; Lu, M.; Imasheva, E. S.; Govindjee, R.; Ebrey, T. G.; Othersen III, B.; Chen, Y.; Crouch, R. K.; Menick, D. R. *Biochem.* **1999**, *38*, 2026-2039.
- (78) Ludmann, K.; Gergely, C.; Va'ro', G. *Biophys. J.* **1998**, *75*, 3110-3119.
- (79) Chizhov, I.; Engelhard, M.; Chernavskii, D. S.; Zubov, B.; Hess, B. *Biophys. J.* **1992**, *61*, 1001-1006.
- (80) Marti, T.; Otto, H.; Mogi, T.; Rösselet, S. J.; Heyn, M. P.; Khorana, H. G. *J. Biol. Chem.* **1991**, *266*, 6919-6927.
- (81) Váró, G.; Lanyi, J. *Biochemistry* **1991**, *30*, 5008-5015.
- (82) Kim, M.-Y.; Maier, C. S.; Reed, D. J.; Deinzer, M. L. *Protein Sci.* **2002**, *11*, 1320-1329.
- (83) Miranker, A.; Robinson, C. V.; Radford, S. E.; Dobson, C. M. *FASEB J.* **1996**, *10*, 93-101.
- (84) Dancsházy, Z.; Tokaji, Z.; Dér, A. *FEBS Lett.* **1999**, *450*, 154-157.
- (85) Maity, H.; Maity, M.; Krishna, M. M. G.; Mayne, L.; Englander, S. W. *Proc. Natl. Acad. Sci. U.S.A.* **2005**, *102*, 4741-4746.
- (86) Weinkam, P.; Zimmermann, J.; Romesberg, F. E.; Wolynes, P. G. *Acc. Chem. Res.* **2010**, *43*, 652-660.
- (87) Xiao, H.; Hoerner, J. K.; Eyles, S. J.; Dobo, A.; Voigtman, E.; Melcuk, A. I.; Kaltashov, I. A. *Protein Sci.* **2005**, *14*, 543-557.
- (88) Jastrzebska, B.; Palczewski, K.; Golczak, M. *J. Biol. Chem.* **2011**, *286*, 18930-18937.
- (89) Curnow, P.; Booth, P. J. *J. Mol. Biol.* **2010**, *403*, 630-642.

Chapter-7 Summary and Future Work

7.1 Summary

The fact that membrane proteins are water insoluble and prone to aggregate makes them a formidable challenge for most analytical techniques. Biochemists require new ways to look at membrane proteins. This work resulted in the first application of laser-induced oxidative labeling coupled with MS for exploring the structure and folding of a membrane protein, bacteriorhodopsin (BR).

In the first step (Chapter-2), native BR in its native lipid environment was exposed to laser-induced oxidative labeling. It was found that the resulting oxidative labeling occurred exclusively at methionine (Met) residues. In contrast to previous studies on water-soluble proteins, the resulting Met oxidative labeling pattern is in excellent agreement with the known structure of native BR. The finding demonstrates that Met oxidative labeling can provide structural information on membrane proteins.

In subsequent studies (Chapter-3), the newly developed labeling strategy was applied to probe the conformational changes of non-native BR samples induced by heat, acid or SDS. It was found that each of the tested denaturing conditions results in unique structural features that give rise to characteristic labeling patterns. The labeling data confirmed the structural resilience of BR against acidic pH. In contrast, both SDS exposure and thermal denaturation induce marked conformational changes. These results demonstrate the capability of laser-induced oxidative labeling as a novel tool for characterizing structural

changes of membrane proteins in response to the alteration of physiochemical environment. Oxidative labeling experiments on BR variants that carry additional Met residues provided even more detailed structural insights that would have been unavailable with the wild-type protein. Combining oxidative labeling with site-directed mutagenesis and fluorescence measurements, this work yielded a detailed structural model of SDS-denatured BR, which has been unobtainable based on previously existing experimental techniques.

In Chapter-4, the oxidative labeling approach was extended further to study the kinetic folding mechanism of BR. A continuous-flow rapid mixing device was coupled with laser labeling for this purpose. After the unfolded BR was mixed quickly with a solution containing lipid/detergent micelles which mimic the native lipid bilayer, short-lived folding intermediates were labeled. In this way, structural properties of membrane folding intermediates were uncovered on the basis of their Met labeling patterns. The combination of pulsed oxidative labeling and stopped-flow spectroscopy revealed unprecedented insights into the pathways by which the protein inserts and folds into lipid bilayers. The work conducted thus far highlights the usefulness of laser-induced oxidative labeling in conjunction with rapid mixing and MS as a new approach for probing temporal structural changes of membrane proteins under various physiochemical conditions.

In addition to covalent labeling, hydrogen/deuterium exchange (HDX) coupled with MS is a potentially powerful approach for investigating the structure and dynamics of membrane proteins. In Chapter-5, in an attempt to enhance the general applicability of HDX/MS to membrane proteins, low-temperature size exclusion chromatography (SEC) was developed

to purify various lipid/detergent-bound BR samples prior to ESI-MS analysis. High quality HDX profiles of BR under various conditions were obtained. Unlike other MS-based approaches, the newly developed low-temperature SEC/ESI-MS allows the labile Schiff-base linkage between the protein and retinal chromophore to be completely preserved, such that HDX properties of co-existing protein sub-populations can be monitored individually. The distinct structural features of native BR, detergent-solubilized BR, and regenerated BR were revealed by their HDX kinetics.

In Chapter-6, comparative HDX experiments of BR were carried out in the dark (resting state) and under steady illumination which induces continuous retinal isomerization that is associated with the vectorial proton transport (functioning state). The HDX kinetics of BR are dramatically accelerated in the presence of light. In contrast, control experiments on retinal-free proteins produced no discernible differences. It was concluded that the extent of thermal fluctuations in BR strongly depends on photon-driven retinal isomerization. The result highlights the potential of HDX/MS for probing the structural dynamics of molecular machines under "engine on" and "engine off" conditions.

7.2 Future Work

7.2.1 Application of Laser-induced Oxidative Labeling

Membrane proteins are key players in many important cellular processes. Due to the difficulties associated with the expression, purification and crystallization of membrane proteins, resolving high-resolution structure of these species remains highly challenging. Topological mapping is thus widely used to provide useful information of the structure and

function of membrane proteins. Using BR as model system, this work has proven that laser-induced Met oxidative labeling is a straightforward method for mapping the surface of membrane proteins. It is especially useful when considering that many of these species are methionine rich.^{1, 2} The introduction of additional Met residues as conformational probes, as well as *in vivo* structural investigations, represents exciting future extensions of this methodology.

Currently, we are applying the laser-induced radical labeling coupled with MS to characterize the structure of WaaL (from *E. coli*). WaaL is a transmembrane enzyme implicated in the biosynthesis of lipopolysaccharides in Gram-negative bacteria.³ The structure of WaaL is unknown. The resulting Met labeling pattern was found to be consistent with the putative topology generated by computational modeling, such that it provides a preliminary experimental validation to the structural model. Oxidative labeling experiments on WaaL variants that are engineered with extra methionines are ongoing. The resulting labeling data will provide more detailed structural information. Also these data can serve as constraints for further refining the structural model. It is expected that this technique can serve as a valuable tool for guiding topology prediction and computational modeling of membrane proteins.^{4, 5}

In addition to providing structural information on native membrane proteins, the laser-induced oxidative labeling has succeeded in investigating the structure of semi-denatured BR and even short-lived BR folding intermediates. The approaches developed in this work should be applicable to other membrane proteins as well.

7.2.2 Application of HDX/MS for Membrane Proteins

HDX/MS is a powerful tool for studying the structure and dynamics of proteins, but thus far this technique has been applied mostly to soluble species. In this work, HDX/MS coupled with low-temperature SEC was developed and validated to be a straightforward strategy to probe the global conformational changes of BR. Unfortunately, the lack of a robust protocol for spatially-resolved membrane protein studies represents a severe impediment for studies in this area. Nonetheless, the ongoing improvements of the HDX and digestion workflow⁶⁻⁹ suggest that membrane proteins will soon become amenable to spatially-resolved HDX/MS studies on a routine basis. The utilization of more efficient Ultra Performance Liquid Chromatography (UPLC) and prior detergent/lipid removal can generally improve the separation.^{10, 11} An alternative future development is the combination of solution-phase HDX with electron-based dissociation techniques for top-down HDX/MS.¹²⁻¹⁴

7.2 References

- (1) Yu, Y.; Gilar, M.; Gebler, J. C. *Rapid Commun. Mass Spectrom.* **2004**, *18*, 711-715.
- (2) Ablonczy, Z.; Kono, M.; Crouch, R. K.; Knapp, D. R. *Anal. Chem.* **2001**, *73*, 4774-4779.
- (3) Pérez, J. M.; McGarry, M. A.; Marolda, C. L.; Valvano, M. A. *Mol. Microbiol.* **2008**, *70*, 1424-1440.
- (4) Barth, P.; Wallner, B.; Baker, D. *Proc. Natl. Acad. Sci. U.S.A.* **2009**, *106*, 1409-1414.
- (5) Elofsson, A.; Heijne, G. V. *Annu. Rev. Biochem.* **2007**, *76*, 125-140.
- (6) Zhang, H. M.; McLoughlin, S. M.; Frausto, S. D.; Tang, H. L.; Emmett, M. R.; Marshall, A. G. *Anal. Chem.* **2010**, *82*, 1450-1454.
- (7) Jones, L. M.; Zhang, H.; Vidavsky, I.; Gross, M. L. *Anal. Chem.* **2010**, *82*, 1171-1174.
- (8) Wales, T. E.; Fadgen, K. E.; Gerhardt, G. C.; Engen, J. R. *Anal. Chem.* **2008**, *80*, 6815-6820.
- (9) Rey, M.; Man, P.; Brandolin, G.; Forest, E.; Pelosi, L. *Rapid Commun. Mass Spectrom.* **2009**, *23*, 3431-3438.
- (10) Hebling, C. M.; Morgan, C. R.; Stafford, D. W.; Jorgenson, J. W.; Rand, K. D.; Engen, J. R. *Anal. Chem.* **2010**, *82*, 5415-5419.
- (11) Rey, M.; Mrzek, H.; Pompach, P.; Novk, P.; Pelosi, L.; Brandolin, G.; Forest, E.; Havlek, V.; Man, P. *Anal. Chem.* **2010**, *82*, 5107-5116.
- (12) Rand, K. D.; Zehl, M.; Jensen, O. N.; Jørgensen, T. J. D. *Anal. Chem.* **2009**, *81*, 5577-5584.
- (13) Pan, J.; Han, J.; Borchers, C. H.; Konermann, L. *J. Am. Chem. Soc.* **2009**, *131*, 12801-12808.
- (14) Pan, J.; Han, J.; Borchers, C. H.; Konermann, L. *Anal. Chem.* **2011**, *83*, 5386-5393.

Appendix-1 Permissions

ELSEVIER LICENSE TERMS AND CONDITIONS

This is a License Agreement between YAN PAN ("You") and Elsevier ("Elsevier") provided by Copyright Clearance Center ("CCC"). The license consists of your order details, the terms and conditions provided by Elsevier, and the payment terms and conditions.

Supplier	Elsevier Limited, The Boulevard,Langford Lane Kidlington,Oxford,OX5 1GB,UK
Registered Company Number	1982084
Customer name	YAN PAN
Customer address	
License number	2732141034410
License date	Aug 18, 2011
Licensed content publisher	Elsevier
Licensed content publication	Journal of Molecular Biology
Licensed content title	Mapping the Structure of an Integral Membrane Protein under Semi-Denaturing Conditions by Laser-Induced Oxidative Labeling and Mass Spectrometry
Licensed content author	Yan Pan,Leonid Brown,Lars Konermann
Licensed content date	18 December 2009
Licensed content volume number	394
Type of Use	reuse in a thesis/dissertation

ELSEVIER LICENSE TERMS AND CONDITIONS

This is a License Agreement between YAN PAN ("You") and Elsevier ("Elsevier") provided by Copyright Clearance Center ("CCC"). The license consists of your order details, the terms and conditions provided by Elsevier, and the payment terms and conditions.

Supplier	Elsevier Limited, The Boulevard,Langford Lane Kidlington,Oxford,OX5 1GB,UK
Registered Company Number	1982084
Customer name	YAN PAN
Customer address	
License number	2732150160004
License date	Aug 18, 2011
Licensed content publisher	Elsevier
Licensed content publication	Journal of the American Society for Mass Spectrometry
Licensed content title	Site-Directed Mutagenesis Combined with Oxidative Methionine Labeling for Probing Structural Transitions of a Membrane Protein by Mass Spectrometry
Licensed content author	Yan Pan,Leonid Brown,Lars Konermann
Licensed content date	November 2010
Licensed content volume number	21
Type of Use	reuse in a thesis/dissertation

ELSEVIER LICENSE TERMS AND CONDITIONS

This is a License Agreement between YAN PAN ("You") and Elsevier ("Elsevier") provided by Copyright Clearance Center ("CCC"). The license consists of your order details, the terms and conditions provided by Elsevier, and the payment terms and conditions.

Supplier	Elsevier Limited, The Boulevard,Langford Lane Kidlington,Oxford,OX5 1GB,UK
Registered Company Number	1982084
Customer name	YAN PAN
Customer address	
License number	2732141403535
License date	Aug 18, 2011
Licensed content publisher	Elsevier
Licensed content publication	Journal of Molecular Biology
Licensed content title	Kinetic Folding Mechanism of an Integral Membrane Protein Examined by Pulsed Oxidative Labeling and Mass Spectrometry
Licensed content author	Yan Pan,Leonid Brown,Lars Konermann
Licensed content date	1 July 2011
Licensed content volume number	410
type of Use	reuse in a thesis/dissertation

ELSEVIER LICENSE TERMS AND CONDITIONS

This is a License Agreement between YAN PAN ("You") and Elsevier ("Elsevier") provided by Copyright Clearance Center ("CCC"). The license consists of your order details, the terms and conditions provided by Elsevier, and the payment terms and conditions.

Supplier	Elsevier Limited, The Boulevard,Langford Lane Kidlington,Oxford,OX5 1GB,UK
Registered Company Number	1982084
Customer name	YAN PAN
Customer address	
License number	2732150060191
License date	Aug 18, 2011
Licensed content publisher	Elsevier
Licensed content publication	International Journal of Mass Spectrometry
Licensed content title	Hydrogen/deuterium exchange mass spectrometry and optical spectroscopy as complementary tools for studying the structure and dynamics of a membrane protein
Licensed content author	Yan Pan,Leonid Brown,Lars Konermann
Licensed content date	30 April 2011
Licensed content volume number	302
Type of Use	reuse in a thesis/dissertation

Dear Yan Pan:

The Royal Society of Chemistry (RSC) hereby grants permission for the use of your paper(s) "Membrane Protein Structural Insights from Chemical Labeling and Mass Spectrometry", *Analyst*, 135, 1191-1200 (2010) in the printed and microfilm version of your thesis. You may also make available the PDF version of your paper(s) that the RSC sent to the corresponding author(s) of your paper(s) upon publication of the paper(s) in the following ways: in your thesis via any website that your university may have for the deposition of theses, via your university's Intranet or via your own personal website. We are however unable to grant you permission to include the PDF version of the paper(s) on its own in your institutional repository. The Royal Society of Chemistry is a signatory to the STM Guidelines on Permissions (available on request).

Please note that if the material specified below or any part of it appears with credit or acknowledgement to a third party then you must also secure permission from that third party before reproducing that material.

Please ensure that the thesis states the following:

Reproduced by permission of The Royal Society of Chemistry

and include a link to the paper on the Royal Society of Chemistry's website.

Please ensure that your co-authors are aware that you are including the paper in your thesis.

Regards

Gill Cockhead

Contracts & Copyright Executive

Gill Cockhead (Mrs), Contracts & Copyright Executive

Royal Society of Chemistry, Thomas Graham House

Science Park, Milton Road, Cambridge CB4 0WF, UK

Tel +44 (0) 1223 432134, Fax +44 (0) 1223 423623

<http://www.rsc.org>



Title: Structural Characterization of an Integral Membrane Protein in Its Natural Lipid Environment by Oxidative Methionine Labeling and Mass Spectrometry

Author: Yan Pan et al.

Publication: Analytical Chemistry

Publisher: American Chemical Society

Date: Jan 1, 2009

Copyright © 2009, American Chemical Society

PERMISSION/LICENSE IS GRANTED FOR YOUR ORDER AT NO CHARGE

This type of permission/license, instead of the standard Terms & Conditions, is sent to you because no fee is being charged for your order. Please note the following:

- Permission is granted for your request in both print and electronic formats.
- If figures and/or tables were requested, they may be adapted or used in part.
- Please print this page for your records and send a copy of it to your publisher/graduate school.
- Appropriate credit for the requested material should be given as follows: "Reprinted (adapted) with permission from (COMPLETE REFERENCE CITATION). Copyright (YEAR) American Chemical Society." Insert appropriate information in place of the capitalized words.
- One-time permission is granted only for the use specified in your request. No additional uses are granted (such as derivative works or other editions). For any other uses, please submit a new request.

Curriculum Vitae

Name: YAN PAN

Education

Ph.D. 2008-2011 The University of Western Ontario, Canada.
M.Sc. 1993-1996 Guangzhou Institute of Chemistry, Chinese Academy of Science.
B.Sc. 1988-1993 Tsinghua University, China.

Selected Scholarships and Awards

NSERC Canada Graduate Scholarship (D), 2010-2012, UWO
NSERC Canada Graduate Scholarship (M), 2009-2010, UWO
Ontario Graduate Scholarship, 2009-2011, (declined to accept NSERC CGS)
Western Graduate Tuition Scholarship, 2009-2012, UWO
Graduate Thesis Research Awards, 2010, 2011, UWO

Work Experience

Research Scientist, 1999-2003, South China University of Technology.
Research Associate, 1996-1999, South China University of Technology.

Peer-reviewed Publications

- 1) **Pan, Y.**, Piyadasa H., O'Neil, J. D., Konermann, L. Conformational Dynamics of a Membrane Transport Protein Probed by H/D Exchange and Covalent Labeling: The Glycerol Facilitator. *J. Mol. Biol.* Submitted, JMB-D-11-01138 (**2011**)
- 2) **Pan, Y.**, Brown, L., Konermann, L. Hydrogen Exchange Mass Spectrometry of Bacteriorhodopsin Reveals Light-Induced Changes in the Structural Dynamics of a Biomolecular Machine. *J. Am. Chem. Soc.* revised, ID: ja-2011-06197h (**2011**)
- 3) Konermann, L., **Pan, Y.** and Stocks, B. B. Protein Folding Mechanisms Studied by Pulsed Oxidative Labeling and Mass Spectrometry. *Curr. Op. Struct. Biol.* 21: 634-640 (**2011**)
- 4) **Pan, Y.**, Brown, L. and Konermann, L. Kinetic Folding Mechanism of an Integral Membrane Protein Examined by Pulsed Oxidative Labeling and Mass Spectrometry. *J. Mol. Biol.* 410:146-158 (**2011**)
- 5) **Pan, Y.**, Brown, L., Konermann, L. Hydrogen/Deuterium Exchange SEC/ESI-MS and Optical Spectroscopy as Complementary Tools for Studying the Structure and Dynamics of a Membrane Protein. *Int. J. Mass Spectrom. [H/D exchange special issue]* 302: 3-11 (**2011**)
- 6) **Pan, Y.**, Brown, L. and Konermann, L. Site-Directed Mutagenesis Combined with

- Oxidative Methionine Labeling for Probing Structural Transitions of a Membrane Protein. *J. Am. Soc. Mass Spectrom.* 21: 1947-1956 (2010)
- 7) **Pan, Y.** and Konermann, L. Membrane Protein Structural Insights from Chemical Labeling and Mass Spectrometry. *Analyst* 135: 1191-1200 (2010)
 - 8) Konermann, L, Stocks, B. B., **Pan, Y.** and Tong, X. Mass Spectrometry Combined with Oxidative Labeling for Exploring Protein Structure and Folding. *Mass Spectrom. Rev.* 29: 651-667 (2010)
 - 9) **Pan, Y.**, Brown, L. and Konermann, L. Mapping the Structure of an Integral Membrane Protein under Semi-Denaturing Conditions by Laser-Induced Oxidative Labeling and Mass Spectrometry. *J. Mol. Biol.* 394: 968-981 (2009)
 - 10) **Pan, Y.**, Stocks, B. B., Brown, L., and Konermann, L. Structural Characterization of an Integral Membrane Protein in its Natural Lipid Environment by Oxidative Methionine Labeling and Mass Spectrometry. *Anal. Chem.* 81:28–35 (2009)
 - 11) Konermann, L., Tong, X., **Pan, Y.** Protein Structure and Dynamics Studied by Mass Spectrometry: H/D exchange, Hydroxyl Radical Labeling, and Related Approaches. *J. Mass Spectrom.* 43:1021-1036 (2008)
 - 12) **Pan, Y.**, Cheng, R., Fu, W. and Xue, F. A New Viscometric Criterion for Polymer-Polymer Interaction. *Eur. Polym. J.* 38:1703-1708 (2002)
 - 13) **Pan, Y.**, Fu, W., Xue, F., Luo, Y., Gu, J. and Cheng, R. The Viscosity Anomaly of Polymer Mixture Solution in Extremely Dilute Concentration Region. *Eur. Polym. J.* 38:359-364 (2002)
 - 14) **Pan, Y.**, Fu, W., Xue, F., Luo, Y. and Gu, J. Miscibility and Crystallization Behavior of Solution-Blended Sulfonated Poly (phenylene oxide)/Poly(styrene-co-4-vinylpyridine) Blend. *J. Appl. Polym. Sci.* 81: 2843-2848 (2001)
 - 15) **Pan, Y.** and Xue, F. Lightly Sulfonated Poly (phenylene oxide)/Poly (styrene-co-4-vinyl pyridine) Blend. Inter-polymer Interactions and Miscibility. *Eur. Polym. J.* 37:247-249 (2001)
 - 16) **Pan, Y.** and Cheng, R. A Novel Interpretation of Concentration Dependence of Viscosity of Dilute Polymer Solution. *Chin. J. Polym. Sci.* 18:57-67 (2000)
 - 17) **Pan, Y.**, Huang, Y., Chen, M., Cong, G. and Leung, L. M. Solution Behavior of Ionomer Blends II. Acid-base Interactions in Blends of Poly (phenylene oxide) Ionomers and Poly (styrene-4-vinylpyridine). *Eur. Polym. J.* 34:213-217 (1998)
 - 18) **Pan, Y.**, Huang, Y., Liao, B., Cong, G. and Leung, L. M. Solution Behavior of Ionomer Blends I. Factors Influencing Inter-polymer Complexes of Ionomer Blends. *Eur. Polym. J.* 34:207-211 (1998)
 - 19) **Pan, Y.**, Huang, Y., Liao, B., Chen, M., Cong, G. and Leung, L. M. Studies on Miscibility of Poly (phenylene oxide)-Based Ionomer/Polystyrene-Based Ionomer Blends. *J. Appl. Polym. Sci.* 62:341-346 (1997)
 - 20) **Pan, Y.**, Huang, Y., Liao, B. and Cong, G. Synthesis and Characterization of Aminated Poly(2,6-dimethyl-1,4-phenylene oxide). *J. Appl. Polym. Sci.* 61:1111-1115 (1996)

Selected Presentations

- 1) **Pan, Y.**, O'Neil, J., Konermann, L. (2011) Conformational Dynamics of an Integral Membrane Protein Probed by HDX and ESI-MS. *Gordon Research Conference, Andover /USA*
- 2) **Pan, Y.**, Brown, L., Konermann, L. (2011) Kinetic Folding Mechanism of an Integral Membrane Protein Examined by Pulsed Oxidative Labeling and Mass Spectrometry. *Oral presentation, 59th ASMS Conference, Denver /USA*
- 3) **Pan, Y.**, Brown, L., Konermann, L. (2010) Conformational Changes of an Integral Membrane Protein Studied by HDX/ESI-MS and Optical Spectroscopy. *58th ASMS Conference, Salt Lake City /USA*
- 4) **Pan, Y.**, Brown, L., Konermann, L. (2009) Structural Characterization of an Integral Membrane Protein by Oxidative Methionine Labeling and Mass Spectrometry. *57th ASMS Conference, Philadelphia /USA*